Novel Resonance Self-Shielding Methods for Nuclear Reactor Analysis

by

Nathan A. Gibson

B.S. Nuclear Engineering, B.S. Physics, 2010
Rensselaer Polytechnic Institute

S.M. Nuclear Science and Engineering, 2013
Massachusetts Institute of Technology

Submitted to the Department of Nuclear Science and Engineering
in Partial Fulfillment for the Degree of

Doctor of Philosophy
at the
Massachusetts Institute of Technology

February 2016

Signature of Author: _____

Nathan A. Gibson
January 25, 2016

Certified by: _____

Benoit Forget, Ph.D.
Associate Professor of Nuclear Science and Engineering
Thesis Supervisor

_____

Kord S. Smith, Ph.D.
KEPCO Professor of the Practice of Nuclear Science and Engineering
Thesis Reader

Accepted by: _____

Ju Li, Ph.D.
Battelle Energy Alliance Professor of Nuclear Science and Engineering
Chair, Department Committee on Graduate Students

Novel Resonance Self-Shielding Methods for Nuclear Reactor Analysis

by

Nathan A. Gibson

Submitted to the Department of Nuclear Science and Engineering on January 25, 2016, in Partial Fulfillment of the Requirements for the Degree of Doctor of Philosophy in Nuclear Science and Engineering

Abstract

In the simulation of the behavior of neutrons in a nuclear reactor, there has long been a dichotomy in solution techniques. One can use Monte Carlo methods, known to be very accurate and problem agnostic but also very costly, or deterministic methods, known to be more computationally efficient but also requiring tuning to a specific application. As designers rely more and more heavily on predictive simulation, higher fidelity and more problem agnostic deterministic methods are desired. This thesis seeks to push these deterministic methods towards that goal of higher fidelity in the context of multigroup cross section generation and resonance self-shielding.

This work has two primary objectives: to quantitatively assess the efficacy of current self-shielding approximations and to propose new self-shielding methods. These objectives are cast primarily in the context of mutual self-shielding, the effect of one nuclide's resonances on the neutron reaction rate with another nuclide.

The first objective is accomplished through the development of a framework for the evaluation of self-shielding methods. This framework is analogous to a unit test suite in software engineering, in that specific aspects of physics modeled by a self-shielding method are isolated. The framework is used on numerous existing methods, and highlights the successes and failures of these methods on very simple problems. This objective is also accomplished via an analysis of the consequences of neglecting the angular dependence of multigroup cross sections in the solution to the multigroup neutron transport equation.

The second objective is accomplished by proposing two new methods: the subgroup method with interference cross sections and ultrafine with simplified scattering. The former uses a fitting method to find the effect of interfering nuclides on the subgroup levels of a primary nuclide, allowing mutual self-shielding effects to be treated natively inside the subgroup method without increasing algorithmic complexity. The latter is a hybrid of the subgroup method and ultrafine methods, using an ultrafine energy mesh on the left hand side of the transport equation with the scatter source of the subgroup method on the right hand side. These two methods are tested in the context of the evaluation framework alongside classical methods. Although it shows promise on some simple problems, the subgroup method with interference cross sections was seen to exhibit shortcomings on problems with many nuclides. Ultrafine with simplified scattering was found to perform very well on all problems in the test suite.

Thesis Supervisor: Benoit Forget
Title: Associate Professor of Nuclear Science and Engineering

Acknowledgments

This research was performed under appointment to the Rickover Fellowship Program in Nuclear Engineering sponsored by the Naval Reactors Division of the U.S. Department of Energy.

First and foremost, I'd like to express my deepest gratitude to my thesis supervisor Prof. Benoit Forget. Over the course of more than five years of working with him, he has gently steered me along a path allowing me to grow from an eager student to a full-fledged academic researcher. This thesis would not be possible without his incredible insight and special ability to guide me in the right direction only when I needed it most.

I'd also like to sincerely thank Prof. Kord Smith for his engagement in my research and for providing me with the opportunity to try my hand at teaching. His vast knowledge and personable demeanor allowed me to learn so much about the state of affairs in industry related to these topics. Taking three classes and assisting a fourth class with him provided me with the bulk of my knowledge of the field.

Next, I'd like to give my appreciation to my fellowship advisor and thesis committee member, Dr. Timothy Trumbull. He began teaching and supporting me all the way back in undergraduate, and I am looking forward to beginning my career alongside him at the Knolls Atomic Power Laboratory.

Both in my undergraduate and graduate education, my learning was enriched and driven by the community of students around me. I'd like to especially thank William Boyd for his assistance with the method of characteristics and cooperation with angular effects on cross sections that supported this research directly. I'd also like to thank my closest friend in the nuclear industry, Dr. Bryan Herman, for being a friend, a classmate, a coworker, and a role model to me for nearly ten years. I will miss the home and office chats with my fellow students, who are too many to list, and who made graduate school a community rather than a simple workplace.

My graduate school career and this research could not have been complete without all the enrichment I received outside my own education and research. Dr. Adam Boyles and the MIT Symphony Orchestra as well as my string quartet—with Daniel Rothenberg, Dan Amrhein, and Lawrence Cheuk—gave my life the gift of music, which propelled me through my time in Cambridge. Co-chairing the ANS 2013 Student Conference and serving as MIT ANS Co-President, with the help of so many others, gave me invaluable leadership experience. And I extend a special thank you to the students of the Fall 2015 22.05 class who I had the distinct pleasure of teaching.

Finally, I must extend my heartfelt love and thanks to those at home. My two wonderful parents, John and Cathy Gibson, have supported me throughout my whopping 23 years of formal education in every way they could, and I am eternally grateful. I'd like to thank them for putting a roof over my head and food in my stomach, including my last semester in graduate school after so long away. I'd like to thank them for agreeing to get me a "real pet" 15 years ago, a cat named Granite that helped in his own way with my homework in high school and again helped with writing this thesis. But most of all, I'd like to thank them simply for being my parents. My last two years were made so much better by the love and support of my amazing girlfriend, Lindsay O'Brien. Words can't describe my gratitude for our time so far and excitement for embarking on a life in upstate New York together.

Contents

Part I

Introduction

Chapter 1

Introduction

1.1 Introduction

In the modeling of a nuclear reactor, a requisite quantity of interest is the distribution of nuclear reaction rates throughout the core. This is accomplished by modeling the distribution of neutrons through the use of the neutron transport equation. This class of problems is known as neutronics or reactor physics.

The independent variable in the neutron transport equation is the neutron flux. When used to describe the distribution of neutrons including their direction of travel, this is the angular flux ψ. When integrated over all angles, the resulting neutron distribution is known as the scalar flux ϕ,

$$\phi = \int_{4\pi} \psi \, \mathrm{d}\hat{\Omega} \quad . \tag{1.1}$$

These fluxes are not the typical definition of flux encountered in physics. Instead the flux is the product of the volume density of neutrons and the speed of the neutrons. An alternative but equivalent definition is the path length traveled by neutrons per unit volume.

The flux is related to the reaction rate $\mathcal{R}$ by a proportionality constant known as a macroscopic cross section Σ,

$$\mathcal{R} = \Sigma\phi \quad . \tag{1.2}$$

The macroscopic cross section varies by material composition, but is related to another quantity known as the microscopic cross section σ by

$$\Sigma = N\sigma \quad , \tag{1.3}$$

where N is the number density of a nuclide. This microscopic cross section is a property of a particular nuclide. It is measured experimentally, evaluated using experimental data and theoretical models, and tabulated. The macroscopic cross section for a material containing

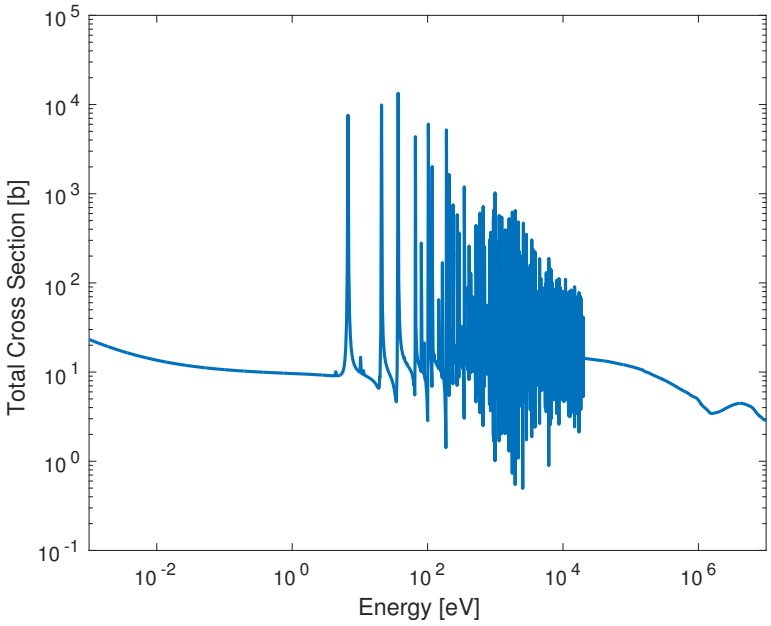

Figure 1.1: Total microscopic cross section of U-238.

multiple nuclides is the sum of the macroscopic cross sections of the constituent nuclides.

The microscopic cross section for a given nuclide can be a wildly varying function of energy. For instance, the cross section of one of the most important nuclides in reactor physics, U-238, is given in Fig. 1.1. The cross section varies several orders of magnitude over an energy interval on the order of an eV near nuclear resonances. This fact, coupled with neutrons in a nuclear reactor covering more than 10 orders of magnitude in energy, provides significant challenges in the solution of the neutron transport equation. This thesis focuses on means of accounting for the effects of resonances on the solution of this equation.

The neutron transport equation is an integro-differential equation, and the flux it models is a function of seven variables. These variables include three variables to describe the position of a neutron, two to describe its direction of travel, one to describe its energy (or equivalently, speed), and one to describe the point in time. It is a balance equation, setting the rate of change of the neutron population equal to the difference in the neutron source rate and the neutron sink rate. In this thesis, only steady-state applications will be considered. The transport equation then requires the sources be balanced exactly by the sink. This implies either a very specific condition be modeled, a fixed source be present, or an eigenvalue to force this balance. The steady state transport equation with a generic source Q is

$$\hat{\Omega}\cdot\nabla\psi(\vec{r},\hat{\Omega},E)+\Sigma_t(\vec{r},E)\psi(\vec{r},\hat{\Omega},E) = \int_0^\infty dE' \int_{4\pi} d\hat{\Omega}'\,\Sigma_s(\vec{r},\hat{\Omega}'\rightarrow\hat{\Omega},E'\rightarrow E)\psi(\vec{r},\hat{\Omega}',E') + Q(\vec{r},\hat{\Omega},E) \quad . \tag{1.4}$$

The subscripts on the cross sections indicate the type of reaction they correspond to. Subscript t indicates the total of all reactions, and s indicates scattering. Other subscripts used in this thesis include a for absorption, γ for radiative capture, and f for fission. The subscript t will sometimes be dropped from Σ_t, and Σ will imply the total cross section in this thesis.

In this equation, the first term on the left hand side represents the streaming of neutrons from one spatial location to another. The second term is the total collision rate for a given volume of phase space. On the right hand side, the first term is the scatter source, representing neutrons that scatter off nuclei at some energy and emerge at the energy of interest. Finally, a source term is included. In a typical reactor physics calculation, this is a fission source including an eigenvalue k,

$$\begin{aligned} Q(\vec{r}, \hat{\Omega}, E) &= \frac{\chi(\vec{r}, E)}{k} \int_0^\infty \mathrm{d}E' \int_{4\pi} \mathrm{d}\hat{\Omega}' \, \nu\Sigma_f(\vec{r}, \hat{\Omega}' \to \hat{\Omega}, E' \to E)\psi(\vec{r}, \hat{\Omega}', E') \\ &\approx \frac{\chi(\vec{r}, E)}{4\pi k} \int_0^\infty \mathrm{d}E' \, \nu\Sigma_f(\vec{r}, E' \to E)\phi(\vec{r}, E') \quad , \end{aligned} \tag{1.5}$$

where χ is the energy spectrum of emerging fission neutrons and ν is the number of neutrons per fission. The approximation is the most commonly used form, as fission neutrons are emitted nearly isotropically.

The neutron transport equation has been solved using a multitude of different approaches. The most accurate and problem agnostic method is the Monte Carlo method, which simulates the behavior of individual neutrons via stochastic methods and infers the distribution of quantities of interests via population statistics. The major downside to the Monte Carlo method is its associated high computational cost.

The alternative to Monte Carlo is to solve the neutron transport equation with a deterministic method. The traditional application of these methods is much more computationally efficient than Monte Carlo, but accurate and problem agnostic results are much more difficult. The objective of this thesis is to provide additional accuracy for deterministic methods, pushing them towards the ideal of being problem agnostic.

1.2 Multigroup Approximation

When using deterministic methods, the neutron transport equation is discretized in each variable, sometimes with the exception of the angular variable, which is expanded with orthogonal polynomials. Spatial discretization follows the well-known approaches used in other fields for the solution of partial differential equations. The energy discretization, however, presents a unique challenge for the neutron transport equation. Because of the large range of important neutron energies in a reactor and the wild energy dependence of the cross sections, the energy discretization must be performed very carefully. The most common approach for

deterministic methods is the multigroup approximation.

The multigroup approximation is formulated in such a way as to preserve reaction rates, as these are the primary quantities of interest. This is accomplished by integrating the neutron transport equation over energy and defining multigroup constants in a consistent manner. In this discussion, the scatter source is assumed to be isotropic, but this assumption is not necessary for the multigroup approximation. Defining an energy group as a contiguous domain of energy, the neutron transport equation is integrated over group g, ranging from $[E_{g+1}, E_g]$,

$$\int_{E_{g+1}}^{E_g} \mathrm{d}E \left(\hat{\Omega} \cdot \nabla \psi(\vec{r}, \hat{\Omega}, E) + \Sigma_t(\vec{r}, E) \psi(\vec{r}, \hat{\Omega}, E) \right) = \int_{E_{g+1}}^{E_g} \mathrm{d}E \left(\frac{1}{4\pi} \int_0^{\infty} \mathrm{d}E' \, \Sigma_s(\vec{r}, E' \rightarrow E) \phi(\vec{r}, E') + Q(\vec{r}, \hat{\Omega}, E) \right) \tag{1.6}$$

$$\hat{\Omega} \cdot \nabla \psi_g(\vec{r}, \hat{\Omega}) + \Sigma_{t,g}(\vec{r}, \hat{\Omega}) \psi_g(\vec{r}, \hat{\Omega}) = \frac{1}{4\pi} \sum_{g'=1}^{G} \Sigma_{s,g' \rightarrow g}(\vec{r}) \phi_{g'}(\vec{r}) + Q_g(\vec{r}, \hat{\Omega}) \quad , \tag{1.7}$$

where the multigroup constants are defined as

$$\psi_g(\vec{r}, \hat{\Omega}) = \int_{E_{g+1}}^{E_g} \mathrm{d}E \, \psi(\vec{r}, E, \hat{\Omega}) \tag{1.8}$$

$$\Sigma_{t,g}(\vec{r}, \hat{\Omega}) = \frac{\int_{E_{g+1}}^{E_g} \mathrm{d}E \, \Sigma_t(\vec{r}, E) \psi(\vec{r}, E, \hat{\Omega})}{\int_{E_{g+1}}^{E_g} \mathrm{d}E \, \psi(\vec{r}, E, \hat{\Omega})} \tag{1.9}$$

$$\Sigma_{s,g' \rightarrow g}(\vec{r}) = \frac{\int_{E_{g'+1}}^{E'_g} \mathrm{d}E' \int_{E_{g+1}}^{E_g} \mathrm{d}E \, \Sigma_s(\vec{r}, E' \rightarrow E) \phi(\vec{r}, E)}{\int_{E_{g'+1}}^{E'_g} \mathrm{d}E' \, \phi(\vec{r}, E')} \tag{1.10}$$

$$Q_g(\vec{r}, \hat{\Omega}) = \int_{E_{g+1}}^{E_g} \mathrm{d}E \, Q(\vec{r}, E, \hat{\Omega}) \quad . \tag{1.11}$$

Note that energy groups with higher indices are lower in energy. This convention stems from the fact that neutrons are born from fission at high energies and slow down to lower energies throughout their life.

The multigroup form of the transport equation presented here is not typically used, as it has the inconvenient property of having an angular dependent total cross section. This angular dependence is a result of collapsing to the multigroup form by integrating with the angular flux. Instead, an approximate multigroup transport equation is much more commonly solved, where the total cross section is collapsed using the scalar flux:

$$\hat{\Omega} \cdot \nabla \psi_g(\vec{r}, \hat{\Omega}) + \Sigma_{t,g}(\vec{r}, \hat{\Omega}) \psi_g(\vec{r}, \hat{\Omega}) = \frac{1}{4\pi} \sum_{g'=1}^{G} \Sigma_{s,g' \rightarrow g}(\vec{r}) \phi_{g'}(\vec{r}) + Q_g(\vec{r}, \hat{\Omega}) \tag{1.12}$$

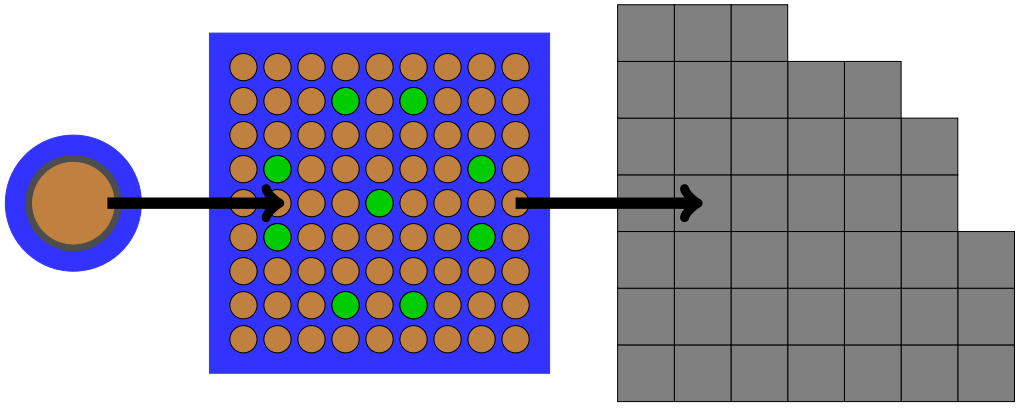

Figure 1.2: Diagram of the multilevel approach used in deterministic reactor physics calculations.

$$\Sigma_{t,g}(\vec{r}) = \frac{\int_{E_{g+1}}^{E_g} \mathrm{d}E\, \Sigma_t(\vec{r}, E)\phi(\vec{r}, E)}{\int_{E_{g+1}}^{E_g} \mathrm{d}E\, \phi(\vec{r}, E)} \quad . \tag{1.13}$$

The consequences of this approximation are explored in Ch. 7.

Other than the approximation for the total multigroup cross section, the multigroup transport equation is an exact representation of the true neutron transport equation. However, the multigroup constants require knowledge of the continuous energy flux, which is not known *a priori*. This difficulty is summarized particularly well by this quote from the NJOY manual [1]:

> *"Wait a minute," you ask, "the purpose of solving the transport equation is to get the flux, but I have to know the flux to compute the multigroup constants!" This conundrum is the source of much of the "art" in using multigroup methods.*

To overcome this challenge, a multi-level framework is usually employed to approximate the flux for use in collapsing multigroup constants. In this framework, a small problem—either an infinite medium or a single unit cell—is solved with continuous or near continuous energy cross sections. This is known as the self-shielding or database level. Next, cross sections are condensed to $O(50 - 500)$ groups, which are used in a larger calculation, typically a reactor fuel assembly. This step is known as the lattice level. Finally, the cross sections are condensed further to $O(2 - 10)$ groups and used in a full-core calculation. A diagram of this process is shown in Fig. 1.2.

In Part II, methods used for the self-shielding level and the lattice level are discussed. Typically, the self-shielding level involves solving the slowing down equation or an approximation to it in an infinite medium, which is discussed in Ch. 2. In recent years, it has become more common to incorporate geometry into this process, usually by means of an ultrafine solution (discuseed in Ch. 5) or by Monte Carlo methods. Traditionally, the lattice level uses equivalence

in dilution methods (Ch. 3) or the subgroup method (Ch. 4). Ultrafine methods can be used to combine the self-shielding and lattice levels by applying the method to a larger geometry, but this is typically associated with a prohibitive computational cost.

1.3 Method of Characteristics

Of the many approaches to solving the neutron transport equation, the primary solver used in this work is the method of characteristics (MOC) [2]. The results given in this thesis were generated by an MOC code developed by the author, inspired by the open source OpenMOC [3]. The method is briefly explained here.

The method of characteristics recognizes that the streaming term in the neutron transport equation is just the rate of change of the angular flux along a straight line path, i.e., a characteristic:

$$\hat{\Omega} \cdot \nabla \psi(\vec{r}, \hat{\Omega}, E) = \frac{\mathrm{d}}{\mathrm{d}s} \psi(\vec{r}_0 + s\hat{\Omega}, E) \quad , \tag{1.14}$$

where $\vec{r} = \vec{r}_0 + s\hat{\Omega}$. The characteristic form of the transport equation, with a generic source that includes scattering, is

$$\frac{\mathrm{d}}{\mathrm{d}s} \psi(\vec{r}_0 + s\hat{\Omega}, E) + \Sigma_t(\vec{r}_0 + s\hat{\Omega}, E)\psi(\vec{r}_0 + s\hat{\Omega}, E) = Q(\vec{r}_0 + s\hat{\Omega}, E) \quad . \tag{1.15}$$

The most common form, and only form considered in this work, separates the geometry into so-called flat source regions, regions of the geometry in which the source is assumed to be constant. The solution to the transport equation is then solved by integrating along many tracks at different angles and starting points along a global boundary and using a numerical quadrature to obtain the scalar flux. An advantage of this approach is, unlike many other deterministic solvers, the method of characteristics can use an exact geometry; it does not require representing boundaries between materials or otherwise with any approximation. Geometry specification is performed by constructive solid geometry. Quadratic surfaces—those that can be represented by quadratic equations in the spatial variables—are used, and geometric regions are defined by a list of bounding surfaces and their orientations.

Following geometry specification, characteristic tracks are layed down across the geometry. Tracks start from one global boundary and extend until they reach another global boundary. The tracks are then segmented, i.e., separated into segments by splitting the track at each flat source region boundary. Tracks are separated by an equal amount approximately, and the amount is input by the user. Similarly, azimuthal angles are chosen to be approximately uniformly spanning the unit circle, and the number of angles used is an input by the user. The track spacing and number of angles are not perfectly uniform, as cyclic tracking is imposed. That is, all tracks must end at the same point that another track begins. This aids in the

modeling of reflective and periodic boundary conditions. The polar angles and associated quadrature used are those which were recommended by Yamamoto and Tabuchi [4].

Starting from a global boundary with a given boundary flux—either specified as the boundary condition or iterated on for reflective or periodic boundary conditions—the neutron transport equation is integrated across each track. The outgoing flux ψ^+ as a function of the incoming flux ψ^- for each segment is given by

$$\psi^+ = \psi^- e^{-\Sigma_t \Delta} + \frac{Q}{\Sigma_t}\left(1 - e^{-\Sigma_t \Delta}\right) \quad , \tag{1.16}$$

where Δ is the length of the segment. The average angular flux along a segment is

$$\overline{\psi} = \frac{1}{\Delta}\left[\frac{\psi^-}{\Sigma_t}\left(1 - e^{-\Sigma_t \Delta}\right) + \frac{\Delta Q}{\Sigma_t}\left(1 - \frac{\left(1 - e^{-\Sigma_t \Delta}\right)}{\Sigma_t \Delta}\right)\right] \quad . \tag{1.17}$$

Once the flux for each segment is computed, the volume-averaged scalar flux in each flat source region is computed by

$$\phi = \frac{1}{V}\int_V d\vec{r} \int_{4\pi} d\hat{\Omega}\psi \quad . \tag{1.18}$$

The integrals are carried out by a numerical quadrature,

$$\phi = \frac{4\pi}{V}\sum_{k \in V} \omega_{m(k)}\omega_{p(k)}\omega_k \Delta \sin\theta_{p(k)}\overline{\psi}_k \quad , \tag{1.19}$$

where k is the index for a particular segment, $\omega_{m(k)}$ is the azimuthal quadrature weight for the segment, $\omega_{p(k)}$ is the polar quadrature weight for the segment, ω_k is the spatial quadrature weight for the segment, $\theta_{p(k)}$ is the polar angle for the segment, and $\overline{\psi}_k$ is the average flux along that segment.

If the source is dependent upon the flux, after the flux is computed, the source is recomputed. An iterative process is followed until the solution converges.

1.4 Motivation and Objectives

Deterministic neutron transport methods require carefully chosen multigroup constants to accurately model the distribution of reaction rates in a nuclear reactor. These multigroup constants are computed using various self-shielding methods, detailed in Part II. However, these self-shielding methods are based on a series of approximations. Such approximations have proven to yield suitable results for the design and analysis of the existing fleet of commercial light water reactors. However, with the reality that large experiments are likely too costly to be incorporated into advance reactor design, predictive capabilities outside of the design space covered by existing reactors is desired. Even small changes to existing designs—

such as pushing to higher burn-up fuel, using mixed oxide fuels, or axial heterogeneity—cause many of the legacy reactor analysis tools to break down.

Furthermore, even without stressing the methods with new designs, higher fidelity simulations are desired. Closer multiphysics coupling is the goal of much of the ongoing work in reactor physics. Thermal hydraulic analysis provides temperature distributions that can be used in neutronics simulations; in return, neutronics simulations provide power distributions to be used in the thermal hydraulic analyses. Fuel performance analyses also are closely coupled with both thermal hydraulics and neutronics. Although such multiphysics coupling is not the subject of this thesis, the requirements of multiphysics coupling provide motivation for better methods. Neutronics methods that can take into account temperature effects in the self-shielding calculation or that predict the effect of a heterogeneous lattice on the rate of depletion in intra-pin zones or be applied to distorted geometries are needed.

There are two primary objectives of this thesis. First, this thesis seeks to quantitatively measure the current status of self-shielding methods. It seeks to identify situations in which the current methods perform well and to also understand their limits. It seeks to find situations that cannot be handled by existing methods and to quantify the adverse effects of applying the existing methods to these situations. And it seeks to do this in a way that is adaptable to problems not studied specifically in this thesis, as a framework for future evaluation of these problems.

Second, the thesis proposes new self-shielding methods. The new methods are not intended to be monumental deviations from the norm, revolutionizing the industry. Instead, the methods are intended to be small changes to existing methods that allow their range of applicability to increase.

For both of these objectives, the thesis primarily—although not exclusively—considers the context of mutual self-shielding. This is the effect of the resonances of one nuclide affecting the reaction rates in the resonances of another nuclide. This particular issue exists in current LWRs, but is exacerbated in the context of higher burnup fuels, mixed oxide fuels, or other alternate materials.

1.5 Outline

This thesis is divided into five parts, each containing chapters.

Part I contains only this chapter, and serves as an introduction to the problems considered and the methods used in this thesis.

Part II is a substantial review of existing self-shielding methods. In it, Ch. 2 is a discussion of neutrons slowing down in infinite media, which is the primary method used at the self-shielding or database level of the multi-level approach and provides the basis of all the other

methods considered. Chapter 3 introduces equivalence in dilution, the primary workhorse of lattice-level cross section generation for many decades. Chapter 4 introduces the subgroup method, which is an alternative to equivalence in dilution that has become increasingly popular in lattice physics codes more recently. And Ch. 5 introduces ultrafine methods, the clear path forward to higher fidelity, but which comes at a high computational cost.

Part III provides several significant contributions to the field. Chapter 6 presents a simple framework for evaluating self-shielding methods. Chapter 7 investigates the approximation made by scalar flux weighting the total multigroup cross section. Chapter 8 discusses the issue of mutual self-shielding in detail and introduces two new methods for accounting for the effects.

Part IV contains a single, long chapter, Ch. 9. This takes the next step from the framework presented in Ch. 6 and compares both old and new methods on realistic but small problems.

Finally, Part V wraps up the thesis, providing conclusions and references.

Part II

Background

Chapter 2

Slowing Down in Infinite Media

2.1 Introduction

The foundation of classical self-shielding methods is the solution of the neutron slowing down equation, which represents how neutrons behave in an infinite medium. The resulting flux is used to generated cross sections, which are used directly in heterogeneous calculations (discussed in Ch. 3) and used to generate subgroup quadratures (discussed in Ch. 4).

The generation of infinite medium cross sections, stored in homogeneous nuclear data tables, is typically the first level of the multi-level approach for multigroup cross section generation. Continuous energy cross sections are collapsed to on the order of hundreds of groups and stored in a database. These then serve as the inputs to lattice-level methods.

In this chapter, the slowing down of neutrons in the resolved resonance range of major actinides is considered. Scattering is assumed to be isotropic in the center of mass, and the implications of this are explored. The slowing down equation is presented, direct solutions are discussed, and approximate solutions are introduced.

2.2 Physics of Elastic Scattering

When a neutron scatters off a target nucleus, its change in energy is directly correlated with the scattering angle. Here, the relationship between energy and angle is demonstrated for a target nucleus at rest. In the resonance region, thermal motion of the nucleus is generally considered negligible compared to the energy of the neutron in regards to the scattering physics (relationship of incoming and outgoing energies of the neutron and nucleus). Although thermal motion affects the center of mass energy of interaction, which has an important impact on resonance behavior, this effect can be accounted for by modifying the cross section through a process known as Doppler broadening [5]. For some nuclides with resonances with large

Table 2.1: Nomenclature used in scattering derivation, Eq. (2.1) through Eq. (2.13).

Symbol	Meaning
$\vec{\cdot}$	Vector; magnitude implied when vector notation is not used
$\hat{z}$	Unit vector in direction z
$\hat{\Omega}$	Unit vector in direction of neutron travel
θ	Angle between $\hat{z}$ and $\hat{\Omega}$
A	Nucleus mass relative to the neutron mass
V_{COM}	Velocity of the center of mass
v_0	Initial velocity of the neutron in the LAB system
v	Final velocity of the neutron in the LAB system
$\mathfrak{u}_0$	Initial velocity of the neutron in the COM system
$\mathfrak{u}$	Final velocity of the neutron in the COM system
U_0	Initial velocity of the nucleus in the COM system
U	Final velocity of the nucleus in the COM system
p_0	Initial total momentum in the COM
p	Final total momentum in the COM
K_0	Total kinetic energy in the COM
K	Final kinetic energy in the COM
E_0	Initial kinetic energy in the LAB
E	Final kinetic energy in the LAB

scattering widths, the small probability of upscattering due to thermal motion can have an important effect, but the associated scattering physics is not discussed here [6].

Now, a derivation of relationships between incoming and outgoing energies of the neutron and nucleus is presented, with nomenclature defined in Tab. 2.1. Consider a neutron with kinetic energy E_0 and corresponding velocity v_0 in direction $\hat{z}$ colliding with a stationary nucleus with mass A times the neutron mass. The velocity of the center of mass is

$$\vec{V}_{COM} = \frac{v_0\hat{z}}{A+1} \quad . \tag{2.1}$$

The corresponding velocities of the neutron and target nucleus, respectively, in the center of mass frame are

$$\vec{\mathfrak{u}}_0 = \vec{v}_0 - \vec{V}_{COM} = \frac{A}{A+1}v_0\hat{z} \tag{2.2}$$

$$\vec{U}_0 = 0 - \vec{V}_{COM} = -\frac{1}{A+1}v_0\hat{z} \quad . \tag{2.3}$$

The total momentum in the center of mass frame before the collision is

$$\begin{aligned} \vec{p}_0 &= \vec{\mathfrak{u}}_0 + A\vec{U}_0 \\ &= \frac{A}{A+1}v_0\hat{z} - A\frac{1}{A+1}v_0\hat{z} = \vec{0} \quad . \end{aligned} \tag{2.4}$$

The total kinetic energy in the center of mass frame before the collision is

$$\begin{aligned} K_0 &= \frac{1}{2}\mathrm{u}_0^2 + \frac{1}{2}AU_0^2 \\ &= \frac{1}{2}\left(\frac{A}{A+1}v_0\right)^2 + \frac{1}{2}A\left(\frac{1}{A+1}v_0\right)^2 = \frac{1}{2}\frac{A}{A+1}v_0^2 \quad . \end{aligned} \tag{2.5}$$

After the collision, the neutron will be travelling in some direction $\hat{\Omega}$ with velocity u, both defined in the center of mass frame. By conservation of linear momentum, the target nucleus must be travelling in the opposite direction of the neutron, and its velocity U can be related to the neutron's by

$$\begin{aligned} \vec{p} &= \vec{p}_0 \\ \mathrm{u} - AU &= 0 \\ \mathrm{u} &= AU \quad . \end{aligned} \tag{2.6}$$

With this relationship, the neutron velocity u can be put in terms of the initial lab velocity v_0 through conservation of kinetic energy:

$$\begin{aligned} K &= K_0 \\ \frac{1}{2}\mathrm{u}^2 + \frac{1}{2}AU^2 &= \frac{1}{2}\frac{A}{A+1}v_0^2 \\ \mathrm{u}^2 + \frac{\mathrm{u}^2}{A} &= \frac{A}{A+1}v_0^2 \\ \mathrm{u}^2 &= \left(\frac{A}{A+1}\right)^2 v_0^2 \end{aligned} \tag{2.7}$$

$$\mathrm{u} = \frac{A}{A+1}v_0 \quad . \tag{2.8}$$

Defining the center of mass scattering angle θ as

$$\cos(\theta) = \hat{\Omega} \cdot \hat{z} \quad , \tag{2.9}$$

the components of the final neutron lab velocity v can be determined. With $\hat{z}$ being the initial neutron direction and $\perp$ representing the perpendicular component, the components are

$$\begin{aligned} v_z &= V_{COM} + \mathrm{u}\cos(\theta) \\ &= \frac{1}{A+1}v_0 + \frac{A}{A+1}v_0\cos(\theta) \end{aligned} \tag{2.10}$$

$$\begin{aligned} v_\perp &= \mathrm{u}\sin(\theta) \\ &= \frac{A}{A+1}v_0\sin(\theta) \quad . \end{aligned} \tag{2.11}$$

The squared magnitude of the final neutron lab velocity is

$$\begin{aligned} v^2 = v_z^2 + v_\perp^2 &= \frac{v_0^2}{(A+1)^2}\left[(1 + A\cos(\theta))^2 + A^2\sin^2(\theta)\right] \\ &= v_0^2\left(\frac{A^2 + 2A\cos(\theta) + 1}{(A+1)^2}\right) \quad . \end{aligned} \tag{2.12}$$

The outgoing neutron energy in the lab system can then be put in terms of the cosine of the center of mass scattering angle $\mu = \cos(\theta)$ as

$$\begin{aligned} E &= \frac{1}{2}v^2 \\ &= E_0\left(\frac{A^2 + 2A\mu + 1}{(A+1)^2}\right) \quad . \end{aligned} \tag{2.13}$$

In the resonance range, elastic scattering is nearly isotropic in the center of mass. If isotropic COM scattering is assumed, the energy distribution can be obtained. To see this, first consider the definition of isotropic scattering:

$$P(\mu)\,\mathrm{d}\mu = \frac{1}{2}\,\mathrm{d}\mu, \quad \mu \in [-1, 1] \quad . \tag{2.14}$$

The equivalent energy distribution can be written as

$$P(E_0 \to E)\,\mathrm{d}E = P(\mu)\,\frac{\mathrm{d}\mu}{\mathrm{d}E}\,\mathrm{d}E \quad . \tag{2.15}$$

Equation (2.13) can be solved in terms of μ and then differentiated to obtain

$$\frac{\mathrm{d}\mu}{\mathrm{d}E} = \frac{(A+1)^2}{2AE_0} \quad . \tag{2.16}$$

Therefore, the energy distribution is

$$\begin{aligned} P(E_0 \to E)\,\mathrm{d}E &= \frac{(A+1)^2}{4AE_0}\,\mathrm{d}E \\ &= \frac{1}{(1-\alpha)E_0}\,\mathrm{d}E \quad , \end{aligned} \tag{2.17}$$

where

$$\alpha = \left(\frac{A-1}{A+1}\right)^2 \quad . \tag{2.18}$$

The bounds on this distribution can be determined by inserting the bounds of μ into Eq. (2.13):

$$\begin{aligned} E\Big|_{\mu=-1} &= \alpha E_0 \\ E\Big|_{\mu=1} &= E_0 \quad . \end{aligned} \tag{2.19}$$

Thus, the probability distribution function for the outgoing energy after an elastic scattering collision isotropic in the center of mass is

$$P(E_0 \to E) = \begin{cases} \dfrac{1}{(1-\alpha)E_0}, & \alpha E_0 \le E \le E_0 \\ 0, & \text{otherwise} \quad . \end{cases} \tag{2.20}$$

With this probability distribution, average quantities can be obtained. Of particular interest is the average logarithmic energy decrement, defined as

$$\xi = \left\langle \ln E_0 - \ln E \right\rangle = \left\langle \ln\left(\frac{E_0}{E}\right) \right\rangle \quad , \tag{2.21}$$

where the angle brackets indicate an average over the outgoing energy. This is obtained by averaging the quantity $\ln(E_0/E)$ in terms of the probability distribution over the energy interval in which the probability is nonzero:

$$\begin{aligned} \xi &= \int_{\alpha E_0}^{E_0} \ln\left(\frac{E_0}{E}\right) \frac{1}{(1-\alpha)E_0} \, \mathrm{d}E \\ &= \frac{1}{(1-\alpha)E_0} \left[E \ln\left(\frac{E_0}{E}\right) - E \right]_{\alpha E_0}^{E_0} \end{aligned} \tag{2.22}$$

$$\xi = 1 + \frac{\alpha}{1-\alpha} \ln \alpha \quad . \tag{2.23}$$

This form is independent of the incoming energy, depending only on the mass of the target nuclide.

Because neutron slowing down is characterized by neutrons losing fractions of their energy in each collision, a common change of variables in the neutron slowing down equation introduces a quantity known as the lethargy u (not to be confused with the COM velocity u used earlier):

$$u = \ln \frac{E_{ref}}{E} \quad , \tag{2.24}$$

where E_{ref} is some reference energy, often taken to be the largest energy encountered in a simulation. Lethargy increases as neutron energy decreases—colloquially, this suggests that neutrons with less energy are more "lethargic". With this definition, ξ of Eq. (2.23) can also be thought of as the average lethargy gain per collision. The elastic scattering kernel in terms of lethargy is

$$\begin{aligned} P(E_0 \to E) \, \mathrm{d}E &= P(u_0 \to u) \, \mathrm{d}u \\ \mathrm{d}u &= -\frac{1}{E} \, \mathrm{d}E \end{aligned} \tag{2.25}$$

$$P(u_0 \to u) = \begin{cases} \frac{1}{1-\alpha} \mathrm{e}^{u-u_0}, & u_0 \le u \le u_0 - \ln \alpha \\ 0, & \text{otherwise} \quad . \end{cases} \tag{2.26}$$

For further references on this topic, see [5, 7, 8].

2.3 Pure Elastic Scatterer

Next, consider the behavior of neutrons slowing down in an infinite medium of a purely scattering material, assuming elastic scattering is isotropic in the center of mass. This thesis is concerned with the resolved resonance range of the actinides, and so this energy range is well below the threshold energies of inelastic scattering and is well below the average energy of fission neutron emission.

Without spatial dependence, the neutron transport equation solely models the energy spectrum of the flux. Because no upscattering is assumed, this equation is known as the neutron slowing down equation. With a pure elastic scatter, the neutron slowing down equation can be written as

$$\begin{aligned}\Sigma_s(E)\phi(E) &= \int_E^{E/\alpha} \Sigma_s(E')P(E' \to E)\phi(E')\mathrm{d}E' + S(E) \\ &= \int_E^{E/\alpha} \frac{\Sigma_s(E')\phi(E')}{(1-\alpha)E'}\,\mathrm{d}E' + S(E) \quad .\end{aligned} \tag{2.27}$$

If the assumption that the source $S(E)$ exists only at high energies and the energy of interest is far below the source energy, the equation can be simplified to represent the flux in its asymptotic form:

$$\Sigma_s(E)\phi(E) = \int_E^{E/\alpha} \frac{\Sigma_s(E')\phi(E')}{(1-\alpha)E'}\,\mathrm{d}E' \quad . \tag{2.28}$$

It is easily verified that the solution to this equation takes the form

$$\phi(E) = \frac{C}{\Sigma_s(E)E} \tag{2.29}$$

by inserting this form into the equation. Because this flux varies as $1/E$, it is often convenient to define the flux in terms of lethargy with

$$\begin{aligned}\phi(E)\,\mathrm{d}E &= \phi(u)\,\mathrm{d}u \\ \phi(u) &= E\phi(E) \quad .\end{aligned} \tag{2.30}$$

This allows the flux to be treated as constant, except for the effects of the cross section. For the remainder of this discussion, the flux will be kept in terms of energy, but this lethargy transformation will be used in subsequent discussions.

To determine the constant C, consider the quantity known as the "slowing down current" $q(E)$. This quantity is the rate at which neutrons with energies greater than E scatter with

outgoing energies less than E. Mathematically, this quantity is defined as

$$q(E) = \int_E^{E/\alpha} \mathrm{d}E' \int_{\alpha E'}^{E} \mathrm{d}E'' \, \Sigma_s(E') P(E' \rightarrow E'') \phi(E') \quad . \tag{2.31}$$

By inserting the flux shape of Eq. (2.29) and the elastic scattering kernel, the slowing down current becomes

$$\begin{aligned} q(E) &= \int_E^{E/\alpha} \mathrm{d}E' \int_{\alpha E'}^{E} \mathrm{d}E'' \, \frac{C}{(1-\alpha)E'^2} \\ &= C\left[1 + \frac{\alpha}{1-\alpha} \ln \alpha\right] = C\xi \quad , \end{aligned} \tag{2.32}$$

where ξ is the average logarithmic energy decrement defined in Eq. (2.23). Now, consider the value of $q(E)$. Below the energy of the source, assuming steady-state behavior and the absence of absorption, the rate of neutrons slowing down past any energy point must be the same as the source rate:

$$q(E) = \int_E^{\infty} S(E') \mathrm{d}E' \equiv S_0 \quad . \tag{2.33}$$

Then, the flux in an infinite medium of a purely elastic scattering material at energies well below the source energy is given by

$$\phi(E) = \frac{S_0}{\xi \Sigma_s(E) E} \quad . \tag{2.34}$$

Up to this point, only energies far below the source energy have been considered. This is a good approximation for the resonance range of heavy nuclides, but a demonstration of this fact is warranted. Consider a simple problem, that of an infinite medium containing a purely elastic scattering constant cross section monoisotopic material with a source given by $S(E) = S_0 \delta(E - E_0)$, where $\delta(E - E_0)$ is the Dirac delta function centered at E_0. Rather than consider the entirety of the flux in this system, consider separately neutrons that have undergone specific numbers of collisions.

First, the uncollided flux ϕ_0 is given simply as

$$\begin{aligned} \Sigma_s \phi_0(E) &= S_0 \delta(E - E_0) \\ \phi_0(E) &= \frac{S_0}{\Sigma_s} \delta(E - E_0) \quad . \end{aligned} \tag{2.35}$$

The flux exists only at the source energy and is nonzero only at a singularity.

Next, the once-collided flux ϕ_1 is a solution to the slowing down equation with the source

coming from scattering from the uncollided flux:

$$\begin{aligned}\Sigma_s\phi_1(E) &= \int_E^{E/\alpha} \frac{\Sigma_s\phi_0(E')}{(1-\alpha)E'}\,\mathrm{d}E' \\ \phi_1(E) &= \begin{cases} \dfrac{S_0}{(1-\alpha)\Sigma_s E_0}, & E \in [\alpha E_0, E_0] \\ 0, & \text{otherwise} \end{cases} .\end{aligned} \tag{2.36}$$

This flux is piecewise constant in energy, featuring a discontinuity at αE_0.

Next, the twice-collided flux ϕ_2 uses the once-collided flux in its scatter source:

$$\Sigma_s\phi_2(E) = \int_E^{E/\alpha} \frac{\Sigma_s\phi_1(E')}{(1-\alpha)E'}\,\mathrm{d}E' \quad . \tag{2.37}$$

Because ϕ_1 is defined piecewise, the integral must be split into pieces. First, the interval $E \in [\alpha E_0, E_0]$ is considered:

$$\begin{aligned}\phi_2(E) &= \int_E^{E_0} \frac{S_0}{(1-\alpha)\Sigma_s E_0}\frac{1}{(1-\alpha)E'}\,\mathrm{d}E' \\ &= \frac{S_0}{(1-\alpha)^2\Sigma_s E_0}\ln\frac{E_0}{E}, \quad E \in [\alpha E_0, E_0] \quad .\end{aligned} \tag{2.38}$$

The flux in the interval $E \in [\alpha^2 E_0, E_0]$ is

$$\begin{aligned}\phi_2(E) &= \int_{\alpha E_0}^{E/\alpha} \frac{S_0}{(1-\alpha)\Sigma_s E_0}\frac{1}{(1-\alpha)E'}\,\mathrm{d}E' \\ &= \frac{S_0}{(1-\alpha)^2\Sigma_s E_0}\ln\frac{E}{\alpha^2 E_0}, \quad E \in [\alpha^2 E_0, \alpha E_0] \quad .\end{aligned} \tag{2.39}$$

The flux is zero below this point. Note that this twice-collided flux is continuous, but exhibits discontinuities in its derivatives at $\alpha^2 E_0$ and αE_0. It is piecewise linear in $\ln E$—or equivalently, in lethargy.

The thrice-collided flux $\phi_3(E)$ uses the twice collided flux in its scatter source:

$$\Sigma_s\phi_3(E) = \int_E^{E/\alpha} \frac{\Sigma_s\phi_2(E')}{(1-\alpha)E'}\,\mathrm{d}E' \quad . \tag{2.40}$$

As with the twice-collided flux, this integral is split to account for the piecewise definition of ϕ_2. In the interval $E \in [\alpha E_0, E_0]$, the flux is

$$\begin{aligned}\phi_3(E) &= \frac{S_0}{(1-\alpha)^2\Sigma_s E_0}\int_E^{E_0} \ln\frac{E_0}{E'}\frac{1}{(1-\alpha)E'}\,\mathrm{d}E' \\ &= \frac{1}{2}\frac{S_0}{(1-\alpha)^3\Sigma_s E_0}\ln^2\frac{E_0}{E}, \quad E \in [\alpha E_0, E_0] \quad .\end{aligned} \tag{2.41}$$

In the interval $E \in [\alpha^2 E_0, \alpha E_0]$, the flux is

$$\begin{aligned}\phi_3(E) &= \frac{S_0}{(1-\alpha)^2 \Sigma_s E_0}\left[\int_{\alpha E_0}^{E/\alpha} \ln\frac{E_0}{E'}\frac{1}{(1-\alpha)E'}\,\mathrm{d}E' + \int_E^{\alpha E_0} \ln\frac{E'}{\alpha^2 E_0}\frac{1}{(1-\alpha)E'}\,\mathrm{d}E'\right] \\ &= \frac{1}{2}\frac{S_0}{(1-\alpha)^3 \Sigma_s E_0}\left[2\ln^2\frac{1}{\alpha} - \ln^2\frac{\alpha E_0}{E} - \ln^2\frac{E}{\alpha^2 E_0}\right], \quad E \in [\alpha^2 E_0, \alpha E_0] \quad .\end{aligned} \tag{2.42}$$

And in the interval $E \in [\alpha^3 E_0, \alpha^2 E_0]$, the flux is

$$\begin{aligned}\phi_3(E) &= \frac{S_0}{(1-\alpha)^2 \Sigma_s E_0}\int_{\alpha^2 E_0}^{E/\alpha} \ln\frac{E'}{\alpha^2 E_0}\frac{1}{(1-\alpha)E'}\,\mathrm{d}E' \\ &= \frac{1}{2}\frac{S_0}{(1-\alpha)^3 \Sigma_s E_0}\ln^2\frac{E}{\alpha^3 E_0}, \quad E \in [\alpha^3 E_0, \alpha^2 E_0] \quad .\end{aligned} \tag{2.43}$$

The flux is zero below this interval. The flux is piecewise quadratic in $\ln E$ and exhibits discontinuities in its second derivative at $\alpha^n E_0$ for $n = 1, 2, 3$. It is continuous and has continuous first derivatives.

This process can be continued for more and more collisions, with the integrals becoming increasingly tedious. However, the trend is clear; each subsequent collision allows the flux to extend an additional factor of α lower in energy, and each collision flux has one additional derivative that is continuous than the previous. Each collision flux is piecewise polynomial in $\ln E$, with the orders increasing with collision. The piecewise nature of the flux is always defined on intervals of the form $[\alpha^n E_0, \alpha^{n-1} E_0]$. These intervals will be referred to as "scattering intervals".

The total flux is the sum of all the collision fluxes:

$$\phi(E) = \sum_{n=0}^{\infty} \phi_n(E) \quad . \tag{2.44}$$

The total flux thus exhibits a discontinuity at αE_0, a discontinuous first derivative at $\alpha^2 E_0$, a discontinuous second derivative at $\alpha^3 E_0$, and so on. Because each of these discontinuities is caused by a single collision flux, the collision fluxes can be used to determine the magnitude of discontinuity. For instance, for the discontinuity at αE_0, the magnitude of the discontinuity is

$$\begin{aligned}\phi^+(\alpha E_0) - \phi^-(\alpha E_0) &= \phi_1^+(\alpha E_0) - \phi_1^-(\alpha E_0) \\ &= \frac{S_0}{(1-\alpha)\Sigma_s E_0} - 0 \\ &= \frac{S_0}{(1-\alpha)\Sigma_s E_0} \quad .\end{aligned} \tag{2.45}$$

In terms of the neutron lethargy, recalling that $\phi(u) = E\phi(E)$ from Eq. (2.30), this is

$$\phi^-(u_0 - \ln\alpha) - \phi^+(u_0 - \ln\alpha) = \frac{S_0}{\Sigma_s}\frac{\alpha}{1-\alpha} \quad . \tag{2.46}$$

Although the higher collision fluxes are tedious to compute analytically, they are easily computed numerically. Figure 2.1 shows the first several collision fluxes per unit energy, plotted on a log scale, with $A = 16$. The piecewise polynomial in $\ln E$ can easily be seen. For the fluxes with higher numbers of collisions, the curves peak lower in energy and increase in magnitude. This suggests the $1/E$ flux shape is taking form. Figure 2.2 shows the total flux per unit lethargy for this same case. The discontinuity at αE_0 and the discontinuities in the derivatives at $\alpha^n E_0$ are easily seen. These discontinuities are known as Placzek transients.

From Fig. 2.2, it is observed that the flux reaches its asymptotic form after only a few scattering intervals. The resolved resonance range for U-238, whose upper bound is 20 keV in ENDF/B-VII.1, is below $\alpha^5 E_0$ for all nuclides $A \geq 6$, assuming E_0 is the average fission energy of 1 MeV. For lighter moderators, the magnitude of the Placzek transients is much smaller, and even for $A = 2$, the flux does not deviate more than 0.2% from the asymptotic value in the resonance range. Furthermore, fission neutrons are actually emitted with a spectrum of energies. This spread in the source energy lessens the effects of the Placzek transients even further, as no sharp discontinuities will be observed in the flux or any of its derivatives when starting from a distributed source. Thus, the assumption that the resonance range can be treated as if energies are far below the source—and thus the flux takes its asymptotic form in this range—is nearly exact.

For further references on this topic, see [5, 8].

2.4 Slowing Down with Absorption

In this section, the effect of absorption on the macroscopic form of the flux is considered. This presentation is most similar to that of [8]. The flux shape near resonances is considered starting in Sec. 2.5. The slowing down equation with absorption and elastic scattering isotropic in the center of mass is

$$\Sigma(E)\phi(E) = \int_E^{E/\alpha} \frac{\Sigma_s(E')\phi(E')}{(1-\alpha)E'}\,\mathrm{d}E' + S(E) \quad . \tag{2.47}$$

Here, only a single nuclide is shown. This is easily extended to multiple nuclides by replacing the integral on the right hand side with a sum of integrals, each corresponding to each nuclide's slowing down source.

2.4.1 Constant Absorption

For the case of $\alpha = 0$, which corresponds to hydrogen, with energy-independent absorption and scattering cross sections, the slowing down equation with absorption can be solved analytically. Although absorption cross sections are never constant in energy in nature, if narrow enough

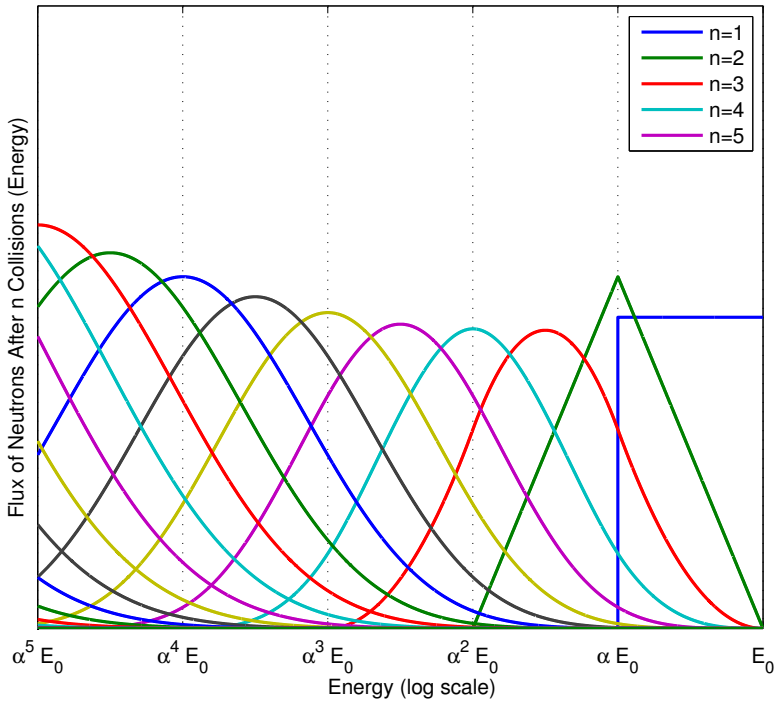

Figure 2.1: Flux after n collisions with a monoenergetic source in a purely scattering infinite medium.

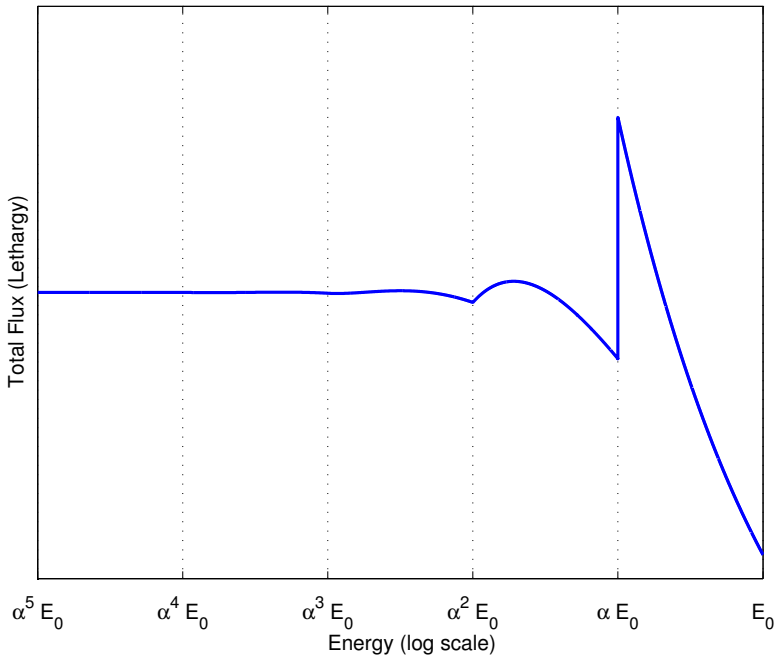

Figure 2.2: Total flux per unit lethargy with a monoenergetic source in a purely scattering infinite medium.

energy groups are used, it can be approximated as such. Furthermore, this analysis should give the reader an appreciation of the effect of absorption over a large energy range. This simplified slowing down equation is given by

$$\Sigma\phi(E) = \int_E^\infty \frac{\Sigma_s\phi(E')}{E'}\,\mathrm{d}E' + S(E) \quad . \tag{2.48}$$

If it is assumed that the source exists only at high energies, then the equation for energies below the source is

$$\Sigma\phi(E) = \int_E^\infty \frac{\Sigma_s\phi(E')}{E'}\,\mathrm{d}E' \quad . \tag{2.49}$$

To solve, this is differentiated on both sides:

$$\frac{\mathrm{d}}{\mathrm{d}E}\phi(E) = -\frac{\Sigma_s}{\Sigma_t}\frac{\phi(E)}{E} \quad . \tag{2.50}$$

This differential equation can be solved by separation of variables. The result is

$$\phi(E) = \phi(E_0)\left(\frac{E_0}{E}\right)^{\Sigma_s/\Sigma} \quad , \tag{2.51}$$

where E_0 is some energy at or below the source in which the flux is known. Note that this result is the familiar $\phi \sim 1/E$ result when the medium is purely scattering. If absorption is present, this flux is always less than the $1/E$ flux, and the relative difference grows as energy decreases.

2.4.2 Effect of Resonances

Now consider a material that is purely scattering aside from a single absorption resonance. Above the resonance, the flux form of Eq. (2.34) holds, as no absorption has been encountered. Far below the resonance, at least a factor of α lower in energy, the flux takes the same asymptotic shape, but the normalization is lower to account for neutrons absorbed in the resonance. Equation (2.34) can be generalized as

$$\phi(E) = \frac{q(E)}{\xi\Sigma_s(E)E} \quad , \tag{2.52}$$

valid when the scattering integrals do not include energies in which absorption cross sections are nonzero. At energies below the resonance, the slowing down density is

$$q(E) = S_0 - \int_E^\infty \Sigma_a(E)\phi(E) \quad , \tag{2.53}$$

which states that the rate at which neutrons slow down past energy E is equal to the difference of the source rate and the absorption rate above E. Thus, the flux below the resonance

eventually regains a $1/E$ shape, but with a magnitude reduced by a factor proportional to the resonance absorption rate.

In the interval between the resonance and regaining the asymptotic flux form, the flux will decrease during the slowing down process, as fewer neutrons from above the resonance will be included in lower energy energy scatter sources. For large A nuclides, this transition region is very small; for small A nuclides, potentially large. However, because the likelihood of jumping over the resonance is higher for lower A nuclides, these exhibit smaller changes in the flux.

2.5 Slowing Down with Single Resonant Absorber

In this section, slowing down in the presence of a single resonant absorber is explored. The resonant nuclide will be denoted with superscript $*$, and admixed moderator—referred to as the "background" moderator—material with superscript $+$. It is assumed that the moderator has a constant cross section, with both the scattering and absorption components possibly nonzero. The background moderator will be shown as a single nuclide for most of this discussion, but simply adding summations over moderator nuclides allows this to be generalized to multiple background nuclides. The resonant nuclide is assumed to have a nonzero absorption cross section only at its resonances. The scattering cross section is constant outside of resonances. To justify these approximations, see Fig. 2.3, which shows the capture and scattering cross section of U-238 below 70 eV. The capture cross section drops to near zero between resonances while the scattering resonance is nearly constant at a nonzero value. The constant value is denoted Σ_p as the potential scattering cross section, but it should be noted that this does not suggest the quantum mechanical definition of potential scattering. Rather, it is merely a matter of notational convenience to distinguish it from the scattering cross section that includes resonance scattering $\Sigma_s(E)$. All scattering is assumed to be isotropic in the center of mass.

2.5.1 Direct Solution of Slowing Down Equation

The most obvious means of determining the neutron spectrum in infinite media is to simply solve the slowing down equation numerically. For a resonant nuclide and background moderator below the source energy, this equation is

$$\left(\Sigma^*(E) + \Sigma^+\right)\phi(E) = \int_E^{E/\alpha^*} \frac{\Sigma_s^*(E')\phi(E')}{(1-\alpha^*)E'}\,\mathrm{d}E' + \int_E^{E/\alpha^+} \frac{\Sigma_p^+\phi(E')}{(1-\alpha^+)E'}\,\mathrm{d}E' \quad . \tag{2.54}$$

By directly solving this equation, no additional approximations are brought into play, other than those involved in writing down the equation itself. The interaction between the resonances and the scatter source is explicitly modeled. Note that the solution to this equation is only

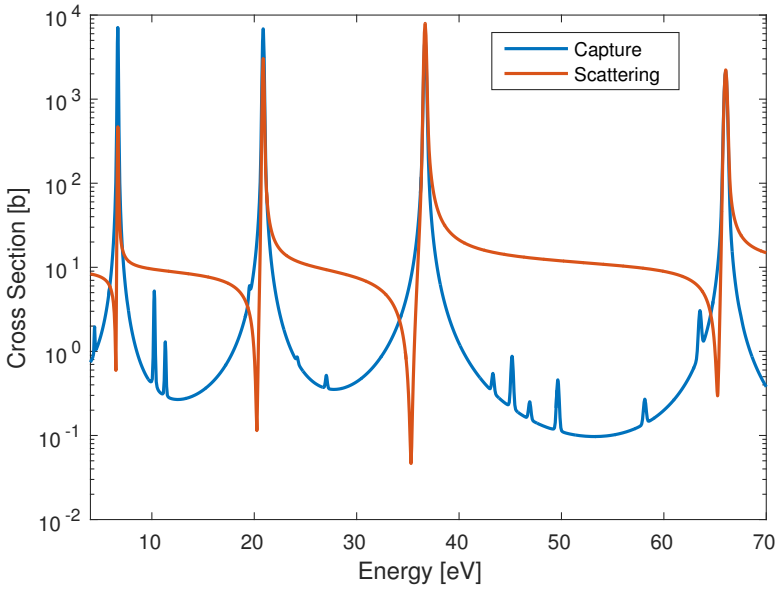

Figure 2.3: Capture and scattering cross section of U-238 below 70 eV.

unique within a multiplicative factor, and so some normalization must be chosen. Physically, this normalization represents the source strength. In practice, the flux is used to generate multigroup cross sections, and so is present both on the top and bottom of a fraction. Thus, the choice of normalization is not significant.

This equation can be easily solved by Monte Carlo methods. This is a class of multigroup cross section generation that has been explored in increasing detail in recent years, but these methods are not explored in this thesis.

In a deterministic framework, this equation must be solved on a solution energy mesh that resolves the resonances of nuclide $*$ sufficiently accurately. Typically, this is done on the pointwise energy mesh on which the cross section is defined, but thinning is possible if so desired.

Computation of the integrals naively requires $O(n^2)$ operations, where n is the number of points. However, this can be reduced to $O(n)$ operations by using cumulative integrals. If the cumulative integral $\mathcal{I}$ for a given nuclide is defined as

$$\mathcal{I}(E) = \int_E^\infty \frac{\Sigma_s(E')}{(1-\alpha)E'}\,\mathrm{d}E' \quad , \tag{2.55}$$

then the nuclide's scatter source is given by

$$\int_E^{E/\alpha} \frac{\Sigma_s(E')}{(1-\alpha)E'}\,\mathrm{d}E' = \mathcal{I}(E) - \mathcal{I}(E/\alpha) \quad . \tag{2.56}$$

Furthermore, the cumulative integral $\mathcal{I}(E)$ can be computed during the solution of the slowing

down equation by cumulatively adding only the lowest energy piece of the scattering integral. If a cumulative integral is known at energy point E_1, the cumulative integral's value at the next energy point E_2 is given simply by

$$\mathcal{I}(E_2) = \mathcal{I}(E_1) + \int_{E_2}^{E_1} \frac{\Sigma_s(E')\phi(E')}{(1-\alpha)E'}\,\mathrm{d}E' \quad . \tag{2.57}$$

Note that the scatter sources must be calculated for each nuclide separately, and so a cumulative integral must be stored for each nuclide to use this technique.

2.5.2 Narrow Resonance Model

In the narrow resonance (NR) model [9, 5], it is assumed that the interval in which neutrons scatter is very large compared to the width of resonances. If the flux is written as

$$\phi(E) = f(E)\varphi(E) \quad , \tag{2.58}$$

where $f(E)$ is a slowly varying function representing the macroscopic behavior of the flux and $\varphi(E)$ is a fine structure function representing the behavior of the flux near the resonance, the narrow resonance assumption implies

$$\int_E^{E/\alpha} \frac{\Sigma_s(E')\phi(E')}{(1-\alpha)E'}\,\mathrm{d}E' \approx \int_E^{E/\alpha} \frac{\Sigma_p f(E')}{(1-\alpha)E'}\,\mathrm{d}E' \quad . \tag{2.59}$$

The quantity $C(E)$ is defined as

$$C(E) = \int_E^{E/\alpha} \frac{f(E')}{(1-\alpha)E'}\,\mathrm{d}E' \quad , \tag{2.60}$$

and is itself a slowing varying function of the energy. Depending upon the choice of $f(E)$, $C(E)$ may depend on the nuclide. If $f(E) = 1/E$, as is often used in practice, $C(E)$ does not depend on the nuclide, but most other choices do result in a nuclide-dependent definition.

The narrow resonance approximation can be made separately for the resonant nuclide and the background moderator. That is, the appropriateness of the use of the NR model is a function of the width of the resonances of a particular nuclide compared to the scattering interval of a given nuclide. For the case of hydrogen, the scattering interval is very large, and all resonances appear narrow in comparison. Here, the narrow resonance model is applied to both the resonant nuclide and the background moderator. The slowing down equation with the narrow resonance model is therefore

$$\left(\Sigma^*(E) + \Sigma^+\right)\phi_{NR}(E) = \Sigma_p^* C^*(E) + \Sigma_p^+ C^+(E) \quad , \tag{2.61}$$

and the flux is

$$\phi_{NR}(E) = \frac{\Sigma_p^* C^*(E) + \Sigma_p^+ C^+(E)}{\Sigma^*(E) + \Sigma^+} \quad . \tag{2.62}$$

It is common to define the background cross section σ_b as

$$\sigma_b = \frac{\Sigma^+}{N^*} \quad , \tag{2.63}$$

and to define the quantity γ as

$$\gamma = \frac{\Sigma_p^+}{\Sigma^+} \quad . \tag{2.64}$$

The background cross section is often also known as the dilution cross section. With these definitions, the NR flux is

$$\phi_{NR} = \frac{\sigma_p^* C^*(E) + \gamma\sigma_b C^+(E)}{\sigma^*(E) + \sigma_b} \quad . \tag{2.65}$$

Finally, in most applications, the macroscopic form of the flux is assumed to be $f(E) \sim 1/E$. Using this form, $C(E)$ is independent of the nuclide and takes the form

$$C(E) = \int_E^{E/\alpha} \frac{1}{(1-\alpha)E'^2}\, \mathrm{d}E' = \frac{1}{E} \quad . \tag{2.66}$$

Assuming a $1/E$ macroscopic form of the flux, the NR flux is

$$\phi_{NR}(E) = \frac{1}{E} \frac{\sigma_p^* + \gamma\sigma_b}{\sigma^*(E) + \sigma_b} \quad . \tag{2.67}$$

2.5.3 Slowing Down Equation with Narrow Resonance Moderator Source

The narrow resonance approximation can be used on the background moderator without being applied to the resonant nuclide. This yields a simplified slowing down equation:

$$\left(\sigma^*(E) + \sigma_b\right)\phi(E) = \int_E^{E/\alpha^*} \frac{\Sigma_s(E')\phi(E')}{(1-\alpha^*)E'}\, \mathrm{d}E' + C(E)\gamma\sigma_b \quad . \tag{2.68}$$

This form is the form used in the NJOY flux calculator [1], which sets $\gamma = 1$. If the macroscopic form of the flux is taken to be $1/E$, then the slowing down equation can be further simplified to

$$\left(\sigma^*(E) + \sigma_b\right)\phi(E) = \int_E^{E/\alpha^*} \frac{\Sigma_s(E')\phi(E')}{(1-\alpha^*)E'}\, \mathrm{d}E' + \frac{\gamma\sigma_b}{E} \quad . \tag{2.69}$$

Here, the solution to the equation does not have a multiplicative degree of freedom and is in fact unique. This is because the assumption that $f(E) = 1/E$ contains the normalization.

2.5.4 Wide Resonance Model

The wide resonance (WR) model [9, 5] assumes that resonances are wide in comparison to the energy interval associated with scattering. Thus, neutrons that scatter at a resonance energy are very likely to remain in the resonance. This allows the slowing down equation to be simplified by assuming that no energy is lost in a scattering collision. The wide resonance scatter source is thus

$$\begin{aligned}\int_E^{E/\alpha} \frac{\Sigma_s(E')\phi(E')}{(1-\alpha)E'}\,\mathrm{d}E' &\approx \lim_{\alpha\to 1}\int_E^{E/\alpha} \frac{\Sigma_s(E')\phi(E')}{(1-\alpha)E'}\,\mathrm{d}E' \\ &= \lim_{\alpha\to 1}\Sigma_s(E)\phi(E)\int_E^{E/\alpha}\frac{1}{(1-\alpha)E'}\,\mathrm{d}E' \\ &= \Sigma_s(E)\phi(E)\lim_{\alpha\to 1}\frac{-\ln\alpha}{1-\alpha} \\ &= \Sigma_s(E)\phi(E) \quad .\end{aligned} \tag{2.70}$$

Because assuming a very small scattering interval is equivalent to assuming $\alpha \to 1$, this approximation is sometimes known as the infinite mass approximation.

As with the narrow resonance model, the wide resonance model can be applied individually to the resonant nuclide and to the background moderator. The wide resonance model is rarely applied to the background moderator, unless the moderator contains multiple nuclides, one of which is heavy. This is because the moderator usually contains a lighter nuclide, and any resonance would be narrow in comparison to a light nuclide's scattering interval. What is commonly presented as the wide resonance model itself is applying the wide resonance approximation to the resonant nuclide but the narrow resonance approximation to the background moderator. This is also known as the narrow resonance-infinite mass (NRIM) approximation:

$$\left(\sigma^*(E)+\sigma_b\right)\phi(E) = \sigma_s(E)\phi(E) + C(E)\gamma\sigma_b \quad . \tag{2.71}$$

Solving this equation for the flux, the wide resonance flux is achieved:

$$\phi_{WR}(E) = \frac{C(E)\gamma\sigma_b}{\sigma_a^*(E)+\sigma_b} \quad . \tag{2.72}$$

Assuming a $1/E$ macroscopic form of the flux, this is

$$\phi_{WR}(E) = \frac{1}{E}\frac{\gamma\sigma_b}{\sigma_a^*(E)+\sigma_b} \quad . \tag{2.73}$$

2.5.5 Intermediate Resonance Model

The narrow resonance and wide resonance models represent two extreme cases, one with resonances being very narrow compared to a scattering interval and one with resonances

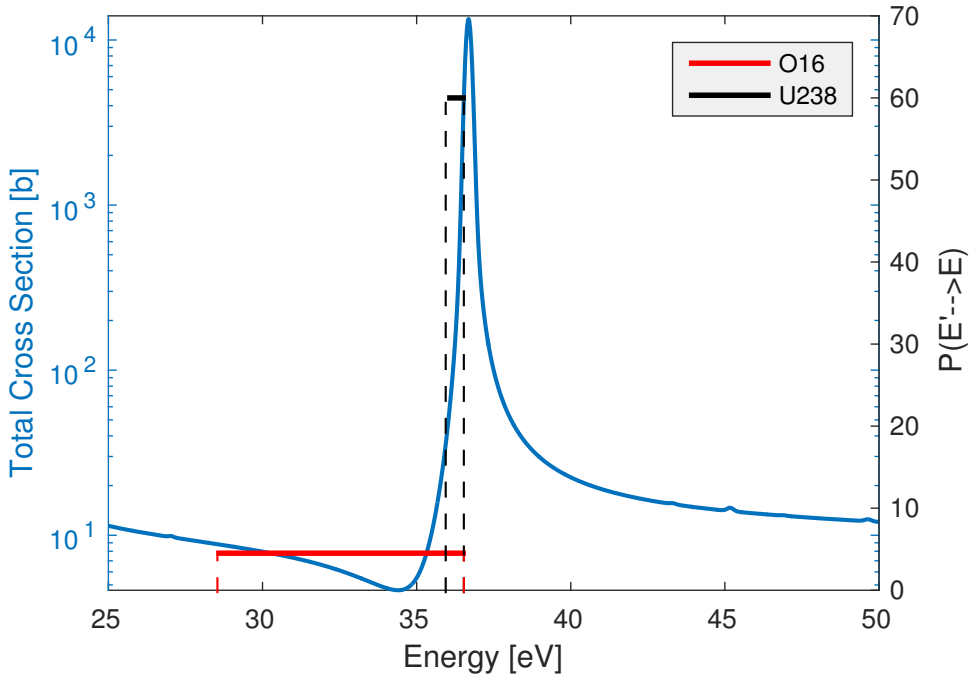

Figure 2.4: Scattering intervals of U-238 and O-16 compared to the 20.8 eV resonance of U-238.

being very wide. Of course, there is an entire spectrum of resonance widths versus scattering intervals. Even in a single material, a resonance may appear wide to one nuclide but narrow to another. To see this, consider Fig. 2.4. The scattering interval of U-238 is on the order of the width of the resonance, whereas the scattering interval of O-16 is much larger. The scattering of U-238 behaves more like the wide resonance model whereas the scattering of O-16 behaves more like the narrow resonance. Note that hydrogen nearly always is well-represented by the narrow resonance model, as it's scatter interval extends to zero energy.

One means of approximating the flux in resonances that are neither narrow nor wide is to use the intermediate resonance (IR) model [10]. The IR scatter source is simply a convex combination with parameter λ of the NR and WR scatter sources:

$$\int_E^{E/\alpha} \frac{\Sigma_s(E')\phi(E')}{(1-\alpha)E'}\,\mathrm{d}E' \approx \lambda C(E)\Sigma_p + (1-\lambda)\Sigma_s(E)\phi(E) \quad . \tag{2.74}$$

Note that this form reduces to the NR approximation when $\lambda = 1$ and to the WR approximation when $\lambda = 0$. Thus, the IR model can be used as a more general case of all three models, and this will be done in subsequent sections.

The IR approximation can be applied separately to the resonant nuclide and the background moderator. In this section, it is applied only to the resonant nuclide; Sec. 2.5.6 discusses the approximation applied to the background moderator. Applying the IR model to the resonant

nuclide and the NR model for the background moderator, the approximated slowing down equation is

$$\left(\sigma_a^*(E) + \lambda\sigma_s^*(E) + \sigma_b\right)\phi(E) = \lambda C^*(E)\sigma_p^* + C^+(E)\gamma\sigma_b \quad , \tag{2.75}$$

and the flux is given by the equation

$$\phi_{IR}(E) = \frac{\lambda C^*(E)\sigma_p^* + C^+(E)\gamma\sigma_b}{\sigma_a^*(E) + \lambda\sigma_s^*(E) + \sigma_b} \quad . \tag{2.76}$$

If the macroscopic form of the flux is assumed to vary as $1/E$, then this simplifies to

$$\phi_{IR}(E) = \frac{1}{E}\frac{\lambda\sigma_p^* + \gamma\sigma_b}{\sigma_a^*(E) + \lambda\sigma_s^*(E) + \sigma_b} \quad . \tag{2.77}$$

The parameter λ is not easily obtained, and various prescriptions and usages can be found in literature. The parameter is best defined in the context of a single resonance, and characterizes the relative width of the resonance compared to the nuclide's scattering interval. However, this requires a means of determining many λ values for each nuclide, and is not easily accomplished in practice.

In other applications, λ has been treated as a parameter for a given nuclide, using only a single value for its entire energy range. Although this makes library generation simple, it is difficult to justify physically. Even if resonance widths are approximately constant in an absolute sense, the widths relative to the energy range are wildly varying. Because scattering intervals are defined as fractions of the neutron energy, resonances at higher energies appear much narrower than those at lower energies, if the width is held constant.

The compromise between these two inconvenient extremes is to use a value of λ for each energy group for each resonant nuclide. This value is determined by comparing the cross sections (or equivalently, effective resonance integrals) with various values of λ to a reference value obtained by direct solution of the slowing down equation. When the cross sections match, λ has been found. This value of λ is technically dependent upon the background moderation level, but is often computed for a representative value and assumed constant.

It should be noted that the scatter source is not truly well-represented by a linear combination of the narrow and wide resonance models. Rather, λ serves more as a correction factor that enables accurate cross sections to be obtained but does not accurately capture the physics at hand. This detail is explored in more detail in Sec. 8.4.2.

2.5.6 Effective Background Cross Section

In the preceding section, application of the intermediate resonance model to the resonant nuclide was considered. Now, consider application of the model to the background moderator.

Because the scattering interval for hydrogen is the entire energy range below the incoming neutron energy, hydrogen's scattering interval is always considered to be very large compared to a resonance width. Thus, hydrogen is very well-represented by the narrow resonance model. A collision with hydrogen at a resonance energy will nearly always cause the neutron to scatter to an energy well below the resonance. For other nuclides, a fraction of scattering events will result in escape from the resonance, but another fraction will result in the neutron remaining within the resonance. Scattering events resulting in neutrons remaining within the resonance are nearly equivalent to the interaction not happening at all. In the narrow resonance model, the value of α does not appear, and so the neutrons that escape from the resonance can be treated as hydrogen without a change in the NR form. Thus, the intermediate resonance model for background moderators is equivalent to replacing the background moderator with a smaller quantity of hydrogen.

A similar procedure for the determination of λ as in the preceding section can be performed for the background moderator, where various values of λ are compared against a reference solution. This is complicated by the fact that λ for the resonant nuclide cannot be easily separated in this calculation. Although procedures for resolving this issue can be found in literature [11], another procedure that is quite intuitive and reliable exists. The procedure is as follows.

First, two background cross section levels are chosen. These should be indicative of the range of background cross sections expected to be encountered in a future simulation, but their selection can be freely chosen. Assume the two levels are σ_{b1} and σ_{b2} with $\sigma_{b2} > \sigma_{b1}$. Next, compute cross sections (or equivalently, effective resonance integrals) using these background levels in a direct solution of the slowing down equation, with the background nuclide set to hydrogen. Let these cross sections be notated σ_1 and σ_2. Next, compute a cross section with a material with an amount of hydrogen equivalent to a background level of σ_{b1} and an amount of the background nuclide of interest equivalent to a background level of $\sigma_{b2} - \sigma_{b1}$, resulting in cross section σ_3. The intermediate resonance parameter is given by

$$\lambda = \frac{\sigma_3 - \sigma_1}{\sigma_2 - \sigma_1} \quad . \tag{2.78}$$

The difference in cross section between σ_2 and σ_1 is caused by the increased fraction of neutrons that escape resonances due to an increase in the amount of hydrogen. The difference between σ_3 and σ_1 is due to the resonance escape due to the presence of the background nuclide of interest. The ratio of these differences gives the equivalent amount of hydrogen that the nuclide of interest provides. This procedure assumes the effect of adding hydrogen has a linear effect on the value of the cross section. This is, of course, most accurate for small changes in the background level, and so σ_{b2} should not be chosen to be too much larger than that of σ_{b1}. Note that the value of λ is dependent on the nuclide mass A and the background level σ_{b1}. As in the previous section, the σ_{b1} dependence is most often ignored.

With this definition, and with a background moderator made up of several nuclides, the effective background cross section that can be used with a narrow resonance approximation while accounting for these mass effects is

$$\sigma_b = \frac{1}{N^*} \sum_{i \in +} \left(\Sigma_a^i + \lambda^i \Sigma_p^i \right) \quad , \tag{2.79}$$

where i denotes the nuclide, and γ for this case is

$$\gamma = \frac{\sum_{i \in +} \lambda^i \Sigma_p^i}{\sum_{i \in +} \left(\Sigma_a^i + \lambda^i \Sigma_p^i \right)} \quad . \tag{2.80}$$

2.5.7 Homogeneous Nuclear Data Tables

As will be shown in subsequent discussion, homogeneous cross sections are particularly valuable quantities for reactor physics simulations, even for heterogeneous geometries. Thus, rather than compute group cross sections for each simulation, it is generally desirable to tabulate homogeneous cross sections into a cross section library.

A library generally consists of all relevant cross sections (or effective resonance integrals) and other nuclear data for a particular group structure. The selection of the group structure is an important consideration for reactor physics simulations but is outside the scope of this thesis. Nuclear data is tabulated as a function of the background level and of the temperature.

The parameter γ is not usually considered a free parameter in the tabulation, but can be included if so desired. However, the flux obtained in this section, used for generation of cross sections or resonance integrals, is unique only within a multiplicative constant. The flux obtained through Eqs. (2.67), (2.69), (2.73) and (2.77) depends upon γ only within the multiplicative constant, and so parameterization by γ is unnecessary. If $C(E)$ is not taken to be $1/E$, or if the direct solution of the full slowing down equation is used, γ may play a—likely very small—role in the obtained cross sections.

The background material used to generate the nuclear data tables is generally chosen to consist solely of hydrogen. This removes the degrees of freedom introduced by allowing for many background nuclides, and is a good approximation, due to the hydrogen equivalence presented in Sec. 2.5.6. Of course, tables could be generated that parameterize the background material, but these are not often seen in practice.

In the cross section table, there are several options of what data can be stored. Most intuitively, the value of the cross section can be stored for each background and temperature point. Alternatively, a cross section at a reference background and temperature can be stored along with multiplicative factors, known as self-shielding factors, that can be used to recover the cross section value. Finally, additive deviations can be stored relative to the reference

value rather than multiplicative self-shielding factors. These additive deviations are generally preferred if the scattering matrix is included as a function of background and temperature in the table. In this case, many entries in the scattering matrix will not change, and the matrix containing deviations will be more sparse than the scattering matrix itself.

Approximating the Group Flux

The group flux is an important quantity for the nuclear data library, as it allows conversion between effective resonance integrals and group cross sections, and it is needed in other aspects of the self-shielding process—e.g., in using n-term rational approximations (see Sec. 3.5.3). However, it is rarely tabulated, as it can be approximated from other tabulated data when using the intermediate resonance model (or equivalent form) and $C(E) = 1/E$.

Consider the group flux of the intermediate resonance model from Eq. (2.77), neglecting the superscripts $*$:

$$\phi(E) = \frac{1}{E} \frac{\lambda\sigma_p + \gamma\sigma_b}{\sigma_a(E) + \lambda\sigma_s(E) + \sigma_b} \quad . \tag{2.81}$$

The group flux is given by integrating this over the bounds of an energy group:

$$\phi_g = \int_g \frac{1}{E'} \frac{\lambda\sigma_p + \gamma\sigma_b}{\sigma_a(E') + \lambda\sigma_s(E') + \sigma_b} \, \mathrm{d}E' \tag{2.82}$$

By adding and subtracting $\sigma_a(E')$ in the numerator, this integral can be rewritten as

$$\phi_g = \int_g \frac{1}{E'} \frac{\sigma_a(E') + \lambda\sigma_p + \gamma\sigma_b}{\sigma_a(E') + \lambda\sigma_s(E') + \sigma_b} \, \mathrm{d}E' - \int_g \frac{1}{E'} \frac{\sigma_a(E')}{\sigma_a(E') + \lambda\sigma_s(E') + \sigma_b} \, \mathrm{d}E' \quad . \tag{2.83}$$

The first term on the right hand side has very nearly the same quantity in the numerator and the denominator, with two differences. First, there is a γ multiplying σ_b in the numerator but not the denominator. However, as previously argued, γ only affects the flux by a multiplicative factor and is chosen to be unity in most situations. For this approximation to be valid, it is assumed that γ is in fact set to unity. Second, σ_p appears in the numerator in the place that $\sigma_s(E')$ appears in the denominator. For the vast majority of resonances, the resonance absorption component is far greater than the scattering component—the 36 eV U-238 resonance being the most notable exception. Thus, even at resonance energies, this ratio is very nearly unity. Even in cases where the ratio may stray from unity, the resonance width is often much smaller than the width of the energy group, and the effect on the integral is negligible. Thus, this first term can be approximated by

$$\int_g \frac{1}{E'} \frac{\sigma_a(E') + \lambda\sigma_p + \gamma\sigma_b}{\sigma_a(E') + \lambda\sigma_s(E') + \sigma_b} \, \mathrm{d}E' \approx \int_g \frac{1}{E'} \, \mathrm{d}E' = \Delta u_g \quad . \tag{2.84}$$

The second term in Eq. (2.83) is exactly represented by

$$\int_g \frac{1}{E'} \frac{\sigma_a(E')}{\sigma_a(E') + \lambda\sigma_s(E') + \sigma_b} \, \mathrm{d}E' = \frac{\Delta u_g I_{a,g}}{\lambda\sigma_p + \sigma_b} \quad , \tag{2.85}$$

maintaining the assumption that $\gamma = 1$. The integrated group flux is thus approximated by

$$\phi_g = \Delta u_g \left(1 - \frac{I_{a,g}}{\lambda\sigma_p + \sigma_b}\right) \quad . \tag{2.86}$$

This result allows the group cross section to be put in terms of effective resonance integrals. The group cross section for reaction ρ is given by

$$\sigma_{\rho,g} = \frac{\Delta u_g I_{\rho,g}}{\phi_g} \quad . \tag{2.87}$$

Inserting Eq. (2.86) into this form gives the cross section defined in terms of the resonance integrals:

$$\sigma_{\rho,g} = \frac{I_{\rho,g}}{1 - I_{a,g}/(\lambda\sigma_p + \sigma_b)} \quad . \tag{2.88}$$

Thus, by only minor approximations in the determination of the group flux, the cross section can be determined from resonance integrals without storing the group flux explicitly.

Finally, by inserting Eq. (2.88) into Eq. (2.86), the group flux can be approximated using only cross sections. First, Eq. (2.88) with ρ as absorption is rearranged to solve for $I_{a,g}$:

$$I_{a,g} = \frac{\sigma_{a,g}}{1 + \sigma_{a,g}/(\lambda\sigma_p + \sigma_b)} \quad . \tag{2.89}$$

This is inserted into Eq. (2.86) to obtain

$$\phi_g = \Delta u_g \left(1 - \frac{\sigma_{a,g}}{\sigma_{a,g} + \lambda\sigma_p + \sigma_b}\right) \quad . \tag{2.90}$$

The information in this section was derived from material in [12].

2.6 Multiple Resonant Absorbers

2.6.1 Direct Solution of Slowing Down Equation

The full slowing down equation can be solved directly, using the same methods as in Sec. 2.5.1. The slowing down equation need not be split into resonant nuclides and background moderators,

instead taking the seemingly simple form

$$\Sigma(E)\phi(E) = \sum_i \int_E^{E/\alpha^i} \frac{\Sigma_s(E')\phi(E')}{(1-\alpha^i)E'}\,\mathrm{d}E' \quad . \tag{2.91}$$

However, the solution energy mesh for this equation must be one that resolves all the resonances of all the resonant nuclides to an acceptable degree of accuracy. This is accomplished by using all of the energy points in the pointwise cross sections of all of the nuclides and subsequently performing some sort of thinning process to reduce the resulting number of energy points. The details of this thinning process are not discussed here.

The results of this process are not easily tabulated, as including multiple resonant nuclides in the material opens a very large solution space, with a degree of freedom for the number density of each nuclide present. This is not feasible for a cross section library in general. Thus, this process would need to be performed for each simulation.

2.6.2 Approximations to Slowing Down Equation

As with slowing down with a single resonant nuclide, with multiple resonant nuclides, each nuclide's scatter source in Eq. (2.91) can be approximated with a resonant model. However, with multiple resonant nuclides, determining if resonances are "wide" or "narrow" cannot be done systematically. Different nuclides have different resonance widths, and an nuclide's scatter source in the full slowing down equation must respect all nuclides' resonances, not just its own. Furthermore, the intermediate resonance model does not produce an accurate shape of the scatter source, but rather produces the correct cross sections (or effective resonance integrals), as was alluded to in Sec. 2.5.5 and is described in more detail in Sec. 8.4.2.

2.6.3 Using Single Resonant Nuclide Tables

Because tabulating nuclear data with multiple resonance integrals is not feasible, it is desired to use nuclear data generated assuming a single resonant nuclide and manipulate it in a way that it can be used in a multiple resonant nuclide setting. With multiple resonant nuclides, the resonances of one nuclide affect the multigroup constants of another nuclide, a phenomenon known as mutual self-shielding, which will be explored in great detail in this thesis, starting in Ch. 8.

Mutual self-shielding takes two forms. First, the non-constant nature of an nuclide's cross sections effectively reduces the group-integrated flux, which increases the cross section of other resonant nuclides. This effect is known as resonance interference without overlap. Second, two resonances can overlap, causing the flux depression for an nuclide's resonance to be greater than would be expected if the nuclide was treated alone. This effect is known as resonance

overlap and reduces the cross section from that of a single nuclide. The effect of resonance interference without overlap can be easily approximated from single resonant nuclide nuclear data tables; resonance overlap cannot, and it requires specialized treatments outside the scope of this section.

Resonance interference without overlap can be accounted for in two ways. First, the effect of resonances of other nuclides on an nuclide of interest can be assumed to be uniform in energy across an energy group, which leads to a procedure of iterating on the background cross section. Second, if the resonances are assumed not to overlap at all, the effect of the resonances of all nuclides can be accounted for together to obtain a group flux. This flux can be used to adjust the single resonant nuclide cross sections. These two methods are described in the following sections.

Background Cross Section Iteration

If one assumes the effect of other nuclides' resonances on an nuclide of interest can be uniformly spread out across an energy group, an iterative procedure for the background cross section can be performed. Resonant cross sections for nuclides other than the nuclide of interest are treated as constant, taking the value of their group-averaged value. If the nuclide of interest is given by the superscript $*$, then the background cross section for that nuclide is

$$\sigma_b^* = \frac{1}{N^*} \sum_{i \neq *} \left(\Sigma_{a,g}^i + \lambda \Sigma_{s,g}^i \right) \quad , \tag{2.92}$$

where λ is defined with respect to the resonances of nuclide $*$. The value of γ is

$$\gamma^* = \frac{\sum_{i \neq *} \lambda \Sigma_{s,g}^i}{\sum_{i \neq *} \left(\Sigma_{a,g}^i + \lambda \Sigma_{s,g}^i \right)} \quad . \tag{2.93}$$

The group-averaged cross sections used here correspond to those generated assuming a single resonant nuclide. Note that each nuclide will have a different background cross section and γ value. Also note that the background cross section relies upon group-averaged cross sections, which themselves rely upon background cross sections for their respective nuclides. Furthermore, those background cross sections rely upon the group-averaged cross section, and thus the background cross section, of the original nuclide. Thus, an iteration procedure is needed. Fortunately, this iteration procedure converges rapidly. The iteration procedure is as follows:

1. Guess σ_b for each nuclide.
2. Compute group-averaged cross sections with these σ_b values.
3. Update σ_b for each nuclide with the new group-averaged cross sections.

4. Repeat steps 2-3 until convergence is obtained on the group-averaged cross sections.

This allows the effect of resonance interference without overlap to be approximated easily.

Flux Correction

An alternative approach to accounting for resonance interference without overlap assumes that the resonances of other nuclides affect a given resonant nuclide's group-averaged cross sections only through the group-integrated flux. First, group-averaged cross sections (or effective resonance integrals) are generated assuming only a single resonant nuclide using

$$\sigma_b^* = \frac{1}{N^*} \sum_{i \neq *} \lambda \Sigma_p^i \quad . \tag{2.94}$$

The other nuclides are assumed to be non-absorbing outside of their resonances. This implies that $\gamma = 1$ unless a non-resonant absorber is also included. The group-integrated flux can then be approximated for this with Eq. (2.86) or Eq. (2.90), reproduced here:

$$\begin{aligned} \phi_g^* &= \Delta u_g \left(1 - \frac{I_{a,g}^*}{\lambda^* \sigma_p^* + \sigma_b^*} \right) \\ &= \Delta u_g \left(1 - \frac{\sigma_{a,g}^*}{\sigma_{a,g}^* + \lambda^* \sigma_p^* + \sigma_b^*} \right) \quad . \end{aligned} \tag{2.95}$$

This flux deviates from the asymptotic value of Δu_g by an amount related to the absorption in the group. With multiple resonant nuclides, each nuclide will provide its own reductions in the flux, and they are assumed to be additive. Thus, the flux assuming multiple resonant nuclides is

$$\begin{aligned} \tilde{\phi}_g &= \Delta u_g \left(1 - \sum_i \frac{I_{a,g}^i}{\lambda^i \sigma_p^i + \sigma_b^i} \right) \\ &= \Delta u_g \left(1 - \sum_i \frac{\sigma_{a,g}^i}{\sigma_{a,g}^i + \lambda^i \sigma_p^i + \sigma_b^i} \right) \quad . \end{aligned} \tag{2.96}$$

Then, the cross sections for each reaction type for each resonant nuclide are adjusted with this new flux:

$$\tilde{\sigma}_{\rho,g}^* = \frac{\sigma_{\rho,g}^* \phi_g^*}{\tilde{\phi}_g} \quad . \tag{2.97}$$

Tables Assuming Admixed U-238

A common approach for accounting for mutual self-shielding effects is to generate nuclear data tables for a particular nuclide, assuming it is admixed with U-238. This is done, as in nearly all commercial reactor designs, actinides are nearly always present alongside a large concentration of U-238, which is the dominate effect on the flux spectrum. These tables require

an approximate ratio of the resonant nuclide to U-238, and multiple tables are needed if the relative concentration of the nuclide compared to U-238 varies in the downstream application.

2.7 Chapter Summary

This chapter considered the slowing down of neutrons through the resolved resonance range of the major actinides. The slowing down equation, assuming isotropic in the center of mass elastic scattering, was the primary tool. Of particular interest was the effect of resonance absorption on the neutron flux, and three approximations were introduced: the narrow resonance model, the wide resonance model, and the intermediate resonance model. With these tools, homogeneous nuclear data tables can be generated, which serve as the foundation of classical self-shielding methods.

Chapter 3

Equivalence in Dilution

3.1 Introduction

One of the two most widely used self-shielding methods is equivalence in dilution. This method is used to relate nuclear data from homogeneous tables to heterogeneous lattice physics calculations. By a clever manipulation of the neutron transport equation with two spatial regions, a heterogeneous geometry can be represented by an equivalent infinite medium. Thus, this manipulation allows cross sections from homogeneous tables to be used directly in the lattice-level calculation.

3.2 Equivalence in Dilution Form

Given a two-region system with one region containing a resonant material (called "fuel" here for simplicity) and the other containing a non-resonant material ("moderator"), the collision probability form of the transport equation can be written as

$$\Sigma^F(E)\phi^F(E)V^F = \left(1 - P^{F\to M}(E)\right) S^F(E)V^F + P^{M\to F}(E)S^M(E)V^M \quad , \tag{3.1}$$

where superscripts F and M indicate the fuel and moderator regions, respectively, ϕ is the flux in the region, Σ is the total macroscopic cross section for the region, V is the volume of the region, S is the source, and $P^{i\to j}$ is the probability a neutron born uniformly and isotropically in region i has its first collision in region j. By invoking the reciprocity relation

$$V^F\Sigma^F P^{F\to M} = V^M\Sigma^M P^{M\to F} \quad , \tag{3.2}$$

this equation can be written such that the only collision probability that appears is $P^{F\to M}$:

$$\Sigma^F(E)\phi^F(E) = \left(1 - P^{F\to M}(E)\right) S^F(E) + P^{F\to M}(E)S^M(E)\frac{\Sigma^F(E)}{\Sigma^M(E)} \quad . \tag{3.3}$$

Next, it is assumed that the moderator has a constant cross section, is purely scattering, and that the narrow resonance model well-represents its source. These approximations are not strictly necessary for this derivation but are typical assumptions in practice and simplify the problem. The transport equation takes the form

$$\Sigma^F(E)\phi^F(E) = \left(1 - P^{F\to M}(E)\right) S^F(E) + P^{F\to M}(E)\frac{\Sigma^F(E)}{E} \quad . \tag{3.4}$$

To obtain the equivalence in dilution form, this equation is first divided through by $1 - P^{F\to M}$:

$$\frac{\Sigma^F(E)}{1 - P^{F\to M}(E)}\phi^F(E) = S^F(E) + \frac{P^{F\to M}(E)\Sigma^F(E)}{1 - P^{F\to M}(E)}\frac{1}{E} \quad . \tag{3.5}$$

Noticing a similarity between the left hand side and the second term on the right hand side, the left hand side is manipulated as

$$\begin{aligned} \frac{\Sigma^F(E)}{1 - P^{F\to M}(E)}\phi^F(E) &= \left(\Sigma^F(E) + \frac{\Sigma^F(E)}{1 - P^{F\to M}(E)} - \Sigma^F(E)\right)\phi^F(E) \\ &= \left(\Sigma^F(E) + \frac{P^{F\to M}(E)\Sigma^F(E)}{1 - P^{F\to M}(E)}\right)\phi^F(E) \quad , \end{aligned} \tag{3.6}$$

and the equivalence cross section is defined as

$$\Sigma_{eq}(E) = \frac{P^{F\to M}(E)\Sigma^F(E)}{1 - P^{F\to M}(E)} \quad . \tag{3.7}$$

This allows the two-region transport equation to be written as

$$\left(\Sigma^F(E) + \Sigma_{eq}(E)\right)\phi^F(E) = S^F(E) + \frac{\Sigma_{eq}(E)}{E} \quad , \tag{3.8}$$

which has the form of a homogeneous problem of the fuel material admixed with a background narrow resonance moderator with cross section Σ_{eq}. This form is known as the equivalence in dilution form, as it casts a heterogeneous problem as an equivalent homogeneous problem by adjusting the background—or dilution—cross section.

Although this takes the form of a homogeneous problem, this still requires the efforts of solving a heterogeneous problem, as Σ_{eq} contains the fuel cross section and the fuel to moderator collision probability. However, if Σ_{eq} were constant in energy, this form would be much more convenient. In that case, several homogeneous problems could be solved and stored in a table, and solutions representing heterogeneous problems could be retrieved via a table lookup, only requiring knowledge of the system's Σ_{eq} value. In practice, this is how equivalence in dilution is performed.

Now, examine the form the fuel to moderator collision probability must take to achieve a

constant Σ_{eq}. To do this, Σ_{eq} is set to a constant value c, and the equation is rearranged:

$$\Sigma_{eq}(E) = \frac{P^{F\to M}(E)\Sigma^F(E)}{1 - P^{F\to M}(E)} = c \tag{3.9}$$

$$P^{F\to M}(E) = \frac{c}{\Sigma^F(E) + c} \quad . \tag{3.10}$$

This form is known as a rational approximation for the collision probability. Consider the limiting behavior of this form. For large fuel cross sections, the collision probability tends toward zero; for small cross sections, the collision probability tends toward one. This behavior is correct physically, which suggests that this form is promising as an approximation model. Selection of the constant c is examined in the following sections.

The information in this section follows the derivation given in [8].

3.3 Escape Probability

Next, consider the analytic form of the escape probability. That is, the probability that a neutron born uniformly and isotropically inside some lump of resonant material ("fuel" here) reaches the lump boundary and exits into surrounding material. Note that this definition only considers the probability of exiting a single lump; it does not take into account the existence of other resonant lumps. For a discussion of those effects, see Sec. 3.6. Because the only cross section that appears in this section is the fuel cross section, the superscript F is dropped. Likewise, the energy dependence of the cross section and escape probability will be implied rather than explicitly shown.

The probability a neutron born at point $\vec{r}$ in volume $\mathrm{d}V$ moving in direction $\hat{\Omega}$ escapes the fuel is

$$p(\vec{r}, \hat{\Omega})\,\mathrm{d}V\,\mathrm{d}\hat{\Omega} = \exp(-\Sigma s)\,\mathrm{d}V\,\mathrm{d}\hat{\Omega} \quad , \tag{3.11}$$

where s is the distance between $\vec{r}$ and the intersection point with the fuel surface in direction $\hat{\Omega}$. A convenient substitution here is to replace the generic volume element by a tube element. With tube elements, the volume can be represented as an integral over the surface with an integral over the length of the tube inside. The tube volume element is

$$\mathrm{d}V = (\hat{n} \cdot \hat{\Omega})\,\mathrm{d}s\,\mathrm{d}S \quad , \tag{3.12}$$

where $\hat{n}$ is a unit vector normal to the surface, $\mathrm{d}S$ is a surface element, s is the position along the tube, and $\mathrm{d}s$ is the length of the tube. The quantity l will be used as the length of the tube, also known as the chord length.

The average collision probability is given by a normalized integral of the collision probability over the volume and over all angles. To avoid double counting tubes, these integrals are

restricted to the halfspace in which $(\hat{n} \cdot \hat{\Omega}) > 0$:

$$P_{esc} = \frac{\iint_{(\hat{n}\cdot\hat{\Omega})>0} \mathrm{d}\hat{\Omega}\,\mathrm{d}S \int_0^l \mathrm{d}s\,(\hat{n}\cdot\hat{\Omega})\exp(-\Sigma s)}{\iint_{(\hat{n}\cdot\hat{\Omega})>0} \mathrm{d}\hat{\Omega}\,\mathrm{d}S \int_0^l \mathrm{d}s\,(\hat{n}\cdot\hat{\Omega})} \quad . \tag{3.13}$$

First, the s integrals are carried out:

$$P_{esc} = \frac{\iint_{(\hat{n}\cdot\hat{\Omega})>0} \mathrm{d}\hat{\Omega}\,\mathrm{d}S\,(\hat{n}\cdot\hat{\Omega})\left[1-\exp(-\Sigma l)\right]\frac{1}{\Sigma}}{\iint_{(\hat{n}\cdot\hat{\Omega})>0} \mathrm{d}\hat{\Omega}\,\mathrm{d}S\,(\hat{n}\cdot\hat{\Omega})l} \quad . \tag{3.14}$$

Next, consider the denominator. For a given angle, the single integral $\int_{(\hat{n}\cdot\hat{\Omega})>0} \mathrm{d}S\,(\hat{n}\cdot\hat{\Omega})l$ is equal to the volume of the region. Because the halfspace of $(\hat{n}\cdot\hat{\Omega}) > 0$ has already been imposed, this leaves an integral over all angles. The denominator thus simplifies to

$$\iint_{(\hat{n}\cdot\hat{\Omega})>0} \mathrm{d}\hat{\Omega}\,\mathrm{d}S\,(\hat{n}\cdot\hat{\Omega})l = \int_{4\pi} \mathrm{d}\hat{\Omega}\,V = 4\pi V \quad . \tag{3.15}$$

The final form of the escape probability without specifying information about the geometry of the fuel lump now be can be written:

$$P_{esc} = \frac{1}{4\pi V\Sigma} \iint_{(\hat{n}\cdot\hat{\Omega})>0} \mathrm{d}\hat{\Omega}\,\mathrm{d}S\,(\hat{n}\cdot\hat{\Omega})\left[1-\exp(-\Sigma l)\right] \quad . \tag{3.16}$$

An important quantity that will be seen to relate to the escape probability is the mean chord length $\bar{l}$. For convex bodies, this is defined as the ratio of the integral of all chord lengths over a uniform and isotropic distribution of surface elements to an integral of the distribution:

$$\bar{l} = \frac{\iint_{(\hat{n}\cdot\hat{\Omega})>0} \mathrm{d}\hat{\Omega}\,\mathrm{d}S\,(\hat{n}\cdot\hat{\Omega})l}{\iint_{(\hat{n}\cdot\hat{\Omega})>0} \mathrm{d}\hat{\Omega}\,\mathrm{d}S\,(\hat{n}\cdot\hat{\Omega})} \quad . \tag{3.17}$$

The numerator is the same as the denominator in the escape probability, and can be simplified to $4\pi V$, as show in Eq. (3.15). In the denominator, the polar angle θ is defined relative to the surface normal. Then, $\hat{\Omega}$ can be expanded into its component angles and the denominator can be simplified:

$$\begin{aligned} \iint_{(\hat{n}\cdot\hat{\Omega})>0} \mathrm{d}\hat{\Omega}\,\mathrm{d}S\,(\hat{n}\cdot\hat{\Omega}) &= \int_0^{2\pi} \mathrm{d}\varphi \int_0^{\pi/2} \sin(\theta)\mathrm{d}\theta \int_S \mathrm{d}S\,\cos(\theta) \\ &= 2\pi S \int_0^{\pi/2} \sin(\theta)\cos(\theta)\,\mathrm{d}\theta = \pi S \quad . \end{aligned} \tag{3.18}$$

Combining the simplified numerator and denominator leads to the simple formula for the mean chord length:

$$\bar{l} = \frac{4V}{S} \quad . \tag{3.19}$$

This derivation was adapted from that of [12].

3.4 Wigner's Rational Approximation

Having formally defined the escape probability, possible values of c in Eq. (3.10) can be explored.

One such choice of c can be derived by enforcing an additional constraint for the black limit: not only should the value tend toward zero for large cross sections, it should do so at the correct rate. Taking the limit as $\Sigma \to \infty$ in Eq. (3.16), the exponential goes to zero:

$$\lim_{\Sigma\to\infty} \frac{1}{4\pi V\Sigma} \iint_{(\hat{n}\cdot\hat{\Omega})>0} \mathrm{d}\hat{\Omega}\,\mathrm{d}S\ (\hat{n}\cdot\hat{\Omega})\left[1-\exp(-\Sigma l)\right] = \frac{1}{4\pi V\Sigma} \iint_{(\hat{n}\cdot\hat{\Omega})>0} \mathrm{d}\hat{\Omega}\,\mathrm{d}S\ (\hat{n}\cdot\hat{\Omega}) \quad . \tag{3.20}$$

The remaining integrals were previously encountered and evaluate to πS. Thus, the true escape probability has the behavior

$$\lim_{\Sigma\to\infty} P_{esc} = \frac{S}{4V\Sigma} = \frac{1}{\bar{l}\Sigma} \quad . \tag{3.21}$$

Now, consider the rational form of Eq. (3.10). As $\Sigma \to \infty$, this form tends toward A/Σ. Thus, $c = 1/\bar{l}$ satisfies the limiting behavior. Defining the escape cross section Σ_e as

$$\Sigma_e = \frac{1}{\bar{l}} \quad , \tag{3.22}$$

this leads to Wigner's Rational Approximation [13]:

$$P_{esc}(E) = \frac{\Sigma_e}{\Sigma(E)+\Sigma_e} \quad . \tag{3.23}$$

Wigner's Rational Approximation results in $\Sigma_{eq}(E) = \Sigma_e$, allowing heterogeneous results to be easily retrieved from a homogeneous table lookup. Furthermore, the table lookup parameter is a very easily computable quantity, only requiring very basic geometric parameters.

3.4.1 Bell Factor

Wigner's Rational Approximation is known to underpredict the escape probability at intermediate values of the fuel cross section. One possibility to account for this is to scale the escape cross section by some factor. Larger values of the escape cross section lead to larger escape probabilities, so this scaling factor should be greater than unity. The scaling factor is usually denoted b and is known as the Bell factor. When incorporated into Wigner's Rational Approximation, the rational form is usually referred to as the Wigner-Bell Rational Approximation [8]:

$$P_{esc}(E) = \frac{b\Sigma_e}{\Sigma(E)+b\Sigma_e} \quad . \tag{3.24}$$

Typical Bell factors range from 1 to 1.5. Note that when $b \neq 1$, this does not preserve the correct rate of decrease of the escape probability for large cross sections.

Figure 3.1 compares the escape probability for a range of cross section values for a cylindrical fuel pin with radius $0.4\,\mathrm{cm}$. Shown are the exact solution (computed numerically from Eq. (3.16)), Wigner's Rational Approximation, and the Wigner-Bell Rational Approximation with $b = 1.15$. Figure 3.2 shows the error in the rational approximations as a function of the cross section.

As is easily seen in Fig. 3.2, Wigner's Rational Approximation accurately predicts the escape probability at the white and black limits, but suffers from nearly 20% errors at intermediate values. The Wigner-Bell form greatly reduces this error—down to approximately 10% for this value of b—but has incorrect behavior at the black limit. Thus, the Bell factor can improve upon Wigner's Rational Approximation, but it must be chosen carefully for the range of cross section values encountered. If large cross sections are encountered, the Bell factor should be driven toward unity; for smaller values, larger Bell factors are appropriate.

3.5 n-Term Rational Approximations

Using the rational form of Eq. (3.10) is convenient in equivalence-based methods, and this form can mimic the behavior of the escape probability with moderate accuracy. However, a higher degree of accuracy is desired, while still maintaining the convenience of Σ_{eq} being constant in energy. This can be achieved by using a multi-term rational approximation.

Consider a linear combination of rational forms:

$$P^{F\to M}(E) = \sum_{i=1}^{n} \beta_i \frac{\alpha_i \Sigma_e}{\Sigma(E) + \alpha_i \Sigma_e} \quad , \tag{3.25}$$

which will be called an n-term rational approximation. Note that the constant c has been replaced by $\alpha_i \Sigma_e$. This is still a constant value, as Σ_e is constant for a given geometry, and as seen in Wigner's Rational Approximation, Σ_e is likely to be a useful quantity. Note that for $n > 1$, this linear combination will not satisfy the condition of Σ_{eq} being constant. However, if the condition

$$\sum_{i=1}^{n} \beta_i = 1 \tag{3.26}$$

is imposed, Eq. (3.4) can be manipulated into a form that takes advantage of the multi-term rational form. The flux is expanded into partial fluxes

$$\phi(E) = \sum_{i=1}^{n} \beta_i \phi_i(E) \quad , \tag{3.27}$$

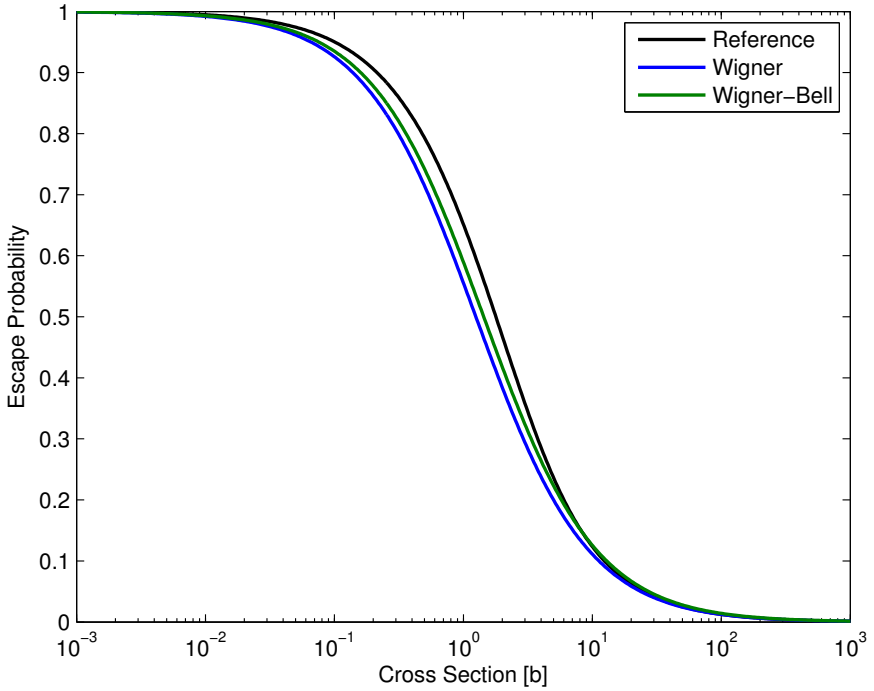

Figure 3.1: Escape probability for a pin of radius $0.4\,\mathrm{cm}$.

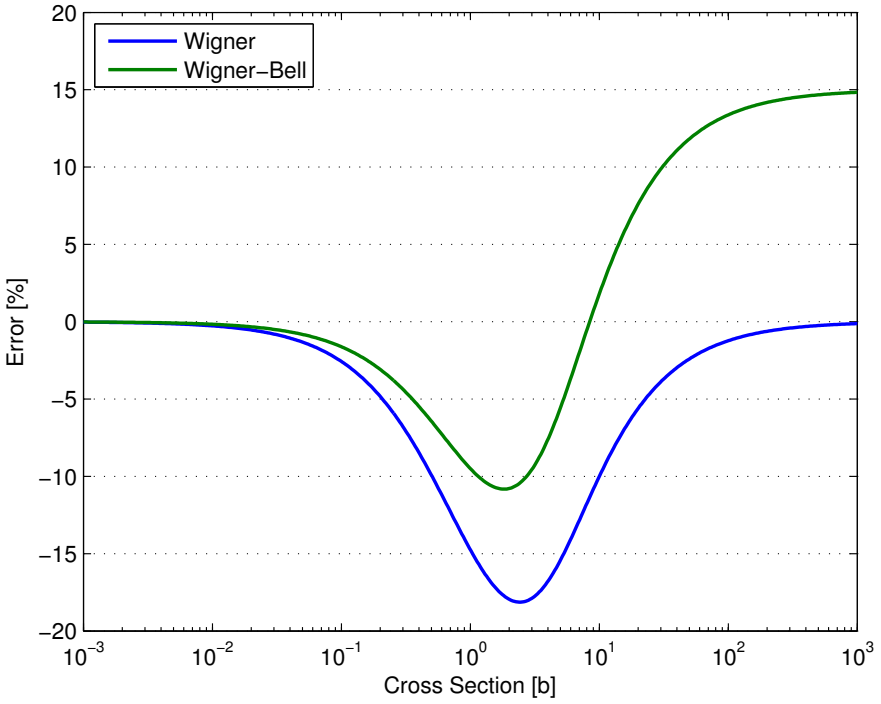

Figure 3.2: Error in rational approximations for a pin of radius $0.4\,\mathrm{cm}$.

and the collision probability is expanded likewise with

$$P^{F\to M}(E) = \sum_{i=1}^{n} \beta_i p_i(E) \quad , \tag{3.28}$$

$$p_i(E) = \frac{\alpha_i \Sigma_e}{\Sigma(E) + \alpha_i \Sigma_e} \quad . \tag{3.29}$$

Inserting these into Eq. (3.4) yields

$$\Sigma(E) \sum_{i=1}^{n} \beta_i \phi_i(E) = \left(\sum_{i=1}^{n} \beta_i - \sum_{i=1}^{n} \beta_i p_i(E) \right) S^F(E) + \sum_{i=1}^{n} \beta_i p_i(E) \frac{\Sigma(E)}{E} \quad . \tag{3.30}$$

Here, note that each term has a summation in it. The summations are collected into a single summation:

$$\sum_{i=1}^{n} \beta_i \left[\Sigma(E)\phi_i(E) - \Big(1 - p_i(E)\Big) S^F(E) - p_i(E) \frac{\Sigma(E)}{E} \right] = 0 \quad . \tag{3.31}$$

One solution to this is obtained when each term is individually zero. This solution is obtained by solving the series of equations

$$\begin{aligned} \Sigma(E)\phi_1(E) &= \Big(1 - p_1(E)\Big) S^F(E) + p_1(E) \frac{\Sigma(E)}{E} \\ \Sigma(E)\phi_2(E) &= \Big(1 - p_2(E)\Big) S^F(E) + p_2(E) \frac{\Sigma(E)}{E} \\ &\vdots \\ \Sigma(E)\phi_n(E) &= \Big(1 - p_n(E)\Big) S^F(E) + p_n(E) \frac{\Sigma(E)}{E} \quad . \end{aligned} \tag{3.32}$$

These equations each take the form of Eq. (3.4), which is equivalent to Eq. (3.8). Furthermore, each $p_i(E)$ takes the rational form of Eq. (3.10), and so the corresponding Σ_{eq} for each is constant in energy. Thus, each equation can be solved via table lookup from a table of homogeneous solutions. The overall flux can be reconstructed from the partial fluxes with Eq. (3.27).

Now that the mechanics of using an n-term rational approximation have been shown, constraints on the $2n$ coefficients β_i and α_i are considered. First, consider the white limit; $P^{F\to M}$ should tend toward unity for small cross sections. Setting the limit of Eq. (3.25) as $\Sigma \to 0$ to unity results in

$$\sum_{i=1}^{n} \beta_i = 1 \quad , \tag{3.33}$$

which is a constraint already imposed for the solution mechanics. For the black limit, the presence of Σ in the denominator of each term in Eq. (3.25) ensures it tends toward zero for large cross sections. Thus, the black and white limits do not impose any additional constraints on the coefficients.

This gives freedom in choosing the coefficients. Additional constraints can be imposed, such

as derivative behavior at the white and black limits. Either in addition to these or alternatively, an optimization procedure can be performed over the coefficients seeking to minimize deviation from some set of reference values.

3.5.1 Carlvik Two-Term Rational Approximation

A widely used rational approximation is Carlvik's Two-Term Rational Approximation [14], which applies to cylindrical fuel regions. In this section, only an isolated pin is considered. For lattice effects, see Sec. 3.6. This rational approximation conserves the derivative behavior at the white and black limits.

To start, consider the general form of a two-term rational approximation for the escape probability, with energy dependences of the cross section and escape probabilities implied:

$$P_{esc} = \beta_1 \frac{\alpha_1 \Sigma_e}{\Sigma + \alpha_1 \Sigma_e} + \beta_2 \frac{\alpha_2 \Sigma_e}{\Sigma + \alpha_2 \Sigma_e} \quad . \tag{3.34}$$

Because the β_i values must sum to unity, these are replaced by β and $1 - \beta$:

$$P_{esc} = \beta \frac{\alpha_1 \Sigma_e}{\Sigma + \alpha_1 \Sigma_e} + (1 - \beta) \frac{\alpha_2 \Sigma_e}{\Sigma + \alpha_2 \Sigma_e} \quad . \tag{3.35}$$

Now, consider the black limit. As seen in Eq. (3.21), the asymptotic behavior for large cross sections is $P_{esc} \to \Sigma_e / \Sigma$. This limit is imposed on the two-term rational approximation:

$$\begin{aligned} \lim_{\Sigma \to \infty} P_{esc} &= \lim_{\Sigma \to \infty} \beta \frac{\alpha_1 \Sigma_e}{\Sigma + \alpha_1 \Sigma_e} + (1 - \beta) \frac{\alpha_2 \Sigma_e}{\Sigma + \alpha_2 \Sigma_e} \\ &= \frac{\beta \alpha_1 \Sigma_e}{\Sigma} + \frac{(1 - \beta) \alpha_2 \Sigma_e}{\Sigma} = \frac{\Sigma_e}{\Sigma} \quad , \end{aligned} \tag{3.36}$$

which gives the condition

$$\beta \alpha_1 + (1 - \beta) \alpha_2 = 1 \quad . \tag{3.37}$$

Next, consider the white limit. The derivative behavior of the exact escape probability can be obtained analytically, although it is a somewhat arduous process. First, because of working with small cross sections, the exponential in Eq. (3.16) can be replaced by a second-order Taylor expansion:

$$\exp(-\Sigma l) \approx 1 - \Sigma l + \frac{1}{2} (\Sigma l)^2 \quad . \tag{3.38}$$

Inserting this into Eq. (3.16) and moving the outer Σ into the integrals gives

$$P_{esc} = \frac{1}{4 \pi V} \iint_{(\hat{n} \cdot \hat{\Omega}) > 0} \mathrm{d}\hat{\Omega} \, \mathrm{d}S \, (\hat{n} \cdot \hat{\Omega}) \left[l - \frac{1}{2} \Sigma l^2 \right] \quad . \tag{3.39}$$

Next, the derivative with respect to Σ is taken:

$$\frac{\mathrm{d}}{\mathrm{d}\Sigma}P_{esc} = -\frac{1}{8\pi V}\iint_{(\hat{n}\cdot\hat{\Omega})>0} \mathrm{d}\hat{\Omega}\,\mathrm{d}S\;(\hat{n}\cdot\hat{\Omega})l^2 \quad . \tag{3.40}$$

For cylindrical geometry, this derivative can be evaluated analytically. The component angles θ and φ of $\hat{\Omega}$ are set to those typical of cylindrical coordinates; θ is the polar angle measured with respect to the central axis of the cylinder, and φ is the azimuthal angle. Because a cylinder is symmetric azimuthally, the azimuthal angle component of $\hat{\Omega}$ can be set to a convenient value in the integrand. Here, an azimuthal angle of 0 is chosen. With this choice,

$$(\hat{n}\cdot\hat{\Omega}) = \cos(\eta)\sin(\theta) \quad , \tag{3.41}$$

where $\eta = \tan(-y/x)$ for some Cartesian coordinate (x, y)—defined with the origin on the central axis—on the surface of cylinder. The condition $(\hat{n}\cdot\hat{\Omega}) > 0$ is satisfied for $\cos(\eta) > 0$, as $\sin(\theta) > 0$ for all polar angles. The chord length l with azimuthal angle $\varphi = 0$ and some polar angle θ is

$$l = \frac{2|x|}{\sin(\theta)} = \frac{2\sqrt{r^2 - y^2}}{\sin(\theta)} \quad . \tag{3.42}$$

Inserting all of these quantities into Eq. (3.40) gives an updated form of

$$\begin{aligned}\frac{\mathrm{d}}{\mathrm{d}\Sigma}P_{esc} &= -\frac{1}{8\pi V}\int_0^{2\pi}\mathrm{d}\varphi\int_0^{\pi}\sin(\theta)\,\mathrm{d}\theta\int_{\cos(\eta)>0}\mathrm{d}S\;\cos(\eta)\sin(\theta)\frac{4(r^2-y^2)}{\sin^2(\theta)} \\ &= -\frac{1}{2\pi V}\int_0^{2\pi}\mathrm{d}\varphi\int_0^{\pi}\mathrm{d}\theta\int_{\cos(\eta)>0}\mathrm{d}S\;\cos(\eta)\,(r^2-y^2) \quad .\end{aligned} \tag{3.43}$$

The surface element $\mathrm{d}S$ can be replaced by $\cos(\eta)\,\mathrm{d}y$, as the axial component of both the surface area and the volume are neglected. Integrating over y for the half surface ranges from $-r$ to r. However, note that the integral is symmetric about $y = 0$, and so the integral is equal to twice the integral from 0 to r. With these transformations, the integral can be evaluated:

$$\begin{aligned}\frac{\mathrm{d}}{\mathrm{d}\Sigma}P_{esc} &= -\frac{1}{\pi V}\int_0^{2\pi}\mathrm{d}\varphi\int_0^{\pi}\mathrm{d}\theta\int_0^{r}\mathrm{d}y\,(r^2-y^2) \\ &= -\frac{2\pi}{V}\left[r^2y - \frac{y^3}{3}\right]_0^r \\ &= -\frac{2\pi}{V}\frac{2r^3}{3} = -\frac{2}{3}\frac{2\pi r^3}{\pi r^2} = -\frac{2}{3}2r \\ &= -\frac{2}{3\Sigma_e} \quad .\end{aligned} \tag{3.44}$$

Now, the derivative of Eq. (3.35) is taken:

$$\frac{\mathrm{d}}{\mathrm{d}\Sigma}P_{esc} = -\beta\frac{\alpha_1\Sigma_e}{(\Sigma+\alpha_1\Sigma_e)^2} - (1-\beta)\frac{\alpha_2\Sigma_e}{(\Sigma+\alpha_2\Sigma_e)^2} \quad . \tag{3.45}$$

This is evaluated at $\Sigma = 0$ and set equal to the result of Eq. (3.44):

$$\frac{\mathrm{d}}{\mathrm{d}\Sigma} P_{esc}\Big|_{\Sigma=0} = -\frac{\beta}{\alpha_1 \Sigma_e} - \frac{1-\beta}{\alpha_2 \Sigma_e} = -\frac{2}{3\Sigma_e} \quad . \tag{3.46}$$

This gives the second condition for the parameters of the Carlvik rational form:

$$\frac{\beta}{\alpha_1} + \frac{1-\beta}{\alpha_2} = \frac{2}{3} \quad . \tag{3.47}$$

The form of Eq. (3.35) has three unknowns (α_1, α_2, β), and now two constraints (Eqs. (3.37) and (3.47)) have been determined. This still leaves a degree of freedom, allowing one parameter to be chosen freely. One convenient choice is to set $\beta = 2$, which results in an integer solution with $\alpha_1 = 2$ and $\alpha_2 = 3$. This particular selection has been quite successful in use in equivalence in dilution applications and is Carlvik's Two-Term Rational Approximation for an isolated pin:

$$P_{esc}(E) = 2\frac{2\Sigma_e}{\Sigma(E) + 2\Sigma_e} - \frac{3\Sigma_e}{\Sigma(E) + 3\Sigma_e} \quad . \tag{3.48}$$

Other two-term rational approximations are possible for an isolated pin, even those that satisfy Eqs. (3.37) and (3.47). However, Carlvik is the most widely used and is quite accurate. Figure 3.3 shows the error in the approximation plotted with the other rational approximations for a pin of radius 0.4 cm. The Carlvik Two-Term Rational Approximation has a peak error less than 3%, much reduced from the one-term approximations.

3.5.2 Román Two-Term Rational Approximation

Of course, cylindrical geometries are not the only ones encountered in reactor analysis. For slab geometry, a suitable two-term rational approximation is given by Román:

$$P_{esc}(E) = 1.1\frac{1.4\Sigma_e}{\Sigma(E) + 1.4\Sigma_e} - .1\frac{5.4\Sigma_e}{\Sigma(E) + 5.4\Sigma_e} \quad . \tag{3.49}$$

This rational approximation obeys the black limit of Eq. (3.37). However, the escape probability for a slab features a logarithmic singularity at $\Sigma = 0$, and so the derivative cannot be taken. Instead, these parameters were generated as a best fit to some set of reference values. Figure 3.4 shows the error in this approximation compared to the other rational approximations for a slab of width 0.4 cm.

Rational approximations can of course be made for other geometries, and there is no single "correct" method of selection of coefficients. Instead, coefficients are sought that yield the best answers for the problems at hand. Furthermore, rational approximations can be generated with more terms if this is deemed necessary for a given application (e.g., [Hebert1991]).

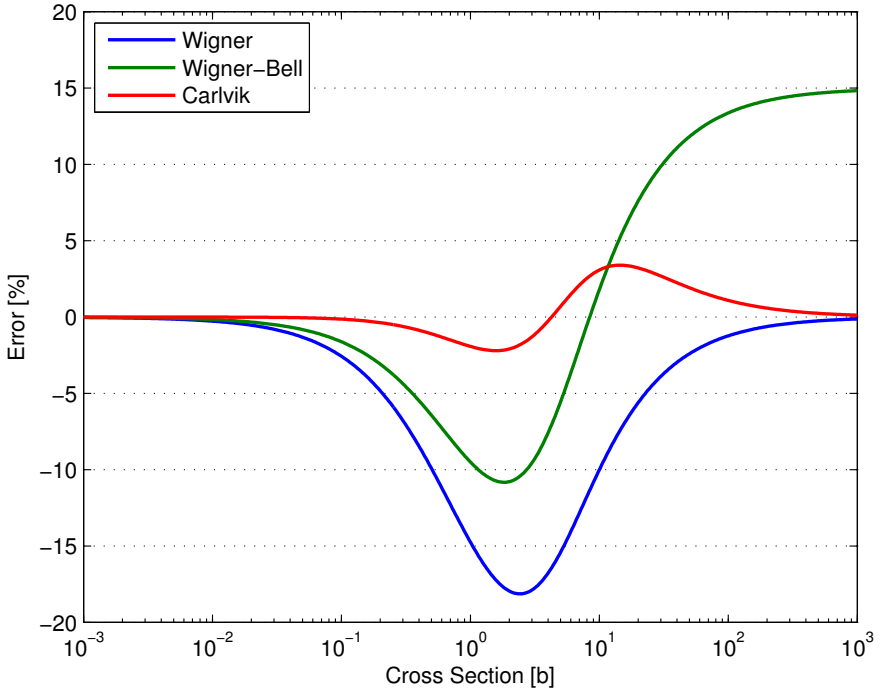

Figure 3.3: Error in rational approximations for a pin of radius $0.4\,\mathrm{cm}$.

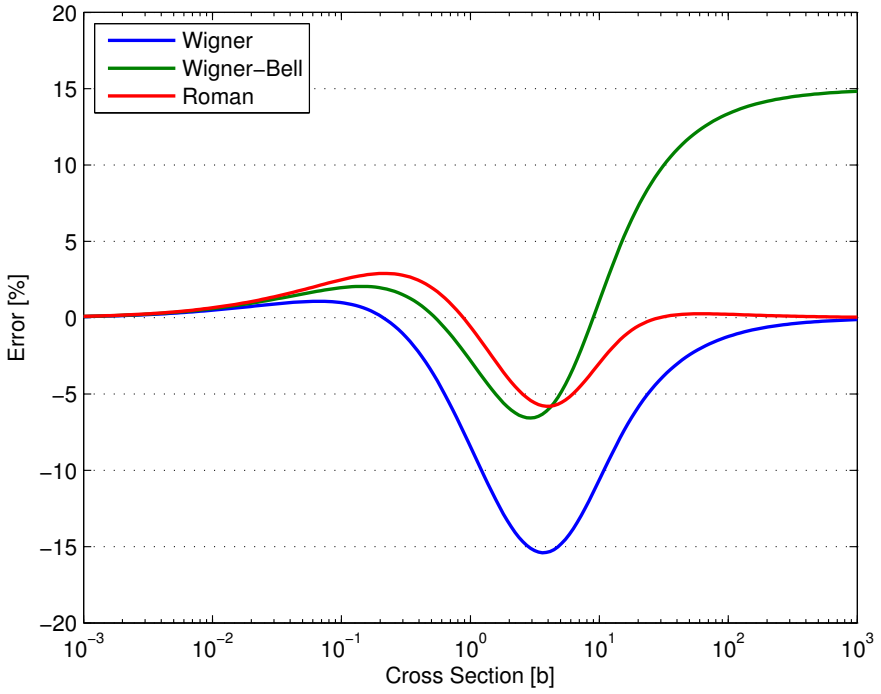

Figure 3.4: Error in rational approximations for a slab of radius $0.4\,\mathrm{cm}$.

3.5.3 Using n-Term Rational Approximations

Although it has been shown that an n-term rational approximation can be used to accurately estimate the flux in a heterogeneous system, effective resonance integrals or cross sections are what is actually desired.

First, consider the effective resonance integral for reaction type ρ, which is defined as

$$I_{\rho,g} = \frac{1}{\Delta u_g} \int_g \sigma_\rho(E)\phi(E)\,\mathrm{d}E \quad . \tag{3.50}$$

Inserting Eq. (3.27) into this definition yields

$$\begin{aligned} I_{\rho,g} &= \frac{1}{\Delta u_g} \int_g \sigma_\rho(E) \sum_{i=1}^{n} \beta_i \phi_i(E)\,\mathrm{d}E \\ &= \frac{1}{\Delta u_g} \sum_{i=1}^{n} \beta_i \int_g \sigma_\rho(E)\phi_i(E)\,\mathrm{d}E \quad . \end{aligned} \tag{3.51}$$

The effective resonance integral defined using a partial flux is recognized in this equation:

$$I_{\rho,g,i} \equiv \frac{1}{\Delta u_g} \int_g \sigma_\rho(E)\phi_i(E)\,\mathrm{d}E \quad . \tag{3.52}$$

This quantity is retrievable from homogeneous nuclear data tables. Then, the true effective resonance integral is simply

$$I_{\rho,g} = \sum_{i=1}^{n} \beta_i I_{\rho,g,i} \quad . \tag{3.53}$$

Next, consider the group-averaged cross section for reaction type ρ:

$$\sigma_{\rho,g} = \frac{\int_g \sigma_\rho(E)\phi(E)\,\mathrm{d}E}{\int_g \phi(E)\,\mathrm{d}E} \quad . \tag{3.54}$$

Inserting Eq. (3.27) into this equation yields

$$\begin{aligned} \sigma_{\rho,g} &= \frac{\int_g \sigma_\rho(E) \sum_{i=1}^{n} \beta_i \phi_i(E)\,\mathrm{d}E}{\int_g \sum_{i=1}^{n} \beta_i \phi_i(E)\,\mathrm{d}E} \\ &= \frac{\sum_{i=1}^{n} \beta_i \int_g \sigma_\rho(E)\phi_i(E)\,\mathrm{d}E}{\sum_{i=1}^{n} \beta_i \int_g \phi_i(E)\,\mathrm{d}E} \quad . \end{aligned} \tag{3.55}$$

The integral in the numerator is recognized as the group cross section multiplied by the group integrated flux using a partial flux:

$$\int_g \sigma_\rho(E)\phi_i(E)\,\mathrm{d}E = \sigma_{\rho,g,i}\phi_{g,i} \quad . \tag{3.56}$$

The integral in the denominator is simply the group integrated flux using a partial flux:

$$\int_g \phi_i(E)\,\mathrm{d}E = \phi_{g,i} \quad . \tag{3.57}$$

These forms are inserted into the group cross section equation to achieve

$$\sigma_{\rho,g} = \frac{\sum_{i=1}^{n} \beta_i \sigma_{\rho,g,i}\phi_{g,i}}{\sum_{i=1}^{n} \beta_i \phi_{g,i}} \quad . \tag{3.58}$$

If the group integrated flux is stored in the homogeneous nuclear data table, this form can be used directly to obtain group cross sections with an n-term rational approximation. If the group integrated flux is not available, it can be approximated as in Sec. 2.5.7:

$$\phi_{g,i} = \Delta u_g \left(1 - \frac{\sigma_{a,g,i}}{\sigma_{a,g,i} + \lambda\sigma_p + \sigma_{b,i}}\right) \quad . \tag{3.59}$$

Inserting this into Eq. (3.58) gives an alternate form for the cross section with an n-term rational approximation:

$$\sigma_{\rho,g} = \frac{\sum_{i=1}^{n} \beta_i \sigma_{\rho,g,i}\left(1 - \frac{\sigma_{a,g,i}}{\sigma_{a,g,i} + \lambda\sigma_p + \sigma_{b,i}}\right)}{\sum_{i=1}^{n} \beta_i \left(1 - \frac{\sigma_{a,g,i}}{\sigma_{a,g,i} + \lambda\sigma_p + \sigma_{b,i}}\right)} \quad . \tag{3.60}$$

3.6 The Dancoff Effect

In the approximations to the fuel to moderator collision probability, it has been assumed that a fuel lump is isolated. However, in real reactor systems, fuel is generally arranged in a regular or semi-regular lattice pattern, with fuel lumps in close enough proximity to each other for neutrons born in one to reach another. In this context, the escape probability—the probability a neutron born in a fuel lump exits that fuel lump—is not the same as the fuel to moderator collision probability. The effect of fuel lumps being present in a lattice rather than being isolated is known as the Dancoff effect [13, 8].

Consider Eq. (3.1) rewritten where the fuel F includes many lumped regions $f' \in F$ and the

moderator M is similarly segmented with regions $m' \in M$. The region of interest is a particular fuel region f. The transport equation for this problem is

$$\Sigma^f(E)\phi^f(E)V^f = P^{f\to f}(E)S^f(E)V^f + \sum_{\substack{f'\in F\\ f'\neq f}} P^{f'\to f}(E)S^{f'}(E)V^{f'} + \sum_{m'\in M} P^{m'\to f}(E)S^{m'}(E)V^{m'} \quad . \tag{3.61}$$

Reciprocity relations are used to transform all the collision probabilities into those originating from the region f. Assuming a generic region $r \neq f$, the reciprocity relation is

$$V^f\Sigma^f P^{f\to r} = V^r\Sigma^r P^{r\to f} \quad . \tag{3.62}$$

The transport equation for this problem is now written as

$$\Sigma^f(E)\phi^f(E) = P^{f\to f}S^f(E) + \sum_{\substack{f'\in F\\ f'\neq f}} P^{f\to f'}(E)S^{f'}(E)\frac{\Sigma^f(E)}{\Sigma^{f'}(E)} + \sum_{m'\in M} P^{f\to m'}(E)S^{m'}(E)\frac{\Sigma^f(E)}{\Sigma^{m'}(E)} \quad . \tag{3.63}$$

If, as before, the moderator cross section is assumed constant and its source is assumed to be that of the narrow resonance model, the moderator regions can be combined with $P^{f\to M}(E) = \sum_{m'\in M} P^{f\to m'}(E)$:

$$\Sigma^f(E)\phi^f(E) = P^{f\to f}S^f(E) + \sum_{\substack{f'\in F\\ f'\neq f}} P^{f\to f'}(E)S^{f'}(E)\frac{\Sigma^f(E)}{\Sigma^{f'}(E)} + P^{f\to M}(E)\frac{\Sigma^f(E)}{E} \quad . \tag{3.64}$$

If all fuel regions, including the region of interest, are assumed to have the same source and the same cross section, this simplifies further to

$$\begin{aligned}\Sigma^f(E)\phi^f(E) &= \left(P^{f\to f} + \sum_{\substack{f'\in F\\ f'\neq f}} P^{f\to f'}(E)\right)S^f(E) + P^{f\to M}(E)\frac{\Sigma^f(E)}{E}\\ &= \left(1 - P^{f\to M}(E)\right)S^f(E) + P^{f\to M}(E)\frac{\Sigma^f(E)}{E} \quad .\end{aligned} \tag{3.65}$$

This is the same form as Eq. (3.4), but the specific meanings of the terms allow for $P^{f\to M}$ to be related to the escape probability. Note that because the cross section of the fuel is the only cross section that appears here, the superscript f will be dropped in subsequent discussion.

3.6.1 Gray Dancoff Factor

Consider the relationship between $P^{f\to M}$ in Eq. (3.65) and the escape probability. $P^{f\to M}$ is the probability that a neutron born in fuel region f both escapes the pin and has its next interaction in the moderator. This is equivalent to a reduction in the escape probability by the

probability the neutron has its next collision in a different fuel element:

$$P^{f\to M}(E) = P_{esc}(E) - \sum_{\substack{f'\in F\\ f'\neq f}} P^{f\to f'}(E) \quad . \tag{3.66}$$

If the quantity $\tilde{C}$ is defined as

$$\tilde{C}(E) = \frac{\sum_{\substack{f'\in F\\ f'\neq f}} P^{f\to f'}(E)}{P_{esc}(E)} \quad , \tag{3.67}$$

then the fuel to moderator probability can be written as

$$P^{f\to M}(E) = \Big(1 - \tilde{C}(E)\Big)P_{esc}(E) \quad . \tag{3.68}$$

This parameter $\tilde{C}$ is known as the gray Dancoff factor. It can be computed for a given configuration using the methods outline in Sec. 3.6.4. It is an energy dependent quantity, and so must be computed for many points along a resonance to accurately model the Dancoff effect. Furthermore, Eq. (3.68) does not satisfy the rational form of Eq. (3.10), and so it cannot be used directly with homogeneous look-up tables. These considerations make the gray Dancoff factor inconvenient to use in practice. Fortunately, a more convenient alternative exists and is the subject of the following section.

3.6.2 Black Dancoff Factor

Consider the fuel to moderator collision probability:

$$\begin{aligned} P^{f\to M}(E) &= 1 - \left(P^{f\to f}(E) + \sum_{\substack{f'\in F\\ f'\neq f}} P^{f\to f'}(E) \right) \\ &= P_{esc} - \sum_{\substack{f'\in F\\ f'\neq f}} P^{f\to f'}(E) \quad . \end{aligned} \tag{3.69}$$

The sum can be expanded as

$$\sum_{\substack{f'\in F\\ f'\neq f}} P^{f\to f'}(E) = \sum_{n=0}^{\infty} P^{f\to nf'}(E) \quad , \tag{3.70}$$

where

- $P^{f\to 0f'}$ is the probability that a neutron born in the fuel escapes, traverses the moderator, and collides in the next fuel element it encounters.

- $P^{f \to 1f'}$ is the probability a neutron born in the fuel escapes, traverses the moderator, traverses another fuel element, again traverses the moderator and collides in the next fuel element.

- $P^{f \to 2f'}$ is the probability a neutron born in the fuel escapes, twice traverses the moderator and a fuel element, traverses the moderator and eventually collides in the next element.

- ...

Thus, n represents the number of fuel lumps a neutron traverses after it escapes and before it eventually collides in a fuel lump. Similarly, define the probability a neutron entering the moderator after traversing n fuel lumps (excluding the lump in which is was born) reaches another fuel lump as C_n. Because the moderator has been assumed to have a constant cross section, C_n is not a function of energy.

Also, define the probability a neutron collides in a given fuel lump after entering the lump through its surface as $P^{S \to f}$. The complementary probability, that a neutron entering a fuel lump through its surfaces traverses it without collision, is notated $P^{S \to S}$. Of course, the complementary relationship holds with these collision probabilities:

$$P^{S \to f}(E) + P^{S \to S}(E) = 1 \quad . \tag{3.71}$$

Next, assume that any neutrons that enter a fuel lump do so uniformly and isotropically across its surface. Likewise, assume any neutrons exiting a fuel lump do so uniformly and isotropically across its surface. These assumptions are not physical, as a great deal of angular structure is present in the probability of traversal, as a neutron is more likely to escape a fuel lump if it travels a shorter distance inside the lump. However, these assumptions work well in the context of equivalence in dilution methods. The first of these approximations gives rise to the reciprocity relation

$$P^{S \to f}(E) = \bar{l}\Sigma(E)P_{esc}(E) \quad . \tag{3.72}$$

It is also assumed that all fuel lumps are the same size and shape. Thus, $P^{S \to f}$ and $P^{S \to S}$ are the same for each fuel lump.

With these definitions and assumptions, the probability of a neutron born in a fuel lump, traversing the moderator, and colliding in the first subsequent fuel lump it encounters can be written

$$P^{f \to 0f'}(E) = P_{esc}(E)C_0P^{S \to f}(E) \quad . \tag{3.73}$$

The probabilities a neutron traverses this fuel lump but collides in a different fuel lump are

$$\begin{aligned} P^{f\to 1f'}(E) &= P_{esc}(E)C_0P^{S\to S}(E)C_1P^{S\to f}(E) \\ P^{f\to 2f'}(E) &= P_{esc}(E)C_0P^{S\to S}(E)C_1P^{S\to S}(E)C_2P^{S\to f}(E) \\ &\vdots \quad . \end{aligned} \tag{3.74}$$

In a regular lattice, with the uniform and isotropic assumptions, each C_n is equal. In irregular lattices, C_n is a function of the geometry. However, the contributions of collision probabilities representing multiple fuel lump traversals diminish rapidly, and so assuming $C_n = C_0$ is an easily justifiable approximation. In this case, using the complementary relationship of Eq. (3.71) and dropping the subscript on C, $P^{f\to nf'}$ can be written

$$P^{f\to nf'}(E) = P_{esc}(E)\left[C\left(1 - P^{S\to f}(E)\right)\right]^n CP^{S\to f}(E) \quad . \tag{3.75}$$

Using the reciprocity relation of Eq. (3.72), this becomes

$$P^{f\to nf'}(E) = P_{esc}(E)\left[C\left(1 - \bar{l}\Sigma(E)P_{esc}(E)\right)\right]^n C\bar{l}\Sigma(E)P_{esc}(E) \quad . \tag{3.76}$$

Because the quantity in square brackets is the product of probabilities, it is guaranteed to be less than unity. Thus, the geometric series form

$$\sum_{n=0}^{\infty} x = \frac{1}{1-x} \tag{3.77}$$

can be invoked. The sum in Eq. (3.70) can now be written

$$\sum_{n=0}^{\infty} P^{f\to nf'}(E) = \frac{P_{esc}^2(E)C\bar{l}\Sigma(E)}{1 - C\left(1 - \bar{l}\Sigma(E)P_{esc}(E)\right)} \quad . \tag{3.78}$$

Finally, this is inserted into Eq. (3.69) to obtain the fuel to moderator collision probability:

$$P^{f\to M}(E) = P_{esc}(E)\left(1 - \frac{P_{esc}(E)C\bar{l}\Sigma(E)}{1 - C\left(1 - \bar{l}\Sigma(E)P_{esc}(E)\right)}\right) \quad . \tag{3.79}$$

By comparison to Eq. (3.68), the gray Dancoff factor has been approximated by

$$\tilde{C}(E) = \frac{P_{esc}(E)C\bar{l}\Sigma(E)}{1 - C\left(1 - \bar{l}\Sigma(E)P_{esc}(E)\right)} \quad . \tag{3.80}$$

Thus, the energy dependent lattice parameter $\tilde{C}(E)$ is replaced by an energy independent lattice parameter C and an equation that appears more complicated. C is the probability a neutron that leaves fuel region f reaches another fuel region without colliding with the moderator. If

Table 3.1: Comparison of using directly computed gray Dancoff factor to using approximation with black Dancoff for an infinite square lattice of fuel pin with radius 0.4 cm, pitch 1.26 cm, and moderator cross section 1.23 cm^{-1}.

Σ [cm^{-1}]	P_{esc}	Gray Dancoff Factor			
		Direct	Approx	Error $\tilde{C}$	Error $(1-\tilde{C})$
1E-01	9.504E-01	0.0225	0.0243	7.64%	-0.18%
1E+00	6.517E-01	0.1413	0.1457	3.12%	-0.51%
1E+01	1.235E-01	0.2447	0.2442	-0.20%	0.06%
1E+02	1.250E-02	0.2465	0.2465	0.00%	0.00%
1E+03	1.250E-03	0.2465	0.2465	0.00%	0.00%
1E+04	1.250E-04	0.2465	0.2465	0.00%	0.00%
1E+05	1.250E-05	0.2465	0.2465	0.00%	0.00%

the fuel cross section were set to a very large value, all neutrons that reach a fuel region collide there. Thus, C can be written as

$$C = \lim_{\Sigma\to\infty} \frac{\sum_{f'\in F,\, f'\neq f} P^{f\to f'}}{P_{esc}} \quad , \tag{3.81}$$

which is the same as the previously encountered gray Dancoff factor evaluated with a very large cross section. Therefore, C is known as the black Dancoff factor. Its computation is discussed in Sec. 3.6.4. Table 3.1 shows a comparison of gray Dancoff factors computed directly versus computed approximately as outlined in this section for an infinite square lattice of fuel pins with radius 0.4 cm, pitch 1.26 cm, and moderator cross section 1.23 cm^{-1}. The Dancoff factor saturates quickly, with the gray Dancoff achieving its black limit with $\Sigma = 100\,cm^{-1}$. With small cross sections, there is a noticeable error in the Dancoff factor, but this can be attributed to the very small value it takes. Because the fuel to moderator probability is actually multiplied by $(1-\tilde{C})$, error in this quantity is perhaps a more appropriate measure, and the approximation leads to almost no error here.

The form of Eq. (3.79) appears very complicated. However, as discussed in the subsequent section, when used in conjunction with a rational approximation, it yields a fuel to moderator probability that takes the same rational form. Thus, it is a very convenient form and can be used directly with homogeneous lookup tables. Furthermore, by defining the quantity A as

$$A = \frac{1-C}{C} \quad , \tag{3.82}$$

using $\Sigma_e = 1/\bar{l}$, and rearranging terms, Eq. (3.79) can be written in a somewhat cleaner form:

$$P^{f\to M}(E) = P_{esc}(E)\left(\frac{A\Sigma_e}{A\Sigma_e + \Sigma(E)P_{esc}(E)}\right) \quad . \tag{3.83}$$

3.6.3 Dancoff Form of Rational Approximations

In the previous section, it was claimed that using the black Dancoff factor with Eq. (3.79) or equivalently Eq. (3.83) in conjunction with a rational approximation for the escape probability yields another rational approximation for the true fuel to moderator collision probability. This claim is proven here for one-term and two-term rational approximations.

Dancoff Form of One-Term Rational Approximation

The Wigner-Bell Rational Approximation can be considered the general form of the one-term rational approximation, as Σ_e is a constant in energy, and so with proper selection of b, $b\Sigma_e$ can evaluate to any constant.

The Wigner-Bell Rational Approximation of Eq. (3.24) is inserted into Eq. (3.83):

$$\begin{aligned} P^{f\to M}(E) &= \frac{b\Sigma_e}{\Sigma(E)+b\Sigma_e}\cdot\frac{A\Sigma_e}{A\Sigma_e+\Sigma(E)\frac{b\Sigma_e}{\Sigma(E)+b\Sigma_e}} \\ &= \frac{Ab\Sigma_e}{A(\Sigma(E)+b\Sigma_e)+b\Sigma(E)} \quad . \end{aligned} \tag{3.84}$$

This can be simplified to a rational approximation:

$$P^{f\to M}(E) = \frac{b^*\Sigma_e}{\Sigma(E)+b^*\Sigma_e} \tag{3.85}$$

$$b^* = \frac{Ab}{A+b} = \frac{(1-C)b}{1-C+Cb} \quad . \tag{3.86}$$

Thus, using Eq. (3.79) with a one-term rational approximation for the escape probability results in a one-term rational approximation for the lattice fuel to moderator probability.

Dancoff Form of Two-Term Rational Approximation

Deriving the two-term rational form including the Dancoff effect is quite a bit more complicated than for the one-term form. However, it can still be done, and is shown here. To simplify notation, explicit dependences of the cross sections and escape probabilities on energy are not shown. First, the general two-term rational expression

$$P_{esc} = \beta\frac{\alpha_1\Sigma_e}{\Sigma+\alpha_1\Sigma_e} + (1-\beta)\frac{\alpha_2\Sigma_e}{\Sigma+\alpha_2\Sigma_e} \tag{3.87}$$

is inserted into Eq. (3.83):

$$P^{f\to M} = \left(\beta\frac{\alpha_1\Sigma_e}{\Sigma+\alpha_1\Sigma_e} + (1-\beta)\frac{\alpha_2\Sigma_e}{\Sigma+\alpha_2\Sigma_e}\right)\frac{A\Sigma_e}{A\Sigma_e+\frac{\Sigma\beta\alpha_1\Sigma_e}{\Sigma+\alpha_1\Sigma_e}+\frac{\Sigma(1-\beta)\alpha_2\Sigma_e}{\Sigma+\alpha_2\Sigma_e}} \quad . \tag{3.88}$$

The numerator and denominator are each multiplied by $(\Sigma + \alpha_1\Sigma_e)(\Sigma + \alpha_2\Sigma_e)$:

$$P^{f\to M} = \frac{(\beta\alpha_1\Sigma_e(\Sigma + \alpha_1\Sigma_e) + (1-\beta)\alpha_2\Sigma_e(\Sigma + \alpha_1\Sigma_e))\, A\Sigma_e}{A\Sigma_e(\Sigma + \alpha_1\Sigma_e)(\Sigma + \alpha_2\Sigma_e) + \Sigma\beta\alpha_1\Sigma_e(\Sigma + \alpha_2\Sigma_e) + \Sigma(1-\beta)\alpha_2\Sigma_e(\Sigma + \alpha_1\Sigma_e)} \quad . \tag{3.89}$$

Next, a factor of Σ_e is noticed to be in each term both in the numerator and denominator, and so can be cancelled. With this and rearranging terms, the form becomes

$$P^{f\to M} = \frac{A\left(\beta\alpha_1 + (1-\beta)\alpha_2\right)\Sigma_e\Sigma + A\alpha_1\alpha_2\Sigma_e^2}{\left(A + \beta\alpha_1 + (1-\beta)\alpha_2\right)\Sigma^2 + \left(A(\alpha_1+\alpha_2) + \alpha_1\alpha_2\right)\Sigma_e\Sigma + A\alpha_1\alpha_2\Sigma_e^2} \quad . \tag{3.90}$$

The desired form for $P^{f\to M}$ is another two-term rational approximation

$$P^{f\to M} = \frac{\beta_1^*\alpha_1^*\Sigma_e}{\Sigma + \alpha_1^*\Sigma_e} + \frac{\beta_2^*\alpha_2^*\Sigma_e}{\Sigma + \alpha_2^*\Sigma_e} \quad , \tag{3.91}$$

and because the denominator of Eq. (3.90) is quadratic in Σ and Σ_e, this form appears possible with a partial fraction expansion. To do this, first, the denominator should be factorized as $(\Sigma + \alpha_1^*)(\Sigma + \alpha_2^*)$, with a leading multiplicative coefficient of γ:

$$\begin{aligned}\mathcal{D} &= \left(A + \beta\alpha_1 + (1-\beta)\alpha_2\right)\Sigma^2 + \left(A(\alpha_1+\alpha_2) + \alpha_1\alpha_2\right)\Sigma_e\Sigma + A\alpha_1\alpha_2\Sigma_e^2 \\ &= \gamma(\Sigma + \alpha_1^*)(\Sigma + \alpha_2^*) = \gamma\left(\Sigma^2 + (\alpha_1^* + \alpha_2^*)\Sigma_e\Sigma + \alpha_1^*\alpha_2^*\Sigma^2\right) \quad .\end{aligned} \tag{3.92}$$

By inspection, the following relationships are implied:

$$\gamma = A + \beta\alpha_1 + (1-\beta)\alpha_2 \tag{3.93}$$

$$\alpha_1^* + \alpha_2^* = \frac{A(\alpha_1+\alpha_2) + \alpha_1\alpha_2}{\gamma} \tag{3.94}$$

$$\alpha_1^*\alpha_2^* = \frac{A\alpha_1\alpha_2}{\gamma} \quad . \tag{3.95}$$

Solving Eq. (3.94) for α_2^* and inserting it into Eq. (3.95), α_1^* is determined:

$$\alpha_1^*\frac{A(\alpha_1+\alpha_2) + \alpha_1\alpha_2}{\gamma} = \frac{A\alpha_1\alpha_2}{\gamma} \tag{3.96}$$

$$\gamma\alpha_1^{*2} - \left(A(\alpha_1+\alpha_2) + \alpha_1\alpha_2\right)\alpha_1^* + A\alpha_1\alpha_2 = 0 \tag{3.97}$$

$$\alpha_1^* = \frac{(A(\alpha_1+\alpha_2) + \alpha_1\alpha_2) \pm \sqrt{(A(\alpha_1+\alpha_2) + \alpha_1\alpha_2)^2 - 4\gamma A\alpha_1\alpha_2}}{2\gamma} \quad . \tag{3.98}$$

By inspection, Eq. (3.95) is satisfied when

$$\alpha_2^* = \frac{(A(\alpha_1+\alpha_2) + \alpha_1\alpha_2) \mp \sqrt{(A(\alpha_1+\alpha_2) + \alpha_1\alpha_2)^2 - 4\gamma A\alpha_1\alpha_2}}{2\gamma} \quad . \tag{3.99}$$

α_1^* and α_2^* are symmetric and thus interchangable in the derivation so far. Thus, the lower signs are chosen without loss of generality:

$$\begin{aligned}\alpha_1^* &= \frac{(A(\alpha_1+\alpha_2)+\alpha_1\alpha_2) - \sqrt{(A(\alpha_1+\alpha_2)+\alpha_1\alpha_2)^2 - 4\gamma A\alpha_1\alpha_2}}{2\gamma} \\ \alpha_2^* &= \frac{(A(\alpha_1+\alpha_2)+\alpha_1\alpha_2) + \sqrt{(A(\alpha_1+\alpha_2)+\alpha_1\alpha_2)^2 - 4\gamma A\alpha_1\alpha_2}}{2\gamma} \quad .\end{aligned} \tag{3.100}$$

Next, Eq. (3.90) can be expanded into partial fractions to obtain the desired form:

$$\begin{aligned}P^{f\to M} &= \frac{A\left(\beta\alpha_1+(1-\beta)\alpha_2\right)\Sigma_e\Sigma + A\alpha_1\alpha_2\Sigma_e^2}{\gamma(\Sigma+\alpha_1^*\Sigma_e)(\Sigma+\alpha_2^*\Sigma_e)} = \frac{C_1}{\Sigma+\alpha_1^*\Sigma_e} + \frac{C_2}{\Sigma+\alpha_2^*\Sigma_e} \\ &= \frac{\beta_1^*\alpha_1^*\Sigma_e}{\Sigma+\alpha_1^*\Sigma_e} + \frac{\beta_2^*\alpha_2^*\Sigma_e}{\Sigma+\alpha_2^*\Sigma_e} \quad ,\end{aligned} \tag{3.101}$$

where C_1 and C_2 are arbitrary constants to be solved for. Because α_1^*, α_2^*, and Σ_e are all constants, C_1 and C_2 can be replaced by $\beta_1^*\alpha_1^*\Sigma_e$ and $\beta_2^*\alpha_2^*\Sigma_e$, respectively, without loss of generality. Multiplying through by the denominator yields

$$\begin{aligned}A\left(\beta\alpha_1+(1-\beta)\alpha_2\right)\Sigma_e\Sigma + A\alpha_1\alpha_2\Sigma_e^2 &= \gamma\beta_1^*\alpha_1^*\Sigma_e(\Sigma+\alpha_2^*\Sigma_e) + \gamma\beta_2^*\alpha_2^*\Sigma_e(\Sigma+\alpha_1^*\Sigma_e) \\ &= \gamma\left(\beta_1^*\alpha_1^*+\beta_2^*\alpha_2\right)\Sigma_e\Sigma + \gamma\left(\beta_1^*+\beta_2^*\right)\alpha_1^*\alpha_2^*\Sigma_e^2 \quad .\end{aligned} \tag{3.102}$$

This gives constraints for β_1^* and β_2^*:

$$\beta_1^*\alpha_1^* + \beta_2^*\alpha_2^* = \frac{A\left(\beta\alpha_1+(1-\beta)\alpha_2\right)}{\gamma} \tag{3.103}$$

$$\beta_1^* + \beta_2^* = \frac{A\alpha_1\alpha_2}{\gamma\alpha_1^*\alpha_2^*} \quad . \tag{3.104}$$

Now, consider the constraint Eq. (3.104). The product $\alpha_1^*\alpha_2^*$ is

$$\begin{aligned}\alpha_1^*\alpha_2^* &= \frac{(A(\alpha_1+\alpha_2)+\alpha_1\alpha_2)^2 - (A(\alpha_1+\alpha_2)+\alpha_1\alpha_2)^2 + 4\gamma A\alpha_1\alpha_2}{4\gamma^2} \\ &= \frac{A\alpha_1\alpha_2}{\gamma} \quad ,\end{aligned} \tag{3.105}$$

and therefore, Eq. (3.104) simplifies to

$$\beta_1^* + \beta_2^* = 1 \quad . \tag{3.106}$$

This ensures the Dancoff form of a two-term rational approximation is also a two-term rational approximation. Finally, this is inserted into Eq. (3.103) to determine the final unknown

parameter:

$$\beta_1^*\alpha_1^* + (1-\beta_1^*)\alpha_2^* = \frac{A\left(\beta\alpha_1 + (1-\beta)\alpha_2\right)}{\gamma} \tag{3.107}$$

$$\beta_1^* = \left(\alpha_2^* - \frac{A\left(\beta\alpha_1 + (1-\beta)\alpha_2\right)}{\gamma}\right)\frac{1}{\alpha_2^* - \alpha_1^*} \quad . \tag{3.108}$$

To summarize, when a two-term rational approximation for the escape probability is used in conjunction with Eq. (3.79), another two-term rational approximation is recovered. This new two-term rational approximation for the fuel to moderator probability in a lattice system is given by

$$P^{f\to M}(E) = \beta^*\frac{\alpha_1^*\Sigma_e}{\Sigma(E) + \alpha_1^*\Sigma_e} + (1-\beta^*)\frac{\alpha_2^*\Sigma_e}{\Sigma(E) + \alpha_2^*\Sigma_e} \quad , \tag{3.109}$$

where

$$\begin{aligned}
\alpha_1^* &= \frac{(A(\alpha_1+\alpha_2)+\alpha_1\alpha_2) - \sqrt{(A(\alpha_1+\alpha_2)+\alpha_1\alpha_2)^2 - 4\gamma A\alpha_1\alpha_2}}{2\gamma} \\
\alpha_2^* &= \frac{(A(\alpha_1+\alpha_2)+\alpha_1\alpha_2) + \sqrt{(A(\alpha_1+\alpha_2)+\alpha_1\alpha_2)^2 - 4\gamma A\alpha_1\alpha_2}}{2\gamma} \\
\beta^* &= \left(\alpha_2^* - \frac{A\left(\beta\alpha_1 + (1-\beta)\alpha_2\right)}{\gamma}\right)\frac{1}{\alpha_2^* - \alpha_1^*} \\
\gamma &= A + \beta\alpha_1 + (1-\beta)\alpha_2 \\
A &= \frac{1-C}{C} \quad .
\end{aligned} \tag{3.110}$$

For the Carlvik Two-Term Rational Approximation with $\alpha_1 = 2$, $\alpha_2 = 3$, and $\beta = 2$, these parameters simplify to

$$\begin{aligned}
\alpha_1^* &= \frac{5A + 6 - \sqrt{A^2 + 36A + 36}}{2A+2} \\
\alpha_2^* &= \frac{5A + 6 + \sqrt{A^2 + 36A + 36}}{2A+2} \\
\beta^* &= \frac{\alpha_2^* - \frac{A}{A+1}}{\alpha_2^* - \alpha_1^*} \quad .
\end{aligned} \tag{3.111}$$

3.6.4 Computation of the Dancoff Factor

To this point, the Dancoff factor has been defined as augmenting the probability that a neutron born in the fuel next collides in some fuel region. The definition of the Dancoff factor in Eq. (3.67) can be applied to a computational procedure directly. First, this equation is transformed such that it contains the collision probabilities $P^{f\to F}$ and $P^{f\to f}$:

$$\tilde{C}(E) = \frac{P^{f\to F}(E) - P^{f\to f}(E)}{1 - P^{f\to f}(E)}. \tag{3.112}$$

These collision probabilities can be determined using a transport solver. To see this, consider the collision probability formulation

$$\Sigma^f(E)\phi(E)V^f = \sum_{f' \in F} P^{f' \to f}(E) S^{f'}(E) V^{f'} + P^{M \to f}(E) S^M(E) V^M \tag{3.113}$$

and set the source in the moderator to zero. If all fuel regions have the same cross section and source and the reciprocity relation of Eq. (3.62) is used, this simplifies to

$$\Sigma^f(E)\phi(E) = \sum_{f' \in F} P^{f \to f'}(E) S^f(E) = P^{f \to F}(E) S^f(E) \quad . \tag{3.114}$$

Thus, by solving a very simple, purely absorbing, fixed source transport equation where $S^f(E)$ is set to a known value and $S^M(E) = 0$, the collision probability $P^{f \to F}$ can be determined:

$$P^{f \to F}(E) = \frac{\Sigma^f(E)\phi(E)}{S^f(E)} \quad . \tag{3.115}$$

$P^{f \to f}$ can be determined in the same manner simply by changing the geometry to include only a single fuel lump in isolation. Because only the flux in the fuel lump is desired, the materials outside the lump are not important, nor are the boundary conditions. If the flux for the isolated case is notated as ϕ^0 and for the lattice case as ϕ^1, then the Dancoff factor is

$$\tilde{C}(E) = \frac{\phi^1(E) - \phi^0(E)}{S^f(E)/\Sigma^f(E) - \phi^0(E)} \quad . \tag{3.116}$$

This procedure, unfortunately, can be difficult, particularly with large cross sections. Fortunately, another approach has been seen to be more successful. This alternate approach is often called the Neutron Current Method [15], and it involves placing the source in the moderator rather than the fuel. Rearranging Eq. (3.68), another formula for the Dancoff factor is obtained:

$$\tilde{C}(E) = \frac{P_{esc}(E) - P^{f \to M}(E)}{P_{esc}(E)} \quad . \tag{3.117}$$

As in the previous method, these collision probabilities can be determined through the solution of a simple transport problem. Start again with Eq. (3.113), but this time set the fuel source to zero. The reciprocity relation is applied, which leads to

$$\Sigma^f(E)\phi(E) = P^{f \to M}(E) S^M(E) \frac{\Sigma^f(E)}{\Sigma^M(E)} \quad . \tag{3.118}$$

The collision probability $P^{f \to M}$ is thus

$$P^{f \to M}(E) = \frac{\Sigma^M(E)\phi(E)}{S^M(E)} \quad . \tag{3.119}$$

The escape probability can be computed similarly, by changing the geometry to that of an isolated fuel lump. To perform this calculation directly, a very large region of moderator would be needed. However, by noting that only the ratio Σ^M/S^M influences the collision probability, one can set the moderator cross section to a large value, adjusting the source accordingly, to allow for a much smaller region of moderator in the solution. (Note, though, that the value of Σ^M does influence the solution of the lattice system, and so must not be changed there.) If the flux for the isolated system is $\phi^0(E)$ and that of the lattice system is $\phi^1(E)$, and assuming the ratio Σ^M/S^M is maintained in both solutions, the Dancoff factor is obtained via the simple formula

$$\tilde{C}(E) = \frac{\phi^0(E) - \phi^1(E)}{\phi^0(E)} \quad . \tag{3.120}$$

In both of these formulations, the gray Dancoff factor $\tilde{C}(E)$ was shown. For the black Dancoff factor, the fuel cross section is simply set to a large value, and the transport solutions require only a single energy point. For both formulations, the flux ϕ^1 can be computed for all fuel regions in a single lattice calculation. The flux ϕ^0 needs to be computed for each unique fuel shape.

3.7 Embedded Self-Shielding Method

A recent extension of equivalence in dilution methods is known as the Embedded Self-Shielding Method (ESSM) [16, 17]. It recognizes that although equivalence in dilution seeks an equivalence between heterogeneous and homogeneous models, the parameters at which this equivalence holds are difficult to determine *a priori*. Instead, ESSM iterates between a heterogeneous model and a homogeneous model until equivalence is obtained.

The homogeneous model is the equivalent homogeneous problem for a two-region fuel-moderator system, as previously encountered in Sec. 3.2. The source in the fuel is left as a generic S^F in this discussion. An intermediate resonance source or true slowing down source can be used. The form of this equation is

$$\left(\Sigma^F(E) + \Sigma_{eq}\right)\phi^F(E) = S^F(E) + \frac{\Sigma_{eq}}{E} \quad , \tag{3.121}$$

where Σ_{eq} is assumed to be constant in energy. As previously discussed, this is equivalent to assuming the fuel to moderator probability is well-represented by a one-term rational approximation. This homogeneous problem is integrated over energy to attain the multigroup form:

$$\left(\Sigma_g^F + \Sigma_{eq,g}\right)\phi_g^F = S_g^F + \Sigma_{eq,g}\Delta u_g \quad , \tag{3.122}$$

where the subscript g is added to $\Sigma_{eq,g}$ to indicate that it only needs to be group-wise constant for this method and S_g^F is simply $S^F(E)$ integrated over the energy group bounds. This equation,

solved for $\Sigma_{eq,g}$, takes the form

$$\Sigma_{eq,g} = \frac{\Sigma_g^F \phi_g^F - S_g^F}{\Delta u_g - \phi_g^F} \quad . \tag{3.123}$$

The heterogeneous model is simply a fixed-source, purely absorbing multigroup neutron transport equation using the geometry of interest. The sources are set to be consistent with the homogeneous model. For fuel regions, the fixed source is set to be S_g^F; for moderator regions it is set to $\Sigma^M \Delta u_g$. The general form of this model is

$$\hat{\Omega} \cdot \nabla \psi_g(\vec{r}, \hat{\Omega}) + \Sigma_g(\vec{r}) \psi_g(\vec{r}, \hat{\Omega}) = \frac{1}{4\pi} \cdot \begin{cases} S_g^F(\vec{r}) & \vec{r} \in F \\ \Sigma_g(\vec{r}) \Delta u_g & \vec{r} \in M \end{cases} \quad . \tag{3.124}$$

The mechanics of the ESSM procedure are as follows:

1. $\Sigma_{eq,g}$ is guessed.
2. Σ_g^F is determined from homogeneous look-up tables using $\Sigma_{eq,g}$.
3. The heterogeneous model of Eq. (3.124) is solved using Σ_g^F to determine ϕ_g^F.
4. ϕ_g^F is inserted into the homogeneous model of Eq. (3.123) to obtain an updated $\Sigma_{eq,g}$.
5. Unless converged, return to step 2.

Convergence can, of course, be measured on a variety of metrics, but ensuring convergence on the cross section Σ^F is the most sensible, as this is the quantity that will be used in subsequent calculations.

Note that this procedure includes all nuclides in the fuel together in the calculation for $\Sigma_{eq,g}$, as this is primarily a geometric parameter. When obtaining Σ_g^F from the homogeneous look-up table, the nuclides are treated separately and combined as

$$\Sigma_g^F = \sum_i N^i \sigma_g^i \left(\sigma_b + \frac{\Sigma_{eq,g}}{N^i} \right) \quad , \tag{3.125}$$

where i denotes the nuclide. Similarly, the source in the fuel contains components from each nuclide. This is straightforward with the narrow resonance model, where the scattering source is given by Σ_p / E, and thus the multigroup combined source is

$$S_g^F = \Delta u_g \sum_i N^i \sigma_p^i \quad . \tag{3.126}$$

However, this treatment is problematic with the the intermediate resonance model. In literature, the scatter source for each nuclide is given as $\lambda \Sigma_p / E + (1 - \lambda) \Sigma_s \phi$ and a summation is

performed:

$$S_g^F = \Delta u_g \sum_i \lambda^i N^i \sigma_p^i + \phi \sum_i (1-\lambda^i) N^i \sigma_s^i \quad . \tag{3.127}$$

The problem with this form is that λ is not well-defined for a system with multiple resonant nuclides. λ models how neutrons scatter with respect to the resonances of a single nuclide, adjusting the effective background cross section that nuclide sees. With multiple resonant nuclides, λ must be chosen to be some representative value for each nuclide for the formulation of this source. This is discussed further in Sec. 8.4.

3.7.1 Heterogeneous Tables

The Embedded Self-Shielding Method has been adapted from its original publications to use small heterogeneous geometries in the table rather than homogeneous tables. These tables are generated by solving a suite of small problems with an ultrafine method. These small problems could also be solved by Monte Carlo or some other fine-energy treatment. Typically unit cell geometries are used. Several variables can be perturbed, including the amount of background moderator in the fuel material, the pin pitch, the pin radius, and the moderator density. The group-averaged cross sections are saved to the table as a function of the effective equivalence cross section, as computed from Eq. (3.123).

The mechanics of the ESSM procedure with heterogeneous tables are as follows:

1. $\Sigma_{eq,g}$ is guessed.
2. Σ_g^F is determined from heterogeneous look-up tables using $\Sigma_{eq,g}$.
3. The full heterogeneous model of Eq. (3.124) is solved using Σ_g^F to determine ϕ_g^F.
4. ϕ_g^F is inserted into the homogeneous model of Eq. (3.123) to obtain an updated $\Sigma_{eq,g}$.
5. Unless converged, return to step 2.

Note that in this process, the cross sections tabulated in the heterogeneous look-up table are potentially multi-valued. That is, a given value of $\Sigma_{eq,g}$ corresponds to more than one group-averaged cross section. This is because changing one variable, e.g., the pin diameter, can have the same effect on $\Sigma_{eq,g}$ as a change in another variable, e.g., the moderator density, despite having different collapsing spectra. Thus, the heterogeneous tables should be generated using as similar geometry and conditions as possible to the real calculation. Multiple heterogeneous tables may be needed if different pins and different conditions are present in the problem of interest.

3.8 Chapter Summary

In this chapter, equivalence in dilution methods were detailed. These methods relate a heterogeneous problem to an equivalent homogeneous problem, allowing cross sections generated in infinite medium calculations to be used directly in a lattice-level calculation.

For this to be possible, the equivalent infinite medium must consist of the fuel material and an admixed moderator with constant cross section. This can be a very good approximation when a rational approximation is used to model the fuel to moderator collision probability. This chapter provided rigorous derivations of the most common rational approximations and a discussion of their use.

The derivations of the rational approximations assumed that a fuel region was isolated. This is almost never the case in a real reactor calculation. Much more often, a repeated geometry is encountered. The Dancoff factor is defined as a correction factor to scale the fuel to moderator probability from a rational approximation to be appropriate in a lattice geometry.

Chapter 4

The Subgroup Method

4.1 Method Description

In the subgroup method [18, 19, 20]—also known as the multiband method—unlike with equivalence in dilution, the self-shielding calculation is performed on a heterogeneous geometry. Rather than finding an equivalent homogeneous problem, the heterogeneous problem can be used directly. Computational efficiency is maintained by a clever change of variables, allowing the integration over an energy group to use the cross section value as the independent variable, rather than the energy. The details are discussed next.

First, the subgroup method is usually formulated with a single resonant nuclide, here denoted with superscript $*$. All other nuclides are lumped into the background moderator, denoted with superscript +, whose cross sections are assumed to be constant across the energy group. The scattering kernel assumes isotropic scattering in the center of mass, and the flux is assumed to be isotropic enough that the scatter source can be treated as isotropic in the transport solution. The transport equation under these conditions is written as

$$\begin{aligned}\hat{\Omega}\cdot\nabla\psi(\vec{r},\hat{\Omega},E)+\left(\Sigma^{*}(\vec{r},E)+\Sigma^{+}(\vec{r})\right)\psi(\vec{r},\hat{\Omega},E)\\ =\frac{1}{4\pi}\int_{E}^{E/\alpha^{*}}\frac{\Sigma_{s}^{*}(\vec{r},E')\phi(\vec{r},E')}{(1-\alpha^{*})E'}\,\mathrm{d}E'+\frac{1}{4\pi}\int_{E}^{E/\alpha^{+}}\frac{\Sigma_{p}^{+}(\vec{r})\phi(\vec{r},E)}{(1-\alpha^{+})E'}\,\mathrm{d}E'\quad,\end{aligned}\tag{4.1}$$

where only a single background moderator nuclide is shown, but generalization to multiple requires only a summation over the nuclides.

Next, the scatter sources are approximated using the intermediate resonance model, discussed in Sec. 2.5.5. The background moderator's source is shown using the narrow resonance model, noting the hydrogen equivalence discussed in Sec. 2.5.6. Also, the macroscopic form of the flux is taken to be $1/E$ and invariant with position. All these approximations lead to the

simplified transport equation

$$\hat{\Omega}\cdot\nabla\psi(\vec{r},\hat{\Omega},E)+\left(\Sigma_a^*(\vec{r},E)+\Sigma^+(\vec{r})\right)\psi(\vec{r},\hat{\Omega},E) = \frac{1}{4\pi}\left(\lambda\frac{\Sigma_p^*(\vec{r})}{E}+(1-\lambda)\Sigma_s^*(\vec{r},E)\phi(\vec{r},E)+\frac{\Sigma_p^+(\vec{r})}{E}\right) \quad . \tag{4.2}$$

The wide resonance model term on the right hand side can be moved to the left hand side by assuming that not only the neutron energy is constant after the collision, but the angle also remains constant. Also, the equation is multiplied through by E and is cast in terms of lethargy rather than energy:

$$\hat{\Omega}\cdot\nabla\psi(\vec{r},\hat{\Omega},u)+\left(\Sigma_a^*(\vec{r},u)+\lambda\Sigma_s^*(\vec{r},u)+\Sigma^+(\vec{r})\right)\psi(\vec{r},\hat{\Omega},u)=\frac{1}{4\pi}\left(\lambda\Sigma_p^*(\vec{r})+\Sigma_p^+(\vec{r})\right) \quad . \tag{4.3}$$

This equation provides the basis for the subgroup method. The lethargy shape of the flux is influenced only by the value of the resonant nuclide's cross sections. Defining the intermediate resonance cross section as

$$\sigma_\lambda(u)=\sigma_a(u)+\lambda\sigma_s(u) \quad , \tag{4.4}$$

the transport equation can be written with functional dependences on σ_λ rather than u:

$$\hat{\Omega}\cdot\nabla\psi(\vec{r},\hat{\Omega},\sigma_\lambda^*)+\left(N^*(\vec{r})\sigma_\lambda^*+\Sigma^+(\vec{r})\right)\psi(\vec{r},\hat{\Omega},\sigma_\lambda^*)=\frac{1}{4\pi}\left(\lambda\Sigma_p^*(\vec{r})+\Sigma_p^+(\vec{r})\right) \quad . \tag{4.5}$$

Note that the functional dependence on σ_λ is matter of notation. The flux is still defined as a quantity per unit lethargy, not per unit cross section.

Now, consider the group-averaged intermediate resonance cross section:

$$\sigma_{\lambda,g}(\vec{r})=\frac{\int_g\sigma_\lambda(u)\phi(\vec{r},u)\,\mathrm{d}u}{\int_g\phi(\vec{r},u)\,\mathrm{d}u} \quad . \tag{4.6}$$

Because ϕ is dependent on lethargy only through the lethargy dependence of the cross section, these integrals can be transformed into integrals over the cross section value,

$$\sigma_{\lambda,g}(\vec{r})=\frac{\int_0^\infty\sigma_\lambda\phi(\vec{r},\sigma_\lambda)p_g(\sigma_\lambda)\,\mathrm{d}\sigma_\lambda}{\int_0^\infty\phi(\vec{r},\sigma_\lambda)p_g(\sigma_\lambda)\,\mathrm{d}\sigma_\lambda} \quad , \tag{4.7}$$

where $p_g(\sigma_\lambda)\mathrm{d}\sigma_\lambda$ is the probability the cross section takes a value between σ_λ and $\sigma_\lambda+\mathrm{d}\sigma_\lambda$ in energy group g. By integrating over the cross section measure in this manner, the integrals are effectively Lebesgue integrals, as opposed to the Riemann integrals appearing in Eq. (4.6).

Next, these integrals are approximated using numerical quadrature. For a given function

$f(\sigma_\lambda)$, a numerical quadrature N base points σ_n and weights w_n is given by

$$\int_0^\infty f(\sigma_\lambda)p(\sigma_\lambda)\,\mathrm{d}\sigma_\lambda \approx \sum_{n=1}^{N} w_n f(\sigma_n) \quad . \tag{4.8}$$

With this and defining the term ϕ_n as

$$\phi_n(\vec{r}) = \phi(\vec{r},\sigma_n) \quad , \tag{4.9}$$

the group-averaged cross section is

$$\sigma_{\lambda,g}(\vec{r}) = \frac{\sum_{n=1}^{N} w_n\sigma_n\phi_n(\vec{r})}{\sum_{n=1}^{N} w_n\phi_n(\vec{r})} \quad . \tag{4.10}$$

This form does not seem much different from a similar approach without transforming the integrals into integrals over cross section. However, the quantities $\sigma_\lambda(u)\phi(u)$ and $\phi(u)$ feature wild fluctuations as a function of the lethargy variable. As such, they require a great many base points in the quadrature to be accurately integrated. Such an approach is known as an ultrafine method because of this, and these methods are described further in Ch. 5. On the other hand $\sigma_\lambda\phi(\sigma_\lambda)$ and $\phi(\sigma_\lambda)$ are very smooth functions of the cross section variable. Thus, a numerical quadrature can be very accurate with many fewer base points.

Now, the subgroup method is presented succinctly. Given a quadrature $Q = \{w_n,\sigma_n\}$ for a specific nuclide, denoted $*$, a subgroup fixed source equation, given by

$$\hat{\Omega}\cdot\nabla\psi_n(\vec{r}) + \left(N^*(\vec{r})\sigma_n + \Sigma^+(\vec{r})\right)\psi_n(\vec{r}) = \frac{1}{4\pi}\left(\lambda\Sigma_p^*(\vec{r}) + \Sigma_p^+(\vec{r})\right) \quad , \tag{4.11}$$

is solved to obtain the scalar subgroup flux ϕ_n. Then, the group-averaged cross section is obtained by inserting the quadrature and these fluxes into

$$\sigma_{\lambda,g}(\vec{r}) = \frac{\sum_{n=1}^{N} w_n\sigma_n\phi_n(\vec{r})}{\sum_{n=1}^{N} w_n\phi_n(\vec{r})} \quad . \tag{4.12}$$

This procedure is repeated for each resonant nuclide. In this form, the subgroup method assumes there are no resonance overlap effects. Resonance interference without overlap can be modeled as in Sec. 2.6, and it is described in Sec. 8.2.3.

Two difficulties arise in using the subgroup method as defined here. First, the quadrature $Q = \{w_n,\sigma_n\}$ is not easily defined. Many of the options for this quadrature are presented in

Sec. 4.2. Second, this process only yields the group-averaged cross section $\sigma_{\lambda,g}$, but not any partial cross sections for other desired reactions. Methods for determining these cross sections are presented in Sec. 4.3.

4.2 Quadrature Generation

4.2.1 Direct Method

One method for defining the subgroup quadrature is known as the direct method or the direct subgroup method. Oftentimes, use of the term "subgroup" implies use of probability tables, as described in the subsequent sections. However, the direct method fits into the definition of the methods of Sec. 4.1, and so is included as a subgroup method here.

In the direct method, explicit energy or lethargy intervals for each subgroup level are defined. A subgroup level corresponds to a specific range of cross section values, given by $[\sigma_{n,\min}, \sigma_{n,\max})$. The cross section used in the quadrature is the continuous energy cross section collapsed across the disjoint lethargy range defined by this cross section interval. Equivalently, defining an indicator function $\mathcal{H}_n$ as

$$\mathcal{H}_n(u) = \begin{cases} 1 & \sigma_{n,\min} \leq \sigma(u) < \sigma_{n,\max} \\ 0 & \text{otherwise,} \end{cases} \tag{4.13}$$

the cross section is a group collapse in which the integrands are multiplied by the indicator function:

$$\sigma_n = \frac{\int_g \sigma(u)\phi(u)\mathcal{H}_n(u)\,\mathrm{d}u}{\int_g \phi(u)\mathcal{H}_n(u)\,\mathrm{d}u} \quad . \tag{4.14}$$

The weights are correspondingly defined as

$$w_n = \frac{\int_g \phi(u)\mathcal{H}_n(u)\,\mathrm{d}u}{\int_g \phi(u)\,\mathrm{d}u} \quad . \tag{4.15}$$

Figure 4.1 shows a conceptual illustration of defining the energy interval based on the cross section value. The subgroup method is sometimes referred to as the "multiband" method, and the cross section interval defining each level is known as a band. This terminology is used in the illustration.

Two issues clearly arise in defining the quadrature in this manner. First, the cross section interval defining a subgroup level is a free parameter. The cross section values defining the boundaries of subgroup levels within a group—and even the number of levels—should be selected in such a way as to minimize the error that this approach imposes. This should be done by comparing cross sections obtained with this approach to those obtained by a reference

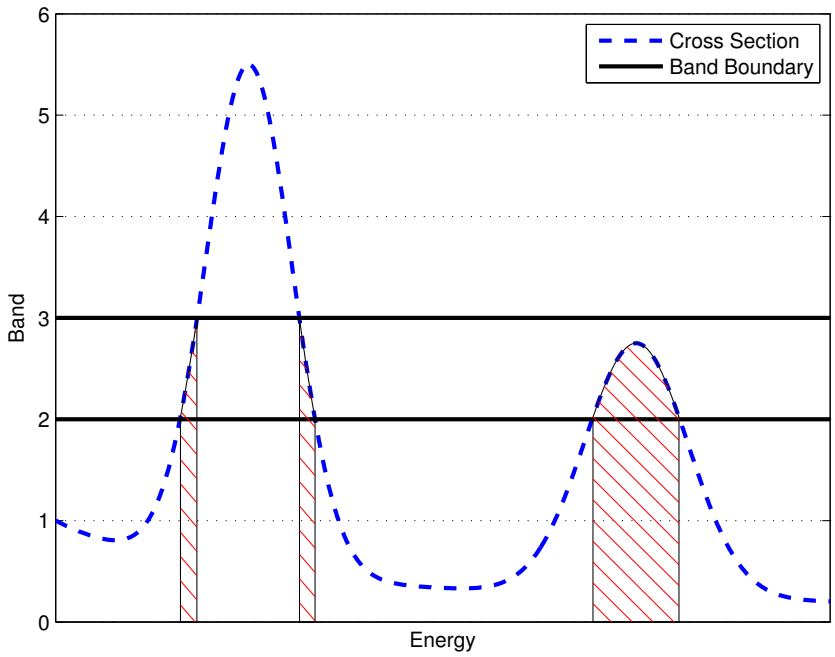

Figure 4.1: A conceptual illustration of the direct subgroup method, reproduced from [21].

solution. Reference solutions should be for problems in which analytic or numerical continuous energy solutions can be obtained. Typically, very simple problems are chosen, such as infinite media or simple pin-cell configurations. However, this process is ultimately one that can vary from implementation to implementation and perhaps even problem to problem.

The second issue is that the quadrature points and weights both depend upon the flux $\phi(u)$ of the system. This is not a known quantity; in fact, the self-shielding calculation, of which the subgroup method itself is an example, is intended to approximate this quantity. Thus, including a dependence on the quantity seems to be a large issue. However, as discussed in Sec. 4.1, the flux as a function of lethargy is a function of only the cross section for the simplified problem solved in the subgroup method. Thus, for relatively small cross section intervals, the flux is not likely to vary much. Certainly, the flux will not exhibit the same wild fluctuations encountered if the entire energy group were to be included by itself. That said, the flux will still exhibit some sort of variation. This is most easily accounted for using equivalence in dilution methods, noting that only a coarse approximation is needed. The escape cross section need not be rigorously calculated; a simple guess will suffice for most applications. For additional accuracy, an iterative scheme similar to ESSM but for multiple cross section levels has been proposed by Yamamoto [22, 23].

4.2.2 Physical Probability Tables

The method of physical probability tables is another method to define the subgroup quadrature. It removes the explicit energy range associated with each subgroup level; instead, weights and quadrature points are defined based on minimizing error associated with using the subgroup method on a set of reference problems. The term "probability table" arises because the quadrature weight is analogous to a probability that a neutron in the energy group falls in the corresponding subgroup level.

Fitting Multigroup Constants

One method for generating physical probability tables—or fit-based subgroup quadratures—is to perform a least squares fitting procedure on multigroup constants—either cross sections or effective resonance integrals.

First, a set of reference solutions are created. These are multigroup constants obtained by solving some configuration either analytically or numerically using continuous energy cross sections. Most commonly, infinite media are used as the configuration references; in this case, the reference solutions are simply entries in the multigroup nuclear data tables for difference background cross section values. Alternatively, other simple geometries, such as pin-cell configurations, can be used [24]. In any case, the reference solution configurations should span the parameter space expected in later simulations. Let the reference solutions for configuration k be given as $I_{g,k}$ or $\sigma_{g,k}$ for effective resonance integrals or group cross sections, respectively.

Next, approximate effective resonance integrals or cross sections are defined. These quantities are functions of the subgroup quadrature $Q = \{w_n, \sigma_n\}$ and of the configuration. Let them be notated $\tilde{I}_{g,k}$ and $\tilde{\sigma}_{g,k}$, and they are defined as

$$\tilde{I}_{g,k}(Q) = \sum_{n=1}^{N} w_n \sigma_n \phi_k(\sigma_n) \tag{4.16}$$

$$\tilde{\sigma}_{g,k}(Q) = \frac{\sum_{n=1}^{N} w_n \sigma_n \phi_k(\sigma_n)}{\sum_{n=1}^{N} w_n \phi_k(\sigma_n)} \quad . \tag{4.17}$$

Note that these definitions require knowledge of the flux in configuration k as a function of the cross section. This flux should be consistent with the flux solution in the references. For infinite medium configurations in which the reference solutions were computed with the intermediate resonance model—or equivalently, the narrow or wide resonance models—the relationship is

analytic:

$$\phi_k(\sigma_n) = \frac{\sigma_{b,k} + \lambda\sigma_p}{\sigma_{b,k} + \sigma_n} \quad , \tag{4.18}$$

where $\sigma_{b,k}$ is the background cross section for configuration k and σ_n has previously been defined as some value of the derived cross section quantity $\sigma_a + \lambda\sigma_s$. For other more complicated reference configurations, the flux must either be tabulated or approximated.

The quadrature is then obtained by a fitting procedure. Generally, the error in some norm is minimized for all reference configurations. The choice of norm varies among implementations, but the most common is the 2-norm for relative error, equally weighting each configuration. Then, this is a non-linear least squares procedure. The quadrature is then given by

$$Q = \arg\min_{Q'} \sum_k \left(\frac{I_{g,k} - \tilde{I}_{g,k}(Q')}{I_{g,k}} \right)^2 \tag{4.19}$$

$$Q = \arg\min_{Q'} \sum_k \left(\frac{\sigma_{g,k} - \tilde{\sigma}_{g,k}(Q')}{\sigma_{g,k}} \right)^2 \quad . \tag{4.20}$$

Constraints are imposed on this procedure. For instance, the weights must sum to unity. Many other constraints are possible and vary by implementation. Such constraints include forcing the weights to be positive, preserving the infinite dilute cross section exactly, and the quadrature points being limited to some range.

Fitting Background Cross Section Curve

Another fit-based quadrature generation technique is described in detail in [9]. With this method, rather than performing a fitting procedure on the subgroup quadrature directly, a fitting procedure is performed on the curve of the multigroup cross section as a function of the background cross section level. Then, a quadrature is generated that can represent the points on this curve exactly, and this is used as the subgroup quadrature. The details of this generation process are not detailed in this thesis, but are spelled out in detail in the literature.

4.2.3 Mathematical Probability Tables

The method of mathematical probability tables is the final method of subgroup quadrature generation detailed here. With this method, a set of cross section moments are preserved in the selection of the quadrature. Unlike with physical probability tables, results are not compared to reference configurations. The term “mathematical probability tables” arises due to the quadrature generation involving only mathematical constructs, as opposed to using results from calculations modeling the physics. The presentation here parallels that of [9, 25]. The method itself was proposed originally by [26].

The lth cross section moment in the gth energy group is defined as

$$M_l = \int_g \sigma(u)^l \, \mathrm{d}u \quad . \tag{4.21}$$

The approximation to this cross section moment using the subgroup method with quadrature $Q = \{w_n, \sigma_n\}$ is

$$\tilde{M}_l(Q) = \sum_{n=1}^{N} w_n \sigma_n^l \quad . \tag{4.22}$$

The quadrature Q is chosen such that M_l and $\tilde{M}_l$ are equivalent for a set of values of l. The constraint $\sum_{n=1}^{N} w_n = 1$ is needed to ensure the weights are consistent with the definitions of the subgroup method. This is equivalent to preserving the 0th moment. This constraint removes one degree of freedom, leaving $2N-1$ unknowns. Thus, $2N-1$ other moments can be preserved.

The most common choice of moments is integer moments ranging from 1 to $2N-1$. However, there is little physics involved in preserving very high order moments. In work by [25], it was suggested that fractional moments between -1 and 0 were perhaps better choices. The -1st moment corresponds to the flux of a fully-shielded configuration. The 0th moment corresponds to the $1/E$ flux encountered in an entirely unshielded configuration. Thus, moments in between these two extremes can be interpreted as intermediate shielding states.

The quadrature can be determined by choosing the moments to preserve and solving the resulting set of nonlinear equations. However, solving a large number of nonlinear equations is not easy in general. Fortunately, a systematic procedure for the moment problem exists. Here, the procedure for conserving integer moments ranging from 0 to $2N-1$ will be shown. It is easily adaptable to other consecutive integer moments, including negative moments, and is even extendible to fractional moments.

Consider the following functional form:

$$F(z) = \sum_{l=0}^{2N-1} z^l M_l \quad . \tag{4.23}$$

Because this function only includes moments preserved by the quadrature generation process, the moments can be replaced by Eq. (4.22). The function can then be rewritten as

$$F(z) = \sum_{l=0}^{2N-1} z^l \sum_{n=1}^{N} w_n \sigma_n^l = \sum_{n=1}^{N} w_n \sum_{l=0}^{2N-1} z^l \sigma_n^l \quad . \tag{4.24}$$

Recognizing the sum over l as the first $2N$ terms in a Taylor expansion, $F(z)$ can be approximated as

$$F(z) = \sum_{n=1}^{N} \frac{w_n}{1 - z\sigma_n} + O(z^{2N}) \quad . \tag{4.25}$$

This form is a simple relation between $F(z)$ and the subgroup quadrature, which is at this point unknown. Next, $F(z)$ will be considered in terms of known quantities and compared back to this form to find the quadrature.

Consider the form of Eq. (4.23) once again. This equation can be approximated to a high degree of accuracy with a Padé approximation:

$$F(z) = \frac{a_0 + a_1 z + \ldots + a_{N-1} z^{N-1}}{1 + b_1 z + \ldots + b_N z^N} + O(z^{2N}) \quad . \tag{4.26}$$

Setting this equal to Eq. (4.23) and multiplying both sides by the denominator, this is

$$\sum_{i=0}^{N-1} a_i z^i = \left(1 + \sum_{j=1}^{N} b_j z^j\right)\left(\sum_{l=0}^{2N-1} z^l M_l\right) + O(z^{2N}) \quad . \tag{4.27}$$

Collecting terms with like powers of z up to order $2N-1$ gives

$$z^0 : \quad a_0 = M_0 \tag{4.28}$$

$$z^1 : \quad a_1 = M_1 + M_0 b_1 \tag{4.29}$$

$$\vdots$$

$$z^{N-1} : \quad a_{N-1} = M_{N-1} + M_{N-2} b_1 + \ldots + M_0 b_{N-1} \tag{4.30}$$

$$z^N : \quad 0 = M_N + M_{N-1} b_1 + \ldots + M_0 b_N \tag{4.31}$$

$$z^{N+1} : \quad 0 = M_{N+1} + M_N b_1 + \ldots + M_1 b_N \tag{4.32}$$

$$\vdots$$

$$z^{2N-1} : \quad 0 = M_{2N-1} + M_{2N-2} b_1 + \ldots + M_{N-1} b_N \quad . \tag{4.33}$$

The equations for terms $z^N, \ldots, z^{2N-1}$ are a linear system for the vector of b coefficients that is easily solved. After the b coefficients are found, another linear system for a could be solved, but this is not necessary for the technique shown here.

Once the b coefficients are known, the denominator of Eq. (4.26) is factored into

$$1 + b_1 z + \ldots + b_N z^N = \prod_{j=1}^{N} (z - z_j) \quad . \tag{4.34}$$

Then, Eq. (4.26) can be written

$$F(z) = \frac{a_0 + a_1 z + \ldots + a_{N-1} z^{N-1}}{\prod_{j=1}^{N} (z - z_j)} + O(z^{2N}) \quad . \tag{4.35}$$

A partial fraction expansion is performed, yielding

$$\begin{aligned} F(z) &= \sum_{n=1}^{N} \frac{c_n}{z - z_n} + O(z^{2N}) \\ &= \sum_{n=1}^{N} \frac{\tilde{c}_n}{1 - z/z_n} + O(z^{2N}) \quad , \end{aligned} \tag{4.36}$$

which is of the same form as Eq. (4.25). By inspection, the quadrature is given by

$$w_n = \tilde{c}_n \quad \forall n \tag{4.37}$$

$$\sigma_n = \frac{1}{z_n} \quad \forall n \quad . \tag{4.38}$$

In practice, the partial fraction expansion does not need to be performed. The quadrature base points can be found during the factorization from Eq. (4.34). Once the base points are found, the weights can be found by solving the simple linear system

$$M_l = \sum_{n=1}^{N} w_n \sigma_n^l \quad . \tag{4.39}$$

The matrix involved in this linear system is a van der Monde matrix, which has an analytic inverse. Alternatively, a numerical solution is very straightforward.

4.3 Partial Cross Sections

Up to this point, discussion has been related to determining the primary cross section needed to solve the subgroup fixed source equations to determine the subgroup level fluxes. If the narrow resonance model is used, this is the total cross section. With the intermediate resonance model, this cross section is the derived cross section $\sigma_\lambda = \sigma_a + \lambda\sigma_s$. However, in the generation of multigroup cross sections for downstream applications, the full gambit of partial cross sections are needed.

Two options are possible. First, for a true subgroup approach, quadratures can be determined for the partial cross sections. Second, for a hybrid subgroup-equivalence approach, a reverse table lookup method can be used.

4.3.1 Partial Cross Section Quadratures

After a quadrature for the primary cross section has been generated, secondary quadratures for each desired partial cross section can be generated. During this process, it must be ensured that the subgroup levels for the partial cross sections correspond to those of the primary cross

section. This is because the subgroup fixed source equations are solved only for the primary cross section, and the resulting flux must be able to be used in the collapsing of the partial cross sections. This is typically accomplished by holding the weights constant between the two quadratures. For probability table methods, the weight is an analogue to the discontiguous energy range that would be attained in a direct subgroup approach, and this ensures the base points are essentially average values of the cross section for these energy ranges.

In a fitting method, reference values of the partial cross section are generated as $\sigma_{\rho,g,k}$ for configuration k. The approximate cross section attained via the subgroup method is

$$\tilde{\sigma}_{\rho,g,k}(Q_\rho, Q_0) = \frac{\sum_{n=1}^{N} w_n \sigma_{\rho,n} \phi_k(\sigma_n)}{\sum_{n=1}^{N} w_n \phi_k(\sigma_n)} \quad , \tag{4.40}$$

where Q_ρ is quadrature for the partial cross sections and Q_0 is the previously determined quadrature of the primary cross section. The flux used in the fitting process is the same as that in the generation of the primary cross section:

$$\sigma_k(\sigma_n) = \frac{\sigma_{b,k} + \lambda \sigma_p}{\sigma_{b,k} + \sigma_n} \quad . \tag{4.41}$$

Then, the base points for the partial cross section quadrature as obtained via

$$Q_\rho = \underset{Q'_\rho : Q_0}{\arg\min} \sum_k \left(\frac{\sigma_{\rho,g,k} - \tilde{\sigma}_{\rho,g,k}(Q'_\rho, Q_0)}{\sigma_{\rho,g,k}} \right)^2 \quad . \tag{4.42}$$

This process can, of course, be performed with effective resonance integrals rather than group cross sections. The straightforward transformation is omitted from this discussion. In this process, additional constraints can be placed upon the optimization routine, such as ensuring the partial cross sections sum to the total cross section for each reference problem. One implementation of such a fitting procedure is described in [27].

In a moment method, partial cross section moments can be defined as

$$M_{\rho,l} = \int \sigma_\rho(E) \sigma^l(E) \, \mathrm{d}E \quad . \tag{4.43}$$

The approximate partial moments using the subgroup quadrature are

$$\tilde{M}_{\rho,l}(Q_\rho, Q_0) = \sum_{n=1}^{N} w_n \sigma_{\rho,n} \sigma_n^l \quad . \tag{4.44}$$

Because there are N unknowns, N partial moments can be conserved. The definition of the partial moments was chosen such that finding the partial cross section base points can be

accomplished by a straightforward linear solve.

Although these methods are similar to their counterparts in the quadrature generation for the primary cross section, it is not strictly necessary to use the same method for both the primary cross section and the partial cross sections. One could use a fitting method for the primary cross section but a moment method for the partial cross sections. However, this is rarely done in practice.

Finally, note that the quadrature generated in this manner does not necessarily correspond exactly to that of the primary cross section. Even in holding the weights constant, a possibly problematic quadrature for the partial cross section can be thought of as shifting the energy range slightly while maintaining the same integrals over the energy range. This is in general a small effect, but care must be taken to ensure the resulting quadratures maintain a fair amount of accuracy. If the desired accuracy is not attained, one can refine the coarse energy group structure or use a correlation matrix for the partial cross sections, similar to the matrix quadrature described in Sec. 8.2.4 and described in [28].

4.3.2 Reverse Table Lookup

Another option for the generation of partial cross sections is to employ a reverse table lookup procedure rather than generating a quadrature. In the context of the moment method, this is often referred to as the Sanchez-Coste approach [28], but it is can be applied to fitting methods just as easily. By this method, a table of the cross section as a function of the background cross section is generated. This can be in the form homogeneous tables or based on heterogeneous calculations in which the background cross section was inferred. Once the primary cross section is generated from the subgroup method, the table is queried to find the background cross section that corresponds to this primary cross section. That background cross section is then used to pull partial cross sections from the table.

This method has the advantage that there is no lack of correlation concerns between the primary and the partial cross sections. However, it suffers from the fact that it still requires the two-region problem assumption from equivalence theory. The subgroup method's primary advantage over equivalence methods is its ability to model complex geometries natively, but the use of the reverse table method brings these issues back. However, this method has been found to be effective in practice and provides an option with much less complication than the partial cross section quadratures.

4.4 Reducing Computational Burden

In general, the subgroup method is associated with a considerably higher computational cost than equivalence in dilution methods, as it requires the solution of transport problems for each

subgroup level, whereas the equivalence-based methods require transport solutions only in the computation of the Dancoff factor. While it is unreasonable to expect subgroup methods to rival equivalence in dilution methods in terms of computational efficiency, there are some tricks that can be employed to reduce the computational burden.

One option is to enforce a condition that each coarse energy group have the same subgroup levels for a particular nuclide. A fitting process is then used to determine the weights for each group, which would be expected to vary from group to group. With this approximation, a subgroup fixed source equation must be solved for each of the global subgroup levels, but it avoids a loop over the coarse groups. In order to obtain sufficient accuracy, more levels per group may be needed, but by avoiding scaling with the number of groups, this still is a significant cost savings. In [29], a particular implementation of this procedure is shown.

Another common approach to reducing the computational burden is to solve the subgroup fixed source equations with a fast but perhaps less accurate neutron transport solver. One example found in literature is the use of the interface current method for these problems when the method of characteristics is used for the lattice physics computation [30]. In this method, simple collision probabilities are used on unit-cell problems, and these problems are coupled to each other through a response matrix. Similarly, an MOC formulation with fewer tracks and segments is possible. These methods provide a significant speed-up and have been found to give sufficient results on some test cases, but such approximation must be carefully managed to ensure it does not inject unwanted bias into the lattice physics calculation.

4.5 Chapter Summary

The subgroup method is used to provide fine-group cross sections to a lattice-level calculation and in recent years has been the most prevalent such method for new code development. It approaches the multigroup cross section generation process by integrating the integrated reaction rate and flux by the cross section value rather than by energy. This clever change of variables leads to a much smoother function, requiring many fewer base points in a numerical quadrature. However, the quadrature is not well-defined, and determining an appropriate quadrature is an arduous process.

Three classes of quadrature generation methods were presented: the direct method, fitting methods, and moment methods. The direct method defines explicit energy ranges for subgroup bands, which makes the definition of the quadrature very easy, but unfortunately leads to a problem-dependent quadrature. Fitting methods compare subgroup approximations for cross sections on simple problems to reference solutions, usually those of the homogeneous tables discussed in Ch. 2, and perform an optimization process for the best fit. Moment methods preserve mathematical constructs based on the cross section.

Chapter 5

Ultrafine Methods

5.1 Background

The goal of reactor physics calculations is to determine the reaction rates throughout the core of a nuclear reactor by solving the neutron transport equation as closely as possible. The steady-state transport equation with explicit scattering and a generic external source,

$$\hat{\Omega} \cdot \nabla \psi(\vec{r}, \hat{\Omega}, E) + \Sigma_t(\vec{r}, E)\psi(\vec{r}, \hat{\Omega}, E) = \int_{4\pi} \mathrm{d}\hat{\Omega}' \int_0^\infty \mathrm{d}E' \, \Sigma_s(\vec{r}, \hat{\Omega}' \to \hat{\Omega}, E' \to E)\psi(\vec{r}, \hat{\Omega}', E') + Q(\vec{r}, \hat{\Omega}, E) \quad , \tag{5.1}$$

is the workhorse of most simulations. Note that eigenvalue calculations, where Q is a function of ψ, use this form of the equation inside fission source iterations.

In approximating a solution to this equation by deterministic methods, the energy variable is often divided into relatively few bins, or energy groups, and great care must be taken in determining the nuclear data at each of these groups. The energy variable is complicated by the existence of large spikes known as resonances in the cross sections at certain energy values. These resonances lead to depressions in the flux, a phenomenon known as self-shielding, both in the energy and spatial variables. However, this self-shielding phenomenon is implicit when enough energy groups are used to resolve the shapes of the resonances in the nuclear cross sections. Spatial self-shielding effects also require sufficient resolution in the spatial and angular solution mesh to be captured implicitly.

Thus, a class of solution techniques to the transport equation known as *ultrafine methods*, in which either a great many very narrow energy groups or true continuous energy dependence is used in the solution, is considered to be the most accurate and flexible means of solution. Unfortunately, this corresponds to very high computational cost, as the number of degrees of freedom in the problem is greatly increased by using so many energy groups. Such a solution on a large problem is not feasible on today's computers. However, as computers are improving, ultrafine methods with certain convenient approximations can be injected more

and more into reactor physics calculations, allowing the field to move away from restricting legacy self-shielding approximations.

If ultrafine methods are seen as a means of generating few-group cross sections for a subsequent calculation, as opposed to being a standalone solution technique, they can be tuned for this purpose. Ultrafine methods can be restricted to the resolved resonance range, as this is the energy range where the methods have the most benefit. At higher energies, because the exact shape of the cross section is not known, using narrower groups does not benefit the solution. At thermal energies, standard energy group structures use narrow enough groups to resolve the effects of the important resonances that exist, and specialized ultrafine methods are not needed. Furthermore, using the ultrafine computation as a means of generating cross sections removes much of the need for coupling the resonance range to higher and lower energies, resulting in a simpler solution method.

5.2 Mechanics of Ultrafine Methods

5.2.1 Scatter Source

The typical method of modeling scattering in a deterministic reactor physics calculation is to use a group-to-group scattering matrix. This is not feasible for an ultrafine calculation, though, as the size of the matrix would be gigantic. Looping over elements in such a matrix would be cost prohibitive in itself, but the memory footprint of the matrix is the true limiting factor. Consider a scatter matrix for a material including hydrogen. Using 10,000 energy groups—a moderate number for ultrafine methods—results in approximately 50 million non-zero entries, requiring a whopping 400 MB to store in double precision. For a 100,000 energy group calculation, this balloons to 5 billion non-zero entries requiring 40 GB to store. Clearly, this is not a feasible tactic.

Fortunately, alternatives exist. In the resolved resonance range, elastic scattering dominates. Inelastic scattering is a threshold reaction that only occurs above resonant energies. For some isotopes, there may be a non-negligible incoming inelastic scatter source at resonance energies, but this is easily included in the external source. With elastic scattering off a stationary nucleus, the group-to-group transfer matrix can be easily computed on the fly, and the source in each group can be computed very efficiently. Although upscattering due to nuclear motion in the resonance range has been found to have a significant effect on the Doppler reactivity coefficient, this is neglected in this discussion.

The elastic scattering kernel has a convenient form for ultrafine calculations. Assuming isotropic scattering in the center of mass, the probability of scattering to a particular energy is

constant within the limits of physically allowable energies:

$$P(E' \to E) = \begin{cases} \dfrac{1}{E'(1-\alpha)} & \alpha E' < E < E' \\ 0 & \text{otherwise} \quad . \end{cases} \tag{5.2}$$

For a given spatial point, the scatter source from scattering off a given isotope is given by

$$Q_s^i(E) = \int_0^\infty \Sigma_s(E' \to E)\phi(E')\,\mathrm{d}E' = \int_0^\infty \Sigma_s^i(E')P(E' \to E)\phi(E')\,\mathrm{d}E' \quad . \tag{5.3}$$

Inserting the elastic scattering kernel, this scatter source becomes

$$Q_s^i(E) = \int_E^{E/\alpha} \frac{\Sigma_s^i(E')\phi(E')}{E'(1-\alpha)}\,\mathrm{d}E' \quad , \tag{5.4}$$

which depends on the energy E only through the bounds on the integral. This has two important implications for efficiently solving an ultrafine problem. First, no up-scattering appears in this equation, which means a single Gauss-Seidel sweep in energy will lead to an exact solution, with no energy iteration needed. Second, the loose dependence on E allows cumulative integrals, described subsequently, to be used to efficiently compute this source.

The integral in Eq. (5.4) can be rewritten as the difference of two integrals with the same integrand and the same upper bound E^*:

$$Q_s^i(E) = \int_E^{E^*} \frac{\Sigma_s^i(E')\phi(E')}{E'(1-\alpha)}\,\mathrm{d}E' - \int_{E/\alpha}^{E^*} \frac{\Sigma_s^i(E')\phi(E')}{E'(1-\alpha)}\,\mathrm{d}E' \quad . \tag{5.5}$$

If the upper bound energy is taken to be the largest energy in the problem—or equivalently, infinity—then these integrals can be interpreted as a cumulative integrals. That is, the integrals can be built by cumulatively adding contributions from each energy solved from the maximum energy down to the energy E. This is easily accomplished during a Gauss-Seidel sweep, and this allows the scatter source at each energy to be computed simply by subtracting two stored values. The algorithmic complexity using cumulative integrals for computing the scatter source is then $\Theta(g)$ where g is the number of groups or energy points, as opposed to the naive $\Theta(g^2)$ algorithm of simply numerically evaluating each integral when encountered.

The details of computing these cumulative integrals and the details of their use vary somewhat depending upon a few assumptions. In particular, the details vary most between ultrafine multigroup calculations and true continuous energy calculations. These details are discussed in the subsequent sections.

Note that this method does not require that cumulative integrals as a function of energy be stored explicitly. For instance, in the lattice physics code AEGIS [31], a single tally of the scatter source is kept. At each energy group, a new contribution to the integral is added and the contributions from higher energies than now possible are subtracted. The mechanics of

this technique varies slightly from that shown here, but it is in essence the same method.

All of the discussion in this section has been for scattering from a single isotope. In a mixture of several isotopes, the scatter source is simply a sum of the scatter source from each individual isotope. Number densities are implied in the use of macroscopic cross sections in this section. The maximum logarithmic energy decrement α is a function of the isotope, but the superscript i is omitted for notational simplicity. The total scatter source Q_s is simply

$$Q_s(E) = \sum_i Q_s^i(E) \quad . \tag{5.6}$$

Multigroup Forms

In the multigroup form of the neutron transport equation, the scatter source Q_{sg} is integrated over the bounds of energy group g,

$$Q_{sg} = \int_g Q_s(E)\,\mathrm{d}E \quad . \tag{5.7}$$

Considering a single isotope with only elastic scattering, Eq. (5.4) is inserted into this equation, leading to a scatter source of the form

$$Q_{sg}^i = \int_g \mathrm{d}E \int_E^{E/\alpha} \mathrm{d}E' \, \frac{\Sigma_s^i(E')\phi(E')}{E'(1-\alpha)} \quad . \tag{5.8}$$

This integral is quite complicated to evaluate using available multigroup data. For simplicity, here it is broken down into three components and each component is examined in turn. The superscript i and subscript s will be implied for the remainder of this discussion. The three components are in-group scatter Q_{gg}, scatter from full energy groups Q_{fg}, and scatter from partial groups Q_{pg}, with

$$Q = Q_{gg} + Q_{fg} + Q_{pg} \quad . \tag{5.9}$$

Full Groups First, consider scatter from full energy groups Q_{fg}. This component is the scattering due to groups higher than the destination group in which it is physically possible for any neutron energy from the scatter group to scatter to any energy in the destination group. This occurs when the upper bound of the scatter group is less than the maximum energy that can scatter to the bottom energy bound of the scatter group,

$$E_{g'} < \frac{E_{g+1}}{\alpha} \quad . \tag{5.10}$$

Then, the scatter source from these full groups is the summation of the scatter source from each of the groups,

$$Q_{fg} = \int_g \mathrm{d}E \sum_{g' \in fg} \int_{g'} \mathrm{d}E' \, \frac{\Sigma_s^i(E')\phi(E')}{E'(1-\alpha)} \quad . \tag{5.11}$$

Because only the group-averaged scatter cross section Σ_{sg}^i and the group-integrated flux ϕ_g are available in a multigroup calculation, the E' integral must be approximated. This is most easily accomplished by inserting group-averaged cross section into the equation with the group-averaged flux, given as the group-integrated flux divided by the width of the energy group,

$$\begin{aligned} Q_{fg} &\approx \int_g \mathrm{d}E \sum_{g' \in fg} \frac{\Sigma_{sg'}^i \phi_{g'}}{\Delta E_{g'}} \int_{g'} \mathrm{d}E' \, \frac{1}{E'(1-\alpha)} \\ &= \Delta E_g \sum_{g' \in fg} \frac{\Sigma_{sg'}^i \phi_{g'} \ln(E_{g'}/E_{g'+1})}{\Delta E_{g'}(1-\alpha)} \quad . \end{aligned} \tag{5.12}$$

Alternatively, the energy E' could also be held constant at some average value $\overline{E_g}$, which leads to a very similar approximation,

$$Q_{fg} \approx \Delta E_g \sum_{g' \in fg} \frac{\Sigma_{sg'}^i \phi_{g'}}{\overline{E_{g'}}(1-\alpha)} \quad . \tag{5.13}$$

In-Group Next, consider the in-group scatter source Q_{gg}. It is assumed that $E_{g+1}/\alpha > E_g$; that is, all neutrons that scatter in the group can lose at least as much energy as to reach the bottom of the group. The in-group scatter source can be written as

$$Q_{gg} = \int_g \mathrm{d}E \int_E^{E_g} \mathrm{d}E' \, \frac{\Sigma_s^i(E')\phi(E')}{E'(1-\alpha)} \quad . \tag{5.14}$$

As with the scatter from full energy groups, the group-average cross section and flux are pulled out of the integral as constants,

$$\begin{aligned} Q_{gg} &\approx \int_g \mathrm{d}E \, \frac{\Sigma_{sg}^i \phi_g}{\Delta E_g} \int_E^{E_g} \mathrm{d}E' \, \frac{1}{E'(1-\alpha)} \\ &= \frac{\Sigma_{sg}^i \phi_g}{\Delta E_g (1-\alpha)} \int_g \mathrm{d}E \, \ln \frac{E_g}{E} \\ &= \frac{\Sigma_{sg}^i \phi_g}{\Delta E_g (1-\alpha)} \left[E \ln \frac{E_g}{E} + E \right]_{E_{g+1}}^{E_g} \\ &= \frac{\Sigma_{sg}^i \phi_g}{(1-\alpha)} \left(1 - \frac{E_{g+1} \ln(E_g/E_{g+1})}{\Delta E_g} \right) \quad . \end{aligned} \tag{5.15}$$

Again, an alternative form comes from using an average energy value $\overline{E_g}$ as a constant and pulling that from the integral,

$$\begin{aligned} Q_{gg} &\approx \frac{\Sigma_{sg}^{i}\phi_g}{\Delta E_g \overline{E_g}(1-\alpha)} \int_g \mathrm{d}E\,(E_g - E) \\ &= \frac{\Sigma_{sg}^{i}\phi_g \Delta E_g}{2\overline{E_g}(1-\alpha)} \quad . \end{aligned} \tag{5.16}$$

This component is very small for ultrafine energy discretization. In AEGIS, this term is neglected altogether. Another approximation that is less drastic is to move this in-group component to the next group's source, so as to avoid source iteration.

Partial Groups Finally, consider the partial-group scatter source Q_{pg}. This is the scatter source due to groups that include energies greater than E_{g+1}/α. When using equal lethargy groups, there are two such groups, (A) the group that contains the point E_{g+1}/α and (B) the group that contains E_g/α. With equal lethargy groups, these two points cannot occur in the same group unless both points fall exactly on the boundary; in that case, the group can be treated as a group containing E_{g+1}/α. If groups have varying lethargy widths, there are two more possibilities, (C) a group can contain both extreme points on its interior and (D) there can exist groups that contain neither extreme point. For each of these four cases, rigorous integrals contributing to Eq. (5.8) can be written down:

$$Q_{pg,A} = \int_{E_{g+1}}^{E_g} \mathrm{d}E \int_{E_{g'+1}}^{E_{g+1}/\alpha} \mathrm{d}E' \, \frac{\Sigma_s^i(E')\phi(E')}{E'(1-\alpha)} + \int_{E_{g+1}/\alpha}^{E_{g'}} \mathrm{d}E' \int_{\alpha E'}^{E_g} \mathrm{d}E \, \frac{\Sigma_s^i(E')\phi(E')}{E'(1-\alpha)} \tag{5.17}$$

$$Q_{pg,B} = \int_{\alpha E_{g'+1}}^{E_g} \mathrm{d}E \int_{E_{g'+1}}^{E/\alpha} \mathrm{d}E' \, \frac{\Sigma_s^i(E')\phi(E')}{E'(1-\alpha)} \tag{5.18}$$

$$Q_{pg,C} = \int_{E_{g+1}}^{E_g} \mathrm{d}E \int_{E_{g'+1}}^{E_{g+1}/\alpha} \mathrm{d}E' \, \frac{\Sigma_s^i(E')\phi(E')}{E'(1-\alpha)} + \int_{E_{g+1}/\alpha}^{E_g/\alpha} \mathrm{d}E' \int_{\alpha E'}^{E_g} \mathrm{d}E \, \frac{\Sigma_s^i(E')\phi(E')}{E'(1-\alpha)} \tag{5.19}$$

$$Q_{pg,D} = \int_{E_{g'+1}}^{E_{g'}} \mathrm{d}E' \int_{\alpha E'}^{E_g} \mathrm{d}E \, \frac{\Sigma_s^i(E')\phi(E')}{E'(1-\alpha)} \quad . \tag{5.20}$$

Note that the order of integration had to be changed in some of these cases due to the bounds depending upon the integration variables. Each of these integrals can be approximated using the same methods as in the full group and in-group cases, but the final forms are omitted from this discussion. Instead, a possible approximation is to treat all partial groups as a single partial group with a form similar to that of case C of Eq. (5.19) with the group-averaged cross

sections and flux from the lowest energy partial group inserted as constants:

$$\begin{aligned} Q_{pg} &\approx \int_{E_{g+1}}^{E_g} \mathrm{d}E \, \frac{\Sigma^i_{sg'}\phi_{g'}}{\Delta E_{g'}(1-\alpha)} \int_{E_{g'+1}}^{E_{g+1}/\alpha} \frac{\mathrm{d}E'}{E'} + \int_{E_{g+1}/\alpha}^{E_g/\alpha} \mathrm{d}E' \, \frac{\Sigma^i_{sg'}\phi_{g'}}{\Delta E_{g'}(1-\alpha)E'} \int_{\alpha E'}^{E_g} \mathrm{d}E \\ &= \frac{\Delta E_g}{\Delta E_{g'}} \frac{\Sigma_{sg'}\phi_{g'}}{(1-\alpha)} \left[\ln \frac{E_{g+1}}{\alpha E_{g'+1}} + \frac{E_g}{\Delta E_g} \ln \frac{E_g}{E_{g+1}} - 1 \right] \quad . \end{aligned} \tag{5.21}$$

This is a very small quantity, so it is not hard to imagine that any approximation to it would not lead to any consequential errors. Thus, AEGIS takes this approximation one step further by treating each group as being defined by its average energy $\overline{E_g}$. If $\alpha\overline{E_{g'}} > \overline{E_g}$, then the group is neglected; otherwise, it is treated as a full scatter group.

In an ultrafine calculation, in order to resolve resonances with the energy discretization, the width of groups will tend to be much less than the scattering interval for even the heaviest of isotopes. Thus, when calculating the scatter source, the vast majority of contributing groups will be considered full groups. The sum in the full group scatter source form can be stored as a cumulative sum (analog of previously discussed integrals), and the width of the destination group can be multiplied on the fly. The in-group and partial group components can be computed for each group.

Continuous Energy Forms

The continuous energy form of the scatter source is much more straightforward. The complications of the second integral from the multigroup form do not exist, and the cumulative integral prescription is much more intuitively applied. However, there still are subtleties that must be carefully considered in this form.

In continuous energy calculations, cross sections are generally assumed to vary linearly between given points. Assuming the solution energy mesh is the same as the cross section energy mesh, this leads to flux values at each energy point, but there is not necessarily a correct interpretation for the shape between the flux points. In computing integrals, including that of the scatter source, some flux shape or quadrature rule must be applied.

The simplest method is to assume a simple quadrature rule, such as the trapezoid rule. Here, given two energy points with corresponding cross section values and flux values, the integral of the reaction rate is given by

$$\int_{E_1}^{E_2} \Sigma(E)\phi(E)\,\mathrm{d}E \approx \frac{1}{2}\left(\Sigma_1\phi_1 + \Sigma_2\phi_2\right)(E_2 - E_1) \quad . \tag{5.22}$$

Although this is likely the simplest option and offers a good degree of accuracy, there are of course many other options. Other quadrature rules are possible, but are not discussed here.

Another possibility is to assume a linear form of the flux and the cross section and to perform the integral analytically.

Regardless of the method taken, barring a one-sided Riemann sum quadrature, the integral of Eq. (5.4) will include a dependence on the flux at the energy point E. Because the flux is not known at that point *a priori*, this requires source iteration or an equivalent solution approach. Although the energy variable is not divided into groups in a continuous energy approach, this is equivalent to in-group scattering. As with the multigroup form, an easily defensible approximation is to move this "in-group" component into the source of the subsequent energy point, foregoing source iteration.

5.2.2 Starting Source

Any fixed source reactor physics calculation requires a specification of the fixed source in order to compute a non-zero flux for the problem. Ultrafine methods, which generally do not solve eigenvalue problems, therefore require some sort of fixed source specification. There are several options for such a source, and two of them are discussed here.

Fission Source

The first option is to use a fission source as the fixed source. An external source Q_{ext} is then defined as

$$Q_{ext}(\vec{r}, E) = \chi(E)\mathcal{R}_f(\vec{r}) \quad , \tag{5.23}$$

where χ is the fission spectrum of the material at the given point and $\mathcal{R}$ is the fission rate. Clearly, this requires knowledge of the spatial fission distribution. Note that because the ultrafine calculation is intended to generate a flux spectrum for cross sections, the absolute value of the fission rates are not important; only their relation to each other survives normalization in the cross section condensation process.

In a simple pin-cell calculation, $\mathcal{R}$ can be set to unity in the fuel region with minimal approximation. The mean free path of a neutron at fission energies is long enough that intra-pin specification of the fission source would not lead to any meaningful gains in accuracy. However, in larger calculations, such as that of a lattice, a fission distribution between pins is needed. This can come from a few-group multigroup calculation with approximate cross sections or can be estimated. If a multigroup calculation is used, it is even possible to turn this into an iterative procedure where ultrafine-calculation-generated cross sections are used in the determination of the spatial fission source, the fission source is piped back into another ultrafine calculation, and this iteration continues until convergence. Of course, such iteration requires multiple ultrafine calculations and so is a very expensive endeavor.

As discussed heretofore, ultrafine calculations generally are restricted to the resonance range and do not have the appropriate physics embedded for the fast range. Unresolved resonances and inelastic scattering are not easily modeled with these methods. Thus, starting from a fission source has the problem of inaccuracies in slowing down from neutron birth to the top of the resonance range.

1/E Source

Another option is to assume a $1/E$ flux with constant potential scattering above the energy range of interest. With this method, no external source is needed; the fixed source is built into the scatter source computation. If using cumulative integrals, this is accomplished by setting negative cumulative integrals at energies above the maximum energy in the problem, consistent with the potential scattering source.

This method has the advantage of separating broad energy groups in well-moderated systems, as information from one broad group only minimally impacts any other broad group outside of the $1/E$ scatter source it provides. By separating the broad groups into separate calculations, an inherent parallelism is achieved.

This method, like the fission source technique, suffers in that the strength of the source spatially is needed. The $1/E$ sources can be scaled spatially if such information is known, but this requires an auxillary few-group multigroup calculation or additional approximation. Note that the subgroup method, which assumes $1/E$ scatter sources, in its standard prescription, assumes the fluxes do not vary spatially in this $1/E$ range, and the only impact on the scatter source spatially comes from varying potential cross sections.

5.3 Existing Ultrafine Implementations

5.3.1 CENTRM

One existing implementation of ultrafine methods is the CENTRM continuous energy discrete ordinates code [32, 33]. CENTRM uses a cylindrical geometry in S_N with white boundary conditions as the spatial solver, and has recently been extended to include a 2-D MOC solver [34]. CENTRM models the energy variable to a very high degree of accuracy, including inelastic scattering and anisotropic scattering. This is made possible by what is called the submoment expansion.

The isotropic in center of mass elastic scattering kernel is able to be computed by cumulative integrals because it is a function only of the incoming energy aside from its energy bounds. The submoment expansion takes other scattering kernels, which do not have this property, and

expand the dependence on the outgoing energy in Legendre polynomials:

$$P(E \to E') \approx \sum_{l=0}^{L} f_l(E)\mathcal{P}_l(E') \quad , \tag{5.24}$$

where $\mathcal{P}_l$ is the lth Legendre polynomial and f_l the lth Legendre moment of the kernel.

With this expansion, each term $f_l(E)$ can be computed as a cumulative integral. Although the overhead associated with this expansion is quite large, this ensures the computation of the scattering kernel is still $\Theta(g)$. For very large numbers of energy groups or energy points as in CENTRM, this expansion leads to significant cost savings over a naive approach.

5.3.2 AEGIS

The Japanese lattice physics code AEGIS [35, 31] contains a 32,000-group ultrafine library. The ultrafine capabilities of the code are used on pin-cell calculations. The AEGIS code is a particularly good example of taking a complicated problem—in this case, the ultrafine discretization of the neutron transport equation—and making justified simplifications in a systematic manner.

First, a study was performed to demonstrate that for the problems of interest, anisotropy does not play a significant role. Thus, AEGIS uses only isotropic scattering. Next, it was shown that satisfactory accuracy could be achieved by using a two-region collision probability model rather than a complete MOC transport solution. This reduced the run time for a pin-cell from several hours to only seconds. Also, approximating the flux as $1/E$ in the moderator was shown not to heavily influence the solution, and this allowed for a factor of 2 reduction in runtime. Finally, rather than model each isotope and its respective scattering source explicitly, AEGIS lumps together isotopes with similar masses as a single isotope. Isotopes are split into categories including hydrogen, other light isotopes, mid-mass isotopes (fission products and structural materials), and heavy isotopes (actinides). This greatly reduces the cost of computing the scatter source for large numbers of isotopes. These approximations allow AEGIS to perform as a very efficient ultrafine code, although they do limit the applicability of it.

5.3.3 MC^2-3

The MC^2-3 code [36] developed by Argonne National Laboratory for fast reactor cross section generation is another existing ultrafine implementation. MC^2-3 takes an innovative approach of a two-level iterative scheme, which allows an eigenvalue calculation to be possible.

The finer energy mesh is known as the hyperfine mesh. This level contains 400,000 energy points, which is likely more than necessary to resolve resonance effects fully implicitly. This calculation inputs source information including the fission source and inelastic scattering

source from the coarser energy mesh. Thus, it is a fully implicit resonance calculation that can take into account the spatial distribution of power and reaction types that are not easily modeled on this fine of a structure. Following the solution of the hyperfine energy mesh, the obtained flux is used to collapse cross sections to the coarser mesh.

The coarser energy mesh is known as the ultrafine mesh, which contrasts with the meaning of the term in this thesis. This level contains approximately 2,000 energy groups complete with a full scattering matrix. At this level, all physics typically included in a multigroup solution is modeled, and an eigenvalue problem is solved. The spatial distribution of the fission source and the inelastic scattering source is fed back to the hyperfine energy mesh, and an iterative procedure is followed until convergence is obtained, usually in only a few iterations.

This procedure can in theory be performed on a variety of geometries, and it is not required that the two levels use the same geometry. However, this is a very costly process, as a single iteration of a 2,000 energy group problem with a full scatter matrix is itself difficult. Furthermore, it is complicated by an iteration scheme requiring the solution multiple times and a 400,000 energy point calculation alongside it. Thus, it is typically used for very small geometries.

5.3.4 RAZOR

The RAZOR code [37] developed at Bettis Atomic Power Laboratory takes a somewhat different approach to the ultrafine problem. RAZOR does not use the cumulative integral approach to computing the scatter source, but rather builds the scatter source for lower energy groups as it sweeps down in energy. This appears to be a $\Theta(g^2)$ approach, but clever implementation ensures that the computational burden is manageable for problems of interest. This scattering approach allows for the treatment of anisotropic scattering without difficulty.

The scatter sources are split into two buffers, a fine-structure buffer including energy groups close to the current group and a coarse-structure buffer for energy groups far away from the current group. This recognizes that the fine structure of the scatter source, including peaks due to resonances, is only significant for neutrons that scatter very small intervals in energy. Neutrons that scatter over larger intervals lead to scatter sources with little to no fine structure; in fact, this is the basis of the narrow resonance approximation, which assumes a scatter source that exhibits no fine structure behavior at all. Thus, a scattering event with a heavy isotope contributes primarily to the fine-structure buffer, but a scattering even with a light isotope (e.g., hydrogen) contributes in small part to the fine-structure buffer but in large part to the coarse-structure buffer. This avoids iterating over all lower energy groups during a scatter event, and ensures the scattering computation scales near linearly with the number of groups.

Furthermore, a coarse energy mesh, with only about 20 groups, is overlaid across the energy

regime. Inelastic scattering is treated only on this coarse mesh, and the resulting source is applied uniformly to the fine groups contained in the coarse group. Because inelastic scattering acts over a very large energy range, the outgoing energies do not exhibit much fine structure. Furthermore, the effect of inelastic scattering on the resonance range is very small. Thus, this approximation is deemed sufficient for these calculations.

5.4 Chapter Summary

Ultrafine methods account for resonance self-shielding effects by discretizing the energy variable enough to resolve the resonances directly. They typically are associated with too high a cost to be used on large geometries, but they can be used for multigroup cross section generation. It is becoming increasingly common for database-level calculations to be based on heterogeneous ultrafine calculations rather than infinite media. Researchers are currently striving to combine the database and lattice levels by applying ultrafine methods directly to larger geometries.

Ultrafine methods require the scatter source to be computed on the fly, as storage of an ultrafine scattering matrix is not practical. The isotropic in center of mass scattering kernel can be computed very efficiently by using an approach based on cumulative integrals. Existing ultrafine implementations such as CENTRM and RAZOR include clever transformations of more general scattering kernels to maintain computational efficiency.

Part III

Contributions

Chapter 6

Framework for Evaluating Self-Shielding Models

6.1 Introduction

Too often new techniques are tested and justified using exclusively large, realistic problems. While realism may sound like the ideal test bed for any method, without coupling it with an isolated analysis of the physics, positive results could be driven by cancellation of error, or the range of applicability may be limited beyond what is desired. In software development, a proper test suite contains both unit tests, which isolate specific aspects of the program, and integral tests, which ensure the program works together as a whole. The framework proposed here is analogous to a unit test; it isolates the physics contained in the self-shielding step and measures a method's performance on this small problem.

The primary content of this chapter is a simple benchmark problem, designed to be the simplest problem in which both spatial and energy effects of resonances can be seen. This represents the first step in the evaluation of a self-shielding model and demonstrates the need for and the use of simple benchmarks in self-shielding analysis.

After this sort of analysis, more realistic problems should be considered, adding complexity to the self-shielding problem. The results of Part IV are framed with this in mind. First, simple changes to the benchmark are considered, such as including the true elastic scattering kernel and multiple nuclides. Then, further complexities are added including larger spatial problems with significant heterogeneity.

6.2 A Simple Benchmark

The benchmark problem presented in this chapter was originally intended to be an educational exercise, to give students an appreciation of the quality of the approximations typically encountered in a reactor physics calculation. However, the results warranted interest beyond a simple educational tool. Although equivalence in dilution methods have been studied extensively on very simple problems [14], side-by-side comparisons of these methods with the subgroup method on problems where both are expected to perform well are not readily found. Furthermore, with the advent of newer self-shielding techniques, it is common to only see performance analysis on large problems. Ignoring very simple problems can lead to overlooking fundamental aspects of a technique and risks relying on cancellation of error for accuracy on specific problems.

Thus, this chapter presents the simplest problem in which both energy and spatial effects are important in a self-shielding problem. It is designed such that the assumptions in self-shielding methods are fully valid, allowing the performance of a method to be understood without complications from poor assumptions. Results are presented for various self-shielding methods with some commentary about the effectiveness and the ease of use of each method.

6.2.1 Overview

The benchmark is representative of light water reactor conditions. Geometrically, equivalence-based self-shielding models assume two regions—fuel and moderator. Thus, this benchmark contains exactly those regions. Because self-shielding models typically only treat one resonant nuclide at a time, this benchmark contains only one such nuclide. This benchmark uses the most common assumption for the scatter source in self-shielding models, the narrow resonance approximation, and only a single energy group is considered.

Two classes of geometries are considered, an isolated slab and an infinite array of identical pin-cells, referred to as a "reflected pin-cell." Various widths of the slab and radii of the pin are considered to test a wide variety of shielding states. Two classes of resonances are considered, a square resonance and a single-level Breit-Wigner resonance. For the purpose of clarity in the results, only a single resonance is included in the resonant material.

The fuel material is assumed to have a constant cross section background moderator representative of U-238 in a light water reactor fuel pin. The resonant nuclide is given a potential scattering cross section equivalent to that of U-238. The moderator material is assumed to be purely scattering. Its properties are chosen to be representative of water in a pressurized water reactor.

The quantity of interest is the group-averaged capture cross section of the resonant nuclide. This is the output from a typical self-shielding calculation. The capture cross section is used

rather than the total cross section, as it considers only the aspect of the cross section affected by self-shielding, whereas the total cross section would in large part be influenced by the constant potential scattering cross section.

This benchmark can be easily extended to cases not considered here, many of which are explored in Part IV. Some simple examples include varying the pin pitch, adding additional resonances to the fuel material, and changing the background level. Larger changes, breaking the assumptions in some self-shielding methods, include introducing cladding to the geometry, including a second resonant nuclide, and using a more realistic scattering model.

6.2.2 Specifications

Geometry

Isolated Slab For the case of the isolated slab, the benchmark geometry is a one-dimensional configuration with a slab of lumped resonant material surrounded by an infinite medium of moderating material. In this case, the only parameter needed to define the configuration is the width of the slab. A slab width of $0.4\,\text{cm}$ is the most analogous case to a pin found in a light water reactor. However, this parameter is varied to evaluate the accuracy of self-shielding methods over a range of configurations. The results presented in this thesis include widths of $0.3\,\text{cm}$, $0.4\,\text{cm}$, and $0.6\,\text{cm}$, but these can be varied over a larger range for methods verification.

The fuel slab should be treated as a single region for the purpose of determining the effective cross section. That is, this benchmark does not attempt to determine the spatial distribution of group cross section within the slab, but rather focuses only on the prediction of the spatial- and energy-averaged cross section. This is to maintain the assumption of a two-region problem.

Reflected Pin-Cell For the case of the reflected pin-cell, the benchmark geometry is a two-dimensional configuration with a cylindrical lump of resonant material surrounded by moderator in an infinitely repeating lattice. The only parameter varied in this benchmark is the fuel radius. The most realistic value for a pressurized water reactor is $0.4\,\text{cm}$, and results are presented for radii of $0.3\,\text{cm}$, $0.4\,\text{cm}$, and $0.6\,\text{cm}$. These can be varied over a larger range for methods verification. The pitch is held constant at $1.26\,\text{cm}$ in this paper but can be varied in subsequent studies.

As with the slab, the pin and the moderator regions should be treated as single regions for the determination of effective cross sections in order to maintain the two-region assumption.

Physics

Energy Group A single energy group is used with group boundaries $1000\,\text{eV}$ and $1100\,\text{eV}$. This benchmark could easily be extended to consider other energy ranges, but this is not

considered here.

Cross Sections The capture cross section of the resonant nuclide contains a single resonance, either a square resonance or a single-level Breit-Wigner resonance, with parameters described subsequently. The nuclide has a potential scattering cross section of 11.4 b and no other reaction channels. The resonant material also contains non-resonant nuclides characterized by a background cross section of 8 b. The number density of the resonant nuclide is $0.022\,{}^{a}/_{\text{b·cm}}$. These values are consistent with U-238 in a light water reactor fuel pin.

The moderator is purely scattering and has macroscopic cross section $1.23\,\text{cm}^{-1}$, representative of water in a pressurized water reactor.

Square Resonance For the case of a square resonance, the capture cross section takes some value in a small range in the center of the energy group and is zero elsewhere,

$$\sigma_\gamma(E) = \begin{cases} f & E_0 - {}^{\delta}/_{2} \le E \le E_0 + {}^{\delta}/_{2} \\ 0 & \text{otherwise} \quad . \end{cases} \tag{6.1}$$

In this benchmark, f is varied, $E_0 = 1050\,\text{eV}$, and $\delta = 0.05\,\text{eV}$.

Single-Level Breit-Wigner Resonance For the case of a single-level Breit-Wigner resonance [8], the capture cross section is a single resonance. The resonance parameters are $\Gamma_n = 0.095\,\text{eV}$ and $\Gamma_\gamma = 0.023\,\text{eV}$, which are taken from the resonance parameters from a real U-238 resonance at a similar energy. The center of the resonance is $E_0 = 1050\,\text{eV}$, and the temperature is $T = 300\,\text{K}$. The formula for the resonance is

$$\sigma_0(E) = \frac{\Gamma_n \Gamma_\gamma}{(\Gamma_n + \Gamma_\gamma)^2} \sqrt{\frac{E_0}{E}} r\psi(x,\xi) \quad , \tag{6.2}$$

where

$$r = \frac{2603911\,\text{b}\cdot\text{eV}}{E_0} \frac{A+1}{A} \tag{6.3}$$

$$x = \frac{2(E - E_0)}{\Gamma_n + \Gamma_\gamma} \tag{6.4}$$

$$\xi = (\Gamma_n + \Gamma_\gamma) \sqrt{\frac{A}{4kTE_0}} \tag{6.5}$$

$$\psi(x,\xi) = \Re\left(\frac{\xi\sqrt{\pi}}{2} W\left(\frac{(x+i)\xi}{2}\right)\right) \quad , \tag{6.6}$$

and $A = 238$ is the atomic mass, k is the Boltzmann constant, and $W(\cdot)$ is the Faddeeva function.

The size of the resonance is varied in this benchmark. This is accomplished by multiplicatively scaling this resonance to obtain a maximum cross section value f,

$$\sigma(E) = \sigma_0(E)\frac{f}{\max\limits_E \sigma_0(E)} \quad . \tag{6.7}$$

Scattering Approximation Scattering is approximated as in the narrow resonance model. That is, all scattering is assumed to come from potential scattering resulting from a $1/E$ spectrum and a constant cross section Σ_p. This gives a scattering source in both fuel and moderator of

$$Q(E) = \frac{\Sigma_p}{E} \quad . \tag{6.8}$$

6.2.3 Transport Calculation

The transport calculation is performed using a collision probability approach. Because this problem has only two regions, this is a very simple calculation. Consider the collision probability form of the neutron transport equation, with the collision probabilities notated as P, the fuel or resonant region indexed as F, the moderator region indexed as M, and volumes given as V,

$$\Sigma^F(E)\phi^F(E)V^F = \left(1 - P^{F\to M}(E)\right) Q^F(E)V^F + P^{M\to F}(E)Q^M(E)V^M \quad . \tag{6.9}$$

Invoking the reciprocity relation

$$V^F\Sigma^F P^{F\to M} = V^M\Sigma^M P^{M\to F} \tag{6.10}$$

and inserting Eq. (6.8), the transport equation simplifies to

$$\Sigma^F(E)\phi^F(E) = \left(1 - P^{F\to M}(E)\right)\frac{\Sigma_p^F}{E} + P^{F\to M}(E)\frac{\Sigma^F(E)}{E} \quad . \tag{6.11}$$

For the case of the 1-D isolated slab, the collision probabilities are analytic,

$$P^{F\to M} = \frac{1}{2\Sigma^F d}\left(1 - 2E_3(\Sigma^F d)\right) \quad , \tag{6.12}$$

where d is the width of the slab and E_3 is the third exponential integral. For the 2-D pin-cell configuration, the collision probabilities were computed using a 2-D method of characteristics code. The MOC parameters included 32 azimuthal angles, a track spacing of 0.01 cm, and a 3-point TY polar quadrature.

6.2.4 Reference Solution

Because of the scattering approximation, the flux at a given energy is decoupled from that of any other energy. Thus, a reference can be obtained by solving a series of one-speed transport equations and performing an integration over energy. For the case of the square resonance, this integral is analytic; for the single-level Breit-Wigner resonance, this requires a numerical approach. The one-speed transport equation is solved using a collision probability model, as described in Sec. 6.2.3.

6.3 Self-Shielding Methods Descriptions

The following self-shielding methods were compared on this benchmark problem. Equivalence in dilution methods included using the Wigner rational model, Wigner-Bell, and a two-term rational expansion (Román for slab, Carlvik for pin). The subgroup method and the Embedded Self-Shielding Method were also tested. These methods and their implementations are described next.

6.3.1 Equivalence in Dilution

First, several equivalence in dilution options were considered. For a detailed description of the theory of these methods, see Ch. 3. The Wigner rational model, the simplest approximation for the escape probability is

$$P^{F\to M} = \frac{\Sigma_e}{\Sigma^F(E) + \Sigma_e} \quad . \tag{6.13}$$

If the Dancoff factor is included, this becomes

$$P^{F\to M} = \frac{(1-C)\Sigma_e}{\Sigma^F(E) + (1-C)\Sigma_e} \quad . \tag{6.14}$$

Next, the Wigner-Bell model was considered, which scales the escape probability for an isolated lump by a factor b. This Bell factor is taken to be 1.15 for this study. This is a representative value for typical light water reactor conditions. Note, though, that the Bell factor does not preserve the correct behavior at the high cross section limit, and so it should be varied and driven to 1 for high cross sections in realistic simulations. The Wigner-Bell collision probability without the Dancoff factor is

$$P^{F\to M} = \frac{b\Sigma_e}{\Sigma^F(E) + b\Sigma_e} \quad , \tag{6.15}$$

and is

$$P^{F\to M} = \frac{\tilde{b}\Sigma_e}{\Sigma^F(E) + \tilde{b}\Sigma_e} \tag{6.16}$$

$$\tilde{b} = \frac{(1-C)b}{1-C+Cb} \tag{6.17}$$

if the Dancoff factor is included.

Two-term rational approximations better approximate the escape probability. These take the form of

$$P^{F\to M} = \beta \frac{\alpha_1 \Sigma_e}{\Sigma^F(E) + \alpha_1 \Sigma_e} + (1-\beta)\frac{\alpha_2 \Sigma_e}{\Sigma^F(E) + \alpha_2 \Sigma_e} \quad , \tag{6.18}$$

where the parameters α_1, α_2, and β are geometry dependent. For an isolated slab, the parameters take the values

$$\alpha_1 = 1.4 \quad \alpha_2 = 5.4 \quad \beta = 1.1 \quad , \tag{6.19}$$

and it is known as the Román rational approximation. For a cylindrical fuel pin, the parameters are given by

$$\begin{aligned} \alpha_1 &= \frac{5A + 6 - \sqrt{A^2 + 36A + 36}}{2A+2} \\ \alpha_2 &= \frac{5A + 6 + \sqrt{A^2 + 36A + 36}}{2A+2} \\ \beta &= \frac{\frac{4A+6}{A+1} - \alpha_1}{\alpha_2 - \alpha_1} \quad , \end{aligned} \tag{6.20}$$

where $A = {}^{(1-C)}/_{C}$, and this is known as Carlvik's rational approximation. Note that in the isolated pin limit, these parameters go to

$$\alpha_1 = 2 \quad \alpha_2 = 3 \quad \beta = 2 \quad . \tag{6.21}$$

To use this in practice, one can use a homogeneous dilution table to obtain two resonance integrals I_1 with added dilution $\alpha_1\Sigma_e$ and I_2 with added dilution $\alpha_2\Sigma_e$. The effective resonance integral is then

$$I = \beta I_1 + (1-\beta) I_2 \quad . \tag{6.22}$$

6.3.2 Embedded Self-Shielding Method

Next, the Embedded Self-Shielding Method (ESSM) [16] is considered. A full description is included in Ch. 3. ESSM searches for a value of the equivalence cross section such that a homogeneous model and heterogeneous model are equivalent. The homogenous model is

$$(\Sigma_g^F + \Sigma_{eq,g})\phi_g^F = \Sigma_p^F \Delta u_g + \Sigma_{eq,g}\Delta u_g \quad , \tag{6.23}$$

which is a simple infinite medium equation with a constant equivalence cross section. The heterogeneous model for this benchmark is the multigroup form of Eq. (6.11),

$$\Sigma_g^F \phi_g^F = \left(1 - P^{F\to M}\right)\Sigma_p^F \Delta u_g + P^{F\to M}\Sigma_g^F \Delta u_g \quad , \tag{6.24}$$

where the collision probabilities are computed using the multigroup cross sections.

With these two models defined, the ESSM procedure is as follows:

1. Guess $\Sigma_{eq,g}$.
2. Compute cross sections from dilution table using $\Sigma_{eq.g}$.
3. Solve Eq. (6.24) with obtained cross sections.
4. Use obtained flux from heterogeneous equation, and solve Eq. (6.23) for $\Sigma_{eq,g}$.
5. Iterate, repeating steps 2–4 to convergence.

6.3.3 Subgroup Method

The subgroup method, fully described in Ch. 4, recognizes that the flux used in self-shielding models (e.g., narrow resonance) depends only on the cross section and the asymptotic $1/E$ spectrum. Thus, in lethargy space, the flux can be written as only a function of the cross section. This allows a change of variables, or in some sense a shift to Lebesgue integration, resulting in an integral over cross section rather than energy in the condensation of multigroup cross sections. This is a convenient transformation, as the flux is a much smoother function of cross section than of energy.

A numerical quadrature is performed for this energy condensation,

$$\sigma_g = \frac{\sum\limits_n w_n \sigma_n \phi(\sigma_n)}{\sum\limits_n w_n \phi(\sigma_n)} \quad . \tag{6.25}$$

In this study, only a fitting procedure is considered for the quadrature generation.

Once a quadrature is obtained, fixed source transport problems are solved for every subgroup level in each group. These problems use the scattering source from the resonance model, resulting in purely absorbing fixed source calculations. Thus, the subgroup fixed source problems are entirely decoupled from one another.

In this benchmark, the subgroup fixed source equations are the equivalent of Eq. (6.11) in lethargy space,

$$N^*(\sigma_n + \sigma_b)\phi = \left(1 - P^{F\to M}\right)\Sigma_p^F + P^{F\to M} N^*(\sigma_n + \sigma_b) \quad , \tag{6.26}$$

where the collision probabilities are computed by using $\Sigma^F = N^*(\sigma_n + \sigma_b)$.

Quadrature Generation

The quadrature is determined by taking a set of reference problems $\{\bar{\sigma}_k\}$, in this case infinite media with varying background levels $\sigma_{b,k}$, and comparing them to cross sections generated by some quadrature $Q = \{w_n, \sigma_n\}$. The approximate cross sections are given as

$$\tilde{\sigma}_k(Q) = \frac{\sum_n \frac{w_n \sigma_n}{\sigma_{b,k} + \sigma_n}}{\sum_n \frac{w_n}{\sigma_{b,k} + \sigma_n}} \quad . \tag{6.27}$$

The quadrature Q is obtained by performing a least squares fitting procedure,

$$Q = \arg\min_{Q'} \sum_k \left(\frac{\bar{\sigma}_k - \tilde{\sigma}_k(Q')}{\bar{\sigma}_k} \right)^2 \quad . \tag{6.28}$$

This process is constrained such that the weights sum to unity and are nonnegative.

In this study, the cross section used in the fitting procedure was the capture cross section, as this allows the parameter of interest in the benchmark to be computed accurately. Note that σ_n in Eq. (6.26) refers to the total cross section, and so σ_p must be added to the cross section generated in this fitting procedure for use in the transport calculation. For all results given here, six subgroup levels were used.

6.4 Results

Each self-shielding technique previously described was tested on the benchmark for various configurations. Results are presented in tabular form, showing the dependence on the height of the resonance. The reference solution is calculated using a calculation with ultrafine energy discretization as described in Sec. 6.2.4. Performance of each method is described as the percent error of the obtained group averaged capture cross section compared to this reference. Positive errors represent obtained cross sections greater than the reference; negative errors represent obtained cross sections less than the reference.

First, results with a square resonance in the 1-D isolated slab geometry are presented. Table 6.1 gives results with a width of 0.3 cm; Tab. 6.2, with a width of 0.4 cm; and Tab. 6.3, with a width of 0.6 cm. Note that subgroup results are not included, as the appropriate selection of a subgroup quadrature results in an exact solution for this simple case.

Next, results with a single-level Breit-Wigner (SLBW) resonance in the 1-D isolated slab geometry are given. Table 6.4 gives results with a width of 0.3 cm; Tab. 6.5, with a width of 0.4 cm; and Tab. 6.6, with a width of 0.6 cm.

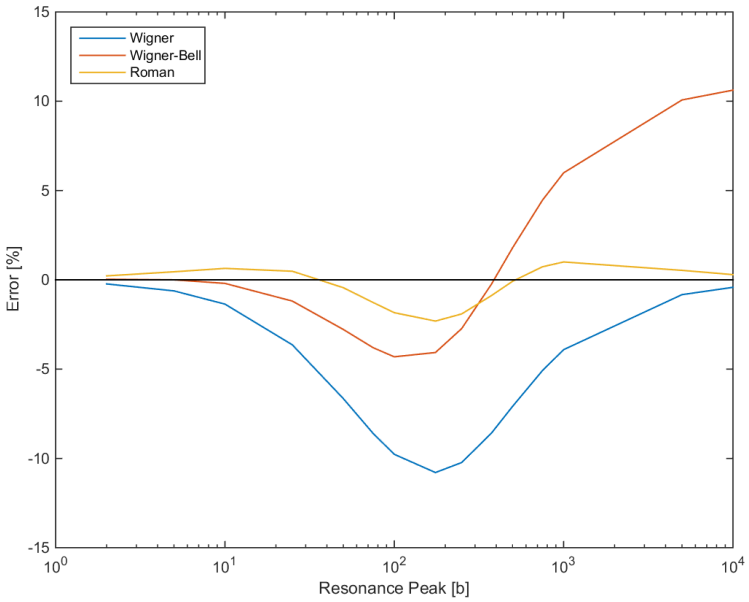

Figure 6.1: Error for equivalence in dilution techniques for 1-D isolated slab and a square resonance.

Finally, results with a SLBW resonance in the 2-D reflected pin-cell geometry are included. Table 6.7 gives results with a pin radius of $0.3\,\text{cm}$; Tab. 6.8, with a pin radius of $0.4\,\text{cm}$; and Tab. 6.9, with a pin radius of $0.6\,\text{cm}$.

6.4.1 Equivalence in Dilution

Fig. 6.1 and Fig. 6.2 plot the error in the capture cross sections generated by equivalence in dilution methods as a function of the resonance peak for the 1-D slab cases with $0.4\,\text{cm}$ width. The results are very familiar curves, behaving consistently with errors known for the rational approximations [14].

Wigner's rational approximation leads to very low error for small resonance peaks. For larger resonance peaks, this approximation does well for the square resonance, and slightly less so for the SLBW resonance. This is because although the peak of the resonance approaches the high cross section limit, the flanks of the resonance are in the intermediate cross section range where the approximation is less accurate. Furthermore, Wigner is seen to consistently under-predict the group averaged capture cross section, and is rather significant for intermediate resonance peaks.

The Wigner-Bell approximation shows the characteristic change of sign in the error at intermediate cross section values. It fares better than Wigner's rational approximation for low and intermediate resonance peaks, but does poorly for large resonance peaks. This is expected,

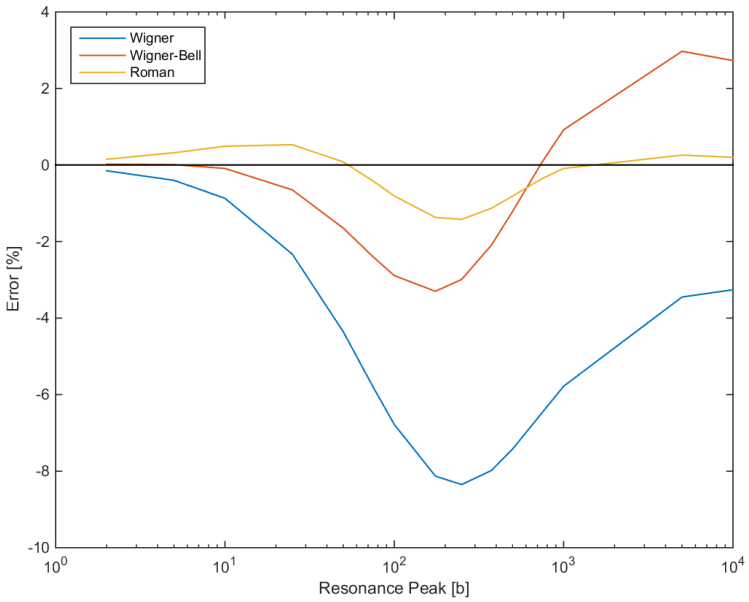

Figure 6.2: Error for equivalence in dilution techniques for 1-D isolated slab and a SLBW resonance.

as a single Bell factor was used for all calculations. At high opacities, it is known that the Bell factor should tend to unity, resulting in Wigner's rational approximation.

Roman's two-term rational approximation for the 1-D slab and Carlvik's two-term rational approximation for the 2-D pin-cell perform very well. For the square resonance case, errors are at or below 2%. For the SLBW resonance cases, nearly all errors fall below 1%. Clearly, a significant improvement is achieved by the inclusion of the second term in the rational approximation.

6.4.2 Embedded Self-Shielding Method

ESSM results are best for smaller resonance peaks, and the method appears to break down for larger resonances. This is somewhat counter-intuitive, as the iteration procedure is essentially searching for the appropriate Dancoff and Bell factor. Thus, one would expect ESSM to perform at least as well as the Wigner and Wigner-Bell approximations.

This can be explained primarily as this ESSM iteration being ill-conditioned. ESSM is forcing equivalence between heterogeneous and homogeneous models, using the flux as the connection. However, the flux varies over a very small range, and small changes in flux lead to very different implied shielding states. For physical intuition of this effect, consider widening the energy group, holding the single resonance constant. The group flux will approach unity for all shielding states, but the effective cross section will still be a strong function of the

background. This means that a small error in flux leads to large errors in the obtained cross sections. For instance, in this benchmark, the heterogeneous problem suffers from small condensation errors, explained in Sec. 7.5, and these errors are enough to impact the results.

Also, ESSM is essentially a direct subgroup method with a single level. Physically, the subgroup method is effective because it can differentiate the behavior of neutrons at resonance energies from those away from resonances. These cannot be separated with a single subgroup level, and the resulting effect is more pronounced for larger resonance peaks. So although it is mathematically possible to obtain an accurate quadrature with a single subgroup level, this is not realistic in practice. Thus, the ESSM procedure cannot be expected to accurately model self-shielding for large resonances.

The poor performance of ESSM is strong evidence of the need for this sort of simple benchmark analysis. This method has been used on large problems with favorable results, but in the form considered in this thesis, it is not suitable for predictive purposes outside of carefully selected regions of design space. The difficulty with ESSM will be revisited in Sec. 7.5, once additional tools for analysis are developed.

Note that more recent ESSM implementations have been based on nuclear data tables generated through heterogeneous calculations, rather than the homogeneous calculations used in this study. This approach is not easily tested on this simple benchmark, but is revisted in Ch. 9.

6.4.3 Subgroup

The results for the subgroup method are very good, with nearly all errors falling below 1%. The variance in the errors can be attributed to the varying quality of the quadrature obtained in the fitting procedure for each configuration, as quadrature generation was found to be a difficult process, even for this simple problem. Adjustment of the subgroup parameters can lead to significant improvements in accuracy, but is not easily generalized. This suggests that subgroup can be an effective self-shielding method, but it requires great care in the generation of the quadrature. For realistic simulations with many energy groups and nuclides, this is likely a very large effort.

It should be noted that using six subgroup levels in this study was an arbitrary choice, and this was more subgroup levels than necessary. Initial results with four subgroup levels provided similar accuracy. The issue of quadrature generation could be further explored using this benchmark and similar problems, comparing various quadrature generation methods and varying numbers of levels.

Table 6.1: Errors in capture capture cross sections for square resonance in 1-D isolated slab configuration with 0.3 cm width.

Peak [b]	Reference [b]	Error [%]			
		Wigner	Wigner-Bell	Roman	ESSM
2	0.0010	-0.13	0.09	0.26	-0.02
5	0.0024	-0.39	0.15	0.55	-0.13
10	0.0046	-0.92	0.09	0.85	-0.44
25	0.0102	-2.81	-0.60	0.97	-1.75
50	0.0174	-5.69	-2.09	0.28	-3.98
75	0.0227	-7.84	-3.29	-0.57	-5.69
100	0.0269	-9.35	-4.11	-1.28	-6.88
175	0.0348	-11.46	-4.89	-2.39	-8.39
250	0.0390	-11.69	-4.30	-2.49	-8.25
375	0.0425	-10.67	-2.36	-1.82	-6.82
500	0.0440	-9.28	-0.35	-0.99	-5.15
750	0.0454	-6.98	2.75	0.20	-2.49
1000	0.0459	-5.47	4.74	0.78	-0.77
5000	0.0472	-1.18	10.37	0.70	4.12
10000	0.0474	-0.60	11.15	0.40	4.79

Table 6.2: Errors in capture capture cross sections for square resonance in 1-D isolated slab configuration with 0.4 cm width.

Peak [b]	Reference [b]	Error [%]			
		Wigner	Wigner-Bell	Roman	ESSM
2	0.0010	-0.23	0.03	0.22	-0.02
5	0.0024	-0.62	-0.00	0.45	-0.14
10	0.0045	-1.36	-0.20	0.64	-0.45
25	0.0098	-3.64	-1.19	0.48	-1.72
50	0.0162	-6.65	-2.78	-0.44	-3.63
75	0.0207	-8.60	-3.80	-1.27	-4.86
100	0.0240	-9.77	-4.31	-1.84	-5.53
175	0.0297	-10.79	-4.07	-2.31	-5.58
250	0.0325	-10.23	-2.73	-1.91	-4.43
375	0.0346	-8.58	-0.24	-0.88	-2.13
500	0.0356	-7.08	1.80	-0.08	-0.22
750	0.0364	-5.08	4.46	0.73	2.28
1000	0.0368	-3.91	5.99	1.00	3.72
5000	0.0378	-0.83	10.07	0.53	7.56
10000	0.0380	-0.42	10.62	0.29	8.08

Table 6.3: Errors in capture capture cross sections for square resonance in 1-D isolated slab configuration with 0.6 cm width.

Peak [b]	Reference [b]	Error [%]			
		Wigner	Wigner-Bell	Roman	ESSM
2	0.0010	-0.38	-0.07	0.14	-0.02
5	0.0023	-0.97	-0.25	0.26	-0.13
10	0.0043	-1.97	-0.64	0.27	-0.42
25	0.0091	-4.57	-1.88	-0.24	-1.43
50	0.0144	-7.31	-3.24	-1.22	-2.55
75	0.0178	-8.63	-3.71	-1.78	-2.85
100	0.0200	-9.14	-3.61	-1.97	-2.64
175	0.0236	-8.64	-1.98	-1.50	-0.80
250	0.0252	-7.39	-0.05	-0.71	1.26
375	0.0263	-5.61	2.41	0.22	3.85
500	0.0269	-4.42	4.00	0.66	5.52
750	0.0274	-3.08	5.79	0.93	7.40
1000	0.0277	-2.35	6.76	0.93	8.41
5000	0.0284	-0.49	9.25	0.33	11.03
10000	0.0285	-0.25	9.58	0.18	11.38

Table 6.4: Errors in capture capture cross sections for SLBW resonance in 1-D isolated slab configuration with 0.3 cm width.

Peak [b]	Reference [b]	Error [%]				
		Wigner	Wigner-Bell	Roman	ESSM	Subgroup
2	0.0260	-0.08	0.06	0.17	-0.01	0.00
5	0.0637	-0.24	0.11	0.38	-0.07	-0.00
10	0.1238	-0.58	0.11	0.62	-0.24	-0.01
25	0.2861	-1.75	-0.24	0.85	-1.00	-0.11
50	0.5129	-3.62	-1.12	0.59	-2.36	-0.32
75	0.7007	-5.11	-1.91	0.14	-3.48	-0.49
100	0.8600	-6.25	-2.52	-0.29	-4.32	0.19
175	1.2244	-8.18	-3.44	-1.13	-5.66	-0.02
250	1.4831	-8.88	-3.55	-1.45	-5.99	-1.02
375	1.7886	-8.97	-3.04	-1.44	-5.67	0.54
500	2.0087	-8.61	-2.30	-1.19	-5.04	0.05
750	2.3256	-7.71	-0.96	-0.70	-3.79	0.93
1000	2.5612	-6.96	0.01	-0.36	-2.82	-0.60
5000	4.4141	-3.95	3.00	0.31	0.80	0.09
10000	5.8114	-3.57	2.96	0.28	1.30	-0.00

Table 6.5: Errors in capture capture cross sections for SLBW resonance in 1-D isolated slab configuration with 0.4 cm width.

Peak [b]	Reference [b]	Error [%]				
		Wigner	Wigner-Bell	Roman	ESSM	Subgroup
2	0.0259	-0.15	0.02	0.15	-0.01	-0.00
5	0.0633	-0.40	0.01	0.32	-0.07	-0.01
10	0.1222	-0.87	-0.09	0.49	-0.25	-0.04
25	0.2782	-2.33	-0.65	0.53	-0.99	-0.19
50	0.4886	-4.36	-1.65	0.08	-2.18	-0.40
75	0.6569	-5.80	-2.40	-0.42	-3.04	-0.53
100	0.7958	-6.78	-2.89	-0.81	-3.60	0.17
175	1.1017	-8.13	-3.30	-1.37	-4.12	-0.03
250	1.3115	-8.35	-2.99	-1.42	-3.85	-0.67
375	1.5558	-7.98	-2.09	-1.13	-2.97	0.49
500	1.7328	-7.42	-1.21	-0.81	-2.08	-0.20
750	1.9929	-6.46	0.09	-0.35	-0.75	1.22
1000	2.1913	-5.78	0.92	-0.09	0.13	-0.54
5000	3.8342	-3.45	2.97	0.26	2.73	0.06
10000	5.1046	-3.26	2.73	0.20	2.83	-0.14

Table 6.6: Errors in capture capture cross sections for SLBW resonance in 1-D isolated slab configuration with 0.6 cm width.

Peak [b]	Reference [b]	Error [%]				
		Wigner	Wigner-Bell	Roman	ESSM	Subgroup
2	0.0258	-0.25	-0.05	0.10	-0.01	-0.01
5	0.0626	-0.64	-0.15	0.19	-0.07	-0.04
10	0.1196	-1.29	-0.39	0.24	-0.23	-0.09
25	0.2656	-3.02	-1.17	0.02	-0.84	-0.30
50	0.4519	-5.01	-2.14	-0.56	-1.60	-0.47
75	0.5932	-6.14	-2.64	-0.97	-1.95	-0.47
100	0.7054	-6.76	-2.82	-1.20	-2.01	0.08
175	0.9419	-7.19	-2.45	-1.26	-1.42	-0.01
250	1.0996	-6.90	-1.71	-1.01	-0.54	0.02
375	1.2842	-6.19	-0.60	-0.59	0.72	0.33
500	1.4210	-5.60	0.22	-0.30	1.63	-0.36
750	1.6285	-4.79	1.23	-0.01	2.76	1.01
1000	1.7911	-4.28	1.80	0.11	3.39	-0.21
5000	3.2125	-2.82	2.76	0.18	4.57	-0.01
10000	4.3359	-2.82	2.37	0.10	4.26	-0.18

Table 6.7: Errors in capture capture cross sections for SLBW resonance in 2-D reflected pin-cell configuration with 0.3 cm diameter.

Peak [b]	Reference [b]	Error [%]				
		Wigner	Wigner-Bell	Carlvik	ESSM	Subgroup
2	0.0260	-0.40	-0.26	-0.05	0.00	0.00
5	0.0639	-0.97	-0.64	-0.13	0.01	-0.00
10	0.1243	-1.83	-1.21	-0.25	0.02	-0.03
25	0.2873	-3.91	-2.58	-0.57	0.13	-0.18
50	0.5115	-6.22	-4.05	-0.93	0.49	-0.47
75	0.6924	-7.62	-4.88	-1.12	1.01	-0.64
100	0.8422	-8.48	-5.31	-1.18	1.62	0.21
175	1.1724	-9.43	-5.44	-0.98	3.58	-0.03
250	1.3991	-9.40	-4.93	-0.61	5.40	-0.67
375	1.6642	-8.83	-3.86	-0.05	7.83	0.56
500	1.8567	-8.19	-2.93	0.33	9.59	-0.22
750	2.1395	-7.18	-1.60	0.74	11.86	1.25
1000	2.3540	-6.48	-0.74	0.90	13.19	-0.47
5000	4.0977	-4.05	1.52	0.71	15.24	0.03
10000	5.4323	-3.85	1.36	0.54	14.07	-0.17

Table 6.8: Errors in capture cross sections for SLBW resonance in 2-D reflected pin-cell configuration with 0.4 cm diameter.

Peak [b]	Reference [b]	Error [%]				
		Wigner	Wigner-Bell	Carlvik	ESSM	Subgroup
2	0.0259	-0.44	-0.29	-0.07	0.00	-0.01
5	0.0631	-1.04	-0.70	-0.17	0.01	-0.03
10	0.1214	-1.93	-1.29	-0.32	0.04	-0.09
25	0.2724	-3.91	-2.59	-0.66	0.23	-0.32
50	0.4676	-5.82	-3.75	-0.95	0.76	-0.53
75	0.6163	-6.79	-4.24	-1.02	1.43	-0.52
100	0.7349	-7.27	-4.38	-0.98	2.14	0.08
175	0.9862	-7.50	-3.99	-0.61	4.13	-0.00
250	1.1552	-7.17	-3.31	-0.24	5.73	0.07
375	1.3539	-6.50	-2.32	0.18	7.60	0.36
500	1.5010	-5.94	-1.59	0.41	8.83	-0.31
750	1.7228	-5.16	-0.64	0.61	10.26	0.89
1000	1.8955	-4.66	-0.08	0.66	11.01	-0.17
5000	3.3810	-3.15	1.09	0.40	11.39	-0.00
10000	4.5462	-3.11	0.84	0.30	10.30	-0.12

6.5 Chapter Summary

In this chapter, a framework for the evaluation of self-shielding methods was introduced. Rather than relying on integral testing—i.e., using large problems with many important aspects of physics—self-shielding methods should first be tested on very simple benchmarks. These benchmarks should isolate the physics of interest and ensure the method performs as desired. Only then should the method be used on more complex problems.

One such simple benchmark has been presented here, which is the simplest possible problem in which both energy and spatial self-shielding effects are important. The benchmark was designed such that the assumptions made in the derivation of self-shielding models are fully valid. This allows self-shielding methods to be evaluated consistently and allows one to separate errors associated with the self-shielding method from any other effects.

This benchmark problem was solved using several techniques, including various equivalence in dilution methods, the Embedded Self-Shielding Method (ESSM), and the subgroup method. The best results were obtained using two-term rational expansions in the equivalence in dilutions methods and using the subgroup method. One-term rational expansion methods lead to much larger errors, as did ESSM.

Table 6.9: Errors in capture cross sections for SLBW resonance in 2-D reflected pin-cell configuration with 0.6 cm diameter.

Peak [b]	Reference [b]	Error [%]				
		Wigner	Wigner-Bell	Carlvik	ESSM	Subgroup
2	0.0254	-0.21	-0.13	-0.01	0.00	-0.02
5	0.0603	-0.48	-0.29	-0.03	0.01	-0.09
10	0.1114	-0.84	-0.51	-0.04	0.03	-0.19
25	0.2293	-1.49	-0.86	-0.04	0.16	-0.35
50	0.3601	-1.92	-1.02	0.01	0.43	-0.09
75	0.4502	-2.03	-0.99	0.10	0.71	0.31
100	0.5186	-2.05	-0.90	0.16	0.94	-0.23
175	0.6606	-1.90	-0.61	0.31	1.48	0.01
250	0.7575	-1.73	-0.38	0.38	1.82	0.63
375	0.8760	-1.52	-0.11	0.43	2.15	-0.40
500	0.9679	-1.37	0.05	0.44	2.34	-0.09
750	1.1130	-1.18	0.24	0.43	2.53	-0.23
1000	1.2309	-1.07	0.34	0.41	2.61	0.01
5000	2.3270	-0.82	0.40	0.28	2.42	0.01
10000	3.2072	-0.83	0.31	0.27	2.29	0.06

Chapter 7

Angular Dependence of Cross Sections

7.1 Introduction

In a reactor physics neutronics simulations , the steady-state neutron transport equation is often the primary workhorse, and is shown here with a generic source:

$$\hat{\Omega} \cdot \nabla \psi(\vec{r}, E, \hat{\Omega}) + \Sigma_t(\vec{r}, E)\psi(\vec{r}, E, \hat{\Omega}) = Q(\vec{r}, E, \hat{\Omega}) \quad . \tag{7.1}$$

This equation can be solved efficiently for many problems by using the multigroup approximation, in which the energy variable is discretized into so-called energy groups. In general, it is not possible to resolve the complex energy behavior of the nuclear data and the neutron flux in a deterministic calculation on a large geometry, and so great care must be taken in the generation of the nuclear data used in group-wise (or "multigroup") solutions of the transport equation.

The multigroup form of the transport equation is attained by integrating Eq. (7.1) over the energies defining a group $[E_{g+1}, E_g]$,

$$\int_{E_g+1}^{E_g} \mathrm{d}E \left(\hat{\Omega} \cdot \nabla \psi(\vec{r}, E, \hat{\Omega}) + \Sigma_t(\vec{r}, E)\psi(\vec{r}, E, \hat{\Omega}) \right) = \int_{E_g+1}^{E_g} \mathrm{d}E \, Q(\vec{r}, E, \hat{\Omega}) \tag{7.2}$$

$$\hat{\Omega} \cdot \nabla \psi_g(\vec{r}, \hat{\Omega}) + \Sigma_{t,g}(\vec{r}, \hat{\Omega})\psi_g(\vec{r}, \hat{\Omega}) = Q_g(\vec{r}, \hat{\Omega}) \quad , \tag{7.3}$$

where the multigroup parameters are given by

$$\psi_g(\vec{r},\hat{\Omega}) = \int_{E_{g+1}}^{E_g} \mathrm{d}E\, \psi(\vec{r},E,\hat{\Omega}) \tag{7.4}$$

$$\Sigma_{t,g}(\vec{r},\hat{\Omega}) = \frac{\int_{E_{g+1}}^{E_g} \mathrm{d}E\, \Sigma_t(\vec{r},E)\psi(\vec{r},E,\hat{\Omega})}{\int_{E_{g+1}}^{E_g} \mathrm{d}E\, \psi(\vec{r},E,\hat{\Omega})} \tag{7.5}$$

$$Q_g(\vec{r},\hat{\Omega}) = \int_{E_{g+1}}^{E_g} \mathrm{d}E\, Q(\vec{r},E,\hat{\Omega}) \quad . \tag{7.6}$$

The multigroup form of the transport equation of Eq. (7.3) has the same form as Eq. (7.1) with one significant caveat: the total cross section in the multigroup form is dependent on the angle. The multigroup total cross section given by Eq. (7.5) is condensed in energy through the use of the angular flux, which gives rise to this newfound angular dependence. Because this angular dependence is not convenient to use in a transport calculation, an approximation is often used in which the scalar flux rather than the angular flux is used in the collapse; this is equivalent to integrating Eq. (7.5) over all angles in both the numerator and denominator:

$$\begin{aligned}\Sigma_{t,g}(\vec{r},\hat{\Omega}) \approx \Sigma_{t,g}(\vec{r}) &= \frac{\int_{4\pi}\mathrm{d}\hat{\Omega}\int_{E_{g+1}}^{E_g}\mathrm{d}E\,\Sigma_t(\vec{r},E)\psi(\vec{r},E,\hat{\Omega})}{\int_{4\pi}\mathrm{d}\hat{\Omega}\int_{E_{g+1}}^{E_g}\mathrm{d}E\,\psi(\vec{r},E,\hat{\Omega})} \\ &= \frac{\int_{E_{g+1}}^{E_g}\mathrm{d}E\,\Sigma_t(\vec{r},E)\phi(\vec{r},E)}{\int_{E_{g+1}}^{E_g}\mathrm{d}E\,\phi(\vec{r},E)} \quad .\end{aligned} \tag{7.7}$$

This leads to an approximate form of the transport equation,

$$\hat{\Omega}\cdot\nabla\psi_g(\vec{r},\hat{\Omega}) + \Sigma_{t,g}(\vec{r})\psi_g(\vec{r},\hat{\Omega}) = Q_g(\vec{r},\hat{\Omega}) \quad , \tag{7.8}$$

which features some error from this alternate condensation equation and whose consequences will be analyzed here.

Note also that the cross section condensation formulas of both Eqs. (7.5) and (7.7) are complicated by the fact the flux is included in the definition. The flux is the output of a solution of the transport equation, and so this requires some estimation of the flux prior to the multigroup solution. This estimation of the flux is the subject of self-shielding techniques that have been studied extensively and developed over the past several decades and are outlined in Part II. However, as higher fidelity flux estimates are used, the condensation errors of Eq. (7.8) are becoming more noticeable.

7.2 Demonstration of Condensation Errors

To demonstrate the existence of errors from approximately collapsing Eq. (7.1) into Eq. (7.8), consider a very simple problem in which the reference flux can be computed precisely. This is an extension of the benchmark problem presented in Ch. 6.

This example problem consists of a unit cell of an infinite array of unclad fuel pins. The fuel material contains U-238 with an atom density of $0.022\,{}^{a}/_{b-cm}$ and a purely scattering nuclide with a constant cross section of $0.176\,\text{cm}^{-1}$, an analog to oxygen in UO_2. The moderator is a pure scatterer with a constant cross section of $1.23\,\text{cm}^{-1}$. The pin radius is $0.4\,\text{cm}$ and the pitch is $1.26\,\text{cm}$. The source is given by

$$Q(\vec{r}, E, \hat{\Omega}) = \frac{1}{4\pi} \frac{\Sigma_p(\vec{r})}{E} \quad , \tag{7.9}$$

which is the scatter source from the narrow resonance approximation.

The reference continuous energy flux is computed by solving Eq. (7.1) for each energy point, and the reference reaction rate is obtained by integrating the flux multiplied by a cross section over an energy range of interest and over the volume of the fuel pin. Next, the collapsed cross section and collapsed source are generated using the reference flux in Eqs. (7.6) and (7.7), respectively. With this collapsed cross section and source, Eq. (7.8) is solved. The collapsed reaction rate is obtained by volume integrating the multigroup flux multiplied by the multigroup cross section over the fuel pin.

This simple problem is solved for the WIMS 69-group energy structure [12] in the resonance range. The results are shown in Tab. 7.1. The condensation errors range from 0.1% in the high energy groups to just over 1% in the lower energy groups, with the exception of group 26. Group 26 sits between the two lowest energy resonances of U-238 and contains no resonance itself, and so it exhibits no significant error. This suggests that the condensation errors are caused by improper self-shielding of the resonances. Furthermore, as the errors increase with lower energy, this suggests that the effect is exacerbated by the magnitude of the resonance peaks. These results are shown in graphical form in Fig. 7.1, plotted against the U-238 total cross section.

In a more realistic simulation, the Monte Carlo code OpenMC [38] was used to generate cross sections for use in the multigroup transport solver OpenMOC [3]. A UO_2 pin-cell modeled after the LWR fuel given in the BEAVRS benchmark [39] was considered, using real cross sections for all materials. The errors observed were very nearly the same as in the simple example problem, and these corresponded to approximately a $200\,\text{pcm}$ underprediction of the eigenvalue. A plot of the errors in the reaction rates of each group plotted alongside the U-238 capture cross section is given in Fig. 7.2.

Table 7.1: U-238 resonance range reaction rates for collapsed cross sections on simple pin-cell.

Group	E_{max} (eV)	Reference	Condensed	Error (%)
15	9118.00	0.12018	0.12030	0.102
16	5530.00	0.11011	0.11027	0.142
17	3519.10	0.11407	0.11444	0.330
18	2239.45	0.10581	0.10630	0.457
19	1425.10	0.11572	0.11625	0.461
20	906.899	0.21110	0.21172	0.294
21	367.263	0.22169	0.22290	0.543
22	148.729	0.16551	0.16649	0.598
23	75.5014	0.10569	0.10621	0.487
24	48.0520	0.14256	0.14394	0.964
25	27.7000	0.13732	0.13867	0.984
26	15.9680	0.09348	0.09348	0.001
27	9.8770*	0.23567	0.23813	1.041

* $E_{min} = 4\,\text{eV}$

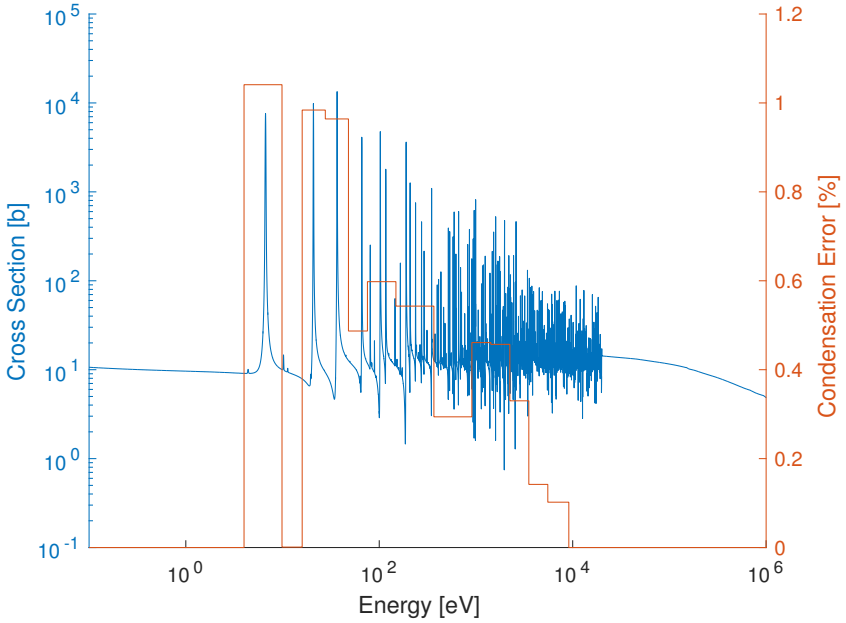

Figure 7.1: Condensation errors in the resonant groups of the WIMS69 group structure, plotted alongside the U-238 cross section.

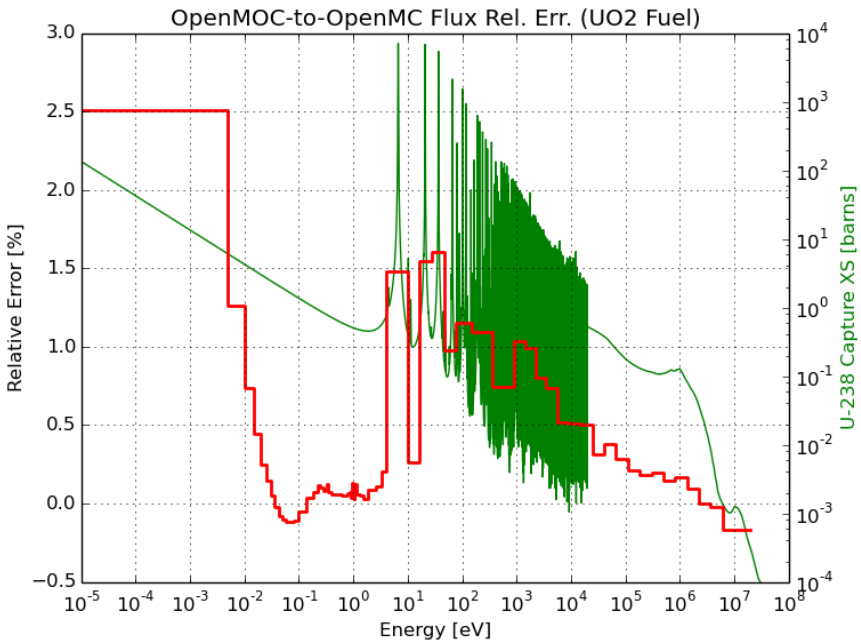

Figure 7.2: Condensation errors in multigroup cross sections generated by OpenMC and used in OpenMOC. *Courtesy of W. Boyd.*

7.3 Diagnosing the Cause of the Errors

It was just shown that errors exist and it was suggested that improper self-shielding was the culprit. In fact, these condensation errors are more precisely due to spatial self-shielding effects. In an infinite medium, there is no variation in angle or space for the angular flux, and so the same results are obtained if one collapses cross sections with the scalar flux as if one collapses with the angular flux. To see this, consider an infinite medium of U-238 with 50 barns of background moderator in a procedure analogous to the previous example. Tab. 7.2 contains the results. The errors are nearly zero in all groups, and the small errors that are seen are entirely attributable to numerical precision.

To understand the cause of these errors, consider how neutrons reach a certain region of a fuel pin. For a region of interest on the exterior of a fuel pin, neutrons may enter directly from the moderator or they may traverse a portion of the fuel pin first, as depicted in Fig. 7.3. The former are unshielded, and the spectrum is that of the asymptotic spectrum, likely $1/E$. The latter, however, are heavily shielded, and the spectrum will have a large depression at the resonance energy. Thus, the resonance reaction rate is much larger for the first case than for the second case.

And in fact, this difference in reaction rates translates to a difference in angular-flux-weighted cross sections. Fig. 7.4 shows the collapsed capture cross section as a function of incoming azimuthal angle for two regions of interest for the 6.67 eV resonance group.

Table 7.2: U-238 resonance range reaction rates (arbitrary units) for collapsed cross sections in an infinite medium.

Group	E_{max} (eV)	Reference	Condensed	Error (%)
15	9118.00	0.33893	0.33891	-0.004
16	5530.00	0.30636	0.30635	-0.003
17	3519.10	0.30631	0.30630	-0.003
18	2239.45	0.29363	0.29362	-0.002
19	1425.10	0.31908	0.31908	-0.001
20	906.899	0.61265	0.61265	0.000
21	367.263	0.61270	0.61270	0.000
22	148.729	0.45950	0.45950	0.000
23	75.5014	0.30625	0.30625	0.000
24	48.0520	0.37338	0.37338	0.000
25	27.7000	0.37333	0.37333	0.000
26	15.9680	0.32560	0.32560	0.000
27	9.8770*	0.61260	0.61260	0.000

* $E_{min} = 4\,\text{eV}$

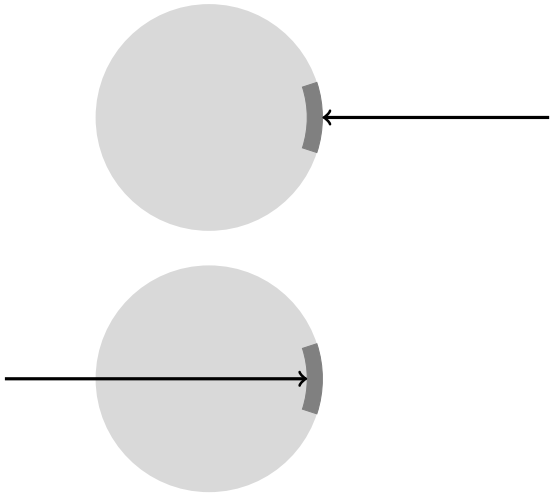

Figure 7.3: Illustration of neutron entering region of interest directly from moderator (top) and after traversing fuel (bottom).

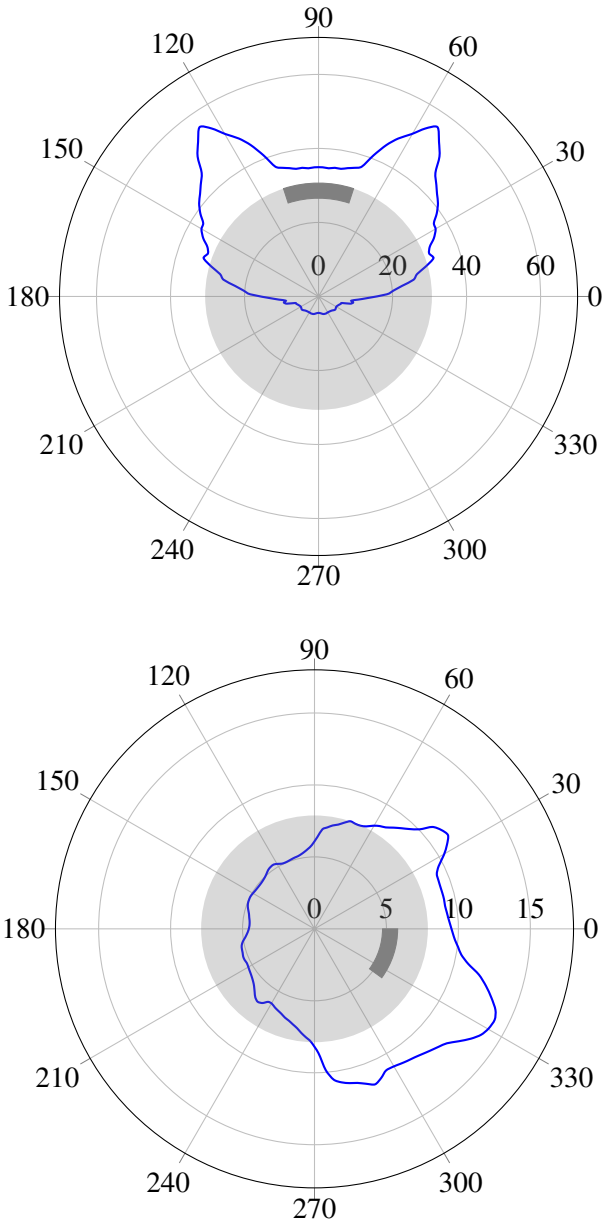

Figure 7.4: Capture cross sections collapsed with angular flux as a function of incoming azimuthal angle into region of interest for the 6.67 eV resonance group. Radial axis in units of barns; azimuthal axis in degrees.

The first region is on the exterior of the fuel pin, and is indicated by the darkly shaded region in the upper half of the figure. The cross section for angles in which neutrons enter from the moderator are all above 30 b, whereas the cross section for neutrons having traversed the fuel pin are as low as 5 b. The peaks near 60° and 120° are due to the square array of pins; at these angles, neutrons can traverse more moderator between pins than at 90°.

The second region is in the interior of the fuel pin, and is indicated by the darkly shaded region in the lower half of the figure. It exhibits the same characteristics of the first region, but the effects are more muted. The maximum value of the cross section is only 15 b, and the minimum value 5 b. A region at the very center of the fuel pin would exhibit almost no angular dependence, as it would be shielded similarly from all directions.

From these plots, it is easy to imagine that accounting for this angular dependence by simply averaging the angular component does not do a suitable job of picking up all the physics at play. It is clearly very important to know whether neutrons are entering directly from the moderator or traversing fuel first. It is conceivable that the vast majority of this effect could be picked up by simply using two cross section values rather than using fully angularly dependent data, but this possibility is not explored in this thesis.

Next, it will be shown that using fully angularly dependent data causes the bias in the group reaction rates to vanish. However, as was noted, the most important aspect of the physics to account for is whether neutrons are entering the region through the fuel pin or directly from the moderator. By simply using angularly dependent data on a single region fuel pin, this cannot be done. A cross section for a given angle would in this case be applied to neutrons entering the fuel pin from the moderator and to neutrons exiting the fuel pin on the opposite side alike. Thus, the fuel pin must be discretized for the error to subside.

The simple pin-cell problem is again used. The reference solution is computed on the ultrafine energy mesh and is used to collapse cross sections. Cross sections for the left hand side of the transport equation are collapsed separately for each angle, weighted by the angular flux for that angle. Then geometry is discretized into rings and sectors. The pin is split up into rings of equal volume. Although the solution is not sensitive to discretization of the moderator, equal width rings are created in the moderator. Sectors are separated by equally spaced angles, and the same angles are used in the fuel and the moderator. Fig. 7.5 shows a schematic of a pin-cell discretized with three fuel rings, two moderator rings, and eight sectors.

Results are shown with no pin discretization in Tab. 7.3, with 3 fuel rings and 4 azimuthal sectors in Tab. 7.4, and with 5 fuel rings and 8 azimuthal sectors in Tab. 7.5. In these tables, the error in the condensed cross section for each resonance group is shown for both scalar flux weighted and angular flux weighted cross sections. The errors resulting from scalar flux weighting remain fairly constant regardless of pin discretization. The errors resulting from angular flux weighting are greatly reduced as pin discretization is increased.

To see this more clearly, see Fig. 7.6 and Fig. 7.7. These figures show the maximum

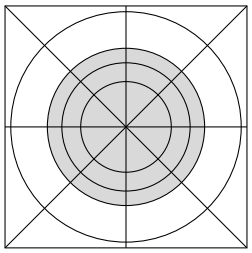

Figure 7.5: Discretized pin-cell system with 3 fuel rings, 2 moderator rings, and 8 sectors.

Table 7.3: Errors of group cross sections when collapsed with scalar vs. angular flux without pin discretization.

		Error (%)	
Group	E_{max} (eV)	Scalar	Angular
15	9.11800E+03	1.05E-01	1.83E-01
16	5.53000E+03	1.42E-01	2.28E-01
17	3.51910E+03	3.29E-01	4.85E-01
18	2.23945E+03	4.57E-01	6.42E-01
19	1.45210E+03	4.61E-01	6.34E-01
20	9.06899E+02	2.94E-01	4.08E-01
21	3.67263E+02	5.43E-01	7.12E-01
22	1.48729E+02	5.98E-01	7.79E-01
23	7.55014E+01	4.87E-01	6.21E-01
24	4.80520E+01	9.64E-01	1.25E+00
25	2.77000E+01	9.84E-01	1.26E+00
26	1.59680E+01	1.19E-03	2.77E-03
27	9.8770E+00*	1.04E+00	1.31E+00

* $E_{min} = 4\,\text{eV}$

Table 7.4: Errors of group cross sections when collapsed with scalar vs. angular flux with 3 fuel rings and 4 azimuthal sectors.

		Error (%)	
Group	E_{max} (eV)	Scalar	Angular
15	9.11800E+03	1.27E-01	4.11E-02
16	5.53000E+03	1.72E-01	5.15E-02
17	3.51910E+03	3.96E-01	1.10E-01
18	2.23945E+03	5.53E-01	1.51E-01
19	1.45210E+03	5.62E-01	1.52E-01
20	9.06899E+02	3.58E-01	9.65E-02
21	3.67263E+02	6.78E-01	1.90E-01
22	1.48729E+02	7.49E-01	2.15E-01
23	7.55014E+01	6.21E-01	1.80E-01
24	4.80520E+01	1.19E+00	3.59E-01
25	2.77000E+01	1.23E+00	3.74E-01
26	1.59680E+01	1.27E-03	7.45E-04
27	9.8770E+00*	1.30E+00	3.89E-01

* $E_{min} = 4$ eV

Table 7.5: Errors of group cross sections when collapsed with scalar vs. angular flux with 5 fuel rings and 8 azimuthal sectors.

		Error (%)	
Group	E_{max} (eV)	Scalar	Angular
15	9.11800E+03	1.29E-01	9.93E-03
16	5.53000E+03	1.75E-01	1.23E-02
17	3.51910E+03	4.04E-01	2.68E-02
18	2.23945E+03	5.67E-01	3.70E-02
19	1.45210E+03	5.75E-01	3.64E-02
20	9.06899E+02	3.65E-01	2.20E-02
21	3.67263E+02	6.99E-01	4.87E-02
22	1.48729E+02	7.75E-01	5.78E-02
23	7.55014E+01	6.47E-01	4.90E-02
24	4.80520E+01	1.24E+00	1.10E-01
25	2.77000E+01	1.27E+00	1.18E-01
26	1.59680E+01	1.29E-03	3.45E-04
27	9.8770E+00*	1.34E+00	1.21E-01

* $E_{min} = 4$ eV

error in any resonance group. Each curve shows a particular number of rings, with the number of sectors plotted on the abscissa. For scalar flux weighting, the errors are nearly constant between 1% and 2%. For angular flux weighting, the error is decreasing with finer discretization.

This demonstrates that the observed condensation errors can be removed by maintaining fine structure in both angle and space in the condensed cross sections. Maintaining one without the other is not sufficient to remove this error. Although this demonstration fully diagnoses the observed errors, this does not suggest that the ultimate solution to condensation errors is to use such fine structure. This would come at a great computational expense, as the spatial discretization increases the cost of the transport solve, and the angular dependent cross sections dramatically increase the memory requirements.

7.4 Alternatives to Explicit Angular Dependent Cross Sections

7.4.1 Transport Correction

One tactic for accounting for angular effects in transport equations without explicitly modeling them is the transport correction. The transport correction has many definitions in the literature, and the discussion here follows that of [1, 40], which are derived from [41]. If the scatter source is written explicitly and the total and scattering reaction rates from Eq. (7.3) are expanded in Legendre polynomials in angle, the transport equation in 1-D slab geometry becomes

$$\mu\frac{\partial}{\partial x}\psi_g(x,\mu)+\sum_{l=0}^{\infty}\frac{2l+1}{2}\mathcal{P}_l(\mu)\Sigma_{t,g,l}(x)\phi_{g,l}(x)=\sum_{l=0}^{\infty}\frac{2l+1}{2}\mathcal{P}_l(\mu)\sum_{g'}\Sigma_{s,g'\rightarrow g,l}(x)\phi_{g',l}(x)+Q_g(x,\mu) \quad . \tag{7.10}$$

The Legendre moments of the flux are defined as

$$\phi_{g,l}(x)=\int_g \mathrm{d}E\int_{-1}^{1}\mathrm{d}\mu\,\mathcal{P}_l(\mu)\psi(x,\mu,E) \quad . \tag{7.11}$$

If the summations over l are brought to the right hand side and $\hat{\Sigma}_{t,g}(x)\psi_g(x,\mu)$ is added to both sides, the transport corrected form of the transport equation is obtained:

$$\begin{aligned}\mu\frac{\partial}{\partial x}\psi_g(x,\mu)+&\hat{\Sigma}_{t,g}(x)\psi_g(x,\mu)=\\ &\sum_{l=0}^{\infty}\frac{2l+1}{2}\mathcal{P}_l(\mu)\sum_{g'}\left[\Sigma_{s,g'\rightarrow g,l}(x)-\left(\Sigma_{t,g,l}(x)-\hat{\Sigma}_{t,g}(x)\right)\delta_{g,g'}\right]\phi_{g',l}(x)+Q_g(x,\mu) \quad ,\end{aligned} \tag{7.12}$$

where $\delta_{g,g'}$ is the Kronecker delta function. No approximations have been made, and so this form is exactly the same equation as the multigroup transport equation. However, in practice,

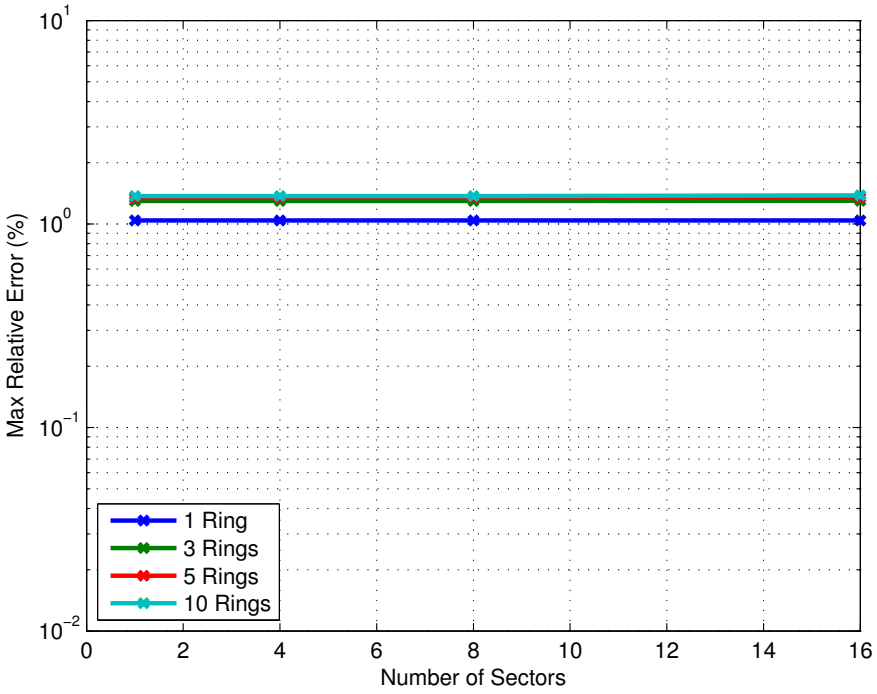

Figure 7.6: Maximum relative error resulting from scalar flux weighting for various pin discretizations.

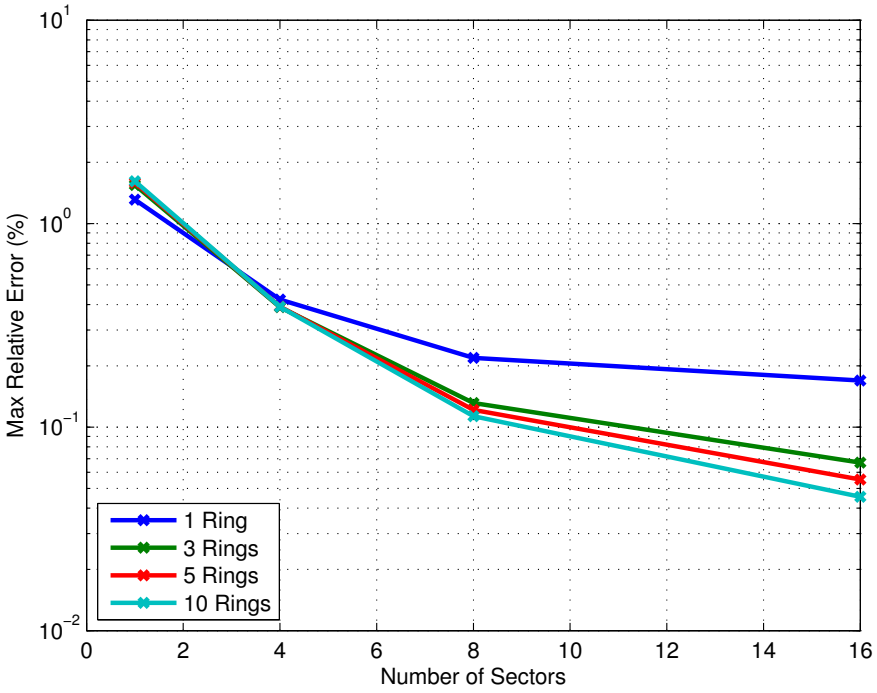

Figure 7.7: Maximum relative error resulting from angular flux weighting for various pin discretizations.

this is an approximation, as the Legendre order is truncated at some maximum value L:

$$\mu\frac{\partial}{\partial x}\psi_g(x,\mu)+\hat{\Sigma}_{t,g}(x)\psi_g(x,\mu) = \sum_{l=0}^{L}\frac{2l+1}{2}\mathcal{P}_l(\mu)\sum_{g'}\left[\Sigma_{s,g'\to g,l}(x)-\left(\Sigma_{t,g,l}(x)-\hat{\Sigma}_{t,g}(x)\right)\delta_{g,g'}\right]\phi_{g',l}(x)+Q_g(x,\mu) \quad . \tag{7.13}$$

The terms in square brackets are the transport corrected scattering matrix $\hat{\Sigma}_{s,g'\to g,l}$. The variable $\hat{\Sigma}_{t,g}$ is a free parameter and can be chosen arbitrarily. Different choices have been dubbed as different forms of the transport approximation. Some possibilities include the Consistent-P transport approximation:

$$\hat{\Sigma}_{t,g} = \Sigma_{t,g,0} \quad , \tag{7.14}$$

the Inconsistent-P transport approximation:

$$\hat{\Sigma}_{t,g} = \Sigma_{t,g,L+1} \quad , \tag{7.15}$$

the Diagonal transport approximation:

$$\hat{\Sigma}_{t,g} = \Sigma_{t,g,L+1} - \Sigma_{s,g'\to g,L+1} \quad , \tag{7.16}$$

the Bell-Hansen-Sandmeier (BHS) approximation:

$$\hat{\Sigma}_{t,g} = \Sigma_{t,g,L+1} - \sum_{g'}\Sigma_{s,g\to g',L+1} \quad , \tag{7.17}$$

and the Inflow transport approximation:

$$\hat{\Sigma}_{t,g} = \Sigma_{t,g,L+1} - \frac{\sum_{g'}\Sigma_{s,g'\to g,L+1}\phi_{g,L+1}}{\phi_{g,L+1}} \quad . \tag{7.18}$$

These approximations, especially the BHS transport approximation, are commonly encountered in existing deterministic neutron transport codes. However, such correction is typically performed to account for one more Legendre moment of anistropic scattering than is explicitly modeled. But even in cases without any anisotropic scattering, the angular dependence of the collapsed cross section can still be modeled in this manner. Rather than explicitly modeling the angular dependence of the cross section, the anisotropy is moved to the right hand side and takes the form of a higher order scattering moment.

Now, consider a simple example of the transport approximation applied to correct condensation errors. Consider an isolated 1-D slab containing UO_2. All uranium is considered to be U-238 with number density $0.022\,\mathrm{a/b\text{–}cm}$. The energy range 4–10 eV is considered. All scattering is considered to be potential scattering, and the narrow resonance model is used as the scatter

Table 7.6: Condensation errors in slab reaction rates using transport corrections.

Legendre Order	Error (%)			
	Scalar	Angular	Consistent-P	Inconsistent-P
0	0.277	0.001	0.277	-0.037
1			-1.152	-0.295
2			-0.084	-0.149
3			-0.148	-0.153
4			-0.031	-0.058
5			-0.047	-0.078

source. The reference solution is that of an ultrafine solution. With the reference continuous energy flux, the cross section is collapsed by the scalar flux, by the angular flux, and into moments. Collapsed cross sections are then used for a one-group simulation and the reaction rates are compared. Two transport corrections are considered, the Consistent-P and the Inconsistent-P. Because all scattering is assumed to be potential scattering, there are no higher order scattering moments, and so the Inconsistent-P is equivalent to the Bell-Hansen-Sandmeier transport correction. Condensation errors are shown in Tab. 7.6.

The scalar collapse results in a positive condensation error, consistent with what was seen in the pin-cell. The angular collapse recovers the reaction rate exactly. Using transport corrections, the error does not behave monatonically with Legendre order, but higher orders are seen to yield better results. Note that with Legendre order 0, the Consistent-P approximation is equivalent to a scalar flux collapse.

7.4.2 SPH Factors

As discussed in Sec. 7.1, multigroup cross sections are defined in such a way as to preserve reaction rates, but an approximation prevents this from being true in general. The left hand side cross sections should be collapsed with the angular flux, but the scalar flux is often used instead to simplify the resulting data. While Sec. 7.3 shows that biases seen in condensation can be attributed to this approximation, it did not present a viable alternative. One such alternative is the *superhomogénéisation* (SPH) factor.

The SPH factor was originally used as a corrective factor to enforce conservation during spatial homogenization [42]. It has been used in cross section condensation without spatial homogenization [28] more recently, but very little discussion of the need for its use has been included in this recent work. Here, the SPH factor is only considered in the case of no spatial homogenization.

The SPH factor is defined as the multiplicative factor needed to adjust cross sections computed from Eq. (7.7) such that reaction rates are preserved. Usually notated as μ, the SPH

factor is thus inserted into the definition of the multigroup cross section, and the new collapsed cross section equation for reaction ρ is

$$\tilde{\sigma}_{\rho,g} = \mu_g \frac{\int_{E_{g+1}}^{E_g} \mathrm{d}E\, \sigma_\rho(\vec{r}, E)\phi(\vec{r}, E)}{\int_{E_{g+1}}^{E_g} \mathrm{d}E\, \phi(\vec{r}, E)} \quad . \tag{7.19}$$

The same SPH factor μ_g is applied to each partial cross section and to the total cross section for each nuclide in a given spatial region. Note that this equation is valid for all cross sections—including the left hand side cross sections.

SPH factors can be determined by simple purely absorbing fixed source equations, coarse group by coarse group. The SPH factor for each coarse group can be computed without knowledge of the other groups, as the equations are not coupled. The equations are solved iteratively, and in practice the equations converge rapidly. The equation solved at iteration n is

$$\hat{\Omega} \cdot \nabla \tilde{\psi}_g^{(n)}(\vec{r}, \hat{\Omega}) + \mu_g^{(n-1)}(\vec{r})\Sigma_t(\vec{r})\tilde{\psi}_g^{(n)}(\vec{r}, \hat{\Omega}) = Q_g(\vec{r}, \hat{\Omega}) \quad . \tag{7.20}$$

This equation yields the SPH-corrected angular flux $\tilde{\psi}_g$ which can be integrated to yield the SPH-corrected scalar flux $\tilde{\phi}_g$. The cross section Σ_t is the uncorrected cross section computed from Eq. (7.7). The source Q_g is the source used in the fine group problem (e.g., ultrafine, Monte Carlo, subgroup) integrated over energy. After solving this problem, the updated SPH factor is computed:

$$\mu_g^{(n)}(\vec{r}) = \frac{\phi_g(\vec{r})}{\tilde{\phi}_g^{(n)}(\vec{r})} \quad , \tag{7.21}$$

where ϕ_g is the uncorrected group-integrated flux, computed from the fine group problem.

Spatial dependence is shown here as continuously varying. However, standard practice is to apply SPH factors by spatial region. For discretizations of spatial regions, one can choose as an implementation decision whether to apply different SPH factors to each discretization zone or only a single to the macro-region. Note that this procedure does not produce unique factors if applied to every spatial domain in a system without leakage. Thus, it is typical to enforce $\mu_g = 1$ for all non-resonant regions (e.g., moderator).

Finally, note that this procedure is intended to preserve reaction rates, not the group-integrated flux. If one desires the flux after a downstream calculation in which SPH-correct cross sections were used, the inverse of the SPH factor must be applied to the resultant flux to attain an estimate of the true flux:

$$\begin{aligned} \phi_g(\vec{r}) &= \mu_g(\vec{r})\tilde{\phi}_g(\vec{r}) \\ \psi_g(\vec{r}, \hat{\Omega}) &= \mu_g(\vec{r})\tilde{\psi}_g(\vec{r}, \hat{\Omega}) \quad . \end{aligned} \tag{7.22}$$

Now, consider an example showing the utility of the SPH factors. The simple problems

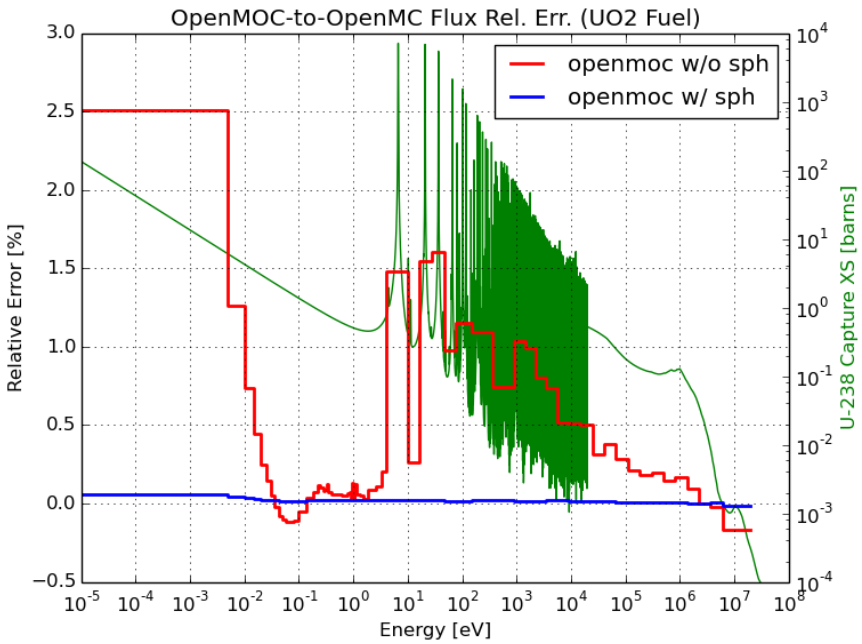

Figure 7.8: Condensation errors in multigroup cross sections generated by OpenMC and used in OpenMOC with and without SPH factors. *Courtesy of W. Boyd.*

considered so far in this Part cannot be used to demonstrate the effectiveness of the SPH process, as the definition of the SPH factor ensures that single-group reaction rates are conserved exactly. However, the Monte Carlo cross section generation discussed briefly in Sec. 7.2 can be revisited. First, consider the errors as plotted in Fig. 7.8. The use of the SPH factor reduces the errors in the reaction rate in each group such that they nearly vanish. The computed eigenvalue error correspondingly vanishes. For a variety of group structures, the bias associated with condensation errors is shown in Tab. 7.7.

7.5 Revisiting ESSM

By understanding these condensation errors, the Embedded Self-Shielding Method, introduced in Sec. 3.7 and whose performance was assessed in Sec. 6.4.2, should be revisited.

As seen previously, ESSM finds an equivalence between a homogeneous problem and a heterogeneous problem, but is prone to large errors in the inferred cross section when small errors are present in the heterogeneous calculation. However, when multigroup cross sections are generated by Eq. (7.7), small errors in the flux should be expected. Here, it will be shown that much of the performance woes of ESSM, highlighted in Sec. 6.4.2 can be attributed to this issue. The same benchmark problem is used with a slightly changed ESSM procedure.

First, the reference SPH factor for the heterogeneous geometry is generated. This is done by solving the reference problem for the ultrafine flux. This flux is used to collapse to a

Table 7.7: Biases due to condensation error in Monte Carlo cross section generation. *Courtesy of W. Boyd.*

Reference	Groups	Bias [pcm]	
		No SPH	With SPH
1.17421 ± 0.00003	1	+69	+7
	2	+49	+11
	4	+51	+11
	8	-91	+11
	16	-99	+11
	25	-164	+9
	40	-178	+10
	70	-187	+10

multigroup cross section. Then, the SPH procedure is performed to ensure the reaction rates in the condensed problem match that of the reference. The resulting SPH factor is stored. For configuration k, let this be notated μ_k.

Then, the ESSM procedure is amended to:

1. Guess $\Sigma_{eq,g}$.
2. Compute cross sections from dilution table using $\Sigma_{eq,g}$.
3. Adjust the cross sections by the SPH factor: $\tilde{\Sigma} = \mu_k \Sigma$.
4. Solve Eq. (6.24) with the corrected cross sections.
5. Un-correct the flux by the SPH factor: $\phi = \mu_k \tilde{\phi}$.
6. Use un-corrected flux from heterogeneous equation, and solve Eq. (6.23) for $\Sigma_{eq,g}$.
7. Iterate, repeating steps 2–6 to convergence.

Several cases of the benchmark problem are solved with this process, and results are compared to the original ESSM results. Results for the 1-D isolated slab with a square resonance are shown in Tables 7.8 to 7.10. Results for the 2-D reflected pin-cell with a single-level Breit-Wigner resonance are shown in Tables 7.11 to 7.13.

ESSM using the SPH factor has considerably better performance than without the SPH factor. In the square resonance cases, the errors essentially vanish. In the SLBW resonance cases, the errors are drastically reduced. If the results are compared to those from Ch. 6, these are seen to outperform the Wigner and Wigner-Bell equivalence in dilution methods, but still exhibit more error than the Carlvik and subgroup results. This is because the errors resulting from errors in the heterogeneous problem have vanished, but the method is still reliant on a one-term rational approximation.

Note that for the slab case with a square resonance the SPH factors are incredibly close to unity. The drastic reduction in error associated with such a small perturbation of the flux suggests that ESSM is quite ill-conditioned for this problem and that the solution is very sensitive to the chosen SPH factor. Fortunately, this is explained in large part by the very small impact on the flux that the square resonance has. For more realistic problems, like those of the SLBW resonance, the SPH factor is further from unity and ESSM is less ill-conditioned. That said, the SPH factors still do not deviate too far from unity.

Although results have drastically improved with this technique, this analysis does not provide a procedure for use in place of existing ESSM implementations. The SPH factor here required knowledge of the reference solution. Of course, if the reference solution were known, no further self-shielding calculation would be needed. Thus, this simply characterizes the observed errors rather than solving them.

However, these results do suggest a path forward with ESSM. Although the originally published descriptions of ESSM use the methods analyzed here, current implementations use heterogeneous tables rather than homogeneous tables. This procedure is revisited in Ch. 9 with more discussion. However, for the purposes of this discussion, the heterogeneous calculations at table generation provide an opportunity to compute the SPH factor save it in the table. These SPH factors are likely to be a good approximation for the true SPH factor for the full geometry.

7.6 Chapter Summary

In this chapter, errors resulting from scalar flux weighting the total cross section were examined. Even if the exact flux spectrum was known—e.g., by using Monte Carlo methods—significant errors can be seen in the multigroup cross section if angular effects are not accounted for. For the large low-lying resonances of U-238, errors were seen to be on the order of 1%.

The use of angular-dependent cross sections can alleviate these issues. However, it must be accompanied by sufficient spatial discretization to be effective. The most important aspect of the angular effect was shown to be accounting for neutrons entering a fuel region directly from the moderator versus neutrons traversing another fuel region first.

Two approaches were considered to account for these issues without directly using angular dependent cross sections. The first is to use a transport correction, where the anisotropic components of the multigroup total reaction rate are moved to the right hand side of the transport equation as part of the scatter source. The other was the SPH factor, which is a correction factor that ensures that the reaction rate in a group is conserved, compared to a fine-group solution.

Table 7.8: Comparison of ESSM with and without SPH factor using a square resonance and a 0.3 cm-width slab.

Peak [b]	Reference [b]	SPH	Error [%]	
			ESSM (No SPH)	ESSM (SPH)
2	0.0009	1.00000	-0.02	0.00
5	0.0023	1.00000	-0.13	0.00
10	0.0045	1.00000	-0.44	0.00
25	0.0101	1.00001	-1.75	0.00
50	0.0173	1.00002	-3.98	0.00
75	0.0227	1.00003	-5.69	0.00
100	0.0268	1.00004	-6.88	0.01
175	0.0347	1.00005	-8.39	0.01
250	0.0390	1.00004	-8.25	0.01
375	0.0424	1.00004	-6.82	0.01
500	0.0440	1.00003	-5.15	0.00
750	0.0453	1.00001	-2.49	0.00
1000	0.0459	1.00000	-0.77	0.00
5000	0.0472	0.99998	4.12	0.00
10000	0.0474	0.99998	4.79	0.00

Table 7.9: Comparison of ESSM with and without SPH factor using a square resonance and a 0.4 cm-width slab.

Peak [b]	Reference [b]	SPH	Error [%]	
			ESSM (No SPH)	ESSM (SPH)
2	0.0009	1.00000	-0.02	0.00
5	0.0023	1.00000	-0.14	0.00
10	0.0044	1.00000	-0.45	0.00
25	0.0097	1.00001	-1.72	0.00
50	0.0161	1.00002	-3.63	0.00
75	0.0206	1.00003	-4.86	0.00
100	0.0239	1.00003	-5.53	0.00
175	0.0297	1.00003	-5.58	0.00
250	0.0325	1.00002	-4.43	0.00
375	0.0346	1.00001	-2.13	0.00
500	0.0355	1.00000	-0.22	0.00
750	0.0364	0.99999	2.28	0.00
1000	0.0368	0.99998	3.72	0.00
5000	0.0378	0.99996	7.56	-0.01
10000	0.0379	0.99996	8.08	-0.01

Table 7.10: Comparison of ESSM with and without SPH factor using a square resonance and a 0.6 cm-width slab.

Peak [b]	Reference [b]	SPH	Error [%]	
			ESSM (No SPH)	ESSM (SPH)
2	0.0009	1.00000	-0.02	0.00
5	0.0023	1.00000	-0.13	0.00
10	0.0043	1.00000	-0.42	0.00
25	0.0091	1.00001	-1.43	0.00
50	0.0143	1.00001	-2.55	0.00
75	0.0177	1.00001	-2.85	0.00
100	0.0200	1.00001	-2.64	0.00
175	0.0236	1.00000	-0.80	0.00
250	0.0251	0.99999	1.26	0.00
375	0.0263	0.99998	3.85	0.00
500	0.0268	0.99997	5.52	-0.01
750	0.0274	0.99997	7.40	-0.01
1000	0.0277	0.99996	8.41	-0.01
5000	0.0284	0.99995	11.03	-0.01
10000	0.0285	0.99995	11.38	-0.01

Table 7.11: Comparison of ESSM with and without SPH factor using a SLBW resonance and a 0.3 cm-radius pin.

Peak [b]	Reference [b]	SPH	Error [%]	
			ESSM (No SPH)	ESSM (SPH)
2	0.0260	1.00000	0.00	0.00
5	0.0639	1.00000	0.01	0.00
10	0.1243	1.00000	0.02	0.00
25	0.2873	0.99998	0.13	0.02
50	0.5115	0.99991	0.49	0.08
75	0.6924	0.99982	1.01	0.17
100	0.8421	0.99970	1.62	0.27
175	1.1724	0.99930	3.58	0.60
250	1.3991	0.99889	5.40	0.91
375	1.6641	0.99831	7.83	1.34
500	1.8566	0.99783	9.59	1.66
750	2.1394	0.99712	11.86	2.12
1000	2.3540	0.99662	13.19	2.44
5000	4.0977	0.99383	15.24	3.82
10000	5.4323	0.99249	14.07	3.89

Table 7.12: Comparison of ESSM with and without SPH factor using a SLBW resonance and a 0.4 cm-radius pin.

Peak [b]	Reference [b]	SPH	Error [%]	
			ESSM (No SPH)	ESSM (SPH)
2	0.0258	1.00000	0.00	0.00
5	0.0631	1.00000	0.01	0.00
10	0.1213	0.99999	0.04	0.01
25	0.2724	0.99996	0.23	0.04
50	0.4675	0.99986	0.76	0.12
75	0.6163	0.99973	1.43	0.23
100	0.7348	0.99958	2.14	0.35
175	0.9862	0.99914	4.13	0.69
250	1.1551	0.99874	5.73	0.96
375	1.3538	0.99822	7.60	1.30
500	1.5010	0.99782	8.83	1.54
750	1.7228	0.99724	10.26	1.88
1000	1.8955	0.99684	11.01	2.11
5000	3.3810	0.99453	11.39	2.96
10000	4.5461	0.99333	10.30	2.86

Table 7.13: Comparison of ESSM with and without SPH factor using a SLBW resonance and a 0.6 cm-radius pin.

Peak [b]	Reference [b]	SPH	Error [%]	
			ESSM (No SPH)	ESSM (SPH)
2	0.0253	1.00000	0.00	0.00
5	0.0602	1.00000	0.01	0.00
10	0.1114	0.99999	0.03	0.01
25	0.2292	0.99997	0.16	0.03
50	0.3600	0.99991	0.43	0.07
75	0.4501	0.99985	0.71	0.12
100	0.5186	0.99979	0.94	0.16
175	0.6605	0.99964	1.48	0.26
250	0.7574	0.99952	1.82	0.32
375	0.8760	0.99937	2.15	0.40
500	0.9679	0.99926	2.34	0.46
750	1.1129	0.99911	2.53	0.54
1000	1.2308	0.99900	2.61	0.58
5000	2.3270	0.99828	2.42	0.67
10000	3.2071	0.99764	2.29	0.55

Chapter 8

Mutual Self-Shielding

8.1 Manifestations

The methods outlined in Part II serve to generate multigroup cross sections in the resonance range when a system contains only a single resonant nuclide. In real reactor applications, this is never the case. Although some discussion of generalizing to multiple nuclides has been included previously in this thesis, the effect of multiple nuclides is explored in more detail here. Because the self-shielding of one nuclide's resonances can impact the flux seen by another nuclide, the effect of multiple resonant nuclides is known as mutual self-shielding.

Figure 8.1 shows a plot of the resonances of several common nuclides encountered in reactor physics in the 4–23 eV energy range. As is easily seen, the resonances do not exist in isolation. Resonances of one nuclide exist at energies very near the resonances of another nuclide, and sometimes the resonances even overlap. Methods that ignore the effect of other nuclides cannot be expected to accurately predict the fine structure of the flux seen by each nuclide.

The effects of mutual self-shielding can be separated into two types, resonance overlap and resonance interference without overlap. In this chapter, these effects will be discussed in detail along with classical approaches to this phenomenon. Also, two new methods for accounting for the effects will be presented in Sections 8.3 and 8.4.

8.1.1 Resonance Overlap

The first type of mutual self-shielding is resonance overlap. This occurs when resonances of two nuclides in a system are centered at energies close enough together that both nuclides have significant resonance cross sections. Then, the flux depression due to one nuclide's resonance will lower the reaction rate in the other nuclide, compared to the nuclides existing in isolation. Thus, by neglecting the effects of resonance overlap, the reaction rate and thus the group averaged cross section will be overpredicted, potentially drastically.

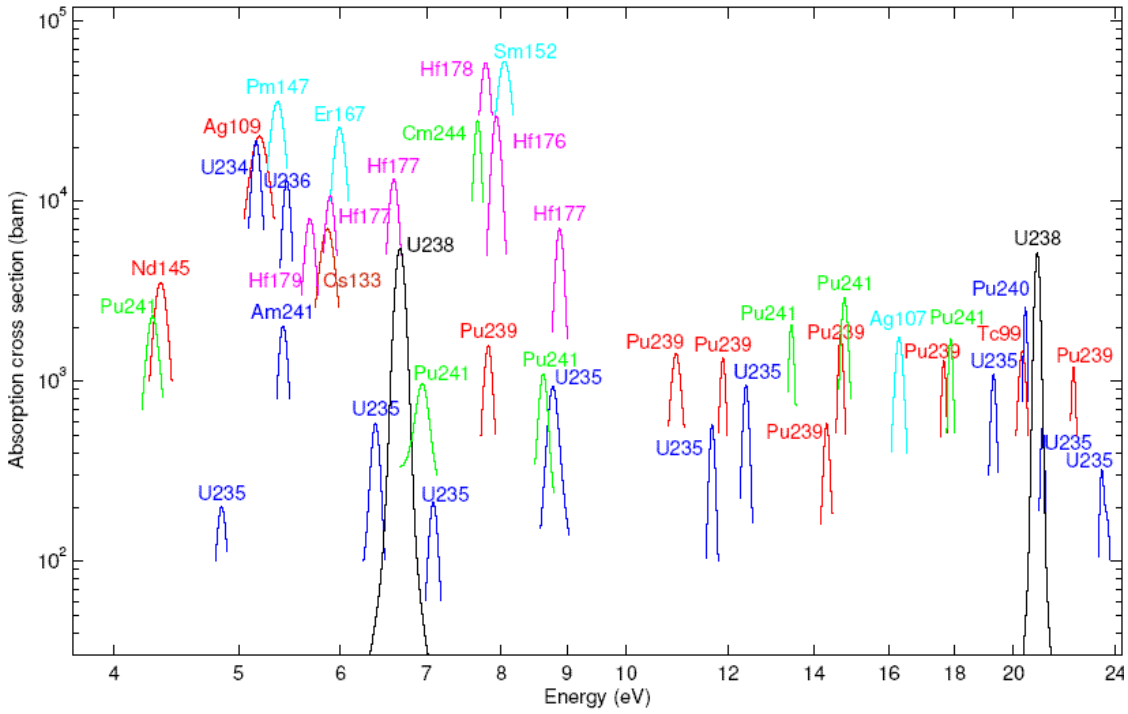

Figure 8.1: Energy location of resonances of several nuclides in the 4-23 eV energy range. Reproduced from [43].

To see this, consider a simple extension of the benchmark presented in Ch. 6. Here, the benchmark contains two nuclides, the primary nuclide and an interfering nuclide. Although similar results could be obtained for more complicated geometries, only an isolated 1-D slab of width 0.4 cm is considered here. The subgroup results are with 6 subgroup levels, with the quadrature generated by a fitting procedure. For the fitting procedure, cross sections from infinite media in varying background states are used as the reference data, and the narrow resonance formulation is used for the subgroup approximation.

Transport calculations for the benchmark are performed using a two-region collision probability model. For the 1-D results presented here, the collision probabilities are analytic. The narrow resonance approximation is used for the scattering source. The reference solution is computed using an ultrafine energy discretization. Results are shown as relative errors, where positive errors represent obtained cross sections greater than the reference and negative errors represent obtained cross sections less than the reference.

For the primary nuclide, as in the original benchmark specification, a single resonance with the shape of a real U-238 resonance at 1050 eV is considered, varying the height by multiplicatively scaling the cross section. For the interfering nuclide, a single resonance is used, with its potential scattering set to 0. Multiplicatively scaling the second resonance is the equivalent of varying the relative number density between the two nuclides. When two nuclides are present in a system, macroscopic cross sections are the appropriate way to combine

Table 8.1: Errors from cross sections generated by subgroup for nuclide without an interfering nuclide.

Peak [b]	Reference [b]	Error [%]
5	0.063	-0.014
25	0.278	-0.008
100	0.796	0.170
375	1.556	0.489
1000	2.191	-0.536

Table 8.2: Errors from cross sections generated by subgroup for primary nuclide with second nuclide resonance overlapping, as in Fig. 8.2.

Peak [b]	Reference [b]	Error [%]
5	0.040	59.325
25	0.182	52.964
100	0.558	42.847
375	1.199	30.414
1000	1.809	20.455

their effects. However, for simplicity, effective microscopic cross sections are used here,

$$\begin{aligned} \sigma^1 &= \frac{\Sigma^1}{N^1} \\ \sigma^2 &= \frac{\Sigma^2}{N^2} \quad . \end{aligned} \tag{8.1}$$

Various spacings in energy between the peak of the primary nuclide resonance and the interfering nuclide resonance are considered so that both resonance overlap and resonance interference without overlap are represented.

Before examples with mutual self-shielding effects are presented, consider the performance of subgroup on an example with only one nuclide, without interference from a second nuclide. Table 8.1 gives these results. All errors are considerably less than 1% and vary in sign.

To illustrate the effect of resonance overlap, an interfering nuclide with resonance height 375 b with a peak at 1051 eV, 1 eV away from the peak of the primary nuclide's resonance, is added as illustrated in Fig. 8.2. Using the traditional subgroup method, the effective group capture cross section is computed for the primary nuclide in this configuration. These effective group cross sections for various primary nuclide peak heights are presented in Tab. 8.2.

The subgroup cross sections show very large errors, as much as 60%. As these errors are all positive, this indicates that neglecting mutual self-shielding leads to a gross overprediction of the cross section. Note that this is a pathological benchmark example, thus errors of this magnitude are not seen for important nuclides in typical reactor analysis. However, when one

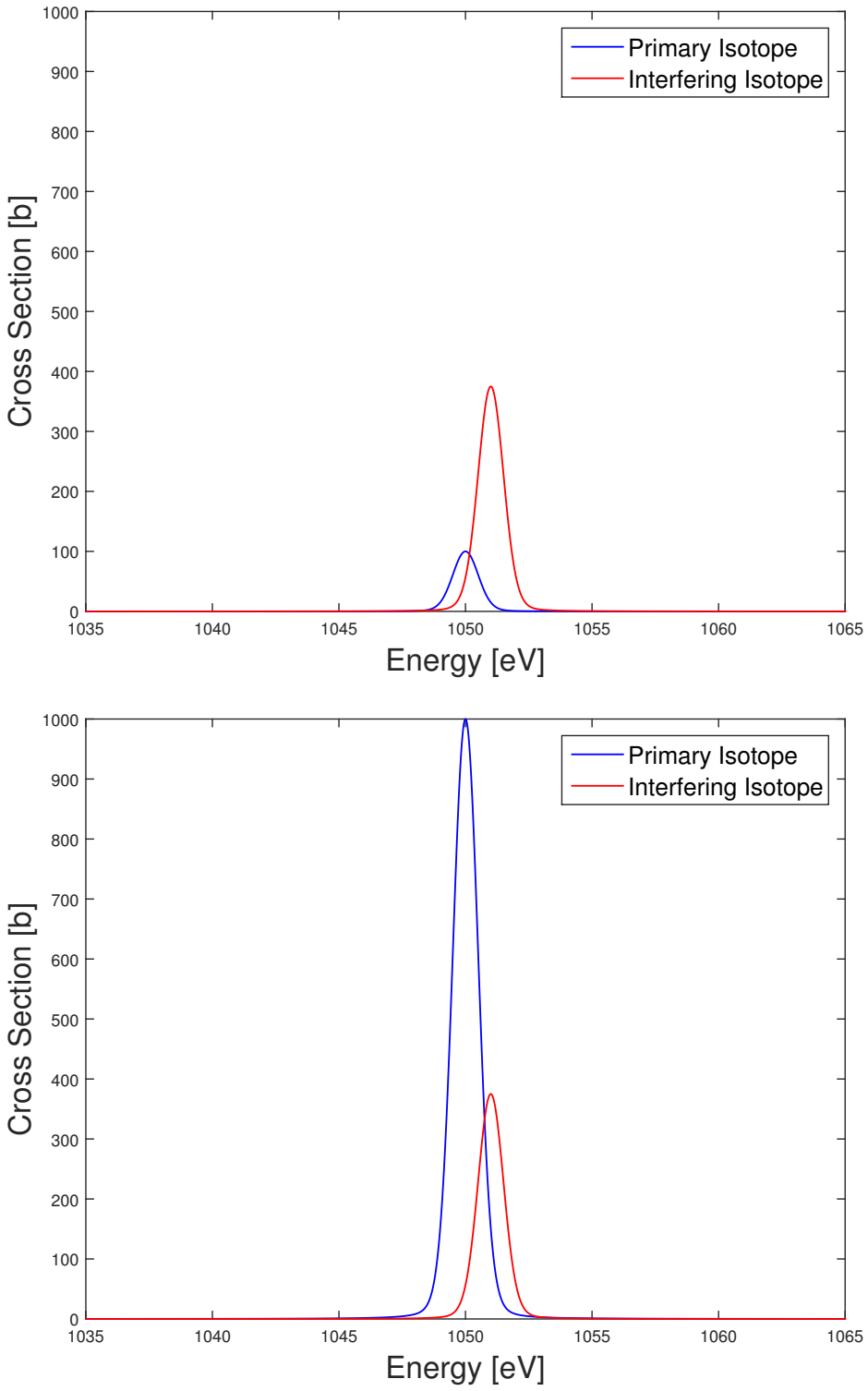

Figure 8.2: Illustration of cross sections for resonance overlap example. Small primary cross section relative to interfering cross section (above); large primary cross section relative to interfering cross section (below).

Table 8.3: Errors from cross sections generated by subgroup for primary nuclide with second nuclide resonance separated in energy, as in Fig. 8.3.

Peak [b]	Reference [b]	Error [%]
5	0.064	-1.605
25	0.283	-1.792
100	0.809	-1.456
375	1.581	-1.122
1000	2.225	-2.052

is interested in reaction rates of minor nuclides, such as in depletion calculations, these sorts of errors are possible.

8.1.2 Resonance Interference without Overlap

The second type of mutual self-shielding is resonance interference without overlap, although it is referred to by various other names throughout the literature. In this case, an nuclide's resonance causes a flux depression away from another nuclide's resonance. This depression should not play a large role in the reaction rate in the second nuclide's resonance, but it does affect the group-integrated flux needed to compute a multigroup cross section. It lowers said flux, raising the group-averaged cross section slightly. Thus, ignoring the effect of resonance interference without overlap leads to multigroup cross sections being slightly underpredicted.

To illustrate resonance interference without overlap, consider the benchmark problem from the previous section, but now take as an example the case where the interfering nuclide having a resonance height of 375 b, centered this time at 1060 eV, 10 eV separated from the primary nuclide's resonance. For various heights of the primary nuclide resonance, as illustrated in Fig. 8.3, effective group capture cross section results for the primary nuclide are presented in Tab. 8.3.

The errors in this case are much smaller than those of the overlapping case. However, these are still several times larger than compared with the single case. Additionally, these errors are all negative, indicating that neglecting the mutual self-shielding effect leads to an underprediction in the effective cross section. These sorts of errors are commonly found in realistic simulations.

8.2 Classical Approaches

8.2.1 Ultrafine Methods

The ultrafine methods described in Ch. 5 are the most direct way to account for mutual self-shielding. By modeling the flux and the cross section on an ultrafine or continuous energy mesh,

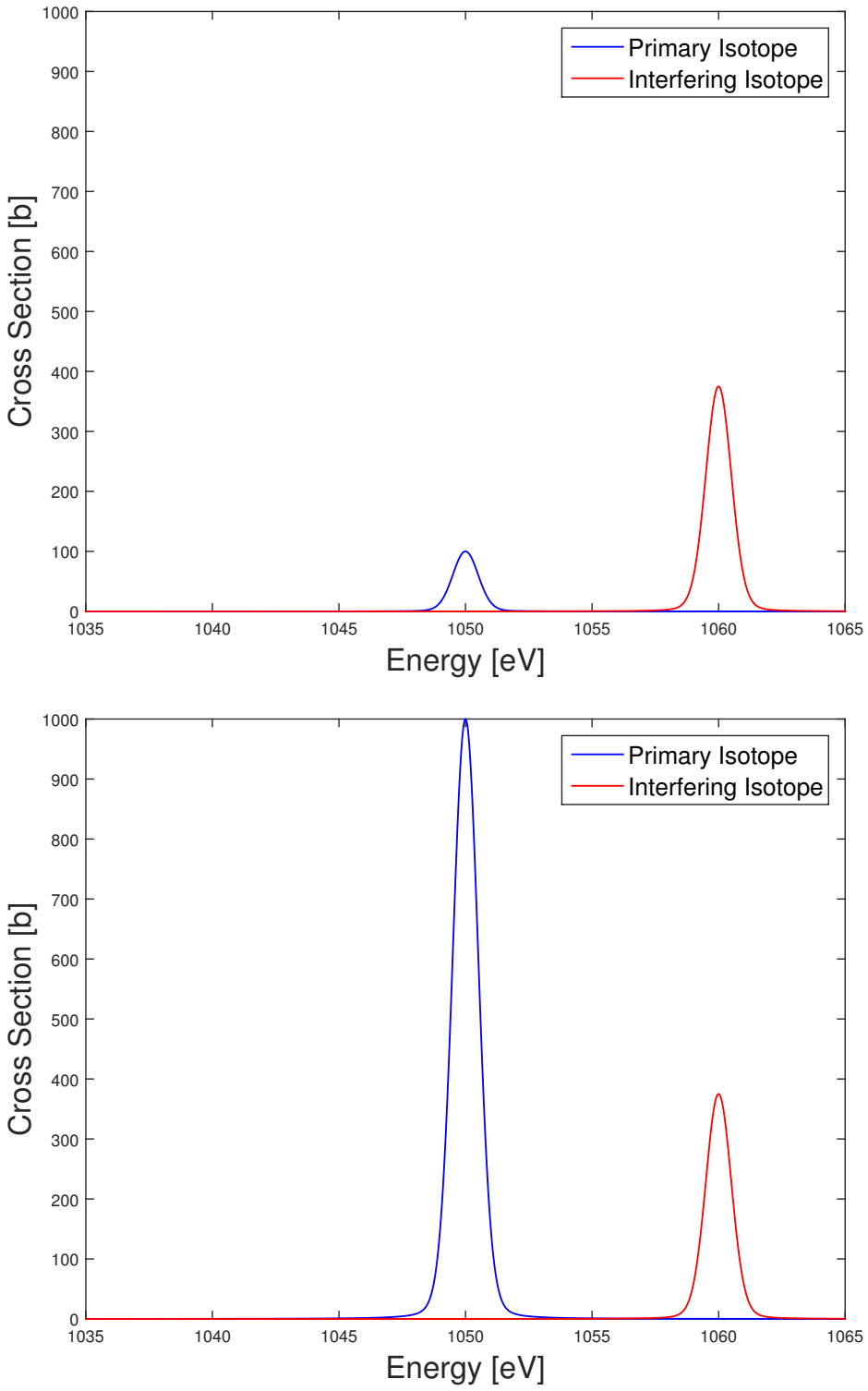

Figure 8.3: Illustration of cross sections for resonance interference without overlap example. Small primary cross section relative to interfering cross section (above); large primary cross section relative to interfering cross section (below).

the effects of self-shielding—and of course, any mutual self-shielding effects—are incorporated implicitly. Existing implementations are discussed in Ch. 5.

8.2.2 Resonance Interference Factors

One means of accounting for mutual self-shielding is an *ad hoc* method commonly referred to as Resonance Interference Factors. This very simple concept has been shown to reduce errors associated with mutual self-shielding in a variety of applications. It is, however, limited in that it merely applies a correction factor to computed quantites rather than modeling the physics directly. Furthermore, implementation for real systems can be very difficult due to the number of nuclides present. While it is simple to use for a small number of nuclides, it quickly becomes unwieldy with large numbers of nuclides.

A resonance interference factor is computed by first creating a resonant cross section table or resonance integral table, as discussed in Ch. 2. For this discussion, it is assumed that cross sections are kept in the table rather than resonance integrals. These tables are generally computed based on infinite media with a single resonant nuclide. However, in recent years, tables based on heterogeneous calculations are becoming more popular. For nuclide i, this gives the cross section as a function of the background cross section, $\sigma_g^i(\sigma_b^i)$.

Next, a table is made using multiple resonant nuclides. This is most often performed using a direct solution of the slowing down equation, but approximate solutions as discussed in Sec. 2.6.2 are also possible. With nuclides $j_1 \dots j_N$ present alongside nuclide i, the table gives the cross section as a function of the background cross section and the relative concentration of each nuclide $n^j = N^j/N^i$, which is notated $\sigma_g^i(\sigma_b^{i,j}, n^{j_1}, n^{j_2}, \dots, n^{j_N})$. This table is potentially very large, as each relative concentration is an independent variable. Also, the definition of the background cross section was adjusted to be

$$\sigma_b^{i,j} = \sigma_b^i - \sum_{k=1}^{N} \lambda^{j_k} n^{j_k} \sigma_p^{j_k} \quad , \tag{8.2}$$

where σ_b^i is the background cross section for analysis with a single resonant nuclide. This is equivalent to the sum of the potential scattering contributions from each nuclide not included in $\{i, j_1, \dots, j_N\}$.

The resonance interference factor is the ratio of values from the two tables,

$$f_{RI}^i(\sigma_b^{i,j}, n^{j_1}, n^{j_2}, \dots, n^{j_N}) = \frac{\sigma_g^i(\sigma_b^{i,j}, n^{j_1}, n^{j_2}, \dots, n^{j_N})}{\sigma_g^i(\sigma_b^i)} \quad . \tag{8.3}$$

The resonance interference factor is used to adjust cross sections generated considering only a single resonant nuclide. If a multigroup cross section is generated from some self-shielding

module as $\sigma^i_{g,0}$, the estimate of the true multigroup cross section is

$$\sigma^i_g = \sigma^i_{g,0} \cdot f^i_{RI}(\sigma^{i,j}_b, n^{j_1}, n^{j_2}, \ldots, n^{j_N}) \quad . \tag{8.4}$$

If the approximation is made that interference between certain nuclides can be treated independently of other nuclides, the resonance interference factor can be split into pieces. If only two nuclides are considered at a time, this is

$$\begin{aligned} f^i_{RI}(\sigma^{i,j}_b, n^{j1}, n^{j2}, \ldots, n^{jN}) &\approx \prod_{k=1}^{N} \frac{\sigma^i_g(\sigma^{i,j_k}_b, n^{j_k})}{\sigma^i_g(\sigma^i_b)} \\ &= \prod_{k=1}^{N} f^{i,j_k}_{RI}(\sigma^{i,j_k}_b, n^{j_k}) \quad . \end{aligned} \tag{8.5}$$

This approximation makes it clear that one can in practice choose which nuclides to include interference effects for and which not to. Neglecting terms close to unity in Eq. (8.5) will not lead to significant errors. Regardless of the number of terms included, this approximation will lead to a considerably smaller table size than Eq. (8.3), and thus may be necessary for practical considerations.

When this method is applied to equivalence in dilution methods, it is equivalent to simply pulling values from the multiple resonant nuclide table and f_{RI} does not need to be computed. In the subgroup method, the explicit f_{RI} table is necessary to apply the method. However, the subgroup method does not supply an appropriate choice of σ_b. One has several options. First, the most straightforward option is for σ_b to be computed as if the self-shielding was being carried out by equivalence in dilution methods. It would not be straightforward to define a procedure using multi-term rational approximations, but the effect should be captured adequately using a single term. Second, a single transport sweep can be used to infer the background cross section, similar to a single iteration of ESSM, as in [27, 44]. Note that [44] uses an additive correction factor rather than a multiplicative one.

By defining f_{RI} as a function of the background cross section, it is implicitly assuming the problem can be modeled as a two-region equivalent geometry. That is, intra-fuel discretization is not accounted for. It can be adapted to have a spatial dependence if f_{RI} were computed on unit cells, although this adds considerable complexity if the design space is at all large. One example of this adaptation can be found in [45].

8.2.3 Resonance Interference without Overlap in the Subgroup Method

Resonance interference without overlap is, in general, somewhat less difficult from a methods perspective than resonance overlap. This is because the effect manifests as a reduction in the group-integrated flux, not in the reaction rate in the resonance of the nuclide of interest.

Thus, knowledge of both nuclides' resonances simultaneously is not strictly necessary. In using homogeneous slowing down tables, two methods to account for resonance interference without overlap were discussed in Sec. 2.6.3. As these tables are used directly in equivalence-based methods, treatment for resonance interference without overlap is easily accomplished in equivalence in dilution.

In the subgroup method, such treatment is less straightforward. However, recent work has created analogs for both methods discussed in Sec. 2.6.3. These methods are described here.

First, in [46], the analog to flux correction is seen. The group-averaged cross section for nuclide i is written as

$$\sigma_g^i = \frac{\sum_n w_n^i \sigma_n^i \phi_n^i}{1 + \sum_j \sum_n w_n^j (\phi_n^j - 1)} \quad . \tag{8.6}$$

Here, j represents each nuclide in the system, and ϕ_n^i is the flux implied by the cross section value. In the fitting process, the intermediate resonance model were used, this is

$$\phi_n^i = \frac{\lambda^i \sigma_p^i + \sigma_b^i}{\sigma_n^i + \sigma_b^i} \quad , \tag{8.7}$$

but other choices are possible. In the paper, the fluxes are computed in a heterogeneous calculation. With this definition of the group-averaged cross section, a fitting process is performed to compute the best fit quadrature. Because it would be difficult to perform this process with many nuclides, the implementation described in the paper considers only two nuclides at a time, the nuclide of interest and the "most important" other nuclide. For LWR applications, the "most important" other nuclide is almost always U-238, aside from the case of U-238 itself. When two nuclides are mutually most important, they must be fit together. Otherwise, the quadrature of the most important nuclide can be held constant during the fitting of the nuclide of interest's quadrature. This fitting is performed for a variety of ratios of number densities of the two nuclides, resulting in a separate quadrature for each ratio.

Second, in [24], an analog to background cross section iteration is developed. Here, a term known as "rest absorption" and given as σ_x is added to the subgroup fixed source equations and is used in the fitting procedure. This rest absorption is defined as

$$\sigma_x^i = \frac{1}{N^i} \sum_j \sigma_a^j \quad . \tag{8.8}$$

Then, the fixed source equations take the form

$$\hat{\Omega} \cdot \nabla \psi_n^i + N^i (\sigma_n^i + \sigma_{x,g}^i) \psi_n^i = Q_{sg}^i \quad . \tag{8.9}$$

In the fitting process, the flux used for the approximate solution is likewise adjusted to

incorporate this rest absorption. If the intermediate resonance model is used, this is

$$\phi_n^i = \frac{\sigma_p^i + \lambda^i \sigma_b^i}{\sigma_n^i + \sigma_{x,g}^i + \sigma_b^i} \quad , \tag{8.10}$$

Note that the rest absorption terms in these equations are the group-averaged rest absorption. This requires knowledge of the group-averaged absorption cross section for each nuclide, thus requiring an iteration process, similar to the iteration described in Sec. 2.6.3.

8.2.4 Matrix Quadrature in Subgroup

To account for mutual self-shielding—both resonance overlap and resonance interference without overlap—in the subgroup method directly has been considered as a topic of research. Most existing forays into this field have constructed the subgroup quadrature as a matrix, such that a subgroup fixed source equation is solved for each of an nuclide's subgroup levels using each level of another nuclide. These methods are discussed here. A new method that does not require a full matrix of solutions is presented in this thesis in Sec. 8.3.

Consider two nuclides whose resonances are known to interfere with each other. This approach generates a quadrature matrix. Rather than computing a vector of weights w_n for nuclide i and another w_m for nuclide j, a matrix of weights $W_{n,m}$ is generated. Then, the group averaged cross section as computed by the subgroup method is

$$\begin{aligned} \sigma_g^i &= \frac{\sum_n \sum_m W_{n,m} \sigma_n \phi_{n,m}}{\sum_n \sum_m W_{n,m} \phi_{n,m}} \\ \sigma_g^j &= \frac{\sum_n \sum_m W_{n,m} \sigma_m \phi_{n,m}}{\sum_n \sum_m W_{n,m} \phi_{n,m}} \quad . \end{aligned} \tag{8.11}$$

Here, $\phi_{n,m}$ is the flux resulting when nuclide i has cross section σ_n and nuclide j has cross section σ_m. This requires solving a subgroup fixed source problem for all combinations of N subgroup levels of nuclide i and M subgroup levels of nuclide j, for a total of $N \times M$ equations.

The weight matrix $W_{n,m}$ is subject to the constraints

$$\sum_n W_{n,m} = 1 \qquad \forall m \tag{8.12}$$

$$\sum_m W_{n,m} = 1 \quad \forall n \quad , \tag{8.13}$$

which is equivalent to enforcing that weights sum to unity in the typical subgroup method. This matrix takes into account correlation effects between the cross section of nuclides i and j. If no such correlation exists—i.e., if the likelihood of cross section i having level n at the same time as nuclide j having level m is equal for all choices of m and vice versa—then the matrix

quadrature is simply

$$W_{n,m} = w_n w_m \quad , \tag{8.14}$$

where w_n and w_m are quadrature weights as generated without considering mutual self-shielding effects.

In the generation of the quadrature, there are several options, just as in the typical subgroup method. In [28], the quadrature is generated by the moment method by considering co-moments of the cross sections,

$$\mathcal{M}_{l,k} = \int \left(\sigma^i(E)\right)^l \left(\sigma^j(E)\right)^k \, \mathrm{d}E \quad . \tag{8.15}$$

In [47], the notation differs considerably, but in essence a direct subgroup formulation is applied, using a $1/E$ flux. In notation consistent with that of this thesis, the quadrature weights are defined as

$$W_{n,m} = \int \mathcal{H}_n(E)\mathcal{H}_m(E)\frac{1}{E}\,\mathrm{d}E \tag{8.16}$$

with

$$\begin{aligned} \mathcal{H}_n(E) &= \begin{cases} 1 & \sigma_{n,min} < \sigma^i(E) \leq \sigma_{n,max} \\ 0 & \text{otherwise} \end{cases} \\ \mathcal{H}_m(E) &= \begin{cases} 1 & \sigma_{m,min} < \sigma^j(E) \leq \sigma_{m,max} \\ 0 & \text{otherwise} \end{cases} \quad . \end{aligned} \tag{8.17}$$

Finally, in [29], the matrix quadrature is applied only in high energy groups in which the assumption of independence of the two nuclides is valid. Thus, matrix weights are generated by Eq. (8.14). No implementation using a fitting method was found during the literature review for this thesis, but such an implementation would be straightforward by fitting to reference problems with multiple resonant nuclides. In fact, although the method introduced in Sec. 8.3 does not create a matrix quadrature, it does apply the fitting method to the problem of mutual self-shielding in the subgroup method.

This procedure could be extended to more than two nuclides. However, the computational burden increases exponentially with the number of nuclides, as the matrix space increases in dimension. If the subgroup fixed source equations are to be solved for every combination of each subgroup level of each nuclide, the cost of the self-shielding method would become infeasible. Also, as presented in Sec. 8.4, a subgroup-like method that can account for mutual self-shielding directly scales much better with additional nuclides.

8.2.5 SHEM Group Structures

Although researchers have studied and found treatments for mutual self-shielding effects, another approach is to reduce the impact of mutual self-shielding. The Santamarina-Hfaiedh

Energy Mesh (SHEM) accomplishes this by discretizing the energy variable finely at energies where mutual self-shielding plays a significant role. This helps a reactor physics calculation be more accurate not only because the mutual self-shielding issue is handled implicitly but also because self-shielding in general is moved closer to being handled implicitly. The SHEM energy structures differ from an ultrafine approach in that by using a relatively small number of groups, these meshes are intended for lattice physics calculations directly, whereas ultrafine methods to date are used only on small geometries as self-shielding treatments prior to lattice calculations.

The first SHEM energy mesh was a 281-group structure known as SHEM281 [43]. This energy mesh was designed to reduce the need for self-shielding up to 23 eV. The structure was explicitly designed to mitigate mutual self-shielding errors arising from improper treatment of U-235/U-238 at 6.7 eV and 21 eV, U-236/U-234 at 5.4 eV, U-238/Pu-240 at 21 eV , Hf-177/Hf-179 at 5.8 eV, and Hf-176/Hf-178 at 7.9 eV. The structure was also designed to reduce other errors resulting from the multigroup approximation, including threshold reactions at higher energies and avoiding splitting resonances throughout the resonance range for a variety of reactor fuel, coolant, and structural materials.

Later, the SHEM energy mesh was extended to 361 groups, SHEM361 [48]. A total of 80 additional groups were added between 22.5 eV and 11.14 keV. This reduces mutual self-shielding and other issues of the multigroup approximation for the majority of the resolved resonance range for actinides. The paper suggests that the mutual self-shielding issue is resolved entirely through the use of this structure. Later work included a 295-group structure SHEM295 [9], where the number of groups was reduced for computational efficiency while maintaining high fidelity results with an implementation of the subgroup method.

8.3 Subgroup with Interference Cross Sections

8.3.1 Method Description

The difficulties in the subgroup method with mutual self-shielding are a result of treating each nuclide independently, assuming the self-shielding effect on one nuclide is separable from that of another nuclide. Thus, a way must be found to incorporate an interfering nuclide's cross section into the self-shielding calculation for a given nuclide. This issue can be addressed through the use of a matrix quadrature, as discussed in Sec. 8.2.4, but here a new method is presented which does not increase the number of subgroup fixed source equations.

Although information about the shape of the cross section is lost in the generation of the subgroup quadrature with mathematical or physical probability tables, the weights can still be interpreted as representing an energy range and the base points as the average cross section in that range, at least to first order. With this in mind, the average cross section of the interfering

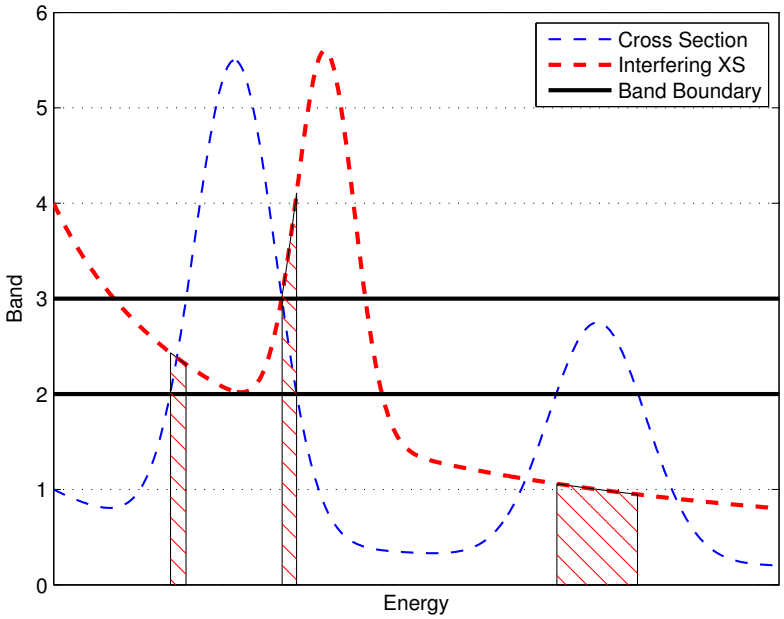

Figure 8.4: Conceptual illustration of inteference cross sections.

nuclide in the energy range corresponding to the quadrature weight is sought. This must be defined consistently with the standard subgroup approximation. A conceptual illustration of this is given in Fig. 8.4.

To do this, consider a homogeneous system with two nuclides, using the narrow resonance approximation for the scattering sources,

$$\begin{aligned}\left(\Sigma_t^1(u) + \Sigma_t^2(u) + \Sigma^+\right)\phi_{NR}^{1,2}(u) \\ = \Sigma_p^1 + \Sigma_p^2 + \Sigma^+ \quad .\end{aligned} \tag{8.18}$$

Rearranging this equation and dividing through by N^1 achieves

$$\phi_{NR}^{1,2}(u) = \frac{\sigma_p^1 + \gamma\sigma_p^2 + \sigma_b}{\sigma_t^1(u) + \gamma\sigma_t^2(u) + \sigma_b} \quad , \tag{8.19}$$

where $\sigma_b = \Sigma^+/N^1$ and $\gamma = N^2/N^1$. This defines the narrow resonance cross section for some reaction ρ for the primary nuclide with interference from the secondary nuclide as

$$\sigma_{\rho,g}^1 = \frac{\int_g \sigma_\rho^1(u)\phi_{NR}^{1,2}(u)\,\mathrm{d}u}{\int_g \phi_{NR}^{1,2}(u)\,\mathrm{d}u} \quad . \tag{8.20}$$

Note that in Eq. (8.19), the flux is not a simple function of the cross section, as the

cross sections of the two nuclides have different energy shapes in general. However, the subgroup approximation is still made, adding an additional parameter to the quadrature for the secondary nuclide cross section.

Assuming the subgroup quadrature for the primary nuclide has already been generated, denoted as $Q_1 = \{w_n, \sigma_n\}$, this quadrature is modified to include an interference cross section $\sigma_n^{1,2}$ as $Q_{1,2} = \{w_n, \sigma_n, \sigma_n^{1,2}\}$. A fitting procedure is then used to determine interference parameters.

First, a set of reference data is generated. Reference group cross sections are generated with Eq. (8.20) with various values of σ_b and γ. Take the set of reference cross sections as $\{\bar{\sigma}_k\}$, with the index k referring to the configuration's background level and density ratio.

Next, the approximate group cross sections are defined as $\{\tilde{\sigma}_k\}$. For configuration k, this is

$$\tilde{\sigma}_k(Q_{1,2}) = \frac{\sum_n \frac{w_n \sigma_n}{\sigma_n + \gamma_k \sigma_n^{1,2} + \sigma_{b,k}}}{\sum_n \frac{w_n}{\sigma_n + \gamma_k \sigma_n^{1,2} + \sigma_{b,k}}} \quad . \tag{8.21}$$

The base points and weights from Q_1 are held fixed, and so $Q_{1,2}$ can be found by a least squares procedure on the interference cross sections,

$$Q_{1,2} = \underset{Q'_{1,2}:Q_1}{\arg\min} \sum_k \left(\frac{\bar{\sigma}_k - \tilde{\sigma}_k(Q'_{1,2})}{\bar{\sigma}_k} \right)^2 \quad . \tag{8.22}$$

For multiple interfering nuclides, each interfering nuclide has its own interference cross section. Each set of interference cross sections can be generated independently of each other. An alternate formulation that takes into account interfering nuclides interfering with each other is possible, but it is not shown here, as this case is unlikely to have a significant impact in realistic applications.

Once the quadrature is appended with the interference cross sections, subgroup fixed source problems are solved. The interference cross sections are added to the collision term. The fixed source problems are otherwise unchanged,

$$\begin{aligned} &\hat{\Omega} \cdot \nabla \psi_n(\vec{r}, \hat{\Omega}) \\ &\quad + N^*(\vec{r}) \left(\sigma_n + \sum_i \gamma_i \sigma_n^{1,i} \right) \psi_n(\vec{r}, \hat{\Omega}) \\ &\quad = \Sigma_p(\vec{r}) \quad . \end{aligned} \tag{8.23}$$

8.3.2 Results and Discussion

Next, results in various configurations of the simple benchmark presented in Ch. 6 are considered. As in the benchmark, in all cases, the subgroup method was implemented with

six levels, generated by a fitting procedure with various infinite medium configurations as references.

Now, consider two nuclides, a primary nuclide and an interfering nuclide. Both nuclides have one resonance, and the heights and spacings between the resonances are varied.

First, consider a case of resonance overlap, where both resonances are centered at 1050 eV. Figure 8.5 shows one example of these cross sections. The heights of the cross sections are varied relative to each other. Results are shown in Tab. 8.4. The column labeled "Peak" gives the peak of the primary nuclide's resonance; the column labeled "Subgroup" shows the error in a subgroup implementation without interference cross sections; and the column labeled "Interference" shows the results for subgroup with interference cross sections as introduced in this section. Positive errors represent obtained cross sections greater than the reference; negative errors represent obtained cross sections less than the reference.

As expected, subgroup errors are seen to greatly magnify as the interfering nuclide's resonance becomes larger. The effect is greatest for smaller primary nuclide resonances. In all cases, the use of interference cross sections greatly reduces the error. This error is below 1% for all cases but one. The one case, a 5 b primary resonance peak with a 1000 b interfering peak, suffers because the primary nuclide has very nearly no effect on the flux near its resonance and because the resulting effective cross section is very small.

Next, consider the case where the resonances are separated by 1 eV. That is, the second resonance is centered at 1051 eV. An example of this is shown in Fig. 8.6. The interference effect is no longer symmetric in the resonance. Errors in the subgroup method are also decreased, but are still very significant. Results are given in Tab. 8.5.

As with the completely overlapping case, use of interference cross sections dramatically decreases the error in all cases. Again, the only instance of errors greater than 1% is for the case of a very small resonance being interfered with by a very large resonance.

Next, consider the case where the resonances are separated by 2 eV. That is, the second resonance is centered at 1052 eV. An example of this is shown in Fig. 8.7. With the resonances further spaced, errors have decreased further, but are still at substantial levels for the cases with large interfering resonances. Results are shown in Tab. 8.6.

In all cases, interference cross sections lead to very small errors in the cross section, less than 1%. For all three resonance overlap cases shown, the resonance interference cross sections are shown to dramatically decrease errors in the subgroup method.

Finally, consider a case of resonance interference without overlap. Here, the second resonance is centered at 1060 eV. An example of this is shown in Fig. 8.8. The errors in the traditional subgroup method are all negative, as expected. Results with the new interference cross section are given in Tab. 8.7.

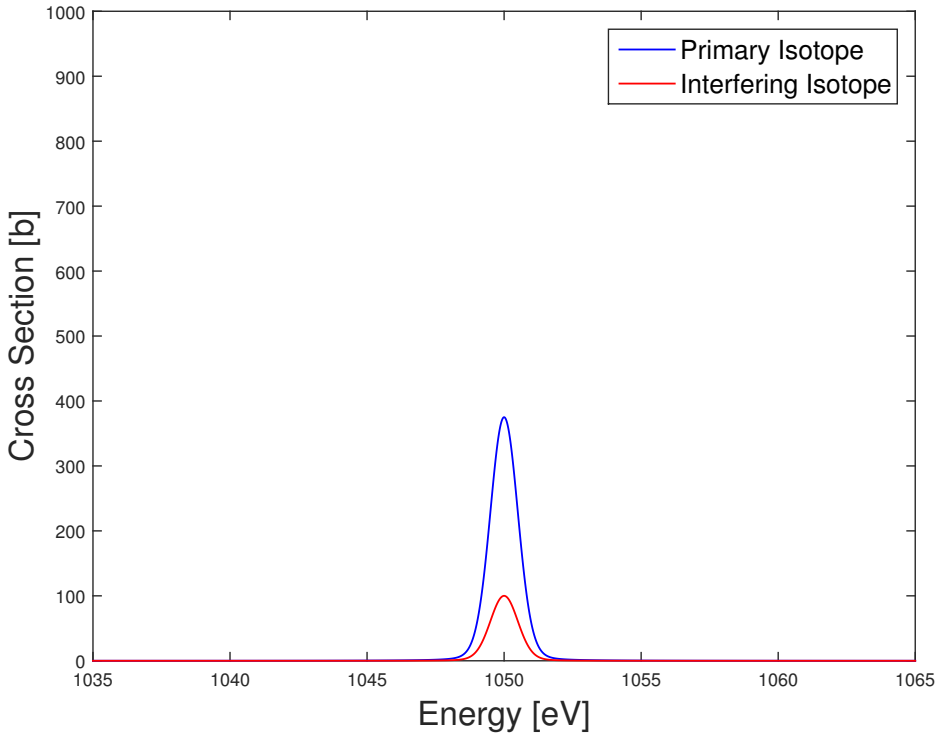

Figure 8.5: Example of cross sections for complete overlap case.

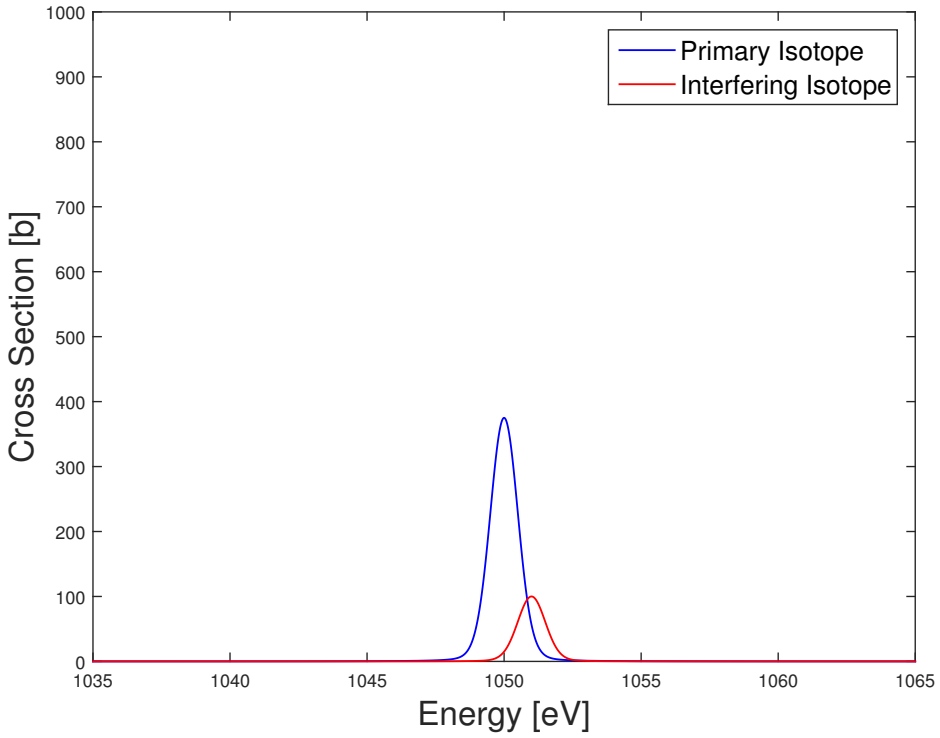

Figure 8.6: Example of cross sections for significant partial overlap case.

Table 8.4: Resonances fully overlap.

Interfering resonance peak: 5b

Peak [b]	Reference [b]	Subgroup Error [%]	Interference Error [%]
5	0.061	3.591	0.002
25	0.270	2.658	-0.273
100	0.782	1.976	0.161
375	1.543	1.304	0.494
1000	2.184	-0.201	-0.537

Interfering resonance peak: 100b

Peak [b]	Reference [b]	Subgroup Error [%]	Interference Error [%]
5	0.039	61.936	0.295
25	0.183	52.051	-0.419
100	0.590	35.170	0.043
375	1.343	16.430	0.522
1000	2.055	6.056	-0.535

Interfering resonance peak: 1000b

Peak [b]	Reference [b]	Subgroup Error [%]	Interference Error [%]
5	0.011	479.580	-2.892
25	0.054	415.307	0.025
100	0.206	287.865	0.083
375	0.663	135.746	-0.893
1000	1.377	58.286	0.241

Table 8.5: Resonances are separated by 1 eV.

Interfering resonance peak: 10b

Peak [b]	Reference [b]	Subgroup Error [%]	Interference Error [%]
5	0.062	1.404	0.111
25	0.275	1.223	0.052
100	0.788	1.141	0.109
375	1.545	1.188	0.462
1000	2.181	-0.050	-0.422

Interfering resonance peak: 100b

Peak [b]	Reference [b]	Subgroup Error [%]	Interference Error [%]
5	0.052	21.443	0.305
25	0.233	19.138	0.156
100	0.689	15.673	0.134
375	1.399	11.764	0.505
1000	2.029	7.437	0.623

Interfering resonance peak: 1000b

Peak [b]	Reference [b]	Subgroup Error [%]	Interference Error [%]
5	0.029	117.527	-2.569
25	0.136	105.045	0.508
100	0.438	82.128	0.609
375	1.011	54.610	-0.985
1000	1.599	36.266	-0.639

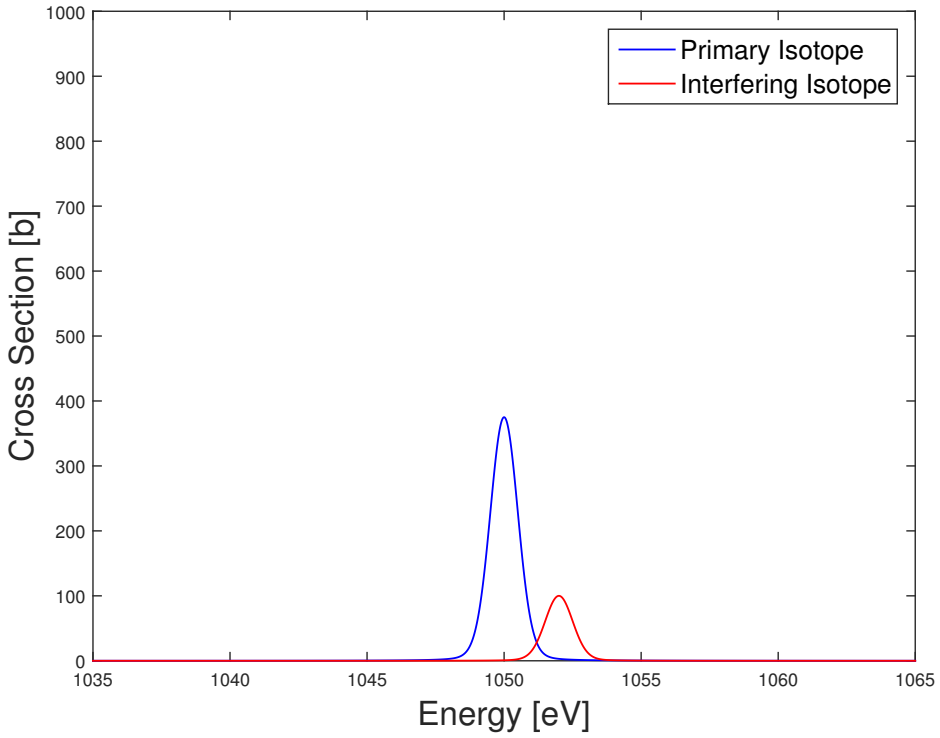

Figure 8.7: Example of cross sections for lesser partial overlap case.

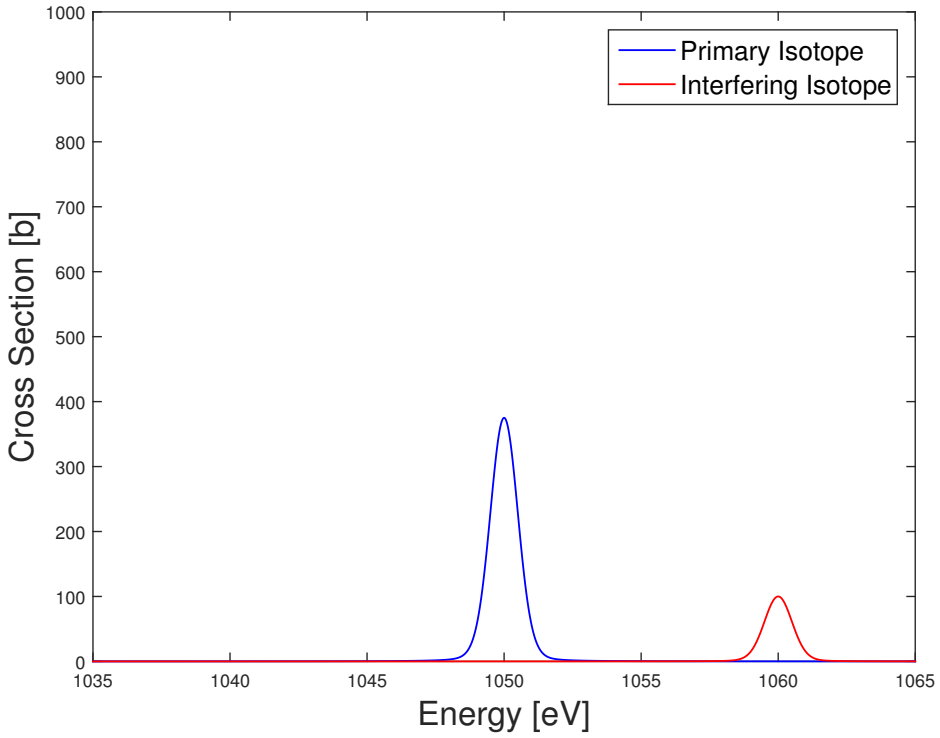

Figure 8.8: Example of cross sections for separated resonances case.

Table 8.6: Resonances are separated by 2 eV.

Interfering resonance peak: 5b

Peak [b]	Reference [b]	Subgroup Error [%]	Interference Error [%]
5	0.063	0.079	-0.014
25	0.278	0.084	-0.009
100	0.795	0.276	0.177
375	1.553	0.650	0.479
1000	2.186	-0.307	-0.447

Interfering resonance peak: 100b

Peak [b]	Reference [b]	Subgroup Error [%]	Interference Error [%]
5	0.062	1.760	0.050
25	0.273	1.700	0.016
100	0.782	1.972	0.249
375	1.519	2.915	0.002
1000	2.122	2.736	0.428

Interfering resonance peak: 1000b

Peak [b]	Reference [b]	Subgroup Error [%]	Interference Error [%]
5	0.056	13.661	0.357
25	0.247	12.556	0.296
100	0.714	11.663	0.067
375	1.391	12.361	-0.708
1000	1.935	12.627	-0.961

Table 8.7: Resonances are separated by 10 eV

Interfering resonance peak: 5b

Peak [b]	Reference [b]	Subgroup Error [%]	Interference Error [%]
5	0.063	-0.086	-0.019
25	0.278	-0.080	-0.071
100	0.796	0.098	0.108
375	1.557	0.418	0.428
1000	2.193	-0.602	-0.592

Interfering resonance peak: 100b

Peak [b]	Reference [b]	Subgroup Error [%]	Interference Error [%]
5	0.064	-0.835	0.043
25	0.280	-0.833	-0.663
100	0.802	-0.659	-0.452
375	1.569	-0.328	-0.138
1000	2.208	-1.303	-1.094

Interfering resonance peak: 1000b

Peak [b]	Reference [b]	Subgroup Error [%]	Interference Error [%]
5	0.065	-2.200	0.224
25	0.285	-2.237	-0.575
100	0.814	-2.112	-0.066
375	1.592	-1.794	0.062
1000	2.240	-2.690	-0.614

Errors are not significant in the cases of the interfering nuclide having a peak of 5 b or 100 b. In these cases, the addition of the interference cross sections does little to improve errors, but it does not harm the accuracy. For the case of a 1000 b interfering cross section peak, the errors are seen to decrease significantly when compared to traditional subgroup, as the flux levels for the lower subgroup levels are more significant and accounted for in this method. Thus, this method is shown to be successful for resonance interference without overlap.

The inclusion of interference cross sections in the subgroup procedure was shown to have a profound impact on the performance of the method for these simple benchmark cases. This new technique improved results both for cases of resonance overlap and for cases of resonance interference without overlap. However, several aspects of this new technique must be considered for it to be useful. First, the generation of the interference cross sections is discussed. Then the computational complexity and some of the flexibility of the method is considered.

By using a range of background cross section values and density ratios, it is assumed that the interference cross section is independent of these. However, this is not true in reality, especially in regards to the density ratio. Over a small range of density ratio values, the interference cross section is seen to be relatively constant; however, this is not true over a very large range of values. Thus, it is recommended that in the generation of parameters, γ values are chosen in a small range around the value expected to be encountered in applications. If a large range of values are expected to be encountered, one can calculate separate parameters for distinct ranges of γ.

In more concrete terms, consider the example of a light water reactor, containing various enrichments in UO_2 fuel pins. When considering U-235, one would expect γ for U-238 to fall in the range of 20 (5% enrichment) to 50 (2% enrichment). When generating interference cross sections, configurations with γ far outside this range need not be considered. However, the γ for fission products with respect to U-235 would be expected to be small fractions, and so γ values near those of U-238 should not be considered.

In this paper, the interference cross sections were generated using a fitting procedure which is applicable regardless of the process used to generate the original subgroup parameters. However, these parameters can be defined by—and in fact, are more theoretically rigorous with—integrating with the explicit energy intervals from the direct subgroup method. Then, average cross sections of interfering nuclides are well defined. The inherent weaknesses of the direct subgroup method, that the assumed flux is dilution dependent, still applies.

The interference cross sections presented in this paper were generated without modifying the original subgroup parameters. However, cases have been observed in which a subgroup quadrature was found to have very good accuracy for an individual nuclide but adequate interference cross sections could not be computed. In these cases, changing the original quadrature, either by shifting the base points or introducing additional subgroup levels, is

necessary. As an example, consider a primary nuclide with a single resonance, and take the corresponding subgroup quadrature to have two levels. One could expect sufficient performance with one level corresponding to areas away from the resonance and one level for the resonance. Consider a resonance from another nuclide with a peak located a small amount in energy from the peak of the primary nuclide's resonance. In this case, this quadrature will not be able to resolve the portion of the primary nuclide's resonance that is being shielded by the interfering resonance.

The addition of a new subgroup parameter for each interfering nuclide may seem cumbersome, costly and memory intensive. However, this is not the case in practice. The calculation of the interference cross sections is a pre-processing step in the generation of the subgroup library. Although the nonlinear optimization required to compute the interference cross sections is difficult in general, because this step is only performed once for each cross section library, this is not of practical concern. The size of the subgroup library increases, which increases memory requirements. However, this increase is not significant. For instance, consider a library of 100 nuclides with 100 resonance groups each with 5 subgroup levels. If one computes for each group the interference effect of each nuclide with each other nuclide, the interference cross sections require only 40 MB of storage in double precision. In practice, much less data is needed, as only important interference effects need be considered. Furthermore, the computational complexity remains the same as in the standard subgroup formulation, as neither the number nor the complexity of the fixed source equations changes.

As was just suggested, it is unnecessary to use this method for each nuclide interfering with each other nuclide in every energy group. One can identify specific groups and nuclides where interference effects are important, and only use this method for those thus cutting down on memory requirements and library generation complexity.

8.4 Ultrafine with Simplified Scattering

The subgroup method is plagued by two approximations, that the neutron flux per unit lethargy is a function of only the cross section of a given nuclide and that each nuclide can be treated independently. Outside of these approximations, the subgroup method has been shown to be very effective, especially in complex geometries in which equivalence-based methods are difficult to use. Much work has been performed addressing each of these weaknesses, but ultimately, such work cannot fully account for the physics lost by these approximations.

The first approximation manifests itself in the difficulty of generating a suitable subgroup quadrature. Three classes of methods—direct, fitting-based, and moment-based—have been discussed in Ch. 4, and each provides an option in the tradeoff continuum of accuracy versus ease of generation. The second approximation manifests itself, as with equivalence-based methods, in the treatment of mutual self-shielding. Options such as resonance interference

factors and matrix subgroup equations were discussed in Sec. 8.2. These methods either provide only an engineering correction or come with great expense.

Here, a new method is presented that is not a subgroup method by its typical definition, but rather is an ultrafine method. However, it retains enough similarity to the subgroup method that it can be seen as a novel way of addressing the two approximations. This method combines the aspects of the subgroup method that have proven to be effective with the aspects of ultrafine methods required to make substantial progress relating to issues such as mutual self-shielding.

8.4.1 Method Description

This proposed method is in essence a direct subgroup method (described in Sec. 4.2.1) with the indicator function $\mathcal{H}_n$ defined contiguously in energy:

$$\mathcal{H}_n(u) = \begin{cases} 1 & u_n \leq u < u_{n+1} \\ 0 & \text{otherwise} \end{cases} . \tag{8.24}$$

Then, as the subgroup base points and weights are defined as

$$\sigma_n = \frac{\int_g \sigma(u)\phi(u)\mathcal{H}_n(u)\,\mathrm{d}u}{\int_g \phi(u)\mathcal{H}_n(u)\,\mathrm{d}u} \tag{8.25}$$

and

$$w_n = \frac{\int_g \phi(u)\mathcal{H}_n(u)\,\mathrm{d}u}{\int_g \phi(u)\,\mathrm{d}u} \quad , \tag{8.26}$$

this process reduces to the standard procedure for collapsing multigroup cross sections. Because $\phi(u)$ is not known *a priori*, a large number of base points are needed for accuracy. Because the quadrature is no longer defined in terms of the cross section value but rather in terms of energy, and because there are a very large number of base points needed, this is by standard definitions an ultrafine method.

This method, though, is differentiated from typical ultrafine methods in that the source is still that of the subgroup method; no attempt is made at a rigorous computation of the slowing down source. The source is assumed to be that of some resonance model, shown here as the intermediate resonance model. Then, the subgroup fixed source equations are

$$\hat{\Omega} \cdot \nabla\psi_n(\vec{r}) + \sum_i N^i(\vec{r})\sigma_n^i\psi_n(\vec{r}) = \frac{1}{4\pi}\sum_i \lambda^i N^i(\vec{r})\sigma_p^i \quad , \tag{8.27}$$

which are solved to obtain the scalar subgroup flux ϕ_n. The group averaged cross section is

obtained by inserting the quadrature and these fluxes into

$$\sigma_{\lambda,g}(\vec{r}) = \frac{\sum_{n=1}^{N} w_n \sigma_n^i \phi_n(\vec{r})}{\sum_{n=1}^{N} w_n \phi_n(\vec{r})} \quad . \tag{8.28}$$

These subgroup fixed source equations differ from those of Sec. 4.1 in that all nuclides are treated together. In this way, mutual self-shielding effects are accounted for, as each nuclide sees the depressions in the flux caused by the resonances of each other nuclide. The effects of mutual self-shielding on the scatter source—e.g., if a peak in the source due to one nuclide's scattering resonance sits atop another nuclide's capture resonance—are not able to be modeled in this method, but this effect is negligible in most situations. The scatter source itself is a subtle issue, explored in more detail in Sec. 8.4.2. The solution of all nuclides concurrently also allows the total number of fixed source solutions to be independent of the number of nuclides and kept at a tractable number.

A further benefit of this approach is its ability to easily model temperature effects natively. Attempts have been made at including temperature dependence in the subgroup method [49, 50, 51], but it is a difficult problem. With this ultrafine method, each transport sweep corresponds to a specific energy range, and the cross section in that energy range is easily determined for each region in the problem, regardless of temperature. For instance, if a pin is discretized radially, one can model a temperature profile across the pellet, with higher temperatures at the pin center.

This number of subgroup fixed source equations warrants further discussion. Although the use of a quadrature based on ultrafine multigroup cross sections requires $O(10{,}000 - 100{,}000)$ base points, by only having one fixed source problem per base point, this is not necessarily a drastic increase in cost compared to other subgroup implementations. As researchers have become increasingly concerned with mutual self-shielding, the number of coarse groups has been increasing. Recent energy meshes SHEM281 [43] and SHEM361 [48] contain 146 and 226 energy groups between 4 eV and 20 keV, respectively. A commonly used mesh XMAS172, [12], contains 52 energy groups in this range. If these three groups were to be used in a depletion analysis following 100 nuclides, each having 5 subgroup levels per coarse group, a total of 73,000, 113,000, or 26,000 subgroup fixed source equations would be required. Of course, these numbers could be reduced—perhaps substantially—by using tricks discussed in Sec. 4.4, but these come at the cost of accuracy. Even with a moderate number of resonance groups such as XMAS172, considering just ten nuclides, using matrix quadratures for mutual self-shielding, coupling each nuclide to one other nuclide, requires 13,000 fixed source solutions. If more nuclides are coupled to each other, this can increase exponentially.

There are two benefits of this approach compared to standard ultrafine methods. First, in

traditional ultrafine methods, the scatter source must be computed for each nuclide separately, causing the simulation time to scale with the number of nuclides. Although there are techniques to reduce this burden (such as in Sec. 5.3.2), this method avoids that through a simple scattering approximation. More significantly, this method fully decouples each group. Thus, this approach can be parallelized over energy groups without difficulty.

The very simple benchmark results shown in this Part cannot be applied to this method, as it is equivalent to the reference solution given the conditions of the benchmark. Thus, results are omitted from this portion. Results relating to this method can be found throughout Part IV.

8.4.2 Intermediate Resonance Scatter Source

A complication of this method is the selection of the scatter source. By using the intermediate resonance model with all nuclides in the same calculation, the intermediate resonance parameter λ is poorly defined. This is the same difficulty that other methods using the intermediate resonance model with multiple nuclides have, including those in the Embedded Self-Shielding Method (Sec. 3.7) and in the approximate solution of the slowing down equation (Sec. 2.6.2).

In the intermediate resonance model, the parameter λ is a measure of the "width" of a resonance. That is, it measures how likely a neutron that scatters near the energy of a resonance is to jump over the resonance's energy range compared to how likely it is to stay near the resonance. For this parameter to be well-defined, there must be a resonance of interest and a mass of the scatterer. In a system with multiple resonant nuclides, a scatter could have one value of λ for one resonance nuclide and another value of λ for another resonant nuclide. In such a system, if the intermediate resonance model is to be used, an effective value of λ must be used, treating each nuclide the same. This is further complicated by the fact that the λ value for a resonant nuclide's scattering compared to its own resonances are usually defined differently from that of a background scatterer compared to another nuclide's resonances, as discussed in Sections 2.5.5 and 2.5.6.

One possible means of dealing with this is a fairly naive approach, but is sufficient for many applications. Recognizing that many systems are dominated by a single nuclide, all λ values can be tuned to that nuclide. For instance, in an LWR fuel pin, the most important nuclide in terms of resonance effects is U-238. In the computation of λ, that of U-238 can be computed as in Sec. 2.5.5, and that each other nuclide can be computed as in Sec. 2.5.6 using U-238 as the reference. This allows the resonance effects of the most important nuclide to be modeled accurately and recognizes that the mutual self-shielding effects will not be greatly influenced by the choice of λ.

Another possible means of finding λ is to perform a search for every unique mixture of nuclides. All nuclides but one can use some value of λ computed separately in an external calculation. The λ for the last nuclide can be determined by matching some quantity (e.g., a

multigroup cross section) computed from a direct solution of the slowing down equation. This uses λ of the final nuclide as a tuning parameter to ensure the quantity of interest is being computed accurately. However, it comes with a significantly higher computational burden than the previous method if many unique mixtures are present.

Next, consider the scatter source given by the intermediate resonance model. Here, it is shown that, regardless of the choice of λ, the intermediate resonance model is not a good approximation for the true shape of the scatter source. Rather, it can only preserve the fraction of neutrons absorbed in resonances versus those that escape. However, this does not imply that this ultrafine-based method using the intermediate resonance model is to be rejected. The method retains the ability to account for flux depressions due to resonant nuclides and incorporate that information into the self-shielding of other resonant nuclides. The inaccuracy of the scatter source is implicit in other self-shielding methods including equivalence-based and subgroup methods.

Consider an infinite medium consisting of a mixture of U-238 and $50\,\mathrm{b}$ of constant cross section background. The scatter source per unit lethargy resulting from a direct solution of the slowing down equation, the wide resonance model, and the narrow resonance model is shown in Fig. 8.9. The true scatter source—that of the direct solution of the slowing down equation—does not always fall between the WR and NR sources. This is seen especially at the interference dips in the scattering cross section on the low energy side of resonances where the true scatter source peaks and the WR source is at a minimum. The intermediate resonance model is a convex combination of the WR and NR models, and so its scatter source will always fall between them. Thus, the IR source cannot be expected to be a good approximation to the scatter source at all energies. This issue is most important in the self-shielding of an nuclide that has a resonance just lower in energy than the resonance of another nuclide that has a large scattering resonance. The IR model in this would underpredict the source at the resonance energy, underpredicting the reaction rate.

8.4.3 Slowing Down Scatter Source

An alternative to using the intermediate resonance scatter source in this method exists. One can use a solution of the slowing down equation to provide the source, analogous to using the slowing down equation rather than the IR approximation to make tables used in equivalence in dilution methods. When using this alternative scattering source, the method of ultrafine with simplified scattering is essentially a hybrid of all three of the classes of methods outlined in Part II: equivalence in dilution, subgroup, and ultrafine methods.

First, one must build the scatter source. This is accomplished by creating an equivalent infinite medium for each resonance region. The infinite medium contains all the nuclides in the region with the same number densities. An additional nuclide is added as a background

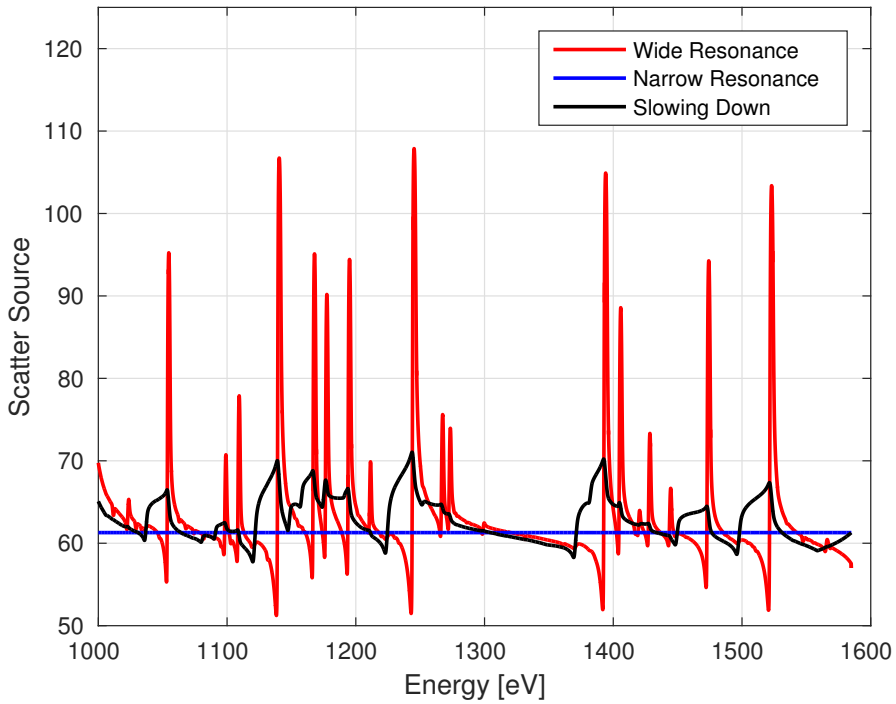

Figure 8.9: Scatter source per unit lethargy from direct slowing down, wide resonance model, and narrow resonance model for infinite medium of U-238 and 50 b of constant cross section background.

moderator, with a macroscopic cross section equal to the equivalence cross section. The simplest choice of equivalence cross section—which will be shown to be very effective in Ch. 9—is to use that of the Wigner Rational Approximation:

$$\Sigma_{eq} = \frac{1 - C}{\bar{l}} \quad , \tag{8.29}$$

where C is the Dancoff factor and

$$\bar{l} = \frac{4V}{S} \quad , \tag{8.30}$$

with V as the volume of the resonant region and S as its surface area. The slowing down equation for the equivalent infinite medium is solved, and the scatter source for eac nuclide at each energy point is tabulated. The scatter source for the subgroup fixed source equations is the sum of the scatter sources of the nuclides that were present in the true resonant region; the scatter source from the added background moderator is discarded. If this scatter source per unit lethargy is given as $Q(u)$, Eq. (8.27) is transformed into

$$\hat{\Omega} \cdot \nabla \psi_n(\vec{r}) + \sum_i N^i(\vec{r}) \sigma_n^i \psi_n(\vec{r}) = \frac{1}{4\pi} Q_n \quad , \tag{8.31}$$

where

$$Q_n = \int_g \mathcal{H}_n(u) Q(u) \, \mathrm{d}u \quad , \tag{8.32}$$

using the indicator function of Eq. (8.24).

Although the solution of the slowing down equation can be performed rapidly, it may not be desired to solve it for every region in a large problem. For instance, in a depleted lattice, every fuel region may have a different composition of nuclides. Fortunately, the solution of the slowing down equation can be moved to a preprocessing step and tabulated. While tabulating the source for a mixtures of many nuclides for every possible configuration is unrealistic—much like tabulating the resonance interference factors from Sec. 8.2.2—the scatter source for individual nuclides at varying background levels can easily be tabulated. If particular interference effects are found to be important, tabulated sources for pairs of nuclides can be generated. After tabulation, selection of the scatter source proceeds much like selecting cross sections from equivalence in dilution methods. Each nuclide's background level is determined from the geometry and concetrations of other nuclides present in the same region. The table is then queried with this background level, and the scatter source for use in the subgroup fixed source equations is retrieved.

8.5 Chapter Summary

Mutual self-shielding is the phenomenon in which the resonances of one nuclide impact the reaction rate for another nuclide. It takes two forms, resonance overlap and resonance interference without overlap. Resonance overlap leads to a significant overprediction of the group cross section, whereas resonance interference without overlap causes an underprediction. Two new methods were presented to account for these effects.

First, the subgroup method with interference cross sections was presented. Cross sections of interfering nuclides are generated for each subgroup level of a primary isotope and are included in the subgroup fixed source problems. This method is fully embedded in the subgroup method, and so the effect is modeled in the self-shielding calculation directly. This offers a more flexible approach than ad hoc correction factors applied after cross sections are determined. Because of the flexibility and the computational efficiency of this method, it is an attractive option when mutual self-shielding effects are important. It allows the effect to be considered when one does not want to rigorously treat these effects in a continuous energy simulation, be it with Monte Carlo or with an ultrafine energy discretization in a deterministic simulation.

Second, ultrafine with simplified scattering was presented. This is a hybrid between ultrafine methods and the subgroup method, solving subgroup fixed source equations on an ultrafine energy grid. This method provides a compromise between the accuracy of ultrafine methods and the efficiency of classical self-shielding approaches. Two potential scatter sources were identified, the intermediate resonance source and one computed from a slowing down solution of an equivalent infinite medium.

Part IV

Results

Chapter 9

Analysis of Multigroup Cross Section Generation Methods

9.1 Introduction

In this chapter, various ultrafine methods are compared side-by-side with equivalence-based and subgroup methods on various pin-based geometries with various materials. Benchmark problems considered are intended to be realistic—both in terms of geometry and cross sections—but are kept small. Errors of group-wise cross sections compared to an ultrafine reference are generated for each nuclide in the problem. Reaction rates integrated across the entire resonance range are also considered.

This analysis is performed as part of the framework introduced in Ch. 6. The cases in this chapter incorporate additional physics compared to that of Ch. 6, but are limited to small geometries. However, the small geometries are chosen in such a way to stress the methods and serve as realistic test cases for most applications. Coupled with the analyses of Ch. 6, this is a nearly complete of test cases for evaluating these methods. One could also incorporate results on full fuel assembly or even full core simulations to measure performance on full-scale calculations, but this would add tremendous cost to testing and would highlight relatively few additional sources of error. Such analysis is beyond the scope of this thesis.

A very simple group structure, the WIMS69 [12] structure, is used to evaluate results. This group structure has 13 resonance range broad groups. The energy bounds of these groups are given in Tab. 9.1. Note that each of the four lowest energy U-238 resonances is in its own group and is approximately at the center of the group. The resonances are in group 27 (6.67 eV), group 25 (20.9 eV), group 24 (36.6 eV), and group 23 (66 eV); no U-238 resonances are in group 26. The selection of a group structure for downstream application is not intended to be the topic of this chapter, although some brief discussion of the implications of the group structure is included.

Table 9.1: Resonance groups of the WIMS69 structure.

Group	E_{max} (eV)	E_{min} (eV)
15	9118.00	5530.00
16	5530.00	3519.10
17	3519.10	2239.45
18	2239.45	1425.10
19	1425.10	906.899
20	906.899	367.263
21	367.263	148.729
22	148.729	75.5014
23	75.5014	48.0520
24	48.0520	27.7000
25	27.7000	15.9680
26	15.9680	9.87700
27	9.87700	4.00000

Throughout this study, ENDF/B-VII.1 cross sections, evaluated at 300 K are used. Only elastic scattering and radiative capture cross sections are included. The total cross section is built as the sum of these two partial cross sections.

Tables of group-averaged cross section values and other metrics will be included in the study. Columns will use abbreviations for the method that generated the results. These abbreviations are included in Tab. 9.2. Each method will be detailed before results are presented with it.

Errors in group-averaged cross sections are shown as percentages, calculated by

$$\epsilon = \frac{\sigma - \sigma_{ref}}{\sigma_{ref}} \times 100\% \quad . \tag{9.1}$$

Positive errors therefore represent an overprediction of the true cross section; negative errors, an underprediction.

9.2 Methods Descriptions

9.2.1 Reference Solution

The reference solution for these problems is created with ultrafine methods, described in more detail in Ch. 5. A rigorously computed elastic scattering source, assumed isotropic in the center of mass, is used. Pins are discretized with 10 equal volume rings in the fuel and 10 equally sized azimuthal sectors. The surrounding moderator in the unit cell is discretized to have 5 equal width rings, and the azimuthal separations are continued into the moderator. The energy variable is discretized by selecting 100,000 points equally spaced in lethargy from 4 eV

Table 9.2: Abbreviations used in tables in this chapter.

Abbreviation	Full Name
REF	Reference Solution, Direct Ultrafine Method
2REG	Ultrafine Method without Spatial Discretization
EQ-SD	Equivalence in Dilution, using Carlvik's Two-Term Rational Approximation and dilution tables based on the slowing down equation
EQ-IR	Equivalence in Dilution, using Carlvik's Two-Term Rational Approximation and dilution tables based on the intermediate resonance model
ESSM	Embedded Self-Shielding Method, based on heterogeneous tables
SUBG	Subgroup method, quadrature generated with a fitting method
S-INT	Subgroup method with interference cross sections, using interference cross sections for all nuclides
UF-IR	Ultrafine with Simplified Scattering, using the intermediate resonance model for the scatter source
UF-SD	Ultrafine with Simplified Scattering, using the scatter source from an infinite medium solved with the slowing down equation
+	Appended to abbreviation when Resonance Interference Factors based on all nuclides in a material are applied
+U	Appended to abbreviation when Resonance Interference Factors based only on a nuclide interfering with U-238 are applied

to 10 keV and is treated as continuous. The problem is solved in the method of characteristics, using 32 azimuthal angles, a 0.01 cm ray spacing, and a 3-point TY polar quadrature.

This ultrafine solver was validated using a fixed source Monte Carlo code on several pin-cell geometries using multiple nuclides. Results matched very closely. The ultrafine solution has a much faster run time, no complications from statistical uncertainties, and better fits with the analyses in this thesis, and so was selected to use as the reference case.

9.2.2 Ultrafine without Discretization

The first approximation is an ultrafine solution without spatial discretization. The pin is treated as a single flat source region, as is the moderator. In an unclad pin-cell, this is a simple two-region problem. The same energy discretization and MOC solution parameters are used as in the reference solution.

Because two-region problems are the basis of equivalence theory and none of the methods tested allow for a spatial distribution of the source, this provides a baseline for the best results that can be obtained from any of the subsequent approximations.

9.2.3 Ultrafine with Simplified Scattering

Next, the method introduced in Sec. 8.4—Ultrafine with Simplified Scattering—is used. This method is an ultrafine method, but instead of modeling elastic scattering physics explicitly, the source term is that of the intermediate resonance model. It is analogous to a subgroup method, where the quadrature is defined by the direct method with contiguous energy ranges. No spatial discretization is imposed, and the MOC solution parameters are the same as in the reference solution.

The intermediate resonance parameters, as discussed in Sec. 8.4.2 are not well-defined for a solution technique that treats multiple resonant nuclides simultaneously. The choice of technique for computing the intermediate resonance parameters is therefore a degree of freedom. In this analysis, the primary method used will be to compute the parameters relative to U-238.

The alternative formulation using a source computed from the slowing down equation as the right hand side is also tested. Results shown here compute the source from an infinite medium containing all the resonant nuclides in the fuel region together. Although the possibility of tabulating the slowing down source for single nuclides was discussed in Sec. 8.4.3, this is not included in the results in this chapter.

9.2.4 Subgroup Method

The subgroup method is described in detail in Ch. 4, but there are many decisions left to implementation. Here, a fitting method is used based on the intermediate resonance derived cross section, $\sigma_\lambda = \sigma_a + \lambda\sigma_s$. For each nuclide, a set of 12 infinite media problems are created. In each, the primary nuclide is admixed with a background moderator with varying concentrations. These infinite media problems are solved assuming the intermediate resonance source, and group-averaged cross sections are generated as the reference values. Note that although the dilution level is varied, the λ parameter is generated at a single dilution corresponding to expected downstream application and held constant throughout the process.

For each group for each nuclide, six subgroup levels are used. They are determined by fitting group-averaged cross sections generated by subgroup to those generated as reference cases. Equation (4.20) is solved using the function `fmincon` in MATLAB [52]. The starting guess for levels is taken to be six equally logarithmic spaced values between $1\,\text{b}$ and $30,000\,\text{b}$, and for weights to be equal for each level. Constraints that weights and levels are positive and that levels not be too large are imposed. The maximum number of function evaluations is increased and the tolerance is tightened compared to the defaults for `fmincon` in order to obtain a suitable quadrature. In nearly all cases, the discrepancy between the reference values and the subgroup approximation is a fraction of a percent.

The partial cross sections and the total cross section are determined using a fitting method. The same reference cases as before are used. The original quadrature is held constant, and base points corresponding to the partial or total cross section are determined via least squares process with `fmincon`. For the total cross section, an additional constraint is imposed that the base points be greater than or equal to those of the original quadrature.

The subgroup fixed source equations are solved for each level of each group for each nuclide using the method of characteristics. The same MOC solution parameters are used for the subgroup fixed source equations as for the reference. The subgroup sources are $\lambda\Sigma_p$ for each nuclide, with λ generated with respect to the primary nuclide. Care is taken to ensure the intermediate resonance parameters are generated at the same dilution as in the quadrature generation and correspond as closely as possible to the problem at hand.

9.2.5 Subgroup with Interference Cross Sections

The method introduced in Sec. 8.3 is used to account for mutual self-shielding effects in the subgroup method. It introduces interference cross sections for the secondary nuclides to be used in the subgroup fixed source equations. A fitting process is used to determine the interference cross sections.

First, reference solutions are created. The reference solutions include a primary nuclide and a secondary nuclide admixed with a background moderator. The same background moderator

levels as in the creation of the subgroup quadrature are used. The ratio of number densities of the primary and secondary nuclides are varied, using four values per nuclide pair. The values are taken to be indicative of the expected ratio of number densities in downstream applications. Intermediate resonance parameters are generated relative to the primary nuclide at a dilution corresponding to downstream applications. The resulting intermediate resonance group-averaged cross sections for the primary nuclide are stored as reference values.

In the fitting process, the original quadrature of the primary nuclide is held constant. By using six levels in the original quadrature, there was a fair amount of freedom to fit the interference cross sections levels. The least squares fitting problem from Eq. (8.22) is solved using MATLAB's `fmincon` function. As with classical subgroup, the options of the optimization routine were altered to obtain a suitable quadrature. Interference cross sections are generated for each nuclide as primary and for each other nuclide as secondary.

The generation of the interference quadratures proved to be a much more difficult process than the base quadrature. While nearly all the reference cases with classical subgroup were able to be represented by the subgroup approximation within a fraction of a percent, many of the interference quadratures had approximations deviating from the reference values by multiple percent. The quadratures used in this study are by no means optimal, obtaining better quadratures has proven to be an arduous process, likely requiring adjusting the base quadrature and a more specialized optimization solver.

The subgroup fixed source equations are then solved for each nuclide for each group and for each level. The subgroup source is the same as that of classical subgroup. The cross section in the collision term, though, has contributions from both the primary nuclide and the secondary nuclides. If more than one secondary nuclide is used, their contributions to the collision term are summed.

A particular challenge in the implementation of this method is for generating interference cross sections for nuclides in groups where the cross section is nearly independent of dilution. This case arises when a nuclide's cross section has no or only very small resonances in an energy group. In this case, for the infinite media that make up the reference problems, the cross sections are independent of the interference cross sections. In the implementation in this study, the optimizer tended to choose very large interference cross sections for these cases. While still providing good agreement with the reference problems, these lead to large errors in downstream applications that involve spatial heterogeneity and include the effects of other nuclides that are not dilution independent. This was addressed in this study by forcing interference cross sections of 0 if the dependence on them was sufficiently small. However, a more elegant solution is an area to be addressed in future work.

9.2.6 Equivalence in Dilution

Also included in this study are equivalence in dilution methods, described in Ch. 3. All geometries in this study are cylindrical fuel pins, and so the Carlvik Two-Term Rational Approximations is used exclusively.

First, for each geometry, the Dancoff factor is determined using the Neutron Current Method, described in Sec. 3.6.4. The black Dancoff factor is used. In lattice problems, the Dancoff factor is computed considering any region containing the nuclide of interest as fuel, regardless of concentration, and all other regions as moderator. The black Dancoff factor cannot account for varying concentrations of a nuclide across spatial regions. Note that this means that in lattice problems, the Dancoff factor can be different for different nuclides present in the same spatial region.

Next, the escape cross section for each resonant region is determined. Because all resonant regions in this problem are cylindrical, the escape cross section is simply

$$\Sigma_e = \frac{1}{2r} \quad , \tag{9.2}$$

where r is the radius of the resonant region.

With the escape cross section, two infinite media configurations are solved. Each contains the primary nuclide. The first region includes a background moderator with constant cross section $\alpha_1^*\Sigma_e/N$; the second, with $\alpha_2^*\Sigma_e/N$, where α_1^* and α_2^* are functions of the Dancoff factor and are given in Eq. (3.111) and N is the number density of the primary nuclide. In each configuration, the background moderator cross section is augmented by $\lambda\Sigma_p^i/N$ for each nuclide i other than the primary nuclide. The intermediate resonance parameters are generated relative to the primary nuclide at a background level corresponding to the background level of the system.

The configurations are solved in one of two ways. First, the slowing down equation is solved directly. Alternatively, the intermediate resonance scatter source is used. These two methods will be compared side-by-side.

Cross sections—total or partial—from these configuration are σ_1 and σ_2, respectively. Assuming differences in the group flux between the two configurations are negligible, the group-averaged cross section is

$$\sigma_g = \beta^*\sigma_1 + (1-\beta^*)\sigma_2 \quad , \tag{9.3}$$

where β^* is also defined in Eq. (3.111).

This process is repeated for each nuclide in each resonant region. Neither iteration for the background iteration nor flux correction is performed to account for any mutual self-shielding effects.

9.2.7 Embedded Self-Shielding Method

The Embedded Self-Shielding Method, presented in Sec. 3.7, is an iterative procedure that relates tabulated cross sections to a fixed source transport solution. The published version of this method alternates between a heterogeneous and a homogeneous model, but this was shown to be problematic in Sec. 6.4.2. A better performing alternative exists, in which the homogeneous model is replaced by a heterogeneous pin-cell calculation. Here, the implementation of ESSM is intended to represent the best-case performance of the method. It is only used on cases with U-238 as a single resonant nuclide, and the tabulated cross sections are generated as closely to the downstream calculation as possible.

First, the heterogeneous tables are generated. These tables are generated using a two-region ultrafine calculation on a pin-cell configuration. The fuel material is taken to be $^{238}UO_2$ with $N = 0.022\,\text{a/b–cm}$. The radius is $0.4096\,\text{cm}$. This number density and radius are the only such values used in downstream applications in this study. The moderator density is varied. For each moderator density, the escape cross section is defined by

$$\Sigma_e = \frac{\Sigma_{t,g}^F \phi_g - \Sigma_{s,g}^F}{\Delta u_g - \phi_g} \quad . \tag{9.4}$$

Next, in the geometry of the downstream application, a two-region fixed source equation is solved for each group. This equation is simply

$$\hat{\Omega} \cdot \nabla \psi_g + \Sigma_{t,g} \psi_g = Q_g \quad , \tag{9.5}$$

where Q_g is the intermediate resonance model scatter source and the cross sections are pulled from the heterogeneous table with a guessed value of Σ_e. The scalar flux in the fuel region is used to compute an updated guess for Σ_e with Eq. (9.4). This solution for the flux and updating of Σ_e is repeated until convergence is obtained.

9.2.8 Resonance Interference Factors

Resonance Interference Factors, originally presented in Sec. 8.2.2, are used to correct the cross sections generated by classical subgroup and equivalence in dilution approaches. Resonance interference factors (RIFs) are computed for each resonant nuclide in each resonant material.

To compute a RIF, first the base case is solved. An infinite medium configuration is setup using the nuclide of interest and a background moderator corresponding to $\lambda\Sigma_p$ for each other nuclide in the material and additional background corresponding to the equivalence cross section. Here, the equivalence cross section is approximated using the Wigner Rational

Approximation and the Dancoff factor,

$$\Sigma_{eq} = \frac{1 - C}{2r} \quad , \tag{9.6}$$

where C is the Dancoff factor and r is the radius of the cylindrical spatial region. The infinite medium is then solved using the slowing down equation, and the total group-averaged cross section σ_g is obtained.

Second, the multi-nuclide case is solved. Here, two approaches are taken. First, all resonant nuclides are included in an infinite medium configuration, and only the equivalence cross section is added as a background moderator. Second, several infinite medium configurations are generated. Each contains the primary nuclide and a single interfering nuclide, along with a background moderator corresponding to both the equivalence cross section and each other nuclide. All these configurations are solved using the slowing down equation, and the total group-averaged cross section of the primary nuclide is obtained $\tilde{\sigma}_g$.

The complete resonance interference factor, given by Eq. (8.3), is determined by

$$f_{IR} = \frac{\tilde{\sigma}_g}{\sigma_g} \quad , \tag{9.7}$$

where $\tilde{\sigma}_g$ corresponds to the configuration including all resonant nuclides.

The partial resonance interference factors, given by Eq. (8.5) is determined by

$$f_{IR}^i = \frac{\tilde{\sigma}_g^i}{\sigma_g} \quad , \tag{9.8}$$

where $\tilde{\sigma}_g^i$ corresponds to the configuration including only the primary nuclide and interfering nuclide i.

These resonance interference factors are applied to the cross sections obtained from classical subgroup or equivalence in dilution methods multiplicatively. With the partial resonance interference factors, each interfering nuclide's RIF can be applied multiplicatively in succession, or only a subset of the partial RIFs can be applied.

9.3 UO_2 Fuel Pin

The first benchmark problem is that of a bare UO_2 fuel pin in an infinite array. This is modeled as a simple pin-cell geometry with reflective boundary conditions. The fuel enrichment, pin radius, and the pin-to-pin pitch are varied. The moderator nuclide concentrations are based on a potential cross section of $1.23\,\mathrm{cm}^{-1}$, and number densities for H-1 and O-16 are derived from this. The concentration of UO_2 molecules is taken to be $0.22\,\mathrm{a/b\text{–}cm}$ regardless of enrichment.

Table 9.3: Errors induced in group-wise constants by using the intermediate resonance scatter source.

Radius [cm]	Rxn Rate	Error [%]	Flux	Error [%]	Cross Section	Error [%]
0.3	9.6033	-0.2197	0.4928	0.9043	19.4872	-1.1140
0.4096	8.4370	-0.0097	0.4802	1.7015	17.5711	-1.6826
0.6	6.4498	3.1975	0.4331	6.6598	14.8932	-3.2461

Enrichments considered included 0%, 1.5%, 3.0%, 4.5%, and 20% by weight. Pin radii were 0.3 cm, 0.4096 cm, and 0.6 cm. Pitch dimensions were 1.0 cm, 1.26 cm, and 1.5 cm. The non-physical case of a 0.6 cm radius with a 1.0 cm pitch was excluded. A subset of the obtained group-averaged cross sections are given here and discussed.

9.3.1 U-238 Alone

First, consider the case of 0% enrichment. In this case, there are no mutual self-shielding effects, as only a single resonant nuclide is present. This provides a baseline for the performance of the methods, similar to the analysis in Ch. 6. The notable difference between this analysis and the previous is the use of the real elastic scattering kernel rather than making a narrow resonance approximation.

Group-averaged cross sections for U-238, averaged across the pin, are generated for equivalence in dilution, subgroup, and ultrafine methods for each of the 8 combinations of pin radius and pitch. The results, given as the reference value and percent deviations from the reference, are given in Tables 9.4 to 9.11.

There are several remarkable results in this suite of test cases. First, note that the error for the two-region ultrafine case is non-negligible for the low energy groups. The error in group 24, which contains the 36.6 eV U-238 resonance, exceeds 1% for several test cases. This error is driven by the large scattering resonances in these groups. The resonances cause the scatter source to exhibit significant self-shielding effects. The approximation that the source is flat throughout the pin, which all methods other than the reference case assume, is a significant source of error.

Next, note that significant errors are seen in the methods making use of the intermediate resonance model's scatter source—ultrafine with simplified scattering, Carlvik with IR, and the subgroup method—especially with larger radii. The cause of this error is the failure of the IR flux to account for the reduction in flux due to absorption. The larger radius pins are at a lower equivalent dilution, and so a higher fraction of neutrons are absorbed in the resonance. To see this effect, see Figs. 9.1 to 9.3. For the larger diameter pins, the discrepancy in the fluxes below the resonance in energy increases. The effects this has on the reaction rate, the group flux, and the group cross section are shown in Tab. 9.3.

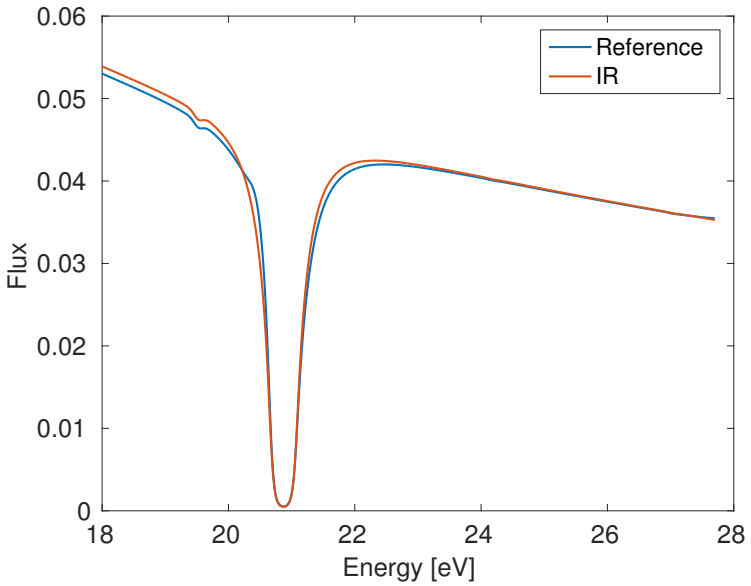

Figure 9.1: Flux in pin cell of radius 0.3 cm with reference scatter source compared to intermediate resonance.

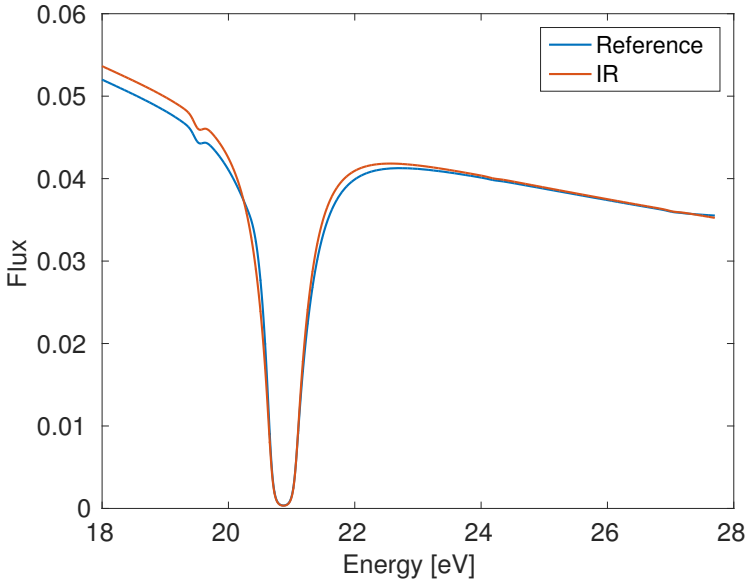

Figure 9.2: Flux in pin cell of radius 0.4096 cm with reference scatter source compared to intermediate resonance.

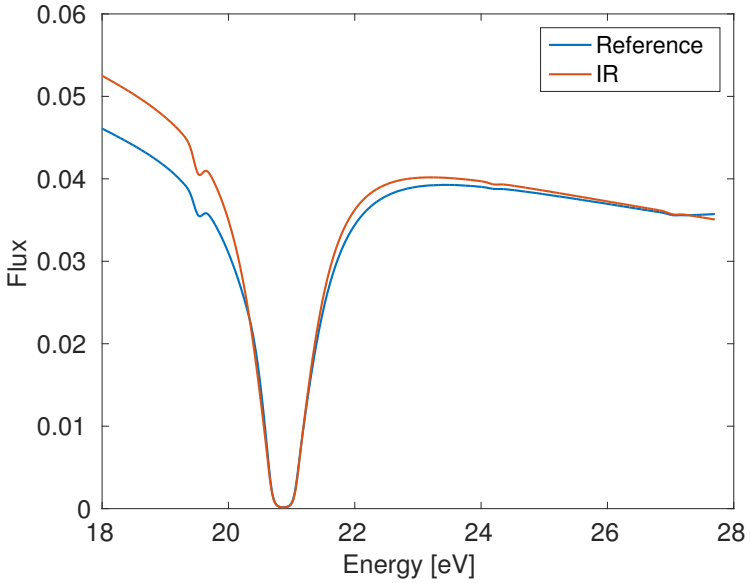

Figure 9.3: Flux in pin cell of radius 0.6 cm with reference scatter source compared to intermediate resonance.

For the $0.3\,\mathrm{cm}$ radius, the reaction rate is slightly underpredicted, driven by the slight flux error on the lower half of the resonance. The flux is overpredicted, resulting in an underprediction of the cross section. For the $0.4\,\mathrm{cm}$ radius, similar behavior is seen, but flux reduction due to absorption causes a cancellation of error for the reaction rate. For the $0.6\,\mathrm{cm}$ radius, the reaction rate is significantly overpredicted due to the flux reduction due to absorption. However, the group flux is overpredicted by an even larger factor, and the group cross section is significantly underpredicted.

This issue can be corrected in one of three ways. First, using data generated by the slowing down equation rather than the intermediate resonance approximation allows this to be taken into account. This is seen by the overall better performance of methods using the slowing down equation than the methods using the IR approximation, including both ultrafine with simplified scattering and equivalence in dilution methods. Second, corrective factors can be applied to address the issue. Similar to resonance interference factors, a corrective factor can be defined as the ratio of a cross section generated with the slowing down equation to that of the intermediate resonance model. These corrective factors can be generated in an equivalent infinite medium and parameterized on the background cross section. Finally, narrower groups can be employed. This increases the complexity of downstream calculations by adding additional groups, but it also prevents the flux from straying too far from $1/E$ in any single group. This approach is employed by the HELIOS 47-group structure [53], which uses many energy groups for the the low-lying U-238 resonances, and very wide groups at higher energies in the resonance range.

Table 9.4: U-238 cross sections with radius 0.3 cm and pitch 1 cm.

			Error (%)					
Group	E_{max} (eV)	REF	2REG	UF-SD	UF-IR	EQ-SD	EQ-IR	SUBG
15	9118.00	14.860	-0.04	-0.04	-0.09	-0.19	-0.21	-0.04
16	5530.00	15.358	0.00	0.00	-0.09	-0.14	-0.25	-0.06
17	3519.10	16.877	0.01	-0.00	-0.22	-0.24	-0.34	-0.20
18	2239.45	15.957	0.00	0.00	-0.26	-0.25	-0.35	-0.24
19	1425.10	16.109	-0.01	-0.01	-0.27	-0.24	-0.34	-0.35
20	906.899	14.252	0.01	0.03	-0.06	-0.10	-0.18	-0.08
21	367.263	16.949	0.11	-0.21	0.31	0.08	0.22	0.75
22	148.729	17.256	0.21	-0.25	0.86	0.38	0.64	1.45
23	75.5014	15.335	0.20	-0.13	0.87	0.50	0.69	1.33
24	48.0520	22.355	0.82	-0.42	1.31	1.77	1.80	2.77
25	27.7000	18.631	0.49	-0.45	-1.23	1.17	-0.55	-0.88
26	15.9680	9.117	-0.00	-0.01	-0.02	-0.02	-0.02	-0.00
27	9.87700	18.559	0.10	-0.39	0.43	1.14	0.53	0.23

Table 9.5: U-238 cross sections with radius 0.3 cm and pitch 1.26 cm.

			Error (%)					
Group	E_{max} (eV)	REF	2REG	UF-SD	UF-IR	EQ-SD	EQ-IR	SUBG
15	9118.00	15.010	-0.02	-0.02	-0.06	-0.21	-0.24	-0.01
16	5530.00	15.539	0.00	0.00	-0.12	-0.19	-0.28	-0.04
17	3519.10	17.246	0.01	-0.01	-0.20	-0.30	-0.40	-0.15
18	2239.45	16.409	0.01	-0.00	-0.26	-0.32	-0.44	-0.20
19	1425.10	16.543	-0.00	-0.01	-0.29	-0.30	-0.38	-0.38
20	906.899	14.530	0.01	0.02	-0.09	-0.15	-0.21	-0.01
21	367.263	17.394	0.15	-0.22	0.06	0.10	0.31	1.40
22	148.729	17.736	0.28	-0.24	0.47	0.45	0.81	2.40
23	75.5014	15.695	0.27	-0.10	0.59	0.62	0.84	2.12
24	48.0520	23.183	1.04	-0.24	1.33	2.24	2.38	4.23
25	27.7000	19.413	0.63	-0.29	-0.74	1.51	0.03	-0.22
26	15.9680	9.118	-0.00	-0.01	-0.01	-0.02	-0.02	0.00
27	9.87700	19.346	0.14	-0.25	0.35	1.28	0.37	0.18

Table 9.6: U-238 cross sections with radius 0.3 cm and pitch 1.5 cm.

			Error (%)					
Group	E_{max} (eV)	REF	2REG	UF-SD	UF-IR	EQ-SD	EQ-IR	SUBG
15	9118.00	15.068	-0.01	-0.01	-0.05	-0.18	-0.20	-0.01
16	5530.00	15.611	0.00	0.00	-0.08	-0.15	-0.24	-0.03
17	3519.10	17.395	0.02	-0.01	-0.20	-0.23	-0.36	-0.11
18	2239.45	16.595	0.01	0.00	-0.22	-0.20	-0.31	-0.18
19	1425.10	16.721	0.00	-0.01	-0.26	-0.18	-0.26	-0.39
20	906.899	14.644	0.01	0.02	-0.02	-0.06	-0.12	0.03
21	367.263	17.577	0.17	-0.21	0.95	0.27	0.50	1.67
22	148.729	17.934	0.31	-0.21	1.86	0.68	1.46	2.80
23	75.5014	15.843	0.30	-0.07	1.77	0.83	1.06	2.47
24	48.0520	23.520	1.13	-0.11	2.82	2.70	2.86	4.84
25	27.7000	19.733	0.69	-0.18	-0.49	1.95	0.59	0.07
26	15.9680	9.118	-0.00	-0.01	-0.01	-0.01	-0.01	0.01
27	9.87700	19.667	0.16	-0.16	0.30	1.63	0.60	0.20

Table 9.7: U-238 cross sections with radius 0.4096 cm and pitch 1 cm.

			Error (%)					
Group	E_{max} (eV)	REF	2REG	UF-SD	UF-IR	EQ-SD	EQ-IR	SUBG
15	9118.00	14.366	-0.09	-0.10	-0.14	-0.14	-0.16	-0.09
16	5530.00	14.790	-0.01	-0.02	-0.12	-0.06	-0.14	-0.10
17	3519.10	15.769	-0.00	-0.01	-0.23	-0.11	-0.24	-0.26
18	2239.45	14.645	-0.01	-0.01	-0.33	-0.15	-0.28	-0.35
19	1425.10	14.865	-0.01	-0.02	-0.28	-0.16	-0.27	-0.32
20	906.899	13.467	0.00	0.03	-0.15	-0.02	-0.12	-0.22
21	367.263	15.699	0.04	-0.23	-1.20	-0.01	0.11	-1.02
22	148.729	15.907	0.10	-0.29	-1.31	0.15	0.33	-1.09
23	75.5014	14.335	0.10	-0.10	-0.86	0.21	0.29	-0.73
24	48.0520	19.926	0.49	-0.70	-1.76	0.63	0.44	-1.04
25	27.7000	16.410	0.28	-0.72	-2.64	0.25	-2.29	-2.54
26	15.9680	9.114	-0.00	-0.04	-0.05	-0.05	-0.05	-0.04
27	9.87700	16.334	0.06	-0.55	1.29	0.83	0.42	0.89

Table 9.8: U-238 cross sections with radius 0.4096 cm and pitch 1.26 cm.

			Error (%)					
Group	E_{max} (eV)	REF	2REG	UF-SD	UF-IR	EQ-SD	EQ-IR	SUBG
15	9118.00	14.670	-0.04	-0.04	-0.09	-0.18	-0.20	-0.05
16	5530.00	15.132	-0.00	-0.00	-0.11	-0.14	-0.20	-0.09
17	3519.10	16.419	0.01	-0.01	-0.25	-0.22	-0.34	-0.28
18	2239.45	15.398	-0.01	-0.01	-0.31	-0.27	-0.38	-0.31
19	1425.10	15.573	-0.02	-0.03	-0.30	-0.27	-0.37	-0.34
20	906.899	13.908	0.00	0.02	-0.08	-0.09	-0.16	-0.15
21	367.263	16.387	0.09	-0.25	0.10	0.00	0.12	0.00
22	148.729	16.636	0.19	-0.28	0.63	0.29	0.56	0.41
23	75.5014	14.863	0.19	-0.11	0.64	0.40	0.59	0.51
24	48.0520	21.180	0.81	-0.41	1.05	1.62	1.50	1.58
25	27.7000	17.569	0.47	-0.47	-1.67	0.99	-1.14	-1.24
26	15.9680	9.116	-0.00	-0.02	-0.02	-0.03	-0.03	-0.01
27	9.87700	17.505	0.10	-0.35	0.66	1.15	0.86	0.73

Table 9.9: U-238 cross sections with radius 0.4096 cm and pitch 1.5 cm.

			Error (%)					
Group	E_{max} (eV)	REF	2REG	UF-SD	UF-IR	EQ-SD	EQ-IR	SUBG
15	9118.00	14.789	-0.02	-0.02	-0.07	-0.16	-0.18	-0.03
16	5530.00	15.270	0.00	-0.00	-0.10	-0.11	-0.17	-0.08
17	3519.10	16.687	0.01	-0.01	-0.24	-0.16	-0.27	-0.26
18	2239.45	15.712	-0.00	-0.01	-0.31	-0.16	-0.27	-0.27
19	1425.10	15.869	-0.01	-0.03	-0.32	-0.16	-0.26	-0.37
20	906.899	14.095	0.00	0.02	-0.09	-0.00	-0.07	-0.10
21	367.263	16.678	0.12	-0.25	-0.06	0.17	0.76	0.46
22	148.729	16.946	0.24	-0.26	0.37	0.54	0.84	1.06
23	75.5014	15.089	0.23	-0.09	0.51	0.64	0.85	1.07
24	48.0520	21.707	0.96	-0.23	0.99	2.30	2.24	2.68
25	27.7000	18.061	0.55	-0.32	-1.25	1.59	-0.35	-0.70
26	15.9680	9.117	-0.00	-0.02	-0.02	-0.02	-0.02	-0.00
27	9.87700	18.001	0.12	-0.23	0.89	1.58	1.01	0.78

Table 9.10: U-238 cross sections with radius 0.6 cm and pitch 1.26 cm.

			Error (%)					
Group	E_{max} (eV)	REF	2REG	UF-SD	UF-IR	EQ-SD	EQ-IR	SUBG
15	9118.00	13.946	-0.11	-0.12	-0.14	-0.10	-0.11	-0.08
16	5530.00	14.344	-0.03	-0.06	-0.21	-0.05	-0.14	-0.10
17	3519.10	14.948	-0.02	-0.03	-0.19	-0.07	-0.19	-0.18
18	2239.45	13.716	-0.02	-0.02	-0.25	-0.14	-0.27	-0.36
19	1425.10	14.001	-0.02	-0.03	-0.15	-0.14	-0.25	-0.35
20	906.899	12.945	-0.01	0.01	-0.02	-0.02	-0.09	-0.29
21	367.263	14.875	0.00	-0.23	0.57	-0.09	-0.29	-2.23
22	148.729	15.046	0.05	-0.27	1.24	-0.10	-0.09	-2.99
23	75.5014	13.716	0.06	0.07	-0.31	-0.06	-0.10	-2.14
24	48.0520	18.413	0.30	-0.70	-3.43	-0.76	-2.83	-4.20
25	27.7000	15.039	0.16	-0.77	-4.18	-0.92	-4.01	-4.22
26	15.9680	9.112	-0.00	-0.13	-0.13	-0.13	-0.13	-0.13
27	9.87700	14.933	0.03	-0.53	-0.07	0.35	0.33	1.69

Table 9.11: U-238 cross sections with radius 0.6 cm and pitch 1.5 cm.

			Error (%)					
Group	E_{max} (eV)	REF	2REG	UF-SD	UF-IR	EQ-SD	EQ-IR	SUBG
15	9118.00	14.296	-0.05	-0.05	-0.10	-0.07	-0.08	-0.06
16	5530.00	14.715	-0.01	-0.02	-0.12	-0.02	-0.10	-0.11
17	3519.10	15.625	-0.00	-0.02	-0.25	-0.04	-0.17	-0.29
18	2239.45	14.476	-0.02	-0.03	-0.36	-0.09	-0.23	-0.40
19	1425.10	14.705	-0.03	-0.05	-0.33	-0.11	-0.22	-0.34
20	906.899	13.363	-0.01	0.01	-0.19	0.04	-0.05	-0.24
21	367.263	15.529	0.04	-0.27	-1.51	0.06	0.19	-1.26
22	148.729	15.711	0.12	-0.29	-1.72	0.29	0.45	-1.38
23	75.5014	14.183	0.13	-0.05	-1.06	0.34	0.89	-0.90
24	48.0520	19.494	0.62	-0.45	-1.95	1.12	0.54	-1.08
25	27.7000	16.046	0.34	-0.55	-2.65	0.63	-2.04	-2.40
26	15.9680	9.113	-0.00	-0.05	-0.06	-0.06	-0.05	-0.05
27	9.87700	15.974	0.08	-0.35	1.78	1.27	1.12	1.34

9.3.2 Enriched UO_2

Next, consider the case of an enriched UO_2 fuel pin. This is the simplest realistic case in which multiple resonant nuclides are present and mutual self-shielding effects are important. Group-averaged cross sections for both U-238 and U-235 are generated for each configuration. A multitude of methods are compared to reference values. For the sake of brevity and clarity, only results with a pitch of 1.26 cm are shown. Results are shown in Tables 9.12 to 9.35. Included are enrichments of 1.5%, 3.0%, 4.5%, and 20% with pin radii of 0.3 cm, 0.4096 cm, and 0.6 cm.

Although the results are presented here as a seemingly endless stream of data points, one can see clear trends in the errors. First, the errors in both U-238 and U-235 for all methods are relatively insensitive to enrichment for the three lowest values of enrichment. For these cases, the errors in U-238 cross sections from the various methods are very similar to those of the unenriched case shown previously. With U-238 nuclei outnumbering U-235 nuclei 20:1 or more, the impact of the additional nuclide on U-238's cross sections is quite small. However, for the 20% enriched case, significant errors are seen in some groups for U-238, demonstrating that the U-235 cross section has a more significant impact on the flux spectrum when it is present in larger quantities.

Next, errors in the cross sections for both nuclides are exacerbated for the largest pin radius. Because the escape cross section is much smaller for the larger pin, the nuclides see a much lower equivalent dilution in this case. Thus, the depressions in the flux in the vicinities of resonances are deeper, and mutual self-shielding effects are magnified.

Mutual self-shielding errors are most easily seen in the lower energy groups of U-235. Methods that do not model the effect exhibit errors over 5% in the lowest energy group (27), which contains the U-238 6.67 eV resonance; errors in the range of 10% in group 25, which contains the U-238 20.9 eV resonance; and errors of 2-3% in group 24, which contains the U-238 36.6 eV resonance. The errors are positive in groups 25 and 27, suggesting that resonance overlap is driving the errors. The errors in group 24 are negative, suggesting that resonance interference without overlap is the primary cause of the errors. These observations are corroborated looking at the cross sections in these groups, Fig. 9.4. The two lowest energy U-238 resonances overlap U-235 resonances significantly. The 36.6 eV resonance sits primarily between U-235 resonances without significant overlap.

Now, consider the ultrafine methods in this study—approximations including the two region approximation, simplified scattering with slowing down, and simplified scatter with the intermediate resonance model. The two region approximation leads to measurable errors in the U-238 cross section in groups with the 20.9 eV and 36.6 eV resonances, as was seen in the unenriched case. No such errors are seen in the cross sections of U-235.

Ultrafine with simplified scattering based on the slowing down equation performs very

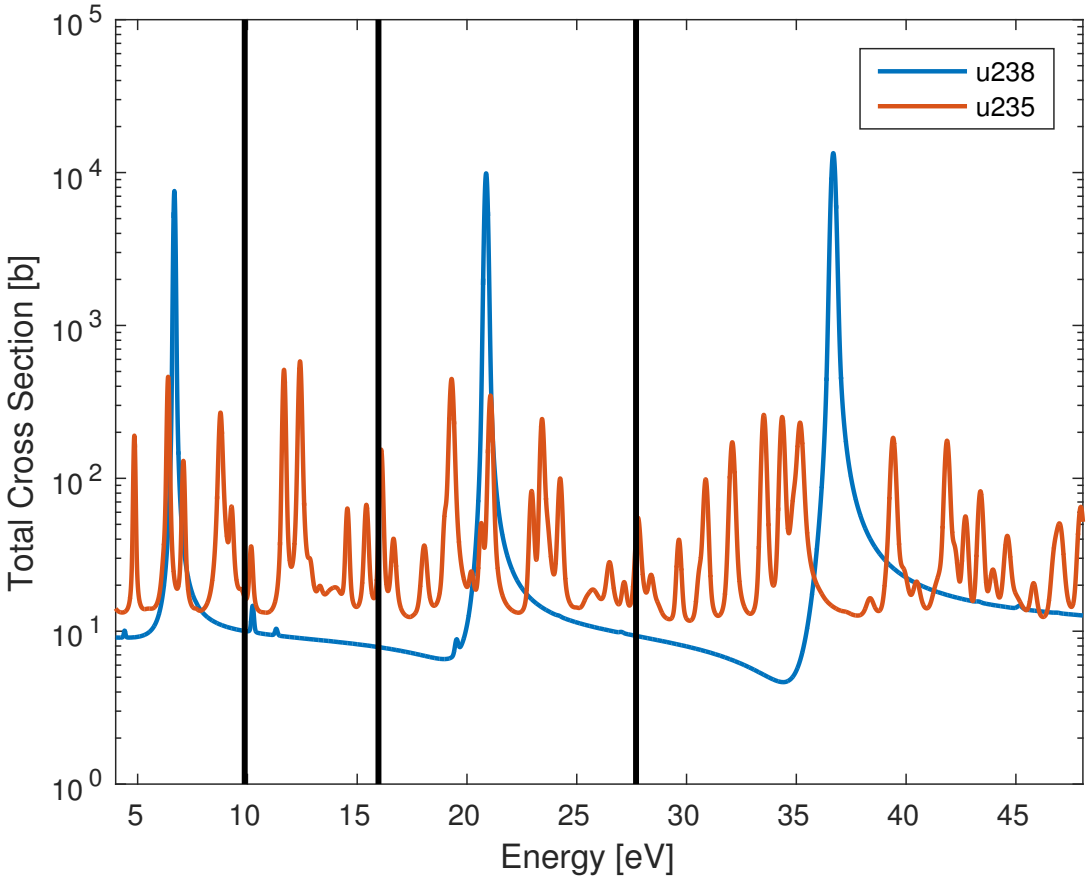

Figure 9.4: Cross sections of U-238 and U-235 for WIMS69 groups 24-27. Black lines show the breakpoints between the groups.

well in nearly all cases. Its largest errors are seen in both U-235 and U-238 in the low energy groups with the 0.6 cm pin for all enrichments. Even in these cases, errors remain below 1% in all configurations other than the 20% enrichment case where the peak error is 1.5%. These errors are driven by the fact that a $1/E$ source is assumed in the moderator, failing to account for the reduction in flux due to absorption. This effect is much smaller than what was seen with the intermediate resonance model and discussed for the unenriched case, as the true flux in the moderator changes much more slowly than that of the pin. This method is by far the most dependable of the methods that do not use a true ultrafine scattering source.

Ultrafine with simplified scattering based on the intermediate resonance model performs similarly to the unenriched cases for these cases. Significant errors are seen in the lower energy groups of U-238 due to the failure to account for flux reduction due to absorption for larger pin radii. For smaller radii, when the resonance escape probability for the low-lying resonances is greater, the method performs better. Similar trends are seen with U-235 cross sections as with U-238 cross sections. However, a particularly interesting data point is group 26 for the 20% enrichment case with a 0.6 cm radius, shown in Tab. 9.35. The error for U-235 in this group is over 3%, by far the highest seen for U-235 in any group. This is because at this low dilution level, the resonances of U-235 make a significant impact on the flux shape. This is a group without a U-238 resonance, and so using an intermediate resonance parameter based on U-238 fails to model the scatter source.

Next, consider the effect of resonance interference factors. The same resonance interference factors were applied to equivalence in dilution with the intermediate resonance model, equivalence in dilution with the slowing down source, and the subgroup method. For the U-238 cross sections, the resonance interference factors were largely unnecessary, as they had very little impact on the already very small errors. Mutual self-shielding errors were most easily seen for the large radius cases; in these cases, the resonance interference factors did reduce errors significantly. For U-235 cross sections, significant errors were seen in the low energy groups for all configurations. Resonance interference factors drove the error below 1% in nearly all cases.

Finally, consider subgroup with interference cross sections. In most cases, this method performs about as well as the methods using resonance interference factors. The largest errors are seen for U-238 with the 0.3 cm radius cases and with the 0.6 cm cases. For the 0.3 cm cases, the errors parallel the errors associated with the subgroup method. As this method uses the same base quadrature as the subgroup method, any issues with the quadrature from the classical subgroup method will not be corrected by using the interference cross sections. The errors in the 0.3 cm case likely arise from the intermediate resonance parameter used in quadrature generation not corresponding to that of the downstream application. In the 0.6 cm cases, the error again parallels that of subgroup without interference factors. For these low dilution cases, where mutual self-shielding effects can be seen in the U-238 cross section, the method does not do an adequate job of picking up the errors. This, however, can be attributed to the true flux's deviation from the $1/E$ spectrum assumed by the method and perhaps problems

with the quadrature. With the U-235 cross sections, subgroup with interference cross sections models the mutual self-shielding effects very well, reducing all the errors seen significantly. In nearly all cases, it is comparable to methods using resonance interference factors.

Table 9.12: U-238 cross sections in 1.5% UO_2 pin with radius 0.3 cm and pitch 1.26 cm.

			Error (%)									
Group	E_{max} (eV)	REF	2REG	UF-SD	UF-IR	EQ-SD	EQ-SD+	EQ-IR	EQ-IR+	SUBG	SUBG+	S-INT
15	9118.00	15.022	-0.02	-0.02	-0.06	-0.20	-0.20	-0.22	-0.22	-0.01	-0.01	-0.01
16	5530.00	15.554	0.00	0.00	-0.08	-0.17	-0.17	-0.27	-0.27	-0.04	-0.04	-0.04
17	3519.10	17.279	0.01	-0.01	-0.20	-0.27	-0.27	-0.37	-0.37	-0.14	-0.14	-0.15
18	2239.45	16.453	0.01	-0.00	-0.23	-0.28	-0.27	-0.40	-0.39	-0.20	-0.19	-0.21
19	1425.10	16.586	-0.00	-0.01	-0.26	-0.26	-0.25	-0.34	-0.33	-0.39	-0.37	-0.38
20	906.899	14.558	0.01	0.02	-0.03	-0.13	-0.11	-0.19	-0.18	-0.01	0.00	-0.00
21	367.263	17.442	0.15	-0.23	0.83	0.14	0.16	0.35	0.37	1.43	1.46	1.46
22	148.729	17.790	0.28	-0.24	1.66	0.50	0.54	0.85	0.89	2.45	2.49	2.50
23	75.5014	15.744	0.27	-0.10	1.57	0.61	0.77	0.85	1.01	2.12	2.29	2.21
24	48.0520	23.324	1.05	-0.26	2.46	2.10	2.63	2.27	2.80	4.08	4.62	4.15
25	27.7000	19.506	0.63	-0.30	-0.69	1.56	1.91	0.12	0.46	-0.25	0.09	-0.20
26	15.9680	9.118	-0.00	-0.01	-0.01	-0.01	-0.03	-0.01	-0.03	0.01	-0.01	0.01
27	9.87700	19.418	0.14	-0.26	0.27	1.40	1.33	0.47	0.40	0.19	0.12	0.15

Table 9.13: U-235 cross sections in 1.5% UO_2 pin with radius 0.3 cm and pitch 1.26 cm.

			Error (%)									
Group	E_{max} (eV)	REF	2REG	UF-SD	UF-IR	EQ-SD	EQ-SD+	EQ-IR	EQ-IR+	SUBG	SUBG+	S-INT
15	9118.00	13.332	0.00	0.00	0.00	0.01	0.01	0.01	0.01	0.07	0.07	-0.01
16	5530.00	13.345	0.00	-0.00	-0.01	0.00	0.00	0.00	0.00	0.01	0.01	0.01
17	3519.10	13.575	0.00	0.00	0.01	-0.01	0.00	-0.01	0.00	0.01	0.01	0.01
18	2239.45	15.033	0.00	0.00	-0.01	0.11	-0.01	0.11	-0.01	0.11	-0.01	0.06
19	1425.10	16.189	0.00	0.00	0.02	-0.02	-0.03	-0.02	-0.03	-0.01	-0.02	-0.08
20	906.899	16.830	-0.00	0.01	0.02	-0.09	0.01	-0.09	0.01	-0.09	0.01	-0.09
21	367.263	21.224	-0.03	-0.01	0.42	0.65	-0.23	0.65	-0.23	0.66	-0.22	0.61
22	148.729	24.499	-0.03	-0.01	0.24	-0.36	-0.09	-0.36	-0.09	-0.37	-0.10	-0.45
23	75.5014	29.798	-0.05	-0.03	0.31	-0.60	-0.16	-0.59	-0.16	-0.63	-0.19	-0.27
24	48.0520	39.471	-0.09	0.06	0.29	-2.47	-0.39	-2.46	-0.38	-2.47	-0.38	-1.42
25	27.7000	41.349	0.01	0.01	0.43	9.55	-0.61	9.59	-0.58	9.63	-0.54	-1.26
26	15.9680	52.263	-0.00	-0.09	-0.19	-0.29	-0.24	-0.22	-0.17	-0.10	-0.06	-0.10
27	9.87700	40.638	-0.00	-0.10	0.69	4.24	-0.76	4.23	-0.77	4.27	-0.74	-2.20

Table 9.14: U-238 cross sections in 1.5% UO_2 pin with radius 0.4096 cm and pitch 1.26 cm.

			Error (%)									
Group	E_{max} (eV)	REF	2REG	UF-SD	UF-IR	EQ-SD	EQ-SD+	EQ-IR	EQ-IR+	SUBG	SUBG+	S-INT
15	9118.00	14.684	-0.04	-0.04	-0.09	-0.16	-0.16	-0.18	-0.18	-0.05	-0.05	-0.05
16	5530.00	15.149	-0.00	-0.00	-0.11	-0.11	-0.11	-0.18	-0.18	-0.09	-0.09	-0.09
17	3519.10	16.453	0.01	-0.01	-0.24	-0.17	-0.17	-0.29	-0.29	-0.28	-0.27	-0.28
18	2239.45	15.439	-0.01	-0.01	-0.31	-0.20	-0.19	-0.32	-0.31	-0.31	-0.29	-0.32
19	1425.10	15.612	-0.02	-0.03	-0.31	-0.21	-0.20	-0.31	-0.30	-0.36	-0.34	-0.34
20	906.899	13.934	0.00	0.02	-0.11	-0.05	-0.04	-0.13	-0.11	-0.16	-0.14	-0.15
21	367.263	16.428	0.09	-0.26	-0.29	0.05	0.08	0.18	0.21	0.03	0.06	0.08
22	148.729	16.683	0.19	-0.29	-0.02	0.34	0.41	0.60	0.67	0.45	0.52	0.52
23	75.5014	14.907	0.19	-0.11	0.16	0.38	0.64	0.60	0.86	0.48	0.74	0.60
24	48.0520	21.321	0.82	-0.44	0.31	1.42	2.27	1.31	2.16	1.33	2.19	1.43
25	27.7000	17.658	0.47	-0.49	-1.63	0.99	1.61	-1.11	-0.50	-1.35	-0.74	-1.28
26	15.9680	9.115	-0.00	-0.02	-0.01	-0.02	-0.05	-0.02	-0.05	0.00	-0.03	0.00
27	9.87700	17.560	0.10	-0.36	0.91	1.31	1.25	1.02	0.96	0.75	0.69	0.77

Table 9.15: U-235 cross sections in 1.5% UO_2 pin with radius 0.4096 cm and pitch 1.26 cm.

			Error (%)									
Group	E_{max} (eV)	REF	2REG	UF-SD	UF-IR	EQ-SD	EQ-SD+	EQ-IR	EQ-IR+	SUBG	SUBG+	S-INT
15	9118.00	13.332	0.00	0.00	0.00	0.01	0.01	0.01	0.01	0.06	0.06	-0.00
16	5530.00	13.345	0.00	-0.00	-0.01	0.00	0.00	0.00	0.00	0.01	0.01	0.01
17	3519.10	13.575	0.00	0.00	0.01	-0.01	0.00	-0.01	0.00	0.00	0.01	0.02
18	2239.45	15.027	0.00	0.01	-0.01	0.14	-0.01	0.14	-0.01	0.14	-0.01	0.07
19	1425.10	16.182	0.00	0.00	0.04	0.01	-0.03	0.01	-0.03	0.02	-0.03	-0.08
20	906.899	16.827	-0.00	0.02	0.02	-0.09	0.01	-0.09	0.01	-0.09	0.01	-0.09
21	367.263	21.182	-0.03	-0.01	0.53	0.77	-0.23	0.77	-0.22	0.79	-0.20	0.70
22	148.729	24.474	-0.03	-0.02	0.21	-0.40	-0.07	-0.40	-0.07	-0.41	-0.08	-0.54
23	75.5014	29.802	-0.05	-0.04	0.34	-0.76	-0.18	-0.75	-0.17	-0.79	-0.21	-0.25
24	48.0520	39.346	-0.08	0.13	0.43	-2.53	-0.47	-2.51	-0.45	-2.53	-0.46	-0.96
25	27.7000	40.799	0.00	0.05	0.44	10.21	-0.65	10.30	-0.57	10.33	-0.54	-0.58
26	15.9680	51.631	-0.00	-0.18	-0.42	-0.45	-0.43	-0.30	-0.28	-0.17	-0.15	-0.21
27	9.87700	39.642	-0.00	-0.22	0.72	6.03	-0.40	6.05	-0.39	6.09	-0.35	-1.63

Table 9.16: U-238 cross sections in 1.5% UO_2 pin with radius 0.6 cm and pitch 1.26 cm.

			Error (%)									
Group	E_{max} (eV)	REF	2REG	UF-SD	UF-IR	EQ-SD	EQ-SD+	EQ-IR	EQ-IR+	SUBG	SUBG+	S-INT
15	9118.00	13.963	-0.10	-0.12	-0.14	-0.04	-0.04	-0.05	-0.05	-0.09	-0.09	-0.09
16	5530.00	14.362	-0.02	-0.06	-0.13	0.02	0.02	-0.08	-0.09	-0.10	-0.10	-0.09
17	3519.10	14.981	-0.02	-0.03	-0.21	0.04	0.05	-0.09	-0.08	-0.19	-0.18	-0.18
18	2239.45	13.755	-0.02	-0.02	-0.33	-0.01	0.04	-0.16	-0.11	-0.39	-0.34	-0.36
19	1425.10	14.037	-0.02	-0.03	-0.26	-0.03	-0.00	-0.14	-0.12	-0.37	-0.35	-0.34
20	906.899	12.967	-0.01	0.01	-0.22	0.05	0.07	-0.02	-0.00	-0.30	-0.28	-0.27
21	367.263	14.911	0.00	-0.24	-2.28	-0.02	0.04	-0.19	-0.13	-2.23	-2.18	-2.14
22	148.729	15.087	0.05	-0.29	-3.02	-0.05	0.24	-0.03	0.26	-2.99	-2.71	-2.87
23	75.5014	13.762	0.06	0.08	-2.10	-0.15	0.57	-0.10	0.62	-2.28	-1.58	-2.10
24	48.0520	18.582	0.31	-0.76	-4.51	-1.18	1.27	-3.15	-0.74	-4.75	-2.38	-4.60
25	27.7000	15.141	0.17	-0.83	-4.16	-1.08	0.80	-4.13	-2.32	-4.56	-2.76	-4.45
26	15.9680	9.108	-0.00	-0.14	-0.07	-0.07	-0.17	-0.07	-0.17	-0.08	-0.18	-0.06
27	9.87700	14.975	0.04	-0.58	1.95	0.54	0.85	0.53	0.84	1.64	1.95	1.75

Table 9.17: U-235 cross sections in 1.5% UO_2 pin with radius 0.6 cm and pitch 1.26 cm.

			Error (%)									
Group	E_{max} (eV)	REF	2REG	UF-SD	UF-IR	EQ-SD	EQ-SD+	EQ-IR	EQ-IR+	SUBG	SUBG+	S-INT
15	9118.00	13.331	0.00	0.01	0.01	0.01	0.01	0.01	0.01	0.05	0.05	0.04
16	5530.00	13.345	0.00	-0.01	-0.01	0.00	-0.01	0.00	-0.01	0.01	0.00	0.01
17	3519.10	13.575	0.00	0.00	0.03	-0.01	0.00	-0.01	0.00	0.00	0.01	0.03
18	2239.45	15.016	0.00	0.01	0.00	0.20	0.00	0.20	0.00	0.20	0.00	0.06
19	1425.10	16.156	0.00	-0.00	0.11	0.15	-0.04	0.15	-0.04	0.16	-0.03	-0.05
20	906.899	16.816	-0.00	0.04	0.03	-0.08	0.04	-0.08	0.04	-0.08	0.04	-0.07
21	367.263	21.045	-0.02	-0.01	0.90	1.15	-0.17	1.16	-0.16	1.21	-0.12	1.01
22	148.729	24.396	-0.02	-0.02	-0.02	-0.52	-0.03	-0.52	-0.03	-0.55	-0.06	-0.85
23	75.5014	29.784	-0.03	-0.18	0.39	-1.23	-0.38	-1.18	-0.32	-1.24	-0.39	-0.07
24	48.0520	38.559	-0.03	0.20	0.86	-1.80	-0.47	-1.73	-0.40	-1.81	-0.48	1.61
25	27.7000	39.275	0.00	-0.06	0.62	11.58	-1.03	12.00	-0.66	11.91	-0.74	1.09
26	15.9680	49.567	-0.00	-0.68	-2.14	-1.14	-1.21	-0.49	-0.56	-0.50	-0.57	-1.03
27	9.87700	37.793	-0.00	-0.59	-0.40	8.10	0.38	8.26	0.53	8.28	0.55	-1.57

Table 9.18: U-238 cross sections in 3.0% UO_2 pin with radius 0.3 cm and pitch 1.26 cm.

			Error (%)									
Group	E_{max} (eV)	REF	2REG	UF-SD	UF-IR	EQ-SD	EQ-SD+	EQ-IR	EQ-IR+	SUBG	SUBG+	S-INT
15	9118.00	15.034	-0.02	-0.02	-0.06	-0.21	-0.21	-0.23	-0.23	-0.01	-0.01	-0.01
16	5530.00	15.570	0.00	0.00	-0.12	-0.19	-0.19	-0.28	-0.28	-0.04	-0.04	-0.04
17	3519.10	17.313	0.01	-0.01	-0.20	-0.31	-0.30	-0.41	-0.40	-0.14	-0.13	-0.15
18	2239.45	16.497	0.01	-0.00	-0.25	-0.33	-0.31	-0.45	-0.43	-0.20	-0.18	-0.22
19	1425.10	16.630	-0.00	-0.01	-0.28	-0.31	-0.29	-0.40	-0.38	-0.39	-0.37	-0.38
20	906.899	14.586	0.01	0.02	-0.08	-0.17	-0.15	-0.23	-0.21	-0.01	0.01	0.00
21	367.263	17.491	0.15	-0.23	0.08	0.07	0.12	0.29	0.33	1.47	1.52	1.52
22	148.729	17.846	0.28	-0.25	0.50	0.41	0.49	0.77	0.85	2.50	2.59	2.59
23	75.5014	15.793	0.27	-0.10	0.61	0.50	0.76	0.73	1.00	2.12	2.39	2.28
24	48.0520	23.467	1.05	-0.29	1.35	1.80	2.64	1.97	2.81	3.94	4.79	4.05
25	27.7000	19.599	0.64	-0.30	-0.69	1.42	1.89	0.01	0.46	-0.27	0.19	-0.16
26	15.9680	9.117	-0.00	-0.01	-0.00	-0.01	-0.04	-0.01	-0.04	0.01	-0.02	0.02
27	9.87700	19.493	0.14	-0.27	0.26	1.34	1.28	0.38	0.32	0.19	0.13	0.11

Table 9.19: U-235 cross sections in 3.0% UO_2 pin with radius 0.3 cm and pitch 1.26 cm.

			Error (%)									
Group	E_{max} (eV)	REF	2REG	UF-SD	UF-IR	EQ-SD	EQ-SD+	EQ-IR	EQ-IR+	SUBG	SUBG+	S-INT
15	9118.00	13.332	0.00	0.00	0.00	0.01	0.01	0.01	0.01	0.06	0.06	-0.01
16	5530.00	13.345	0.00	-0.00	-0.01	0.00	0.00	0.00	0.00	0.01	0.01	0.01
17	3519.10	13.574	0.00	0.00	0.01	-0.01	0.00	-0.01	0.00	0.00	0.01	0.01
18	2239.45	15.032	0.00	0.00	-0.01	0.10	-0.01	0.10	-0.01	0.10	-0.01	0.05
19	1425.10	16.187	0.00	0.00	0.02	-0.02	-0.03	-0.02	-0.03	-0.02	-0.02	-0.08
20	906.899	16.824	-0.00	0.01	0.02	-0.09	0.01	-0.09	0.01	-0.09	0.01	-0.09
21	367.263	21.194	-0.03	-0.01	0.41	0.63	-0.23	0.63	-0.23	0.67	-0.20	0.61
22	148.729	24.433	-0.03	-0.02	0.22	-0.37	-0.10	-0.37	-0.10	-0.37	-0.11	-0.46
23	75.5014	29.715	-0.05	-0.03	0.33	-0.60	-0.18	-0.60	-0.18	-0.64	-0.22	-0.30
24	48.0520	39.195	-0.09	0.06	0.36	-2.49	-0.41	-2.49	-0.41	-2.49	-0.40	-1.48
25	27.7000	40.901	0.01	-0.01	0.38	9.32	-0.59	9.32	-0.59	9.39	-0.53	-0.98
26	15.9680	51.027	-0.00	-0.14	-0.31	-0.31	-0.34	-0.31	-0.34	-0.09	-0.12	-0.14
27	9.87700	40.228	-0.00	-0.12	0.73	3.90	-0.60	3.82	-0.67	3.91	-0.59	-2.10

Table 9.20: U-238 cross sections in 3.0% UO_2 pin with radius 0.4096 cm and pitch 1.26 cm.

			Error (%)									
Group	E_{max} (eV)	REF	2REG	UF-SD	UF-IR	EQ-SD	EQ-SD+	EQ-IR	EQ-IR+	SUBG	SUBG+	S-INT
15	9118.00	14.699	-0.04	-0.04	-0.09	-0.18	-0.18	-0.21	-0.20	-0.05	-0.04	-0.05
16	5530.00	15.166	-0.00	-0.00	-0.11	-0.14	-0.14	-0.21	-0.20	-0.09	-0.09	-0.09
17	3519.10	16.487	0.01	-0.01	-0.24	-0.23	-0.22	-0.35	-0.34	-0.28	-0.27	-0.28
18	2239.45	15.481	-0.01	-0.01	-0.30	-0.28	-0.25	-0.40	-0.37	-0.31	-0.28	-0.33
19	1425.10	15.653	-0.02	-0.03	-0.30	-0.29	-0.26	-0.39	-0.36	-0.37	-0.34	-0.34
20	906.899	13.960	0.00	0.02	-0.08	-0.11	-0.08	-0.19	-0.16	-0.16	-0.13	-0.14
21	367.263	16.471	0.09	-0.26	0.14	-0.04	0.02	0.09	0.16	0.07	0.13	0.14
22	148.729	16.731	0.19	-0.30	0.68	0.22	0.35	0.49	0.61	0.49	0.61	0.60
23	75.5014	14.953	0.19	-0.11	0.66	0.22	0.61	0.44	0.83	0.44	0.83	0.65
24	48.0520	21.463	0.82	-0.48	0.92	0.99	2.25	0.89	2.14	1.10	2.36	1.26
25	27.7000	17.746	0.47	-0.50	-1.64	0.74	1.55	-1.33	-0.55	-1.44	-0.65	-1.30
26	15.9680	9.114	-0.00	-0.03	0.00	-0.01	-0.07	-0.01	-0.07	0.01	-0.05	0.02
27	9.87700	17.617	0.10	-0.38	0.60	1.22	1.17	0.93	0.88	0.77	0.72	0.73

Table 9.21: U-235 cross sections in 3.0% UO_2 pin with radius 0.4096 cm and pitch 1.26 cm.

			Error (%)									
Group	E_{max} (eV)	REF	2REG	UF-SD	UF-IR	EQ-SD	EQ-SD+	EQ-IR	EQ-IR+	SUBG	SUBG+	S-INT
15	9118.00	13.332	0.00	0.00	0.00	0.01	0.01	0.01	0.01	0.05	0.05	-0.01
16	5530.00	13.345	0.00	-0.00	-0.01	0.00	0.00	0.00	0.00	0.01	0.01	0.01
17	3519.10	13.575	0.00	0.00	0.01	-0.01	0.00	-0.01	0.00	0.00	0.01	0.01
18	2239.45	15.026	0.00	0.01	-0.01	0.13	-0.01	0.13	-0.01	0.13	-0.01	0.06
19	1425.10	16.179	0.00	0.00	0.04	0.01	-0.04	0.01	-0.04	0.02	-0.03	-0.08
20	906.899	16.819	-0.00	0.02	0.02	-0.10	0.01	-0.10	0.01	-0.09	0.02	-0.08
21	367.263	21.138	-0.03	-0.01	0.52	0.74	-0.23	0.74	-0.23	0.80	-0.18	0.71
22	148.729	24.376	-0.03	-0.02	0.18	-0.41	-0.09	-0.41	-0.09	-0.41	-0.09	-0.54
23	75.5014	29.676	-0.05	-0.04	0.29	-0.76	-0.20	-0.76	-0.20	-0.80	-0.24	-0.29
24	48.0520	38.944	-0.08	0.12	0.26	-2.57	-0.49	-2.56	-0.48	-2.57	-0.49	-1.06
25	27.7000	40.148	0.01	0.02	0.33	9.93	-0.60	9.94	-0.59	10.01	-0.52	-0.19
26	15.9680	49.860	0.00	-0.26	-0.70	-0.38	-0.48	-0.37	-0.47	-0.13	-0.23	-0.29
27	9.87700	39.086	0.00	-0.25	0.53	5.46	-0.19	5.34	-0.30	5.46	-0.18	-1.54

Table 9.22: U-238 cross sections in 3.0% UO_2 pin with radius 0.6 cm and pitch 1.26 cm.

			Error (%)									
Group	E_{max} (eV)	REF	2REG	UF-SD	UF-IR	EQ-SD	EQ-SD+	EQ-IR	EQ-IR+	SUBG	SUBG+	S-INT
15	9118.00	13.981	-0.10	-0.12	-0.14	-0.12	-0.11	-0.12	-0.12	-0.10	-0.09	-0.09
16	5530.00	14.380	-0.02	-0.06	-0.16	-0.06	-0.06	-0.15	-0.15	-0.11	-0.10	-0.09
17	3519.10	15.015	-0.02	-0.02	-0.18	-0.09	-0.06	-0.22	-0.19	-0.20	-0.18	-0.18
18	2239.45	13.794	-0.02	-0.02	-0.24	-0.18	-0.10	-0.33	-0.25	-0.41	-0.33	-0.36
19	1425.10	14.073	-0.02	-0.04	-0.14	-0.18	-0.13	-0.30	-0.24	-0.39	-0.34	-0.33
20	906.899	12.989	-0.01	0.01	-0.01	-0.06	-0.01	-0.13	-0.08	-0.32	-0.27	-0.27
21	367.263	14.947	0.00	-0.25	0.64	-0.19	-0.07	-0.36	-0.25	-2.24	-2.12	-2.09
22	148.729	15.127	0.05	-0.31	1.32	-0.24	0.12	-0.22	0.14	-2.99	-2.64	-2.80
23	75.5014	13.808	0.06	0.09	-0.20	-0.43	0.50	-0.36	0.57	-2.42	-1.50	-2.12
24	48.0520	18.742	0.31	-0.83	-3.31	-1.96	1.11	-3.89	-0.88	-5.24	-2.27	-4.96
25	27.7000	15.234	0.17	-0.89	-4.18	-1.61	0.56	-4.65	-2.54	-4.85	-2.74	-4.62
26	15.9680	9.104	-0.00	-0.16	-0.02	-0.03	-0.21	-0.03	-0.21	-0.04	-0.21	-0.01
27	9.87700	15.016	0.04	-0.61	-0.15	0.32	0.64	0.31	0.63	1.60	1.92	1.66

Table 9.23: U-235 cross sections in 3.0% UO_2 pin with radius 0.6 cm and pitch 1.26 cm.

			Error (%)									
Group	E_{max} (eV)	REF	2REG	UF-SD	UF-IR	EQ-SD	EQ-SD+	EQ-IR	EQ-IR+	SUBG	SUBG+	S-INT
15	9118.00	13.331	0.00	0.01	0.01	0.01	0.01	0.01	0.01	0.04	0.03	0.03
16	5530.00	13.345	0.00	-0.01	-0.01	0.00	-0.01	0.00	-0.01	0.01	-0.00	0.01
17	3519.10	13.575	0.00	0.00	0.03	-0.01	0.00	-0.01	0.00	-0.00	0.01	0.03
18	2239.45	15.013	0.00	0.01	0.00	0.20	0.00	0.20	0.00	0.19	-0.00	0.06
19	1425.10	16.149	0.00	-0.00	0.11	0.14	-0.04	0.14	-0.04	0.15	-0.03	-0.06
20	906.899	16.798	-0.00	0.04	0.01	-0.08	0.04	-0.08	0.04	-0.07	0.05	-0.06
21	367.263	20.954	-0.02	-0.01	0.79	1.11	-0.17	1.11	-0.17	1.21	-0.07	1.02
22	148.729	24.198	-0.02	-0.02	-0.26	-0.52	-0.05	-0.51	-0.04	-0.54	-0.07	-0.85
23	75.5014	29.511	-0.03	-0.19	-0.07	-1.15	-0.36	-1.15	-0.36	-1.19	-0.40	-0.14
24	48.0520	37.786	-0.03	0.18	0.10	-1.87	-0.43	-1.85	-0.41	-1.96	-0.52	1.27
25	27.7000	38.057	0.00	-0.13	0.19	11.21	-0.74	11.24	-0.72	11.25	-0.71	1.59
26	15.9680	46.332	0.00	-0.79	-3.63	-0.44	-0.66	-0.45	-0.67	-0.36	-0.58	-1.23
27	9.87700	36.786	-0.00	-0.60	-1.69	6.96	0.80	6.69	0.55	6.79	0.64	-1.65

Table 9.24: U-238 cross sections in 4.5% UO_2 pin with radius 0.3 cm and pitch 1.26 cm.

			Error (%)									
Group	E_{max} (eV)	REF	2REG	UF-SD	UF-IR	EQ-SD	EQ-SD+	EQ-IR	EQ-IR+	SUBG	SUBG+	S-INT
15	9118.00	15.047	-0.02	-0.02	-0.06	-0.20	-0.19	-0.22	-0.22	-0.01	-0.01	-0.01
16	5530.00	15.586	0.00	0.00	-0.08	-0.17	-0.17	-0.27	-0.26	-0.04	-0.03	-0.03
17	3519.10	17.348	0.01	-0.01	-0.20	-0.28	-0.27	-0.38	-0.36	-0.14	-0.12	-0.15
18	2239.45	16.542	0.01	-0.00	-0.22	-0.29	-0.26	-0.41	-0.38	-0.20	-0.17	-0.23
19	1425.10	16.674	-0.00	-0.01	-0.25	-0.28	-0.24	-0.36	-0.33	-0.40	-0.36	-0.37
20	906.899	14.615	0.01	0.02	-0.02	-0.15	-0.11	-0.21	-0.17	-0.01	0.02	0.01
21	367.263	17.541	0.15	-0.24	0.94	0.11	0.18	0.32	0.39	1.51	1.59	1.57
22	148.729	17.902	0.28	-0.26	1.84	0.45	0.57	0.80	0.92	2.56	2.69	2.69
23	75.5014	15.844	0.28	-0.10	1.72	0.49	0.85	0.72	1.08	2.12	2.49	2.35
24	48.0520	23.611	1.05	-0.31	2.63	1.67	2.80	1.85	2.98	3.80	4.96	3.97
25	27.7000	19.692	0.64	-0.31	-0.63	1.48	2.05	0.11	0.67	-0.28	0.28	-0.12
26	15.9680	9.117	-0.00	-0.01	0.00	-0.00	-0.05	-0.00	-0.05	0.02	-0.03	0.02
27	9.87700	19.571	0.14	-0.28	0.19	1.46	1.41	0.47	0.42	0.19	0.14	0.07

Table 9.25: U-235 cross sections in 4.5% UO_2 pin with radius 0.3 cm and pitch 1.26 cm.

			Error (%)									
Group	E_{max} (eV)	REF	2REG	UF-SD	UF-IR	EQ-SD	EQ-SD+	EQ-IR	EQ-IR+	SUBG	SUBG+	S-INT
15	9118.00	13.332	0.00	0.00	0.00	0.01	0.01	0.01	0.01	0.06	0.06	-0.01
16	5530.00	13.345	0.00	-0.00	-0.01	0.00	0.00	0.00	0.00	0.01	0.01	0.01
17	3519.10	13.574	0.00	0.00	0.01	-0.01	0.00	-0.01	0.00	0.00	0.01	0.01
18	2239.45	15.031	0.00	0.00	-0.01	0.10	-0.01	0.10	-0.01	0.10	-0.01	0.05
19	1425.10	16.185	0.00	0.00	0.02	-0.03	-0.03	-0.03	-0.03	-0.02	-0.02	-0.08
20	906.899	16.819	-0.00	0.01	0.02	-0.09	0.01	-0.09	0.01	-0.09	0.01	-0.08
21	367.263	21.165	-0.03	-0.01	0.40	0.61	-0.24	0.61	-0.23	0.67	-0.18	0.62
22	148.729	24.368	-0.03	-0.02	0.21	-0.38	-0.11	-0.38	-0.11	-0.38	-0.11	-0.46
23	75.5014	29.633	-0.05	-0.03	0.29	-0.62	-0.21	-0.61	-0.20	-0.64	-0.24	-0.31
24	48.0520	38.929	-0.09	0.06	0.22	-2.54	-0.45	-2.51	-0.42	-2.50	-0.42	-1.53
25	27.7000	40.482	0.01	-0.02	0.33	8.98	-0.68	9.08	-0.58	9.17	-0.50	-0.72
26	15.9680	49.900	0.00	-0.18	-0.42	-0.52	-0.60	-0.36	-0.44	-0.08	-0.16	-0.18
27	9.87700	39.836	0.00	-0.14	0.67	3.50	-0.55	3.46	-0.59	3.59	-0.46	-2.00

Table 9.26: U-238 cross sections in 4.5% UO_2 pin with radius 0.4096 cm and pitch 1.26 cm.

			Error (%)									
Group	E_{max} (eV)	REF	2REG	UF-SD	UF-IR	EQ-SD	EQ-SD+	EQ-IR	EQ-IR+	SUBG	SUBG+	S-INT
15	9118.00	14.713	-0.04	-0.04	-0.08	-0.16	-0.15	-0.18	-0.18	-0.05	-0.04	-0.05
16	5530.00	15.183	-0.00	-0.00	-0.10	-0.11	-0.11	-0.18	-0.17	-0.09	-0.08	-0.08
17	3519.10	16.522	0.01	-0.01	-0.23	-0.19	-0.17	-0.30	-0.28	-0.28	-0.26	-0.28
18	2239.45	15.523	-0.01	-0.01	-0.30	-0.22	-0.18	-0.34	-0.29	-0.32	-0.27	-0.34
19	1425.10	15.694	-0.02	-0.03	-0.30	-0.23	-0.19	-0.33	-0.29	-0.38	-0.33	-0.34
20	906.899	13.986	0.00	0.02	-0.10	-0.07	-0.03	-0.15	-0.11	-0.17	-0.12	-0.14
21	367.263	16.514	0.09	-0.27	-0.18	0.01	0.10	0.14	0.23	0.10	0.19	0.20
22	148.729	16.780	0.20	-0.31	0.14	0.27	0.44	0.52	0.70	0.53	0.70	0.69
23	75.5014	14.999	0.19	-0.11	0.26	0.20	0.72	0.41	0.93	0.41	0.93	0.70
24	48.0520	21.605	0.82	-0.52	0.43	0.81	2.45	0.72	2.36	0.88	2.52	1.11
25	27.7000	17.834	0.48	-0.52	-1.59	0.77	1.73	-1.27	-0.33	-1.51	-0.57	-1.30
26	15.9680	9.114	-0.00	-0.03	0.01	0.00	-0.08	0.00	-0.08	0.02	-0.06	0.03
27	9.87700	17.676	0.10	-0.39	0.80	1.38	1.33	1.09	1.04	0.79	0.74	0.69

Table 9.27: U-235 cross sections in 4.5% UO_2 pin with radius 0.4096 cm and pitch 1.26 cm.

			Error (%)									
Group	E_{max} (eV)	REF	2REG	UF-SD	UF-IR	EQ-SD	EQ-SD+	EQ-IR	EQ-IR+	SUBG	SUBG+	S-INT
15	9118.00	13.332	0.00	0.00	0.00	0.01	0.01	0.01	0.01	0.05	0.05	-0.01
16	5530.00	13.345	0.00	-0.00	-0.01	0.00	0.00	0.00	0.00	0.01	0.01	0.01
17	3519.10	13.575	0.00	0.00	0.01	-0.01	0.00	-0.01	0.00	0.00	0.01	0.01
18	2239.45	15.025	0.00	0.01	-0.01	0.13	-0.01	0.13	-0.01	0.13	-0.01	0.06
19	1425.10	16.176	0.00	0.00	0.04	0.01	-0.04	0.01	-0.04	0.01	-0.03	-0.09
20	906.899	16.811	-0.00	0.02	0.02	-0.10	0.01	-0.10	0.01	-0.09	0.02	-0.08
21	367.263	21.094	-0.03	-0.01	0.50	0.71	-0.24	0.72	-0.23	0.80	-0.15	0.72
22	148.729	24.283	-0.03	-0.02	0.14	-0.42	-0.11	-0.41	-0.10	-0.41	-0.10	-0.55
23	75.5014	29.554	-0.05	-0.05	0.29	-0.79	-0.25	-0.76	-0.22	-0.79	-0.25	-0.30
24	48.0520	38.564	-0.08	0.11	0.26	-2.64	-0.54	-2.59	-0.49	-2.60	-0.50	-1.14
25	27.7000	39.555	0.01	-0.01	0.25	9.42	-0.76	9.63	-0.57	9.71	-0.49	0.14
26	15.9680	48.312	0.00	-0.32	-0.88	-0.70	-0.86	-0.40	-0.56	-0.12	-0.28	-0.35
27	9.87700	38.564	0.00	-0.28	0.74	4.78	-0.19	4.76	-0.21	4.93	-0.05	-1.46

Table 9.28: U-238 cross sections in 4.5% UO_2 pin with radius 0.6 cm and pitch 1.26 cm.

			Error (%)									
Group	E_{max} (eV)	REF	2REG	UF-SD	UF-IR	EQ-SD	EQ-SD+	EQ-IR	EQ-IR+	SUBG	SUBG+	S-INT
15	9118.00	13.999	-0.10	-0.12	-0.14	-0.06	-0.04	-0.07	-0.05	-0.10	-0.09	-0.09
16	5530.00	14.398	-0.02	-0.05	-0.12	0.02	0.02	-0.09	-0.08	-0.11	-0.10	-0.09
17	3519.10	15.049	-0.02	-0.02	-0.21	0.02	0.06	-0.11	-0.08	-0.22	-0.18	-0.19
18	2239.45	13.833	-0.02	-0.02	-0.32	-0.05	0.05	-0.20	-0.10	-0.43	-0.32	-0.36
19	1425.10	14.110	-0.02	-0.04	-0.25	-0.07	0.01	-0.19	-0.11	-0.41	-0.33	-0.33
20	906.899	13.012	-0.01	0.01	-0.21	0.01	0.08	-0.06	0.01	-0.33	-0.27	-0.26
21	367.263	14.983	0.00	-0.27	-2.15	-0.11	0.06	-0.30	-0.13	-2.24	-2.07	-2.04
22	148.729	15.167	0.05	-0.33	-2.85	-0.17	0.27	-0.15	0.29	-2.99	-2.57	-2.73
23	75.5014	13.854	0.06	0.10	-2.02	-0.49	0.65	-0.39	0.75	-2.54	-1.42	-2.12
24	48.0520	18.897	0.32	-0.89	-4.40	-2.27	1.37	-4.10	-0.53	-5.68	-2.17	-5.28
25	27.7000	15.322	0.17	-0.95	-4.13	-1.65	0.79	-4.66	-2.29	-5.08	-2.73	-4.74
26	15.9680	9.102	-0.00	-0.17	0.02	0.00	-0.24	-0.00	-0.24	-0.00	-0.24	0.03
27	9.87700	15.057	0.04	-0.64	1.77	0.54	0.86	0.53	0.85	1.56	1.88	1.59

Table 9.29: U-235 cross sections in 4.5% UO_2 pin with radius 0.6 cm and pitch 1.26 cm.

			Error (%)									
Group	E_{max} (eV)	REF	2REG	UF-SD	UF-IR	EQ-SD	EQ-SD+	EQ-IR	EQ-IR+	SUBG	SUBG+	S-INT
15	9118.00	13.331	0.00	0.01	0.01	0.01	0.01	0.01	0.01	0.03	0.02	0.03
16	5530.00	13.345	0.00	-0.01	-0.01	0.00	-0.01	0.00	-0.01	0.01	-0.00	0.01
17	3519.10	13.574	0.00	0.00	0.03	-0.01	0.00	-0.01	0.00	-0.00	0.00	0.03
18	2239.45	15.010	0.00	0.01	0.00	0.19	0.00	0.19	0.00	0.19	-0.00	0.06
19	1425.10	16.142	0.00	-0.00	0.11	0.14	-0.04	0.14	-0.04	0.14	-0.04	-0.06
20	906.899	16.782	-0.00	0.04	0.02	-0.08	0.04	-0.08	0.04	-0.06	0.06	-0.05
21	367.263	20.867	-0.02	-0.01	0.80	1.05	-0.19	1.07	-0.17	1.22	-0.03	1.03
22	148.729	24.016	-0.02	-0.03	-0.33	-0.50	-0.05	-0.48	-0.03	-0.54	-0.08	-0.86
23	75.5014	29.256	-0.03	-0.20	0.12	-1.23	-0.50	-1.10	-0.37	-1.13	-0.40	-0.18
24	48.0520	37.100	-0.03	0.15	0.07	-2.08	-0.52	-1.94	-0.37	-2.09	-0.53	0.98
25	27.7000	37.045	0.01	-0.20	-0.15	10.05	-1.21	10.75	-0.58	10.65	-0.67	1.89
26	15.9680	43.858	0.01	-0.85	-3.41	-1.13	-1.39	-0.29	-0.56	-0.31	-0.58	-1.30
27	9.87700	35.900	0.00	-0.60	0.06	5.41	0.49	5.53	0.60	5.65	0.72	-1.73

Table 9.30: U-238 cross sections in 20% UO_2 pin with radius 0.3 cm and pitch 1.26 cm.

			Error (%)									
Group	E_{max} (eV)	REF	2REG	UF-SD	UF-IR	EQ-SD	EQ-SD+	EQ-IR	EQ-IR+	SUBG	SUBG+	S-INT
15	9118.00	15.183	-0.02	-0.01	-0.05	-0.20	-0.17	-0.22	-0.20	-0.01	0.01	-0.02
16	5530.00	15.760	0.00	0.00	-0.06	-0.18	-0.16	-0.26	-0.24	-0.03	-0.01	-0.01
17	3519.10	17.736	0.01	-0.01	-0.18	-0.33	-0.27	-0.45	-0.39	-0.11	-0.05	-0.21
18	2239.45	17.059	0.01	-0.01	-0.17	-0.37	-0.24	-0.46	-0.34	-0.21	-0.09	-0.32
19	1425.10	17.190	0.00	-0.01	-0.19	-0.37	-0.22	-0.47	-0.32	-0.44	-0.29	-0.33
20	906.899	14.948	0.01	0.01	0.02	-0.26	-0.10	-0.32	-0.15	-0.04	0.13	0.05
21	367.263	18.136	0.16	-0.29	1.63	-0.07	0.27	0.13	0.48	1.96	2.30	2.21
22	148.729	18.570	0.30	-0.32	2.92	0.22	0.73	0.59	1.11	3.27	3.80	3.86
23	75.5014	16.443	0.30	-0.09	2.51	-0.14	1.21	0.17	1.51	2.23	3.60	3.23
24	48.0520	25.248	1.09	-0.53	3.73	-0.37	3.45	-0.15	3.68	2.66	6.60	3.33
25	27.7000	20.733	0.69	-0.38	-0.23	1.51	2.55	0.54	1.57	0.03	1.05	0.76
26	15.9680	9.116	0.00	-0.02	0.04	0.02	-0.14	0.02	-0.14	0.04	-0.12	0.07
27	9.87700	20.542	0.16	-0.35	-0.23	1.57	1.73	0.32	0.48	0.01	0.18	-0.42

Table 9.31: U-235 cross sections in 20% UO_2 pin with radius 0.3 cm and pitch 1.26 cm.

			Error (%)									
Group	E_{max} (eV)	REF	2REG	UF-SD	UF-IR	EQ-SD	EQ-SD+	EQ-IR	EQ-IR+	SUBG	SUBG+	S-INT
15	9118.00	13.332	0.00	0.00	0.00	0.01	0.01	0.01	0.01	0.03	0.03	-0.02
16	5530.00	13.345	0.00	-0.00	-0.01	0.00	0.00	0.00	0.00	0.01	0.01	0.01
17	3519.10	13.574	0.00	0.00	0.01	-0.00	0.00	-0.00	0.00	-0.00	0.01	0.00
18	2239.45	15.022	0.00	0.00	-0.01	0.08	-0.01	0.08	-0.01	0.08	-0.01	0.04
19	1425.10	16.162	0.00	0.00	0.01	-0.05	-0.03	-0.05	-0.03	-0.04	-0.02	-0.10
20	906.899	16.763	-0.00	0.01	0.01	-0.11	-0.01	-0.11	-0.01	-0.06	0.04	-0.06
21	367.263	20.880	-0.03	-0.01	0.34	0.44	-0.27	0.45	-0.27	0.72	-0.00	0.67
22	148.729	23.789	-0.03	-0.03	0.09	-0.45	-0.20	-0.43	-0.18	-0.38	-0.13	-0.46
23	75.5014	28.868	-0.04	-0.04	0.18	-0.70	-0.41	-0.66	-0.37	-0.53	-0.25	-0.31
24	48.0520	36.620	-0.08	0.02	-0.10	-2.71	-0.57	-2.70	-0.56	-2.58	-0.43	-1.83
25	27.7000	37.236	0.02	-0.16	-0.02	6.87	-0.66	7.00	-0.54	7.34	-0.23	0.71
26	15.9680	42.105	0.02	-0.37	-0.92	-0.74	-0.94	-0.69	-0.89	-0.11	-0.32	-0.29
27	9.87700	36.588	0.01	-0.25	0.53	1.42	-0.02	1.18	-0.27	1.62	0.17	-1.34

Table 9.32: U-238 cross sections in 20% UO_2 pin with radius 0.4096 cm and pitch 1.26 cm.

			Error (%)									
Group	E_{max} (eV)	REF	2REG	UF-SD	UF-IR	EQ-SD	EQ-SD+	EQ-IR	EQ-IR+	SUBG	SUBG+	S-INT
15	9118.00	14.874	-0.03	-0.03	-0.08	-0.18	-0.14	-0.20	-0.16	-0.06	-0.02	-0.05
16	5530.00	15.374	0.00	-0.00	-0.08	-0.13	-0.10	-0.24	-0.21	-0.09	-0.06	-0.06
17	3519.10	16.914	0.01	-0.01	-0.20	-0.24	-0.15	-0.35	-0.26	-0.27	-0.18	-0.30
18	2239.45	16.010	-0.00	-0.02	-0.24	-0.31	-0.12	-0.41	-0.22	-0.35	-0.16	-0.44
19	1425.10	16.169	-0.01	-0.04	-0.23	-0.34	-0.13	-0.43	-0.23	-0.49	-0.28	-0.34
20	906.899	14.294	0.00	0.02	-0.05	-0.20	0.01	-0.28	-0.06	-0.22	-0.01	-0.08
21	367.263	17.025	0.11	-0.34	0.48	-0.21	0.22	-0.10	0.33	0.49	0.92	0.87
22	148.729	17.352	0.22	-0.41	1.10	-0.04	0.59	0.23	0.87	1.07	1.71	1.78
23	75.5014	15.531	0.21	-0.10	0.91	-0.68	1.08	-0.53	1.23	0.18	1.96	1.45
24	48.0520	23.166	0.87	-0.86	1.21	-1.92	3.00	-1.83	3.09	-0.95	4.01	-0.01
25	27.7000	18.754	0.52	-0.66	-1.27	0.34	2.11	-1.37	0.37	-1.68	0.06	-0.69
26	15.9680	9.111	0.00	-0.05	0.08	0.04	-0.19	0.04	-0.19	0.06	-0.17	0.11
27	9.87700	18.426	0.12	-0.49	0.30	1.57	1.66	0.99	1.07	0.69	0.78	0.11

Table 9.33: U-235 cross sections in 20% UO_2 pin with radius 0.4096 cm and pitch 1.26 cm.

			Error (%)									
Group	E_{max} (eV)	REF	2REG	UF-SD	UF-IR	EQ-SD	EQ-SD+	EQ-IR	EQ-IR+	SUBG	SUBG+	S-INT
15	9118.00	13.332	0.00	0.00	0.00	0.01	0.01	0.01	0.01	0.02	0.02	-0.02
16	5530.00	13.345	0.00	-0.00	-0.01	0.00	0.00	0.00	0.00	0.01	0.00	0.01
17	3519.10	13.574	0.00	0.00	0.01	-0.01	0.00	-0.01	0.00	-0.01	0.00	0.00
18	2239.45	15.011	0.00	0.01	-0.01	0.10	-0.01	0.10	-0.01	0.11	-0.01	0.05
19	1425.10	16.143	0.00	0.00	0.03	-0.03	-0.04	-0.03	-0.04	-0.02	-0.03	-0.11
20	906.899	16.730	-0.00	0.02	0.00	-0.11	-0.01	-0.11	-0.01	-0.05	0.06	-0.05
21	367.263	20.692	-0.03	-0.01	0.39	0.48	-0.28	0.49	-0.27	0.84	0.07	0.77
22	148.729	23.488	-0.02	-0.04	-0.09	-0.48	-0.18	-0.44	-0.14	-0.44	-0.14	-0.56
23	75.5014	28.464	-0.04	-0.06	0.09	-0.84	-0.49	-0.75	-0.40	-0.59	-0.24	-0.29
24	48.0520	35.499	-0.07	0.05	-0.38	-2.88	-0.56	-2.95	-0.63	-2.82	-0.49	-1.71
25	27.7000	35.420	0.02	-0.21	-0.34	6.89	-0.67	6.90	-0.67	7.39	-0.21	1.50
26	15.9680	39.038	0.02	-0.52	-1.49	-0.57	-0.83	-0.44	-0.71	-0.14	-0.41	-0.41
27	9.87700	34.553	0.02	-0.41	0.63	1.90	0.36	1.69	0.15	2.01	0.47	-1.06

Table 9.34: U-238 cross sections in 20% UO_2 pin with radius 0.6 cm and pitch 1.26 cm.

			Error (%)									
Group	E_{max} (eV)	REF	2REG	UF-SD	UF-IR	EQ-SD	EQ-SD+	EQ-IR	EQ-IR+	SUBG	SUBG+	S-INT
15	9118.00	14.199	-0.11	-0.12	-0.14	-0.12	-0.04	-0.14	-0.05	-0.18	-0.10	-0.11
16	5530.00	14.607	-0.02	-0.05	-0.10	-0.03	0.03	-0.13	-0.07	-0.16	-0.11	-0.09
17	3519.10	15.435	-0.01	-0.02	-0.18	-0.09	0.09	-0.23	-0.05	-0.36	-0.18	-0.18
18	2239.45	14.283	-0.01	-0.01	-0.27	-0.27	0.13	-0.42	-0.02	-0.64	-0.24	-0.36
19	1425.10	14.535	-0.02	-0.05	-0.17	-0.29	0.06	-0.41	-0.06	-0.60	-0.25	-0.24
20	906.899	13.275	-0.00	0.01	-0.14	-0.19	0.13	-0.30	0.01	-0.50	-0.19	-0.20
21	367.263	15.402	0.01	-0.38	-1.42	-0.53	0.18	-0.75	-0.04	-2.16	-1.46	-1.35
22	148.729	15.611	0.06	-0.51	-1.86	-0.65	0.34	-0.80	0.18	-2.74	-1.78	-1.70
23	75.5014	14.347	0.06	0.19	-1.70	-2.07	1.02	-2.09	1.00	-3.62	-0.57	-1.76
24	48.0520	20.402	0.36	-1.48	-3.79	-6.35	1.46	-7.47	0.24	-8.96	-1.37	-7.20
25	27.7000	16.123	0.19	-1.42	-3.78	-3.14	0.59	-5.90	-2.28	-6.29	-2.69	-4.66
26	15.9680	9.094	-0.00	-0.29	0.21	0.12	-0.47	0.12	-0.47	0.12	-0.47	0.24
27	9.87700	15.537	0.05	-0.83	1.12	0.64	0.90	0.66	0.93	1.24	1.51	0.95

Table 9.35: U-235 cross sections in 20% UO_2 pin with radius 0.6 cm and pitch 1.26 cm.

			Error (%)									
Group	E_{max} (eV)	REF	2REG	UF-SD	UF-IR	EQ-SD	EQ-SD+	EQ-IR	EQ-IR+	SUBG	SUBG+	S-INT
15	9118.00	13.331	-0.00	0.01	0.01	0.01	0.01	0.01	0.01	-0.01	-0.01	-0.00
16	5530.00	13.345	0.00	-0.01	-0.01	0.00	-0.01	0.00	-0.00	0.01	-0.00	0.01
17	3519.10	13.573	0.00	0.00	0.03	-0.01	-0.00	-0.01	0.00	-0.01	-0.00	0.01
18	2239.45	14.981	0.00	0.00	-0.01	0.16	-0.00	0.16	-0.00	0.15	-0.01	0.05
19	1425.10	16.075	0.00	-0.01	0.09	0.07	-0.05	0.07	-0.05	0.07	-0.04	-0.12
20	906.899	16.625	-0.00	0.04	-0.01	-0.09	0.04	-0.09	0.04	-0.03	0.10	-0.02
21	367.263	20.142	-0.02	-0.00	0.47	0.70	-0.20	0.72	-0.18	1.09	0.19	0.97
22	148.729	22.707	-0.01	-0.06	-1.04	-0.48	-0.01	-0.61	-0.15	-0.64	-0.18	-0.94
23	75.5014	27.270	-0.02	-0.26	-0.44	-1.02	-0.61	-0.82	-0.42	-0.75	-0.35	-0.29
24	48.0520	32.622	-0.03	0.03	-1.98	-2.82	-0.18	-3.05	-0.42	-3.11	-0.48	-0.84
25	27.7000	31.533	0.02	-0.56	-1.49	6.46	-0.83	6.81	-0.50	6.66	-0.64	1.90
26	15.9680	33.213	0.02	-0.90	-3.38	-0.32	-0.56	-0.31	-0.56	-0.41	-0.65	-0.89
27	9.87700	30.420	0.02	-0.48	0.58	1.46	1.31	1.21	1.06	1.12	0.96	-2.06

9.4 MOX Fuel Pin

The next benchmark problem is a bare MOX fuel pin in an infinite array, modeled as a simple pin-cell geometry with reflective boundary conditions. The uranium enrichment is held constant at 3.0% by weight, and the relative weight fractions of transuranics are held constant at the values shown in Tab. 9.36. As with the previous benchmark, moderator nuclide concentrations are based on a potential cross section of $1.23\,\mathrm{cm}^{-1}$, and number densities for H-1 and O-16 are derived from this. The concentration of molecules in the MOX fuel is taken to be $0.22\,{}^{\mathrm{a}}/_{\mathrm{b-cm}}$ regardless of composition.

The ratio of transuranics to uranium by weight was varied, using values 5%, 10%, and 20%. The pitch was held constant at $1.26\,\mathrm{cm}$ and the pin radius was varied between $0.3\,\mathrm{cm}$, $0.4096\,\mathrm{cm}$, and $0.6\,\mathrm{cm}$. For each configuration, group-averaged cross sections for each of the resonance groups in the WIMS69 structure for each nuclide were created. A multitude of cross section generation methods were compared to an ultrafine reference case.

This benchmark problem is intended to stress each method further in terms of mutual self-shielding. Figure 9.5 shows the cross sections for WIMS69 groups 23-27 for the three highest concentration nuclides in MOX fuel: U-238, Pu-239, and Pu-240. Each nuclide's cross section features large resonances that have a significant impact on the flux. Furthermore, several cases of significant resonance overlap are easily seen. U-238 and Pu-240 have overlapping resonances at $20\,\mathrm{eV}$; Pu-239 and Pu-240 overlap at $41\,\mathrm{eV}$; and all three nuclides have significantly overlapping resonances at $66\,\mathrm{eV}$. Furthermore, several more nuclides are present in the fuel, albeit at lower concentrations, and each presents its own challenge with mutual self-shielding.

Results are presented in two formats at the end of this section. First, for each nuclide and for each of the full suite of cases considered, approximate errors in the total isotopic reaction rate for the entire resonance region are shown. The reaction rates are obtained by solving for the group-integrated flux for each group in the reference solution and subsequently multiplying these reference fluxes by the cross sections obtained in each method. The total

Table 9.36: Relative weight fraction of transuranics in MOX benchmark.

Nuclide	Weight Fraction
Np-237	0.05343
Pu-238	0.02636
Pu-239	0.48407
Pu-240	0.21778
Pu-241	0.10506
Pu-242	0.06222
Am-241	0.03368
Am-242	0.01740

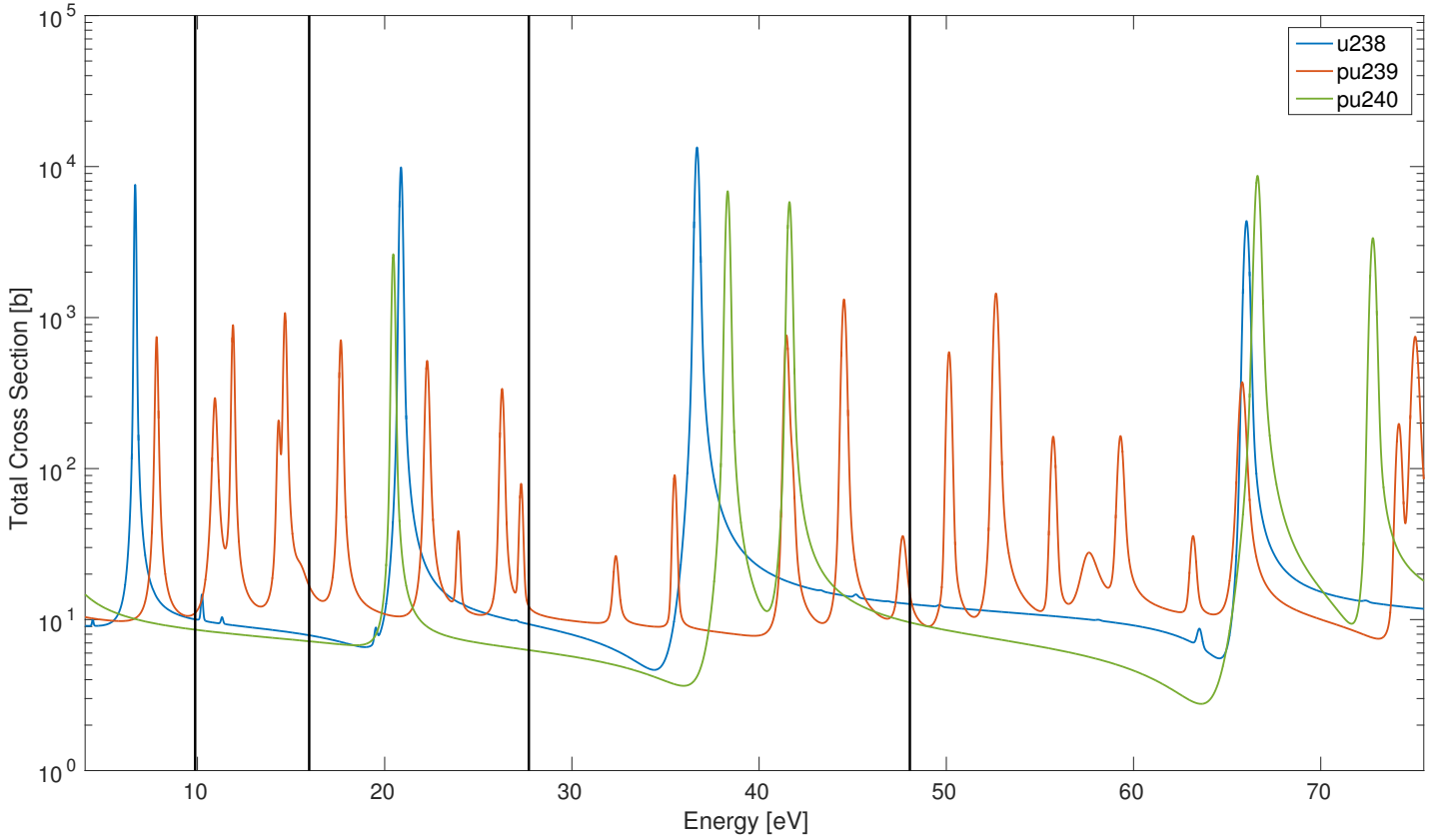

Figure 9.5: Cross sections of U-238, Pu-239, and Pu-240 for WIMS69 groups 23-27. Black lines show the breakpoints between the groups.

Table 9.37: Summary table. Errors in integrated reaction rate in resonance range for MOX fuel pin benchmark with 10% transuranics, radius 0.4096 cm, and pitch 1.26 cm.

		Error (%)									
Nuclide	REF	2REG	UF-SD	UF-IR	EQ-SD	EQ-SD+	EQ-IR	EQ-IR+	SUBG	SUBG+	S-INT
U-238	100.1	0.17	-0.26	0.06	0.04	0.49	-0.13	0.32	0.07	0.52	0.15
U-235	152.0	-0.02	-0.04	0.27	0.69	-0.12	0.67	-0.13	0.72	-0.08	0.31
Np-237	311.8	0.02	-0.02	0.04	-1.10	-0.04	-1.10	-0.04	-1.25	-0.20	-1.95
Pu-238	209.5	-0.04	0.14	1.09	-2.02	-0.40	-2.02	-0.40	-2.67	-1.08	-1.51
Pu-239	177.1	-0.01	-0.26	-1.22	-1.62	0.27	-1.66	0.22	-1.36	0.54	-1.82
Pu-240	185.2	0.11	-0.35	-0.33	1.09	0.67	1.14	0.72	1.73	1.32	-2.54
Pu-241	186.6	-0.01	0.13	0.13	-1.42	-0.42	-1.39	-0.39	-1.53	-0.54	-1.29
Pu-242	173.4	-0.01	-0.21	1.23	-1.55	-0.26	-1.52	-0.24	-2.45	-1.21	-1.91
Am-241	284.2	0.02	0.27	0.66	-0.22	-0.28	-0.22	-0.28	-0.43	-0.49	-0.59
Am-242	133.0	0.02	-0.33	-0.59	4.25	-0.30	4.24	-0.31	4.23	-0.31	-1.91

reaction rate is the sum of the reaction rates for each group. Note that this is not a perfect metric for evaluating the quality of each multigroup cross section generation method, as it is quite possible for unpredicted reaction rates in one group to cancel with overpredicted reaction rates in another. However, by looking at this metric for a large number of cases, it does provide a good feeling for the quality of the approximations. These results are shown in Tables 9.38 to 9.47.

Second, the group-averaged cross sections for each nuclide are shown for a single configuration, the $0.4096\,\text{cm}$ radius pin with 10% transuranics by weight in the MOX fuel. These results, coupled with the integrated reaction rate errors, paint a clearer picture of the performance of each method. The configuration used is intended to be the most typical configuration encountered in a realistic MOX-fueled light water reactor. These results are shown in Tables 9.48 to 9.57.

A summary table is shown in Tab. 9.37. This table shows the integrated reaction rates across the entire resonance range for each nuclide for the same single configuration, the $0.4096\,\text{cm}$ radius pin with 10% transuranics by weight in the MOX fuel. This table compares all nuclides side-by-side and serves to simplify the large amount of data presented in subsequent tables.

Consider first the classical self-shielding methods, equivalence in dilution and the subgroup method. Even without using resonance interference factors, the integrated reaction rates for U-238 and U-235 are quite accurate. For U-238, this is because mutual self-shielding plays a minor role in its cross sections, as it is by far the dominant nuclide in the material. For U-235, this is a result of cancellation of error. By consulting Tab. 9.49, it is seen that positive errors in groups 25 and 27 cancel with negative errors in groups 23, 24, and 26. For other nuclides, mutual self-shielding errors are significant. In all cases, resonance interference factors greatly reduce any large errors, and the integrated reaction rates are accurate within a fraction of a percent.

Comparing equivalence in dilution and subgroup, the methods perform very similarly for most cases. However, for some cases, the subgroup method does exhibit slightly higher deviations from reference. Subgroup results are consistently less than ideal for $0.3\,\text{cm}$ radius pin configurations, which can be attributed to the intermediate resonance parameters used in quadrature generation not being compatible with the downstream application. Dispersed in the various groups of various nuclides, a few other larger errors are encountered. As these errors do not show a systematic trend, this is likely due to less than optimal quadratures.

Next, consider ultrafine with simplified scatter using the slowing down source. This method, as it was with the UO_2 fuel pin is very reliable, providing the smallest errors of any of the methods that do not use a true ultrafine scatter source. For all integrated reaction rates for all nuclides and all configurations, this method shows less than 0.5% error, and the majority of cases are considerably less than this.

A more interesting case is ultrafine with simplified scattering using the intermediate resonance approximation. As expected, errors are slightly higher than that of its sister method using the slowing down source, but errors remain quite small in most cases. However, large errors are seen in a few groups of Pu-238, Pu-239, Pu-240, and Pu-242. These errors arise due to the flux reduction due to absorption in U-238, similar to what was described previously in Sec. 9.3. The most striking example of this is in the Pu-239's and Pu-240's cross sections in group 24, which contains the U-238 $36.6\,\text{eV}$ resonance. As seen in Fig. 9.5, both Pu-239 and Pu-240 have two large resonances higher in energy than the U-238 resonance but no large resonances lower in energy. The ultrafine with simplified scattering method accurately predicts the reaction rate for these resonances above the U-238 resonance, but by failing to account for the reduction in the flux below the resonance, the denominator in the cross section condensation is much too large and causes large errors. Consulting Tables 9.52 and 9.53, the errors for Pu-239 and Pu-240 in this group are -3.37% and -0.85%, respectively. When the radius is increased to $0.6\,\text{cm}$, the flux reduction becomes much more significant, and the errors balloon to -10.62% and -12.89%, respectively.

Finally, consider subgroup with interference cross sections. The errors seen in the integrated reaction rates for these cases are, quite frankly, unacceptably high. Looking at the group-wise errors in the cross sections, one can see the method performs well in some groups but quite poorly in others. Overall, the method is not dependable with the quadratures generated in this study. Many of the single nuclide quadratures obtained were able to accurately preserve single nuclide cross sections in downstream applications, but the quadratures did not lend much insight into the shape of the cross section in the group. That is, the quadrature base points and weights did not appear to be representative of ranges of cross section values and the support of the domain, as would be obtained in a direct subgroup method. Without this property, the interference cross sections were not able to be fitted adequately. The errors seen in these cases correlate with errors seen on the infinite media references used in the quadrature generation process.

Table 9.38: Errors in integrated reaction rate in resonance range for U-238 in MOX fuel pin benchmark.

			Error (%)									
Frac TU	Radius	REF	2REG	UF-SD	UF-IR	EQ-SD	EQ-SD+	EQ-IR	EQ-IR+	SUBG	SUBG+	S-INT
5	0.3	114.1	0.23	-0.18	0.08	0.30	0.58	0.14	0.42	0.83	1.11	0.87
5	0.4096	101.3	0.16	-0.23	0.05	0.13	0.45	-0.03	0.29	0.08	0.39	0.14
5	0.6	71.8	0.03	-0.26	-0.21	-0.31	0.15	-0.65	-0.19	-1.25	-0.80	-1.07
10	0.3	113.8	0.24	-0.20	0.06	0.20	0.63	0.03	0.46	0.82	1.25	0.87
10	0.4096	100.1	0.17	-0.26	0.06	0.04	0.49	-0.13	0.32	0.07	0.52	0.15
10	0.6	68.6	0.03	-0.28	-0.09	-0.39	0.15	-0.70	-0.17	-1.24	-0.71	-1.00
20	0.3	114.0	0.26	-0.23	0.06	-0.01	0.73	-0.18	0.56	0.81	1.56	0.90
20	0.4096	98.6	0.19	-0.28	0.11	-0.19	0.57	-0.36	0.39	0.03	0.79	0.19
20	0.6	64.4	0.04	-0.30	0.12	-0.60	0.17	-0.87	-0.11	-1.30	-0.53	-0.87

Table 9.39: Errors in integrated reaction rate in resonance range for U-235 in MOX fuel pin benchmark.

			Error (%)									
Frac TU	Radius	REF	2REG	UF-SD	UF-IR	EQ-SD	EQ-SD+	EQ-IR	EQ-IR+	SUBG	SUBG+	S-INT
5	0.3	169.8	-0.02	-0.03	0.27	0.96	-0.20	0.95	-0.21	1.00	-0.16	0.54
5	0.4096	156.1	-0.02	-0.05	0.22	1.04	-0.16	1.02	-0.18	1.08	-0.12	0.46
5	0.6	109.5	-0.01	-0.13	-0.14	0.81	-0.13	0.79	-0.15	0.80	-0.13	0.04
10	0.3	167.3	-0.02	-0.02	0.30	0.68	-0.14	0.67	-0.15	0.72	-0.11	0.40
10	0.4096	152.0	-0.02	-0.04	0.27	0.69	-0.12	0.67	-0.13	0.72	-0.08	0.31
10	0.6	102.0	-0.01	-0.13	0.02	0.40	-0.14	0.38	-0.16	0.39	-0.15	-0.04
20	0.3	163.2	-0.02	-0.02	0.33	0.21	-0.07	0.20	-0.08	0.24	-0.04	0.18
20	0.4096	145.6	-0.02	-0.04	0.34	0.13	-0.08	0.12	-0.09	0.16	-0.05	0.11
20	0.6	91.7	-0.01	-0.14	0.20	-0.11	-0.19	-0.13	-0.20	-0.12	-0.19	-0.01

Table 9.40: Errors in integrated reaction rate in resonance range for Np-237 in MOX fuel pin benchmark.

			Error (%)									
Frac TU	Radius	REF	2REG	UF-SD	UF-IR	EQ-SD	EQ-SD+	EQ-IR	EQ-IR+	SUBG	SUBG+	S-INT
5	0.3	354.1	0.02	0.01	0.06	-1.07	0.01	-1.07	0.01	-1.15	-0.07	-1.88
5	0.4096	325.1	0.02	-0.00	0.08	-1.07	-0.01	-1.07	-0.01	-1.18	-0.13	-1.90
5	0.6	222.2	0.01	-0.14	-0.24	-0.99	-0.15	-0.99	-0.15	-1.15	-0.31	-1.85
10	0.3	345.2	0.02	-0.00	0.04	-1.09	-0.02	-1.09	-0.02	-1.23	-0.16	-1.98
10	0.4096	311.8	0.02	-0.02	0.04	-1.10	-0.04	-1.10	-0.04	-1.25	-0.20	-1.95
10	0.6	201.0	0.01	-0.16	-0.44	-1.01	-0.16	-1.01	-0.16	-1.18	-0.33	-1.81
20	0.3	330.3	0.02	-0.02	0.02	-1.13	-0.04	-1.13	-0.04	-1.29	-0.21	-1.98
20	0.4096	290.7	0.02	-0.04	-0.01	-1.15	-0.05	-1.15	-0.05	-1.30	-0.20	-1.92
20	0.6	173.0	0.02	-0.17	-0.64	-1.08	-0.14	-1.08	-0.14	-1.21	-0.27	-1.72

Table 9.41: Errors in integrated reaction rate in resonance range for Pu-238 in MOX fuel pin benchmark.

			Error (%)									
Frac TU	Radius	REF	2REG	UF-SD	UF-IR	EQ-SD	EQ-SD+	EQ-IR	EQ-IR+	SUBG	SUBG+	S-INT
5	0.3	231.0	-0.04	0.10	0.75	-1.72	-0.34	-1.72	-0.34	-2.11	-0.75	-1.14
5	0.4096	216.7	-0.05	0.14	1.07	-1.82	-0.40	-1.82	-0.41	-2.32	-0.92	-0.93
5	0.6	161.8	-0.03	0.04	2.03	-1.41	-0.51	-1.42	-0.52	-2.03	-1.14	0.26
10	0.3	226.2	-0.04	0.10	0.79	-1.89	-0.34	-1.89	-0.34	-2.47	-0.95	-1.71
10	0.4096	209.5	-0.04	0.14	1.09	-2.02	-0.40	-2.02	-0.40	-2.67	-1.08	-1.51
10	0.6	149.3	-0.03	0.03	1.82	-1.58	-0.46	-1.59	-0.47	-2.20	-1.10	-0.19
20	0.3	218.0	-0.04	0.10	0.83	-2.14	-0.34	-2.15	-0.35	-2.83	-1.07	-2.21
20	0.4096	197.7	-0.04	0.14	1.10	-2.30	-0.39	-2.31	-0.40	-2.94	-1.08	-1.89
20	0.6	131.6	-0.03	0.00	1.52	-1.76	-0.37	-1.80	-0.40	-2.23	-0.86	-0.33

Table 9.42: Errors in integrated reaction rate in resonance range for Pu-239 in MOX fuel pin benchmark.

			Error (%)									
Frac TU	Radius	REF	2REG	UF-SD	UF-IR	EQ-SD	EQ-SD+	EQ-IR	EQ-IR+	SUBG	SUBG+	S-INT
5	0.3	209.0	-0.02	-0.17	-0.62	-1.45	0.27	-1.46	0.26	-1.41	0.31	-1.56
5	0.4096	191.6	-0.02	-0.24	-1.03	-1.74	0.26	-1.76	0.24	-1.64	0.36	-1.82
5	0.6	133.0	-0.00	-0.25	-2.68	-2.16	0.34	-2.21	0.30	-2.14	0.37	-2.35
10	0.3	197.8	-0.02	-0.20	-0.76	-1.39	0.21	-1.41	0.19	-1.15	0.45	-1.56
10	0.4096	177.1	-0.01	-0.26	-1.22	-1.62	0.27	-1.66	0.22	-1.36	0.54	-1.82
10	0.6	116.0	0.00	-0.18	-2.85	-1.94	0.46	-2.02	0.38	-2.00	0.40	-2.29
20	0.3	181.0	0.00	-0.21	-0.90	-1.30	0.28	-1.34	0.23	-0.90	0.68	-1.55
20	0.4096	157.3	0.01	-0.23	-1.34	-1.48	0.42	-1.56	0.34	-1.24	0.67	-1.80
20	0.6	96.7	0.01	-0.06	-2.64	-1.78	0.58	-1.88	0.47	-2.08	0.26	-2.09

Table 9.43: Errors in integrated reaction rate in resonance range for Pu-240 in MOX fuel pin benchmark.

			Error (%)									
Frac TU	Radius	REF	2REG	UF-SD	UF-IR	EQ-SD	EQ-SD+	EQ-IR	EQ-IR+	SUBG	SUBG+	S-INT
5	0.3	237.9	0.08	-0.28	0.37	2.15	-0.04	2.18	-0.02	3.20	0.97	-1.18
5	0.4096	211.2	0.08	-0.36	-0.02	2.37	0.34	2.38	0.35	3.32	1.27	-2.07
5	0.6	142.6	0.04	-0.24	-3.26	0.80	0.94	0.77	0.91	0.95	1.12	-4.71
10	0.3	213.5	0.11	-0.31	0.34	1.22	0.30	1.30	0.38	2.28	1.34	-1.49
10	0.4096	185.2	0.11	-0.35	-0.33	1.09	0.67	1.14	0.72	1.73	1.32	-2.54
10	0.6	119.4	0.05	-0.16	-3.47	-0.88	1.07	-0.90	1.05	-1.16	0.79	-4.67
20	0.3	183.5	0.16	-0.30	0.20	0.51	0.72	0.63	0.85	1.02	1.24	-1.85
20	0.4096	155.8	0.15	-0.30	-0.53	0.11	0.99	0.20	1.08	0.10	0.98	-2.82
20	0.6	95.8	0.06	-0.07	-2.90	-1.87	1.10	-1.91	1.06	-2.61	0.30	-4.06

Table 9.44: Errors in integrated reaction rate in resonance range for Pu-241 in MOX fuel pin benchmark.

			Error (%)									
Frac TU	Radius	REF	2REG	UF-SD	UF-IR	EQ-SD	EQ-SD+	EQ-IR	EQ-IR+	SUBG	SUBG+	S-INT
5	0.3	216.5	-0.01	0.08	0.10	-1.37	-0.39	-1.36	-0.38	-1.49	-0.52	-1.23
5	0.4096	196.7	-0.01	0.15	0.18	-1.51	-0.41	-1.49	-0.39	-1.65	-0.55	-1.17
5	0.6	128.9	-0.01	0.26	0.35	-1.52	-0.38	-1.49	-0.35	-1.64	-0.50	-0.61
10	0.3	209.5	-0.01	0.07	0.07	-1.28	-0.43	-1.26	-0.40	-1.42	-0.57	-1.33
10	0.4096	186.6	-0.01	0.13	0.13	-1.42	-0.42	-1.39	-0.39	-1.53	-0.54	-1.29
10	0.6	115.0	-0.01	0.21	0.14	-1.51	-0.35	-1.46	-0.30	-1.52	-0.37	-0.83
20	0.3	198.2	-0.01	0.05	0.04	-1.23	-0.42	-1.18	-0.37	-1.30	-0.49	-1.43
20	0.4096	171.4	-0.01	0.10	0.08	-1.42	-0.37	-1.36	-0.31	-1.41	-0.36	-1.41
20	0.6	97.6	-0.01	0.16	0.01	-1.65	-0.28	-1.59	-0.22	-1.53	-0.16	-1.01

Table 9.45: Errors in integrated reaction rate in resonance range for Pu-242 in MOX fuel pin benchmark.

			Error (%)									
Frac TU	Radius	REF	2REG	UF-SD	UF-IR	EQ-SD	EQ-SD+	EQ-IR	EQ-IR+	SUBG	SUBG+	S-INT
5	0.3	199.1	-0.03	-0.08	0.87	-1.24	-0.26	-1.25	-0.27	-2.33	-1.38	-1.72
5	0.4096	185.5	-0.03	-0.13	1.07	-1.40	-0.29	-1.39	-0.28	-2.53	-1.46	-1.77
5	0.6	138.7	-0.01	-0.34	0.51	-1.52	-0.29	-1.54	-0.30	-2.47	-1.28	-1.41
10	0.3	189.5	-0.02	-0.16	1.10	-1.43	-0.30	-1.41	-0.27	-2.49	-1.40	-2.11
10	0.4096	173.4	-0.01	-0.21	1.23	-1.55	-0.26	-1.52	-0.24	-2.45	-1.21	-1.91
10	0.6	123.8	-0.00	-0.38	0.23	-1.61	-0.20	-1.63	-0.21	-2.31	-0.93	-1.19
20	0.3	175.6	-0.00	-0.25	1.16	-1.54	-0.22	-1.48	-0.15	-2.23	-0.93	-1.97
20	0.4096	157.2	0.01	-0.29	1.13	-1.58	-0.13	-1.53	-0.07	-2.14	-0.71	-1.61
20	0.6	106.5	0.01	-0.41	-0.05	-1.65	-0.11	-1.67	-0.13	-2.28	-0.79	-0.83

Table 9.46: Errors in integrated reaction rate in resonance range for Am-241 in MOX fuel pin benchmark.

			Error (%)									
Frac TU	Radius	REF	2REG	UF-SD	UF-IR	EQ-SD	EQ-SD+	EQ-IR	EQ-IR+	SUBG	SUBG+	S-INT
5	0.3	324.8	0.02	0.17	0.51	-0.67	-0.32	-0.67	-0.32	-0.79	-0.44	-0.96
5	0.4096	296.8	0.02	0.27	0.71	-0.53	-0.31	-0.53	-0.31	-0.69	-0.47	-0.54
5	0.6	199.1	0.01	0.36	1.15	0.26	-0.24	0.26	-0.24	0.07	-0.43	0.82
10	0.3	316.1	0.02	0.17	0.47	-0.36	-0.32	-0.36	-0.32	-0.55	-0.51	-0.96
10	0.4096	284.2	0.02	0.27	0.66	-0.22	-0.28	-0.22	-0.28	-0.43	-0.49	-0.59
10	0.6	180.6	0.01	0.33	0.97	0.30	-0.22	0.29	-0.23	0.10	-0.41	0.42
20	0.3	302.3	0.02	0.18	0.42	-0.06	-0.23	-0.07	-0.24	-0.29	-0.46	-1.00
20	0.4096	265.4	0.02	0.28	0.62	-0.05	-0.16	-0.06	-0.17	-0.28	-0.39	-0.80
20	0.6	156.6	0.01	0.30	0.76	-0.01	-0.16	-0.02	-0.17	-0.15	-0.30	-0.24

Table 9.47: Errors in integrated reaction rate in resonance range for Am-242 in MOX fuel pin benchmark.

			Error (%)									
Frac TU	Radius	REF	2REG	UF-SD	UF-IR	EQ-SD	EQ-SD+	EQ-IR	EQ-IR+	SUBG	SUBG+	S-INT
5	0.3	149.0	0.00	-0.25	-0.64	3.79	-0.44	3.79	-0.44	3.79	-0.44	-1.61
5	0.4096	136.7	0.01	-0.32	-0.58	4.67	-0.36	4.67	-0.36	4.67	-0.36	-1.91
5	0.6	96.7	0.01	-0.28	-0.41	5.11	-0.08	5.11	-0.08	5.10	-0.09	-1.69
10	0.3	146.8	0.01	-0.25	-0.63	3.48	-0.38	3.48	-0.39	3.48	-0.39	-1.63
10	0.4096	133.0	0.02	-0.33	-0.59	4.25	-0.30	4.24	-0.31	4.23	-0.31	-1.91
10	0.6	90.1	0.02	-0.30	-0.36	4.36	-0.08	4.35	-0.09	4.34	-0.09	-1.63
20	0.3	143.0	0.01	-0.26	-0.61	2.92	-0.28	2.91	-0.29	2.90	-0.30	-1.63
20	0.4096	127.2	0.02	-0.34	-0.62	3.49	-0.22	3.49	-0.23	3.48	-0.23	-1.89
20	0.6	81.0	0.02	-0.32	-0.30	3.27	-0.10	3.26	-0.10	3.25	-0.11	-1.52

Table 9.48: Cross sections for U-238 in a MOX pin with radius 0.4096 cm, pitch 1.26 cm, and 10% transuranic concentration.

			Error (%)									
Group	E_{max} (eV)	REF	2REG	UF-SD	UF-IR	EQ-SD	EQ-SD+	EQ-IR	EQ-IR+	SUBG	SUBG+	S-INT
15	9118.00	14.797	-0.03	-0.04	-0.08	-0.20	-0.16	-0.23	-0.19	-0.06	-0.02	-0.08
16	5530.00	15.283	0.00	-0.00	-0.10	-0.17	-0.13	-0.24	-0.19	-0.11	-0.06	-0.14
17	3519.10	16.730	0.01	-0.01	-0.24	-0.34	-0.20	-0.45	-0.31	-0.34	-0.20	-0.33
18	2239.45	15.775	-0.00	-0.02	-0.27	-0.40	-0.20	-0.51	-0.31	-0.40	-0.20	-0.50
19	1425.10	15.943	-0.01	-0.03	-0.30	-0.43	-0.22	-0.53	-0.31	-0.52	-0.30	-0.41
20	906.899	14.152	0.00	0.01	-0.06	-0.28	-0.05	-0.35	-0.12	-0.29	-0.06	-0.25
21	367.263	16.806	0.10	-0.32	0.34	-0.42	0.16	-0.30	0.28	0.04	0.62	0.52
22	148.729	17.091	0.22	-0.47	0.53	-0.15	0.39	0.06	0.61	0.61	1.15	0.96
23	75.5014	15.048	0.29	-0.19	-0.86	1.08	0.93	1.27	1.11	1.69	1.53	0.19
24	48.0520	21.865	0.92	-0.80	1.25	1.59	2.25	1.47	2.14	2.23	2.91	2.67
25	27.7000	18.304	0.49	-0.65	-1.30	0.30	1.94	-1.59	0.03	-1.72	-0.11	-2.43
26	15.9680	9.122	-0.00	-0.02	0.07	-0.08	-0.15	-0.08	-0.15	-0.06	-0.13	0.01
27	9.87700	18.231	0.11	-0.43	0.63	0.28	1.37	-0.13	0.95	-0.30	0.78	0.44

Table 9.49: Cross sections for U-235 in a MOX pin with radius 0.4096 cm, pitch 1.26 cm, and 10% transuranic concentration.

			Error (%)									
Group	E_{max} (eV)	REF	2REG	UF-SD	UF-IR	EQ-SD	EQ-SD+	EQ-IR	EQ-IR+	SUBG	SUBG+	S-INT
15	9118.00	13.332	0.00	0.00	0.00	0.01	0.01	0.01	0.01	0.06	0.06	0.06
16	5530.00	13.345	0.00	-0.00	-0.01	0.00	0.00	0.00	0.00	0.01	0.01	0.01
17	3519.10	13.574	0.00	0.00	0.01	-0.00	0.00	-0.00	0.00	0.00	0.01	0.00
18	2239.45	15.029	0.00	0.01	-0.01	0.12	-0.01	0.12	-0.01	0.12	-0.01	0.05
19	1425.10	16.180	0.00	0.00	0.04	0.01	-0.04	0.01	-0.04	0.01	-0.03	-0.03
20	906.899	16.819	-0.00	0.02	0.03	-0.08	0.01	-0.08	0.01	-0.08	0.01	-0.07
21	367.263	21.164	-0.03	0.01	0.59	0.67	-0.25	0.67	-0.25	0.72	-0.20	0.70
22	148.729	24.368	-0.03	-0.04	0.08	-0.30	-0.14	-0.29	-0.14	-0.30	-0.14	-0.60
23	75.5014	29.947	-0.06	-0.03	0.60	-1.57	-0.21	-1.57	-0.21	-1.61	-0.25	0.48
24	48.0520	39.083	-0.09	0.21	0.60	-2.71	-0.53	-2.71	-0.53	-2.71	-0.53	-1.17
25	27.7000	41.120	0.00	0.06	0.44	7.73	-0.27	7.74	-0.27	7.81	-0.21	4.51
26	15.9680	51.189	0.01	-0.33	-0.08	-2.31	-0.27	-2.30	-0.26	-2.08	-0.03	-0.95
27	9.87700	39.925	0.00	-0.22	0.45	3.65	0.31	3.54	0.21	3.65	0.31	0.21

Table 9.50: Cross sections for Np-237 in a MOX pin with radius 0.4096 cm, pitch 1.26 cm, and 10% transuranic concentration.

			Error (%)									
Group	E_{max} (eV)	REF	2REG	UF-SD	UF-IR	EQ-SD	EQ-SD+	EQ-IR	EQ-IR+	SUBG	SUBG+	S-INT
15	9118.00	17.325	0.00	0.01	0.00	0.02	0.01	0.02	0.01	0.03	0.02	0.09
16	5530.00	18.714	0.00	-0.00	-0.03	0.01	-0.00	0.01	-0.00	0.02	0.01	0.02
17	3519.10	20.299	0.00	0.00	-0.00	0.01	0.00	0.01	0.00	0.02	0.01	0.01
18	2239.45	22.247	-0.00	0.00	0.03	0.00	0.00	0.00	0.00	0.01	0.01	0.00
19	1425.10	24.744	0.00	0.00	-0.02	0.01	-0.00	0.02	-0.00	0.02	0.01	1.23
20	906.899	29.900	-0.00	0.01	0.09	-0.07	-0.08	-0.07	-0.08	-0.04	-0.06	-1.46
21	367.263	41.657	0.06	0.01	-0.59	-0.22	0.01	-0.22	0.01	-0.13	0.11	-1.22
22	148.729	53.254	0.15	0.15	-0.99	-1.93	0.19	-1.93	0.19	-1.91	0.20	-0.72
23	75.5014	82.730	0.02	-0.07	-0.24	0.96	-0.51	0.96	-0.51	0.73	-0.74	-0.61
24	48.0520	64.919	-0.09	-0.17	0.60	1.32	-0.16	1.32	-0.16	1.14	-0.35	-0.44
25	27.7000	112.638	0.03	-0.44	-1.77	-2.45	1.05	-2.45	1.06	-2.61	0.88	-5.70
26	15.9680	113.171	0.00	-0.14	0.27	-0.55	-1.10	-0.53	-1.08	-0.72	-1.27	-1.62
27	9.87700	95.783	0.02	0.38	2.18	-4.26	0.02	-4.28	-0.01	-4.83	-0.57	-4.01

Table 9.51: Cross sections for Pu-238 in a MOX pin with radius 0.4096 cm, pitch 1.26 cm, and 10% transuranic concentration.

			Error (%)									
Group	E_{max} (eV)	REF	2REG	UF-SD	UF-IR	EQ-SD	EQ-SD+	EQ-IR	EQ-IR+	SUBG	SUBG+	S-INT
15	9118.00	16.073	0.00	0.01	0.00	0.02	0.01	0.02	0.01	0.03	0.02	0.03
16	5530.00	17.335	0.00	-0.00	-0.03	0.01	-0.00	0.01	-0.00	0.02	0.01	0.13
17	3519.10	18.851	0.00	0.00	-0.00	0.01	0.00	0.01	0.00	0.26	0.25	0.00
18	2239.45	20.662	-0.00	0.00	0.03	0.00	0.00	0.00	0.00	0.01	0.01	0.10
19	1425.10	22.939	0.00	0.00	-0.02	0.01	-0.00	0.01	-0.00	0.02	0.00	0.03
20	906.899	30.495	-0.01	0.01	0.22	-0.49	-0.10	-0.49	-0.10	-0.50	-0.11	0.36
21	367.263	52.249	-0.09	0.05	2.24	-0.46	-0.62	-0.47	-0.63	-0.88	-1.04	-1.90
22	148.729	63.248	-0.13	-0.15	0.71	-2.28	-0.30	-2.28	-0.31	-3.10	-1.14	-3.44
23	75.5014	21.389	-0.05	-0.03	0.27	-2.40	0.40	-2.40	0.40	-2.42	0.37	-2.40
24	48.0520	15.513	-0.00	0.03	0.13	0.54	-0.11	0.54	-0.11	0.54	-0.11	0.03
25	27.7000	102.473	-0.02	0.83	2.67	-7.12	-1.24	-7.12	-1.24	-9.62	-3.91	-2.57
26	15.9680	30.551	-0.00	0.02	0.74	-2.78	-0.62	-2.78	-0.62	-2.76	-0.59	-1.55
27	9.87700	17.818	-0.00	0.20	0.00	-0.75	0.41	-0.76	0.40	-0.75	0.40	-0.54

Table 9.52: Cross sections for Pu-239 in a MOX pin with radius 0.4096 cm, pitch 1.26 cm, and 10% transuranic concentration.

			Error (%)									
Group	E_{max} (eV)	REF	2REG	UF-SD	UF-IR	EQ-SD	EQ-SD+	EQ-IR	EQ-IR+	SUBG	SUBG+	S-INT
15	9118.00	14.675	0.00	0.01	0.01	0.02	0.02	0.02	0.02	0.04	0.03	0.05
16	5530.00	15.597	-0.00	-0.00	-0.01	0.02	-0.00	0.02	-0.00	0.03	0.00	0.03
17	3519.10	16.320	-0.00	0.00	0.01	-0.15	0.01	-0.15	0.01	-0.16	0.00	-0.11
18	2239.45	16.861	0.00	0.00	-0.12	-0.03	-0.02	-0.03	-0.02	-0.02	-0.01	-0.21
19	1425.10	17.775	0.01	0.01	-0.12	0.46	-0.03	0.46	-0.03	0.48	-0.02	0.22
20	906.899	20.178	0.02	-0.04	-0.50	-1.36	0.10	-1.37	0.09	-1.33	0.13	-1.01
21	367.263	28.596	-0.01	-0.08	-0.25	-1.41	-0.11	-1.43	-0.13	-1.30	-0.00	-0.72
22	148.729	33.335	-0.09	-0.16	0.31	0.67	-0.60	0.65	-0.62	0.97	-0.30	-0.42
23	75.5014	49.424	0.07	0.27	-3.61	1.00	0.49	1.02	0.50	1.66	1.14	-1.52
24	48.0520	30.294	-0.07	-0.56	-3.37	-1.26	1.31	-1.24	1.34	-0.60	2.00	-5.61
25	27.7000	44.270	-0.03	-0.20	-0.56	-6.34	-0.04	-6.32	-0.02	-6.02	0.31	-3.24
26	15.9680	79.864	0.02	-0.36	-1.40	0.31	-0.42	0.18	-0.56	0.75	0.02	-0.73
27	9.87700	28.537	-0.02	-1.66	-3.91	-10.28	3.06	-10.51	2.80	-10.11	3.25	-7.72

Table 9.53: Cross sections for Pu-240 in a MOX pin with radius 0.4096 cm, pitch 1.26 cm, and 10% transuranic concentration.

			Error (%)									
Group	E_{max} (eV)	REF	2REG	UF-SD	UF-IR	EQ-SD	EQ-SD+	EQ-IR	EQ-IR+	SUBG	SUBG+	S-INT
15	9118.00	16.350	0.00	0.02	0.02	-0.11	0.05	-0.11	0.05	-0.11	0.05	0.01
16	5530.00	15.052	-0.00	0.01	0.11	-0.59	0.06	-0.59	0.06	-0.58	0.07	-0.29
17	3519.10	17.117	0.01	-0.01	-0.23	-1.00	0.15	-1.00	0.14	-0.99	0.15	-0.42
18	2239.45	18.274	0.04	-0.01	-1.27	-1.78	0.41	-1.79	0.41	-1.75	0.44	-1.16
19	1425.10	22.357	-0.01	0.02	0.72	0.70	-0.24	0.69	-0.25	0.65	-0.28	0.65
20	906.899	21.359	0.01	-0.06	-0.74	-1.49	-0.13	-1.54	-0.18	-1.71	-0.36	-1.48
21	367.263	30.166	0.06	0.02	-0.17	-5.21	0.34	-5.26	0.29	-5.43	0.11	-1.99
22	148.729	45.250	-0.09	-0.51	0.11	0.53	-0.60	0.49	-0.64	0.52	-0.61	-2.62
23	75.5014	75.902	0.09	-0.61	2.17	10.23	2.04	10.46	2.25	13.23	4.81	-2.78
24	48.0520	93.142	-0.02	-1.46	-0.85	-4.47	2.26	-4.28	2.47	-2.61	4.25	-7.04
25	27.7000	31.976	1.66	1.34	-6.41	21.26	-0.12	21.29	-0.10	19.73	-1.38	-0.41
26	15.9680	7.878	-0.00	-0.02	0.04	0.04	-0.11	0.04	-0.11	0.07	-0.08	0.06
27	9.87700	10.815	0.00	0.21	0.64	-0.25	-0.65	-0.26	-0.65	-0.26	-0.65	0.92

Table 9.54: Cross sections for Pu-241 in a MOX pin with radius 0.4096 cm, pitch 1.26 cm, and 10% transuranic concentration.

			Error (%)									
Group	E_{max} (eV)	REF	2REG	UF-SD	UF-IR	EQ-SD	EQ-SD+	EQ-IR	EQ-IR+	SUBG	SUBG+	S-INT
15	9118.00	12.580	0.00	0.00	0.00	0.01	0.01	0.01	0.01	0.02	0.02	0.02
16	5530.00	13.102	0.00	-0.00	-0.01	0.00	-0.00	0.00	-0.00	0.01	0.01	0.01
17	3519.10	13.584	0.00	0.00	-0.00	0.00	-0.00	0.00	-0.00	0.01	0.01	0.01
18	2239.45	14.364	-0.00	0.00	0.02	0.00	0.00	0.00	0.00	0.01	0.01	0.01
19	1425.10	14.826	0.00	-0.00	-0.00	0.00	-0.00	0.00	-0.00	0.00	-0.00	0.00
20	906.899	16.454	-0.00	0.00	0.08	0.05	-0.09	0.05	-0.09	0.05	-0.09	-0.13
21	367.263	20.304	-0.01	-0.00	0.19	-0.87	0.06	-0.87	0.06	-0.89	0.03	-0.81
22	148.729	25.041	-0.03	0.09	0.60	-1.03	-0.35	-1.03	-0.35	-1.03	-0.35	-1.14
23	75.5014	18.268	0.02	-0.03	-0.00	3.60	0.06	3.60	0.06	3.61	0.06	-3.07
24	48.0520	22.871	-0.05	0.07	0.33	-1.94	-0.19	-1.94	-0.19	-1.95	-0.21	-1.60
25	27.7000	55.669	-0.01	0.44	1.15	-1.54	-1.30	-1.54	-1.30	-1.71	-1.46	-0.30
26	15.9680	92.763	-0.00	-0.13	-1.42	1.23	0.78	1.24	0.80	1.25	0.80	0.27
27	9.87700	92.092	-0.01	0.36	0.58	-5.05	-1.40	-4.94	-1.29	-5.44	-1.80	-3.64

Table 9.55: Cross sections for Pu-242 in a MOX pin with radius 0.4096 cm, pitch 1.26 cm, and 10% transuranic concentration.

			Error (%)									
Group	E_{max} (eV)	REF	2REG	UF-SD	UF-IR	EQ-SD	EQ-SD+	EQ-IR	EQ-IR+	SUBG	SUBG+	S-INT
15	9118.00	17.300	0.00	0.01	0.00	0.02	0.01	0.02	0.01	0.21	0.20	0.21
16	5530.00	18.591	0.00	-0.00	-0.03	0.01	-0.00	0.01	-0.00	0.12	0.11	0.50
17	3519.10	20.152	0.00	0.00	-0.00	0.01	0.00	0.01	0.00	0.01	0.00	-0.00
18	2239.45	22.080	-0.00	0.00	0.03	0.00	0.00	0.00	0.00	0.01	0.01	-0.05
19	1425.10	24.453	0.01	0.01	-0.11	-0.10	0.02	-0.10	0.02	-0.14	-0.02	-0.25
20	906.899	26.355	-0.02	-0.02	0.60	2.64	-0.29	2.63	-0.30	2.33	-0.59	1.80
21	367.263	34.252	0.04	0.03	0.94	-0.49	0.17	-0.58	0.08	-0.96	-0.30	-1.18
22	148.729	23.038	-0.09	-0.19	0.01	-1.59	-0.09	-1.61	-0.11	-2.79	-1.30	-5.86
23	75.5014	142.007	-0.04	-0.68	3.64	-5.72	-0.80	-5.58	-0.66	-8.28	-3.50	-5.25
24	48.0520	10.716	0.01	-0.26	-0.26	-1.94	0.07	-1.94	0.07	-1.93	0.07	-2.66
25	27.7000	14.790	-0.02	-0.38	-0.64	-3.13	0.59	-3.13	0.59	-3.14	0.58	-4.70
26	15.9680	12.679	0.01	-0.07	-0.35	4.68	-0.57	4.68	-0.57	4.71	-0.54	4.02
27	9.87700	13.978	0.00	0.22	0.60	-0.58	-0.65	-0.58	-0.65	-0.58	-0.65	1.28

Table 9.56: Cross sections for Am-241 in a MOX pin with radius 0.4096 cm, pitch 1.26 cm, and 10% transuranic concentration.

			Error (%)									
Group	E_{max} (eV)	REF	2REG	UF-SD	UF-IR	EQ-SD	EQ-SD+	EQ-IR	EQ-IR+	SUBG	SUBG+	S-INT
15	9118.00	16.245	0.00	0.01	0.00	0.02	0.01	0.02	0.01	0.02	0.02	0.02
16	5530.00	17.429	0.00	-0.00	-0.04	0.01	0.00	0.01	0.00	0.02	0.01	0.06
17	3519.10	18.951	0.00	0.00	-0.00	0.01	0.00	0.01	0.00	0.01	0.00	0.01
18	2239.45	20.424	-0.00	0.00	0.03	0.00	-0.00	0.00	-0.00	0.00	0.00	-0.08
19	1425.10	22.575	0.00	0.00	-0.01	0.01	-0.00	0.01	-0.00	0.02	0.01	-0.16
20	906.899	27.392	-0.00	-0.00	0.06	0.03	-0.08	0.04	-0.08	0.07	-0.05	-0.03
21	367.263	36.500	0.00	0.02	0.11	0.06	-0.08	0.06	-0.08	0.08	-0.06	0.11
22	148.729	49.430	0.01	-0.05	-0.18	-0.51	0.12	-0.51	0.12	-0.50	0.14	-0.96
23	75.5014	59.316	0.24	0.14	-1.60	-0.53	0.46	-0.53	0.46	-0.51	0.48	-1.95
24	48.0520	54.117	-0.07	-0.13	0.91	11.70	-0.38	11.70	-0.38	11.55	-0.52	1.15
25	27.7000	73.945	-0.04	0.24	0.20	-6.28	0.32	-6.28	0.32	-6.31	0.29	-3.86
26	15.9680	87.103	0.01	-0.17	-1.12	12.32	-1.68	12.32	-1.68	11.64	-2.28	3.30
27	9.87700	130.648	0.02	1.09	3.26	-6.74	-0.58	-6.75	-0.60	-7.30	-1.18	-1.67

Table 9.57: Cross sections for Am-242 in a MOX pin with radius 0.4096 cm, pitch 1.26 cm, and 10% transuranic concentration.

			Error (%)									
Group	E_{max} (eV)	REF	2REG	UF-SD	UF-IR	EQ-SD	EQ-SD+	EQ-IR	EQ-IR+	SUBG	SUBG+	S-INT
15	9118.00	12.633	0.00	0.00	0.00	0.01	0.01	0.01	0.01	0.02	0.02	0.02
16	5530.00	13.094	0.00	-0.00	-0.01	0.00	-0.00	0.00	-0.00	0.01	0.01	0.01
17	3519.10	13.581	0.00	0.00	-0.00	0.00	0.00	0.00	0.00	0.01	0.01	0.01
18	2239.45	14.131	-0.00	0.00	0.01	0.00	0.00	0.00	0.00	0.01	0.01	0.01
19	1425.10	14.793	0.00	0.00	-0.01	0.01	-0.00	0.01	-0.00	0.13	0.12	0.14
20	906.899	16.099	-0.00	-0.00	0.03	0.02	-0.04	0.02	-0.04	0.02	-0.03	0.02
21	367.263	18.537	0.00	0.01	0.06	0.06	-0.05	0.06	-0.05	0.06	-0.05	-0.58
22	148.729	22.342	-0.00	0.02	0.25	-0.37	-0.03	-0.37	-0.03	-0.36	-0.02	0.67
23	75.5014	28.765	0.13	0.04	-0.60	0.70	-0.05	0.70	-0.05	0.71	-0.05	-0.43
24	48.0520	26.544	0.02	-0.81	2.77	5.36	-0.78	5.36	-0.78	5.36	-0.79	-3.17
25	27.7000	25.954	-0.00	0.03	0.58	4.24	-0.74	4.24	-0.74	4.20	-0.77	3.06
26	15.9680	33.818	-0.00	0.03	-0.47	-1.28	0.91	-1.29	0.90	-1.24	0.95	-1.29
27	9.87700	44.726	0.03	-1.52	-4.43	20.01	-1.39	19.99	-1.41	19.89	-1.49	-9.75

9.5 Lattice with Water Hole

Next, consider a small lattice consisting of UO_2 fuel pins in water. The lattice is 3 cells by 3 cells, with the central cell consisting only of water and the surrounding cells containing fuel pins. A visual depiction of this geometry is given in Fig. 9.6. Reflective boundary conditions are imposed. As in previous benchmarks, the water is H_2O with its density selected such that the potential scattering cross section to be $1.23\,\mathrm{cm}^{-1}$. The fuel is 3% enriched UO_2 with a number density of $0.022\,{}^{\mathrm{a}}/_{\mathrm{b-cm}}$. The pitch is $1.26\,\mathrm{cm}$, and the radius is varied, taking the values of $0.3\,\mathrm{cm}$, $0.4096\,\mathrm{cm}$, and $0.6\,\mathrm{cm}$. Due to the symmetry of the geometry, there are only two distinct values of the pin-averaged cross sections: one for corner pins and another for pins face-adjacent to the water hole.

Total cross sections are compared for a multitude of methods for both pin locations. Results are given in Tables 9.58 to 9.69. These results show only small differences in cross sections between the two pin locations, and the trends in the errors closely match that of the pin in a uniform lattice.

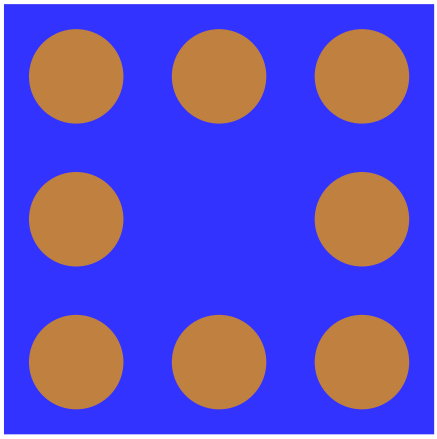

Figure 9.6: 3x3 lattice of UO_2 fuel pins with central water hole.

Table 9.58: U-238 cross sections in UO_2 lattice with water hole, corner pin with radius 0.3 cm.

			Error (%)								
Group	E_{max} (eV)	REF	2REG	UF-SD	UF-IR	EQ-SD	EQ-SD+	EQ-IR	EQ-IR+	SUBG	SUBG+
15	9118.00	15.042	-0.01	-0.01	-0.06	-0.20	-0.19	-0.22	-0.22	-0.01	-0.01
16	5530.00	15.582	-0.01	-0.01	-0.12	-0.18	-0.18	-0.28	-0.28	-0.09	-0.09
17	3519.10	17.338	0.00	-0.02	-0.20	-0.30	-0.29	-0.39	-0.38	-0.14	-0.13
18	2239.45	16.526	0.01	-0.00	-0.24	-0.30	-0.28	-0.42	-0.40	-0.20	-0.18
19	1425.10	16.657	0.00	-0.01	-0.27	-0.29	-0.26	-0.37	-0.35	-0.39	-0.37
20	906.899	14.604	0.01	0.02	-0.09	-0.15	-0.13	-0.21	-0.19	-0.09	-0.06
21	367.263	17.521	0.16	-0.23	-0.39	0.10	0.15	0.32	0.37	1.36	1.41
22	148.729	17.879	0.29	-0.24	-0.02	0.44	0.52	0.80	0.89	2.35	2.44
23	75.5014	15.818	0.29	-0.08	0.29	0.52	0.79	0.76	1.02	2.02	2.29
24	48.0520	23.524	1.08	-0.25	0.26	1.87	2.69	2.04	2.87	3.99	4.84
25	27.7000	19.653	0.66	-0.27	-0.84	1.48	1.94	0.08	0.54	-0.20	0.25
26	15.9680	9.118	-0.00	-0.01	-0.00	-0.01	-0.04	-0.01	-0.04	0.01	-0.02
27	9.87700	19.546	0.16	-0.22	0.28	1.40	1.33	0.42	0.36	-0.25	-0.31

Table 9.59: U-235 cross sections in UO_2 lattice with water hole, corner pin with radius 0.3 cm.

			Error (%)								
Group	E_{max} (eV)	REF	2REG	UF-SD	UF-IR	EQ-SD	EQ-SD+	EQ-IR	EQ-IR+	SUBG	SUBG+
15	9118.00	13.332	0.00	0.00	0.00	0.01	0.01	0.01	0.01	0.06	0.06
16	5530.00	13.345	0.00	-0.00	-0.01	0.00	0.00	0.00	0.00	0.01	0.01
17	3519.10	13.574	0.00	0.00	0.01	-0.01	0.00	-0.01	0.00	0.00	0.01
18	2239.45	15.032	0.00	0.00	-0.01	0.10	-0.01	0.10	-0.01	0.10	-0.01
19	1425.10	16.187	0.00	0.00	0.02	-0.03	-0.03	-0.03	-0.03	-0.02	-0.02
20	906.899	16.824	-0.00	0.01	0.02	-0.09	0.01	-0.09	0.01	-0.09	0.01
21	367.263	21.196	-0.03	-0.01	0.41	0.63	-0.23	0.63	-0.23	0.66	-0.20
22	148.729	24.434	-0.03	-0.02	0.22	-0.37	-0.10	-0.37	-0.10	-0.38	-0.11
23	75.5014	29.716	-0.05	-0.04	0.33	-0.60	-0.18	-0.60	-0.18	-0.67	-0.25
24	48.0520	39.201	-0.09	0.05	0.36	-2.49	-0.40	-2.49	-0.40	-2.49	-0.41
25	27.7000	40.921	0.01	-0.01	0.37	9.30	-0.59	9.31	-0.59	9.25	-0.64
26	15.9680	51.053	-0.00	-0.13	-0.30	-0.29	-0.32	-0.29	-0.32	-0.19	-0.22
27	9.87700	40.248	-0.00	-0.09	0.75	3.89	-0.58	3.81	-0.65	3.82	-0.64

Table 9.60: U-238 cross sections in UO_2 lattice with water hole, corner pin with radius 0.4096 cm.

			Error (%)								
Group	E_{max} (eV)	REF	2REG	UF-SD	UF-IR	EQ-SD	EQ-SD+	EQ-IR	EQ-IR+	SUBG	SUBG+
15	9118.00	14.715	-0.03	-0.03	-0.08	-0.18	-0.17	-0.21	-0.21	-0.04	-0.04
16	5530.00	15.188	-0.01	-0.02	-0.12	-0.16	-0.15	-0.24	-0.24	-0.17	-0.17
17	3519.10	16.528	-0.01	-0.02	-0.24	-0.26	-0.25	-0.41	-0.40	-0.28	-0.26
18	2239.45	15.526	-0.01	-0.01	-0.29	-0.29	-0.26	-0.45	-0.42	-0.30	-0.27
19	1425.10	15.694	-0.01	-0.02	-0.28	-0.30	-0.27	-0.43	-0.40	-0.36	-0.33
20	906.899	13.986	0.01	0.02	-0.09	-0.12	-0.09	-0.20	-0.17	-0.25	-0.22
21	367.263	16.512	0.10	-0.26	-0.51	-0.07	-0.01	0.04	0.11	0.00	0.07
22	148.729	16.776	0.21	-0.29	-0.31	0.16	0.28	0.42	0.55	0.39	0.51
23	75.5014	14.985	0.21	-0.09	0.28	0.19	0.57	0.42	0.80	0.43	0.81
24	48.0520	21.537	0.86	-0.42	-0.37	0.84	2.07	0.77	2.00	1.28	2.51
25	27.7000	17.816	0.51	-0.45	-1.74	0.48	1.26	-1.49	-0.73	-1.31	-0.54
26	15.9680	9.115	-0.00	-0.03	-0.00	-0.01	-0.07	-0.01	-0.07	0.01	-0.05
27	9.87700	17.684	0.12	-0.30	0.67	0.81	0.75	0.84	0.78	0.39	0.34

Table 9.61: U-235 cross sections in UO_2 lattice with water hole, corner pin with radius 0.4096 cm.

			Error (%)								
Group	E_{max} (eV)	REF	2REG	UF-SD	UF-IR	EQ-SD	EQ-SD+	EQ-IR	EQ-IR+	SUBG	SUBG+
15	9118.00	13.332	0.00	0.00	0.00	0.01	0.01	0.01	0.01	0.06	0.05
16	5530.00	13.345	0.00	-0.00	-0.01	0.00	0.00	0.00	0.00	0.01	0.01
17	3519.10	13.575	0.00	0.00	0.01	-0.01	0.00	-0.01	0.00	0.00	0.01
18	2239.45	15.026	0.00	0.01	-0.01	0.13	-0.01	0.13	-0.01	0.13	-0.01
19	1425.10	16.179	0.00	0.00	0.04	0.01	-0.04	0.01	-0.04	0.01	-0.03
20	906.899	16.819	-0.00	0.02	0.02	-0.10	0.01	-0.10	0.01	-0.09	0.02
21	367.263	21.142	-0.03	-0.01	0.51	0.73	-0.23	0.73	-0.23	0.77	-0.19
22	148.729	24.380	-0.03	-0.02	0.18	-0.41	-0.09	-0.41	-0.09	-0.41	-0.10
23	75.5014	29.680	-0.05	-0.05	0.29	-0.76	-0.20	-0.76	-0.20	-0.86	-0.30
24	48.0520	38.962	-0.08	0.11	0.29	-2.57	-0.49	-2.57	-0.48	-2.58	-0.50
25	27.7000	40.191	0.01	0.01	0.32	9.90	-0.60	9.91	-0.59	9.71	-0.77
26	15.9680	49.925	0.00	-0.25	-0.66	-0.37	-0.46	-0.36	-0.45	-0.35	-0.44
27	9.87700	39.124	-0.00	-0.19	0.61	5.45	-0.16	5.33	-0.27	5.30	-0.29

Table 9.62: U-238 cross sections in UO_2 lattice with water hole, corner pin with radius 0.6 cm.

			Error (%)								
Group	E_{max} (eV)	REF	2REG	UF-SD	UF-IR	EQ-SD	EQ-SD+	EQ-IR	EQ-IR+	SUBG	SUBG+
15	9118.00	14.025	-0.08	-0.09	-0.11	-0.19	-0.18	-0.20	-0.19	-0.07	-0.06
16	5530.00	14.430	-0.04	-0.07	-0.18	-0.17	-0.17	-0.26	-0.26	-0.27	-0.27
17	3519.10	15.100	-0.04	-0.05	-0.20	-0.24	-0.21	-0.37	-0.35	-0.23	-0.20
18	2239.45	13.883	-0.04	-0.04	-0.20	-0.32	-0.25	-0.47	-0.39	-0.39	-0.32
19	1425.10	14.154	-0.03	-0.05	-0.13	-0.29	-0.24	-0.41	-0.35	-0.34	-0.28
20	906.899	13.034	-0.01	0.01	0.02	-0.10	-0.06	-0.17	-0.12	-0.40	-0.35
21	367.263	15.014	0.01	-0.28	-0.25	-0.23	-0.12	-0.39	-0.28	-2.13	-2.02
22	148.729	15.185	0.07	-0.31	-0.16	-0.20	0.14	-0.16	0.19	-2.82	-2.48
23	75.5014	13.841	0.08	0.11	-0.68	-0.33	0.56	-0.22	0.67	-2.17	-1.30
24	48.0520	18.784	0.42	-0.66	-4.07	-1.49	1.45	-3.30	-0.41	-4.48	-1.63
25	27.7000	15.283	0.24	-0.69	-3.95	-1.20	0.88	-4.20	-2.18	-4.24	-2.23
26	15.9680	9.107	-0.00	-0.15	-0.03	-0.05	-0.22	-0.05	-0.22	-0.05	-0.21
27	9.87700	15.056	0.08	-0.29	0.37	0.77	1.05	0.75	1.02	1.89	2.17

Table 9.63: U-235 cross sections in UO_2 lattice with water hole, corner pin with radius 0.6 cm.

			Error (%)								
Group	E_{max} (eV)	REF	2REG	UF-SD	UF-IR	EQ-SD	EQ-SD+	EQ-IR	EQ-IR+	SUBG	SUBG+
15	9118.00	13.331	0.00	0.01	0.01	0.01	0.01	0.01	0.01	0.04	0.04
16	5530.00	13.345	0.00	-0.01	-0.01	0.00	-0.01	0.00	-0.01	0.01	-0.00
17	3519.10	13.575	0.00	0.00	0.03	-0.01	0.00	-0.01	0.00	-0.00	0.00
18	2239.45	15.014	-0.00	0.01	0.00	0.19	-0.00	0.19	-0.00	0.19	-0.01
19	1425.10	16.152	0.00	-0.01	0.10	0.13	-0.05	0.13	-0.05	0.12	-0.06
20	906.899	16.800	-0.00	0.04	0.02	-0.09	0.03	-0.09	0.03	-0.07	0.05
21	367.263	20.975	-0.02	-0.03	0.77	1.04	-0.22	1.04	-0.22	1.10	-0.16
22	148.729	24.213	-0.02	-0.02	-0.19	-0.53	-0.07	-0.53	-0.07	-0.54	-0.08
23	75.5014	29.542	-0.03	-0.20	-0.06	-1.19	-0.41	-1.20	-0.41	-1.45	-0.67
24	48.0520	37.914	-0.04	0.19	0.16	-2.07	-0.57	-2.05	-0.55	-2.09	-0.60
25	27.7000	38.245	0.01	-0.12	0.21	10.95	-0.90	10.98	-0.88	10.09	-1.67
26	15.9680	46.622	0.02	-0.69	-3.11	-0.63	-0.85	-0.63	-0.86	-1.07	-1.30
27	9.87700	36.776	0.01	-0.28	-1.06	7.30	1.04	7.03	0.79	6.72	0.50

Table 9.64: U-238 cross sections in UO_2 lattice with water hole, face-adjacent pin with radius 0.3 cm.

			Error (%)								
Group	E_{max} (eV)	REF	2REG	UF-SD	UF-IR	EQ-SD	EQ-SD+	EQ-IR	EQ-IR+	SUBG	SUBG+
15	9118.00	15.056	-0.01	-0.01	-0.05	-0.20	-0.20	-0.23	-0.22	-0.01	-0.00
16	5530.00	15.599	-0.00	-0.00	-0.12	-0.19	-0.19	-0.28	-0.28	-0.08	-0.08
17	3519.10	17.371	0.00	-0.02	-0.20	-0.30	-0.30	-0.40	-0.39	-0.14	-0.13
18	2239.45	16.568	0.01	-0.01	-0.25	-0.31	-0.29	-0.42	-0.41	-0.20	-0.18
19	1425.10	16.697	-0.00	-0.01	-0.28	-0.29	-0.27	-0.37	-0.35	-0.40	-0.38
20	906.899	14.629	0.01	0.02	-0.09	-0.15	-0.13	-0.21	-0.19	-0.09	-0.06
21	367.263	17.561	0.16	-0.23	-0.37	0.12	0.17	0.34	0.39	1.40	1.45
22	148.729	17.921	0.29	-0.24	0.01	0.47	0.55	0.84	0.92	2.41	2.50
23	75.5014	15.849	0.29	-0.08	0.32	0.56	0.82	0.80	1.06	2.08	2.34
24	48.0520	23.591	1.09	-0.23	0.31	1.96	2.78	2.13	2.95	4.12	4.95
25	27.7000	19.718	0.66	-0.26	-0.81	1.57	2.01	0.19	0.63	-0.15	0.29
26	15.9680	9.118	-0.00	-0.01	-0.00	-0.01	-0.04	-0.01	-0.04	0.01	-0.02
27	9.87700	19.615	0.15	-0.23	0.26	1.44	1.38	0.44	0.38	-0.28	-0.34

Table 9.65: U-235 cross sections in UO_2 lattice with water hole, face-adjacent pin with radius 0.3 cm.

			Error (%)								
Group	E_{max} (eV)	REF	2REG	UF-SD	UF-IR	EQ-SD	EQ-SD+	EQ-IR	EQ-IR+	SUBG	SUBG+
15	9118.00	13.332	0.00	0.00	0.00	0.01	0.01	0.01	0.01	0.06	0.06
16	5530.00	13.345	0.00	-0.00	-0.01	0.00	0.00	0.00	0.00	0.01	0.01
17	3519.10	13.574	0.00	0.00	0.01	-0.00	0.00	-0.00	0.00	0.00	0.01
18	2239.45	15.032	0.00	0.00	-0.01	0.10	-0.01	0.10	-0.01	0.10	-0.01
19	1425.10	16.187	0.00	0.00	0.02	-0.03	-0.03	-0.03	-0.03	-0.02	-0.02
20	906.899	16.825	-0.00	0.01	0.02	-0.09	0.01	-0.09	0.01	-0.09	0.01
21	367.263	21.199	-0.03	-0.02	0.40	0.62	-0.24	0.62	-0.24	0.65	-0.21
22	148.729	24.437	-0.03	-0.02	0.22	-0.37	-0.10	-0.37	-0.10	-0.38	-0.11
23	75.5014	29.719	-0.05	-0.04	0.32	-0.60	-0.18	-0.60	-0.18	-0.67	-0.25
24	48.0520	39.213	-0.09	0.05	0.35	-2.50	-0.41	-2.49	-0.41	-2.50	-0.41
25	27.7000	40.952	0.01	-0.02	0.36	9.27	-0.60	9.27	-0.60	9.23	-0.64
26	15.9680	51.099	-0.00	-0.13	-0.29	-0.30	-0.33	-0.30	-0.32	-0.18	-0.21
27	9.87700	40.295	-0.00	-0.09	0.74	3.81	-0.61	3.74	-0.68	3.76	-0.65

Table 9.66: U-238 cross sections in UO_2 lattice with water hole, face-adjacent pin with radius 0.4096 cm.

			Error (%)								
Group	E_{max} (eV)	REF	2REG	UF-SD	UF-IR	EQ-SD	EQ-SD+	EQ-IR	EQ-IR+	SUBG	SUBG+
15	9118.00	14.743	-0.02	-0.02	-0.07	-0.17	-0.17	-0.21	-0.21	-0.04	-0.03
16	5530.00	15.220	-0.01	-0.01	-0.11	-0.15	-0.15	-0.23	-0.23	-0.16	-0.16
17	3519.10	16.591	-0.00	-0.02	-0.24	-0.25	-0.24	-0.41	-0.40	-0.28	-0.27
18	2239.45	15.601	-0.01	-0.02	-0.29	-0.29	-0.26	-0.44	-0.42	-0.31	-0.28
19	1425.10	15.766	-0.02	-0.03	-0.30	-0.30	-0.28	-0.44	-0.41	-0.38	-0.35
20	906.899	14.031	0.00	0.02	-0.09	-0.12	-0.09	-0.19	-0.17	-0.26	-0.23
21	367.263	16.582	0.11	-0.26	-0.46	-0.05	0.01	0.07	0.14	0.08	0.14
22	148.729	16.850	0.22	-0.29	-0.22	0.20	0.32	0.47	0.59	0.51	0.63
23	75.5014	15.038	0.21	-0.10	0.35	0.23	0.60	0.46	0.84	0.54	0.91
24	48.0520	21.657	0.89	-0.39	-0.25	1.00	2.19	0.94	2.14	1.53	2.73
25	27.7000	17.931	0.52	-0.44	-1.68	0.59	1.35	-1.33	-0.59	-1.20	-0.46
26	15.9680	9.115	-0.00	-0.02	-0.00	-0.01	-0.06	-0.01	-0.06	0.01	-0.05
27	9.87700	17.808	0.12	-0.33	0.61	0.83	0.77	0.85	0.79	0.31	0.25

Table 9.67: U-235 cross sections in UO_2 lattice with water hole, face-adjacent pin with radius 0.4096 cm.

			Error (%)								
Group	E_{max} (eV)	REF	2REG	UF-SD	UF-IR	EQ-SD	EQ-SD+	EQ-IR	EQ-IR+	SUBG	SUBG+
15	9118.00	13.332	0.00	0.00	0.00	0.01	0.01	0.01	0.01	0.06	0.06
16	5530.00	13.345	0.00	-0.00	-0.01	0.00	0.00	0.00	0.00	0.01	0.01
17	3519.10	13.575	0.00	0.00	0.01	-0.01	0.00	-0.01	0.00	0.00	0.01
18	2239.45	15.027	0.00	0.01	-0.01	0.13	-0.01	0.13	-0.01	0.13	-0.01
19	1425.10	16.180	0.00	0.00	0.03	0.00	-0.04	0.00	-0.04	0.01	-0.03
20	906.899	16.820	-0.00	0.02	0.02	-0.10	0.01	-0.10	0.01	-0.09	0.02
21	367.263	21.148	-0.04	-0.02	0.49	0.72	-0.24	0.72	-0.24	0.76	-0.20
22	148.729	24.386	-0.03	-0.02	0.18	-0.41	-0.10	-0.41	-0.10	-0.41	-0.10
23	75.5014	29.686	-0.05	-0.05	0.28	-0.75	-0.21	-0.75	-0.21	-0.84	-0.30
24	48.0520	38.998	-0.08	0.10	0.27	-2.59	-0.50	-2.59	-0.50	-2.60	-0.51
25	27.7000	40.260	0.01	0.00	0.32	9.85	-0.61	9.85	-0.60	9.69	-0.75
26	15.9680	50.040	0.00	-0.24	-0.63	-0.38	-0.46	-0.37	-0.45	-0.33	-0.41
27	9.87700	39.226	-0.00	-0.20	0.60	5.31	-0.21	5.20	-0.32	5.19	-0.33

Table 9.68: U-238 cross sections in UO_2 lattice with water hole, face-adjacent pin with radius 0.6 cm.

			Error (%)								
Group	E_{max} (eV)	REF	2REG	UF-SD	UF-IR	EQ-SD	EQ-SD+	EQ-IR	EQ-IR+	SUBG	SUBG+
15	9118.00	14.110	-0.06	-0.06	-0.10	0.00	0.01	-0.01	-0.00	-0.05	-0.04
16	5530.00	14.525	-0.03	-0.05	-0.16	-0.00	0.00	-0.09	-0.09	-0.25	-0.25
17	3519.10	15.280	-0.03	-0.04	-0.20	-0.02	0.00	-0.15	-0.13	-0.25	-0.23
18	2239.45	14.092	-0.04	-0.03	-0.23	-0.10	-0.03	-0.24	-0.18	-0.44	-0.38
19	1425.10	14.350	-0.04	-0.05	-0.18	-0.12	-0.07	-0.23	-0.19	-0.40	-0.35
20	906.899	13.154	-0.01	0.01	0.00	-0.02	0.02	-0.12	-0.08	-0.40	-0.36
21	367.263	15.205	0.01	-0.24	-0.05	-0.10	0.00	-0.22	-0.11	-1.85	-1.75
22	148.729	15.389	0.08	-0.27	0.10	-0.06	0.22	0.04	0.32	-2.41	-2.13
23	75.5014	13.989	0.08	0.06	-0.50	-0.22	0.55	-0.22	0.55	-1.89	-1.14
24	48.0520	19.150	0.45	-0.61	-3.84	-1.02	1.50	-2.39	0.10	-3.83	-1.38
25	27.7000	15.632	0.24	-0.75	-3.94	-0.91	0.86	-3.77	-2.05	-4.07	-2.35
26	15.9680	9.107	-0.00	-0.12	-0.02	-0.02	-0.16	-0.02	-0.16	-0.03	-0.17
27	9.87700	15.442	0.04	-0.52	-0.11	0.66	0.83	0.60	0.76	1.33	1.50

Table 9.69: U-235 cross sections in UO_2 lattice with water hole, face-adjacent pin with radius 0.6 cm.

			Error (%)								
Group	E_{max} (eV)	REF	2REG	UF-SD	UF-IR	EQ-SD	EQ-SD+	EQ-IR	EQ-IR+	SUBG	SUBG+
15	9118.00	13.331	0.00	0.01	0.01	0.01	0.01	0.01	0.01	0.04	0.04
16	5530.00	13.345	0.00	-0.00	-0.01	0.00	-0.00	0.00	-0.00	0.01	0.00
17	3519.10	13.575	0.00	0.00	0.03	-0.01	0.00	-0.01	0.00	-0.00	0.01
18	2239.45	15.016	-0.00	0.01	-0.00	0.19	0.00	0.19	0.00	0.18	-0.00
19	1425.10	16.156	0.00	-0.00	0.09	0.11	-0.03	0.11	-0.03	0.10	-0.04
20	906.899	16.803	-0.00	0.04	0.02	-0.08	0.03	-0.08	0.03	-0.07	0.04
21	367.263	20.998	-0.03	-0.02	0.72	1.03	-0.18	1.03	-0.18	1.05	-0.15
22	148.729	24.238	-0.02	-0.03	-0.14	-0.47	-0.04	-0.47	-0.04	-0.54	-0.10
23	75.5014	29.560	-0.04	-0.16	-0.02	-1.07	-0.31	-1.07	-0.31	-1.36	-0.60
24	48.0520	38.084	-0.05	0.14	0.12	-2.08	-0.41	-2.05	-0.39	-2.23	-0.57
25	27.7000	38.535	-0.00	-0.11	0.17	11.05	-0.58	11.06	-0.57	9.97	-1.54
26	15.9680	47.098	-0.00	-0.68	-2.87	-0.24	-0.46	-0.24	-0.46	-1.04	-1.26
27	9.87700	37.157	-0.01	-0.45	-1.10	7.18	0.75	6.94	0.53	6.36	-0.02

Perhaps a more interesting quantity of interest is the capture cross section. Consider now a similar lattice with the enrichment reduced to 0%. Only a radius of $0.4096\,\text{cm}$ is included in this analysis. To allow the reader to more easily see the effect of the water hole, cross sections corresponding to three configurations are included in the same table: uniform lattice, corner pin, and face-adjacent pin. For this analysis, the Embedded Self-Shielding Method is included. For the uniform lattice, this implementation of ESSM reproduces the value of the two region ultrafine solution exactly. Results are given in Tables 9.70 to 9.72.

The capture cross sections for the lower energy groups, which contain large resonances, exhibit an increase of over 2% from the uniform lattice to the face-adjacent pin. This is caused by the effective dilution of the face-adjacent pin being higher; i.e., neutrons emerging from the water hole are less shielded than those from other directions. For these methods, the errors remain close to constant for each pin location. Also, the error induced by the self-shielding of the scatter source—most significantly in group 24—is seen much more clearly with capture cross sections than with the total cross section.

Table 9.70: Capture cross sections for U-238 in lattice with water hole.

					Error [%]					
		REF			2REG			ESSM		
Group	E_{max} (eV)	Uniform	Corner	Face	Uniform	Corner	Face	Uniform	Corner	Face
15	9118.00	0.700	0.701	0.703	0.01	0.04	0.04	0.01	0.07	0.09
16	5530.00	0.737	0.739	0.742	-0.00	0.05	0.05	-0.00	0.08	0.11
17	3519.10	0.952	0.955	0.961	0.01	0.06	0.05	0.01	-0.05	0.02
18	2239.45	0.846	0.851	0.858	0.02	0.03	0.02	0.02	-0.12	0.04
19	1425.10	1.216	1.223	1.234	0.02	0.03	0.02	0.02	-0.28	-0.10
20	906.899	1.363	1.373	1.388	0.04	0.05	0.04	0.04	-0.25	-0.01
21	367.263	1.568	1.580	1.598	0.48	0.51	0.51	0.48	-0.10	0.17
22	148.729	2.453	2.471	2.499	0.84	0.88	0.89	0.84	0.34	0.65
23	75.5014	2.124	2.140	2.164	1.17	1.23	1.25	1.17	0.93	1.26
24	48.0520	4.678	4.712	4.763	2.17	2.27	2.31	2.17	1.78	2.12
25	27.7000	6.339	6.392	6.477	1.06	1.13	1.14	1.06	0.52	0.92
26	15.9680	0.473	0.473	0.473	-0.00	-0.00	-0.00	-0.00	-0.06	-0.05
27	9.87700	8.102	8.170	8.289	0.22	0.26	0.24	0.22	-0.19	0.12

Table 9.71: Capture cross sections for U-238 in lattice with water hole.

					Error [%]					
		REF			UF-SD			UF-IR		
Group	E_{max} (eV)	Uniform	Corner	Face	Uniform	Corner	Face	Uniform	Corner	Face
15	9118.00	0.700	0.701	0.703	-0.02	0.02	0.01	-0.04	-0.01	-0.02
16	5530.00	0.737	0.739	0.742	0.02	0.08	0.07	-0.14	-0.07	-0.08
17	3519.10	0.952	0.955	0.961	-0.01	0.04	0.03	0.07	0.14	0.12
18	2239.45	0.846	0.851	0.858	0.06	0.07	0.06	0.13	0.16	0.14
19	1425.10	1.216	1.223	1.234	-0.07	-0.06	-0.08	-0.87	-0.85	-0.85
20	906.899	1.363	1.373	1.388	0.08	0.08	0.06	-0.89	-0.91	-0.90
21	367.263	1.568	1.580	1.598	-0.28	-0.27	-0.28	-1.67	-2.96	-2.71
22	148.729	2.453	2.471	2.499	-0.19	-0.16	-0.17	-3.92	-5.84	-5.53
23	75.5014	2.124	2.140	2.164	0.07	0.13	0.12	-2.91	-4.36	-4.03
24	48.0520	4.678	4.712	4.763	0.34	0.41	0.46	-2.47	-5.09	-4.85
25	27.7000	6.339	6.392	6.477	-0.20	-0.13	-0.13	-3.25	-3.49	-3.42
26	15.9680	0.473	0.473	0.473	-0.07	-0.07	-0.06	-0.15	-0.15	-0.14
27	9.87700	8.102	8.170	8.289	-0.18	-0.08	-0.15	3.60	3.77	3.54

Table 9.72: Capture cross sections for U-238 in lattice with water hole.

					Error [%]					
		REF			EQ-SD			EQ-IR		
Group	E_{max} (eV)	Uniform	Corner	Face	Uniform	Corner	Face	Uniform	Corner	Face
15	9118.00	0.700	0.701	0.703	-0.21	-0.19	-0.21	-0.22	-0.21	-0.22
16	5530.00	0.737	0.739	0.742	-0.29	-0.25	-0.26	-0.43	-0.39	-0.39
17	3519.10	0.952	0.955	0.961	-0.46	-0.42	-0.43	-0.29	-0.24	-0.26
18	2239.45	0.846	0.851	0.858	-0.44	-0.42	-0.43	-0.27	-0.25	-0.26
19	1425.10	1.216	1.223	1.234	-0.53	-0.52	-0.51	-1.31	-1.29	-1.28
20	906.899	1.363	1.373	1.388	-0.36	-0.33	-0.32	-1.43	-1.39	-1.35
21	367.263	1.568	1.580	1.598	0.76	0.80	0.89	-1.58	-1.44	-1.20
22	148.729	2.453	2.471	2.499	1.54	1.58	1.71	-4.00	-3.85	-3.56
23	75.5014	2.124	2.140	2.164	2.58	2.66	2.83	-2.95	-2.80	-2.52
24	48.0520	4.678	4.712	4.763	3.91	4.03	4.27	-1.96	-1.80	-0.75
25	27.7000	6.339	6.392	6.477	1.51	1.60	1.74	-2.91	-2.77	-2.54
26	15.9680	0.473	0.473	0.473	-0.15	-0.15	-0.14	-0.21	-0.20	-0.19
27	9.87700	8.102	8.170	8.289	1.20	1.27	1.27	3.88	3.93	3.89

9.6 UO_2-MOX Lattice

The final benchmark case considered in this study is a small lattice with alternating UO_2 and MOX pins. This is modeled as a 2 cell by 2 cell geometry with periodic boundary conditions. A visual depiction of the geometry is given in Fig. 9.7.

As with previous benchmarks, the moderator is H_2O with a density corresponding to a potential scatter cross section of $1.23\,\mathrm{cm}^{-1}$. The fuel has number density $0.022\,\mathrm{a/b\text{–}cm}$ and a transuranic concentration of 10%. The relative concentrations of the transuranic isotopes are given in Tab. 9.36. The uranium is enriched to 3%. The pitch is $1.26\,\mathrm{cm}$ and the radius is varied with values $0.3\,\mathrm{cm}$, $0.4096\,\mathrm{cm}$, and $0.6\,\mathrm{cm}$.

Results are shown for the four most prevalent nuclides in MOX: U-238, U-235, Pu-239, and Pu-240. The quantity of interest is the total cross section. Results are shown in Tables 9.73 to 9.90.

In this benchmark problem, not all resonant nuclides are present in all fuel regions. The uranium isotopes are present in each fuel pin, but the transuranics are only present in alternating fuel pins. This means in equivalence-based methods, the Dancoff factor is not the same for different nuclides in the MOX pin.

Also, mutual self-shielding effects can arise from the resonances of uranium isotopes affecting the reaction rate of the transuranics in a different pin. This spatial mutual self-shielding effect cannot be modeled by resonance interference factors. This effect is fairly small for most cases, but can be seen clearly in the cross sections for Pu-240 with radius $0.6\,\mathrm{cm}$ (Tab. 9.90). In group 25, where a significant resonance overlap with U-238 occurs, errors greater than 10% persist even after using resonance interference factors. Ultrafine with simplified scattering using a slowing down source is able to model this effect without any correction factors.

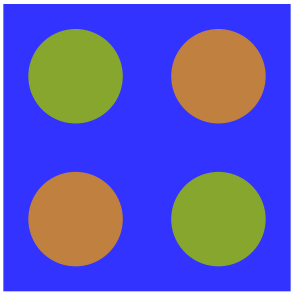

Figure 9.7: 2x2 lattice with alternating UO_2 and MOX fuel pins.

Table 9.73: Cross sections for U-238 in a UO_2 pin in a UO_2-MOX lattice with radius 0.3 cm, pitch 1.26 cm, and 10% transuranic concentration.

			Error (%)						
Group	E_{max} (eV)	REF	2REG	UF-SD	UF-IR	EQ-SD	EQ-SD+	EQ-IR	EQ-IR+
15	9118.00	15.038	-0.01	-0.01	-0.05	-0.23	-0.35	-0.26	-0.37
16	5530.00	15.576	-0.00	-0.00	-0.12	-0.22	-0.36	-0.32	-0.45
17	3519.10	17.324	0.01	-0.01	-0.19	-0.37	-0.60	-0.46	-0.70
18	2239.45	16.507	0.01	-0.00	-0.28	-0.38	-0.69	-0.50	-0.80
19	1425.10	16.638	0.00	-0.01	-0.28	-0.36	-0.65	-0.44	-0.74
20	906.899	14.592	0.01	0.02	-0.09	-0.21	-0.41	-0.27	-0.47
21	367.263	17.502	0.16	-0.23	-0.35	0.02	-0.20	0.23	0.01
22	148.729	17.857	0.29	-0.24	-0.09	0.35	0.17	0.71	0.53
23	75.5014	15.779	0.27	-0.02	0.29	0.59	0.64	0.83	0.88
24	48.0520	23.473	1.06	-0.25	0.60	1.78	2.40	1.96	2.57
25	27.7000	19.622	0.64	-0.32	-0.77	1.31	1.55	-0.11	0.13
26	15.9680	9.117	-0.00	-0.00	0.01	-0.01	-0.04	-0.01	-0.04
27	9.87700	19.516	0.15	-0.26	0.26	1.23	1.02	0.27	0.07

Table 9.74: Cross sections for U-235 in a UO_2 pin in a UO_2-MOX lattice with radius 0.3 cm, pitch 1.26 cm, and 10% transuranic concentration.

			Error (%)						
Group	E_{max} (eV)	REF	2REG	UF-SD	UF-IR	EQ-SD	EQ-SD+	EQ-IR	EQ-IR+
15	9118.00	13.332	0.00	0.00	0.00	0.01	0.01	0.01	0.01
16	5530.00	13.345	0.00	-0.00	-0.01	0.00	0.00	0.00	0.00
17	3519.10	13.574	0.00	0.00	0.01	-0.00	0.00	-0.00	0.00
18	2239.45	15.032	0.00	0.00	-0.01	0.10	-0.01	0.10	-0.01
19	1425.10	16.187	0.00	0.00	0.02	-0.02	-0.03	-0.02	-0.03
20	906.899	16.824	-0.00	0.01	0.02	-0.09	0.01	-0.09	0.01
21	367.263	21.195	-0.03	-0.01	0.42	0.63	-0.24	0.63	-0.24
22	148.729	24.432	-0.03	-0.02	0.21	-0.37	-0.10	-0.37	-0.10
23	75.5014	29.729	-0.05	-0.02	0.38	-0.65	-0.23	-0.65	-0.23
24	48.0520	39.203	-0.09	0.06	0.42	-2.51	-0.43	-2.51	-0.43
25	27.7000	40.958	0.01	-0.01	0.39	9.17	-0.74	9.17	-0.74
26	15.9680	51.103	-0.00	-0.12	-0.24	-0.46	-0.51	-0.45	-0.50
27	9.87700	40.285	-0.00	-0.14	0.70	3.75	-0.75	3.67	-0.83

Table 9.75: Cross sections for U-238 in a UO_2 pin in a UO_2-MOX lattice with radius 0.4096 cm, pitch 1.26 cm, and 10% transuranic concentration.

			Error (%)						
Group	E_{max} (eV)	REF	2REG	UF-SD	UF-IR	EQ-SD	EQ-SD+	EQ-IR	EQ-IR+
15	9118.00	14.706	-0.02	-0.02	-0.08	-0.23	-0.41	-0.25	-0.43
16	5530.00	15.177	-0.01	-0.01	-0.12	-0.21	-0.41	-0.28	-0.47
17	3519.10	16.504	-0.00	-0.02	-0.26	-0.34	-0.68	-0.46	-0.80
18	2239.45	15.497	-0.01	-0.02	-0.32	-0.39	-0.81	-0.51	-0.92
19	1425.10	15.667	-0.02	-0.03	-0.32	-0.38	-0.78	-0.48	-0.88
20	906.899	13.970	0.00	0.02	-0.11	-0.18	-0.45	-0.26	-0.53
21	367.263	16.490	0.09	-0.28	-0.41	-0.16	-0.43	-0.02	-0.29
22	148.729	16.742	0.20	-0.29	-0.01	0.16	-0.04	0.43	0.22
23	75.5014	14.929	0.18	0.00	0.19	0.38	0.51	0.60	0.73
24	48.0520	21.445	0.83	-0.41	0.11	1.07	2.05	0.97	1.95
25	27.7000	17.782	0.47	-0.54	-1.76	0.54	1.07	-1.53	-1.01
26	15.9680	9.114	-0.00	-0.01	0.03	-0.00	-0.06	-0.00	-0.06
27	9.87700	17.653	0.10	-0.38	0.69	1.02	0.78	0.73	0.49

Table 9.76: Cross sections for U-235 in a UO_2 pin in a UO_2-MOX lattice with radius 0.4096 cm, pitch 1.26 cm, and 10% transuranic concentration.

			Error (%)						
Group	E_{max} (eV)	REF	2REG	UF-SD	UF-IR	EQ-SD	EQ-SD+	EQ-IR	EQ-IR+
15	9118.00	13.332	0.00	0.00	0.00	0.01	0.01	0.01	0.01
16	5530.00	13.345	0.00	-0.00	-0.01	0.00	0.00	0.00	0.00
17	3519.10	13.575	0.00	0.00	0.01	-0.01	0.00	-0.01	0.00
18	2239.45	15.026	0.00	0.01	-0.01	0.13	-0.01	0.13	-0.01
19	1425.10	16.179	0.00	0.00	0.04	0.01	-0.04	0.01	-0.04
20	906.899	16.819	-0.00	0.02	0.02	-0.10	0.01	-0.10	0.01
21	367.263	21.140	-0.03	-0.00	0.54	0.73	-0.25	0.73	-0.25
22	148.729	24.374	-0.03	-0.01	0.17	-0.40	-0.08	-0.40	-0.08
23	75.5014	29.707	-0.05	-0.03	0.42	-0.86	-0.31	-0.86	-0.31
24	48.0520	38.969	-0.08	0.12	0.34	-2.63	-0.56	-2.63	-0.56
25	27.7000	40.282	0.01	0.01	0.37	9.56	-0.95	9.57	-0.94
26	15.9680	50.030	0.00	-0.21	-0.49	-0.72	-0.86	-0.71	-0.85
27	9.87700	39.215	-0.00	-0.30	0.55	5.11	-0.54	4.99	-0.66

Table 9.77: Cross sections for U-238 in a UO_2 pin in a UO_2-MOX lattice with radius 0.6 cm, pitch 1.26 cm, and 10% transuranic concentration.

			Error (%)						
Group	E_{max} (eV)	REF	2REG	UF-SD	UF-IR	EQ-SD	EQ-SD+	EQ-IR	EQ-IR+
15	9118.00	13.998	-0.07	-0.07	-0.10	-0.24	-0.23	-0.25	-0.24
16	5530.00	14.403	-0.03	-0.06	-0.15	-0.23	-0.23	-0.32	-0.31
17	3519.10	15.056	-0.03	-0.03	-0.18	-0.36	-0.34	-0.50	-0.47
18	2239.45	13.840	-0.03	-0.02	-0.20	-0.52	-0.44	-0.66	-0.59
19	1425.10	14.112	-0.03	-0.02	-0.13	-0.46	-0.40	-0.57	-0.52
20	906.899	13.014	-0.01	0.04	0.01	-0.25	-0.20	-0.31	-0.27
21	367.263	15.006	0.01	-0.19	0.09	-0.59	-0.47	-0.76	-0.64
22	148.729	15.123	0.04	0.01	0.20	-0.22	0.14	-0.20	0.16
23	75.5014	13.781	0.02	0.45	-0.95	-0.24	0.69	-0.17	0.76
24	48.0520	18.601	0.31	-0.02	-3.89	-1.22	1.87	-3.17	-0.14
25	27.7000	15.332	0.17	-0.80	-4.12	-2.24	-0.08	-5.26	-3.16
26	15.9680	9.101	-0.00	-0.11	0.13	0.01	-0.17	0.01	-0.17
27	9.87700	15.103	0.03	-0.58	0.03	-0.26	0.05	-0.27	0.04

Table 9.78: Cross sections for U-235 in a UO_2 pin in a UO_2-MOX lattice with radius 0.6 cm, pitch 1.26 cm, and 10% transuranic concentration.

			Error (%)						
Group	E_{max} (eV)	REF	2REG	UF-SD	UF-IR	EQ-SD	EQ-SD+	EQ-IR	EQ-IR+
15	9118.00	13.331	0.00	0.01	0.01	0.01	0.01	0.01	0.01
16	5530.00	13.345	0.00	-0.01	-0.01	0.00	-0.01	0.00	-0.01
17	3519.10	13.574	0.00	0.00	0.03	-0.01	0.00	-0.01	0.00
18	2239.45	15.014	-0.00	0.01	0.00	0.19	-0.00	0.19	-0.00
19	1425.10	16.149	0.00	-0.00	0.11	0.14	-0.04	0.14	-0.04
20	906.899	16.798	-0.00	0.04	0.02	-0.08	0.04	-0.08	0.04
21	367.263	20.961	-0.02	0.02	0.92	1.08	-0.21	1.08	-0.21
22	148.729	24.177	-0.02	0.00	-0.22	-0.43	0.04	-0.43	0.04
23	75.5014	29.605	-0.03	-0.16	0.53	-1.46	-0.68	-1.46	-0.68
24	48.0520	37.896	-0.03	0.05	0.27	-2.16	-0.72	-2.14	-0.70
25	27.7000	38.564	0.01	-0.27	0.42	9.75	-2.05	9.78	-2.03
26	15.9680	46.844	-0.00	-0.60	-2.25	-1.53	-1.75	-1.54	-1.76
27	9.87700	37.214	-0.00	-0.66	-1.67	5.73	-0.36	5.46	-0.61

Table 9.79: Cross sections for U-238 in a MOX pin in a UO_2-MOX lattice with radius 0.3 cm, pitch 1.26 cm, and 10% transuranic concentration.

			Error (%)						
Group	E_{max} (eV)	REF	2REG	UF-SD	UF-IR	EQ-SD	EQ-SD+	EQ-IR	EQ-IR+
15	9118.00	15.109	-0.01	-0.01	-0.05	-0.16	-0.45	-0.19	-0.47
16	5530.00	15.670	-0.00	-0.00	-0.11	-0.17	-0.50	-0.26	-0.59
17	3519.10	17.539	0.01	-0.01	-0.18	-0.31	-0.88	-0.44	-1.01
18	2239.45	16.792	0.01	-0.00	-0.24	-0.33	-1.09	-0.44	-1.20
19	1425.10	16.928	0.00	-0.01	-0.27	-0.35	-1.07	-0.43	-1.15
20	906.899	14.783	0.01	0.01	-0.07	-0.25	-0.70	-0.31	-0.76
21	367.263	17.849	0.16	-0.27	0.11	-0.12	-0.43	0.08	-0.23
22	148.729	18.272	0.30	-0.37	0.15	0.03	-0.08	0.37	0.25
23	75.5014	16.046	0.40	-0.40	-1.67	0.68	0.25	0.91	0.47
24	48.0520	24.081	1.13	-0.57	1.32	1.93	2.16	2.07	2.29
25	27.7000	20.233	0.67	-0.38	-0.12	1.23	1.91	0.03	0.70
26	15.9680	9.124	0.00	-0.02	0.03	-0.08	-0.10	-0.08	-0.10
27	9.87700	20.184	0.16	-0.28	0.44	0.71	1.42	-0.40	0.30

Table 9.80: Cross sections for U-235 in a MOX pin in a UO_2-MOX lattice with radius 0.3 cm, pitch 1.26 cm, and 10% transuranic concentration.

			Error (%)						
Group	E_{max} (eV)	REF	2REG	UF-SD	UF-IR	EQ-SD	EQ-SD+	EQ-IR	EQ-IR+
15	9118.00	13.332	0.00	0.00	0.00	0.01	0.01	0.01	0.01
16	5530.00	13.345	0.00	-0.00	-0.01	0.00	0.00	0.00	0.00
17	3519.10	13.574	0.00	0.00	0.01	-0.00	0.00	-0.00	0.00
18	2239.45	15.034	0.00	0.00	-0.01	0.09	-0.01	0.09	-0.01
19	1425.10	16.188	0.00	0.00	0.02	-0.03	-0.03	-0.03	-0.03
20	906.899	16.824	-0.00	0.01	0.02	-0.08	0.00	-0.08	0.00
21	367.263	21.213	-0.03	-0.00	0.47	0.58	-0.25	0.58	-0.25
22	148.729	24.434	-0.03	-0.04	0.12	-0.32	-0.16	-0.32	-0.16
23	75.5014	29.910	-0.05	-0.02	0.67	-1.19	-0.12	-1.20	-0.13
24	48.0520	39.265	-0.10	0.14	0.64	-2.53	-0.47	-2.53	-0.47
25	27.7000	41.568	0.01	0.02	0.50	7.84	-0.21	7.85	-0.21
26	15.9680	51.942	0.00	-0.19	-0.01	-1.59	-0.03	-1.59	-0.02
27	9.87700	40.786	0.00	-0.08	0.68	2.75	-0.07	2.68	-0.13

Table 9.81: Cross sections for Pu-239 in a MOX pin in a UO_2-MOX lattice with radius 0.3 cm, pitch 1.26 cm, and 10% transuranic concentration.

			Error (%)						
Group	E_{max} (eV)	REF	2REG	UF-SD	UF-IR	EQ-SD	EQ-SD+	EQ-IR	EQ-IR+
15	9118.00	14.676	0.00	0.01	0.00	0.02	0.02	0.02	0.02
16	5530.00	15.598	-0.00	-0.00	-0.01	0.02	-0.00	0.02	-0.00
17	3519.10	16.319	-0.00	0.00	0.01	-0.12	0.01	-0.12	0.01
18	2239.45	16.886	0.00	0.00	-0.10	-0.06	-0.02	-0.06	-0.02
19	1425.10	17.821	0.01	0.01	-0.11	0.44	-0.04	0.44	-0.04
20	906.899	20.258	0.02	-0.04	-0.46	-1.19	0.03	-1.20	0.02
21	367.263	29.133	-0.02	-0.06	-0.39	-1.35	-0.38	-1.36	-0.39
22	148.729	34.651	-0.09	-0.13	-0.09	0.22	-1.26	0.21	-1.26
23	75.5014	52.354	0.07	0.03	-3.21	1.04	-0.46	1.06	-0.44
24	48.0520	32.490	-0.11	-0.51	-3.39	-1.44	-0.50	-1.42	-0.47
25	27.7000	45.945	-0.04	-0.17	-0.43	-5.76	-0.59	-5.75	-0.57
26	15.9680	85.210	0.01	-0.24	-0.91	-0.19	-1.19	-0.25	-1.25
27	9.87700	29.356	-0.04	-1.03	-2.75	-8.11	2.50	-8.27	2.33

Table 9.82: Cross sections for Pu-240 in a MOX pin in a UO_2-MOX lattice with radius 0.3 cm, pitch 1.26 cm, and 10% transuranic concentration.

			Error (%)						
Group	E_{max} (eV)	REF	2REG	UF-SD	UF-IR	EQ-SD	EQ-SD+	EQ-IR	EQ-IR+
15	9118.00	16.349	0.00	0.01	0.01	-0.07	0.05	-0.07	0.05
16	5530.00	15.060	-0.00	0.01	0.09	-0.46	0.02	-0.46	0.02
17	3519.10	17.142	0.00	-0.01	-0.22	-0.75	0.08	-0.75	0.08
18	2239.45	18.318	0.04	-0.02	-1.12	-1.40	0.25	-1.40	0.25
19	1425.10	22.630	-0.01	0.02	0.52	0.65	-0.36	0.65	-0.37
20	906.899	21.790	0.01	-0.07	-0.75	-1.47	-0.45	-1.50	-0.48
21	367.263	31.109	0.04	-0.03	-1.36	-4.54	-0.37	-4.56	-0.39
22	148.729	49.187	-0.10	-0.42	-2.08	-0.17	-2.09	-0.18	-2.09
23	75.5014	88.339	0.07	-0.74	-5.41	10.38	-0.28	10.68	-0.02
24	48.0520	109.012	-0.08	-1.27	-7.76	-3.78	-1.09	-3.57	-0.87
25	27.7000	37.535	1.74	1.23	-7.08	14.31	-0.63	14.33	-0.60
26	15.9680	7.880	0.00	-0.01	0.02	0.01	-0.08	0.01	-0.08
27	9.87700	10.827	0.00	0.11	0.37	-0.36	-0.56	-0.36	-0.56

Table 9.83: Cross sections for U-238 in a MOX pin in a UO_2-MOX lattice with radius 0.4096 cm, pitch 1.26 cm, and 10% transuranic concentration.

			Error (%)						
Group	E_{max} (eV)	REF	2REG	UF-SD	UF-IR	EQ-SD	EQ-SD+	EQ-IR	EQ-IR+
15	9118.00	14.783	-0.02	-0.02	-0.01	-0.11	-0.56	-0.13	-0.58
16	5530.00	15.273	-0.01	-0.01	-0.03	-0.10	-0.60	-0.17	-0.66
17	3519.10	16.710	-0.00	-0.02	-0.07	-0.22	-1.05	-0.33	-1.16
18	2239.45	15.754	-0.01	-0.02	-0.01	-0.26	-1.31	-0.37	-1.42
19	1425.10	15.923	-0.02	-0.04	-0.06	-0.31	-1.29	-0.41	-1.39
20	906.899	14.139	0.00	0.00	0.10	-0.18	-0.80	-0.26	-0.88
21	367.263	16.782	0.10	-0.33	0.49	-0.27	-0.63	-0.15	-0.51
22	148.729	17.076	0.22	-0.52	0.76	-0.06	-0.41	0.15	-0.19
23	75.5014	15.065	0.31	-0.37	-1.07	0.97	0.13	1.15	0.31
24	48.0520	21.864	0.92	-0.93	1.68	1.59	1.64	1.48	1.52
25	27.7000	18.258	0.50	-0.65	-1.03	0.55	1.61	-1.34	-0.30
26	15.9680	9.123	0.00	-0.04	0.06	-0.09	-0.16	-0.09	-0.16
27	9.87700	18.184	0.12	-0.42	1.02	0.54	1.35	0.12	0.93

Table 9.84: Cross sections for U-235 in a MOX pin in a UO_2-MOX lattice with radius 0.4096 cm, pitch 1.26 cm, and 10% transuranic concentration.

			Error (%)						
Group	E_{max} (eV)	REF	2REG	UF-SD	UF-IR	EQ-SD	EQ-SD+	EQ-IR	EQ-IR+
15	9118.00	13.332	0.00	0.00	0.00	0.01	0.01	0.01	0.01
16	5530.00	13.345	0.00	-0.00	-0.01	0.00	-0.00	0.00	-0.00
17	3519.10	13.574	0.00	0.00	0.01	-0.01	0.00	-0.01	0.00
18	2239.45	15.028	0.00	0.01	-0.01	0.12	-0.01	0.12	-0.01
19	1425.10	16.180	0.00	0.00	0.04	0.01	-0.04	0.01	-0.04
20	906.899	16.819	-0.00	0.02	0.03	-0.08	-0.00	-0.08	-0.00
21	367.263	21.161	-0.03	0.00	0.61	0.68	-0.27	0.68	-0.27
22	148.729	24.372	-0.03	-0.05	0.08	-0.31	-0.20	-0.31	-0.20
23	75.5014	29.923	-0.06	-0.03	0.76	-1.49	-0.17	-1.50	-0.17
24	48.0520	39.061	-0.09	0.24	0.59	-2.65	-0.58	-2.65	-0.58
25	27.7000	40.994	0.00	0.07	0.51	8.07	-0.13	8.07	-0.13
26	15.9680	51.023	0.01	-0.36	-0.12	-1.99	-0.21	-1.98	-0.20
27	9.87700	39.797	0.00	-0.18	0.57	3.98	0.51	3.87	0.41

Table 9.85: Cross sections for Pu-239 in a MOX pin in a UO_2-MOX lattice with radius 0.4096 cm, pitch 1.26 cm, and 10% transuranic concentration.

			Error (%)						
Group	E_{max} (eV)	REF	2REG	UF-SD	UF-IR	EQ-SD	EQ-SD+	EQ-IR	EQ-IR+
15	9118.00	14.676	0.00	0.01	0.01	0.02	0.02	0.02	0.02
16	5530.00	15.597	-0.00	-0.00	-0.01	0.02	-0.00	0.02	-0.00
17	3519.10	16.321	-0.00	0.00	0.01	-0.16	-0.01	-0.16	-0.01
18	2239.45	16.868	0.00	0.00	-0.13	-0.04	-0.04	-0.04	-0.04
19	1425.10	17.790	0.01	0.00	-0.14	0.44	-0.09	0.44	-0.09
20	906.899	20.229	0.02	-0.04	-0.52	-1.46	-0.13	-1.47	-0.13
21	367.263	28.778	-0.01	-0.08	-0.61	-1.54	-0.58	-1.56	-0.59
22	148.729	33.795	-0.09	-0.19	-0.39	0.17	-1.58	0.16	-1.59
23	75.5014	50.416	0.07	0.03	-4.24	0.46	-0.93	0.49	-0.91
24	48.0520	31.158	-0.07	-0.68	-5.12	-2.36	-0.93	-2.33	-0.90
25	27.7000	45.010	-0.03	-0.27	-0.66	-6.83	-1.22	-6.81	-1.19
26	15.9680	81.762	0.01	-0.38	-1.41	-0.49	-1.73	-0.61	-1.85
27	9.87700	29.044	-0.02	-1.69	-4.18	-10.63	1.70	-10.84	1.46

Table 9.86: Cross sections for Pu-240 in a MOX pin in a UO_2-MOX lattice with radius 0.4096 cm, pitch 1.26 cm, and 10% transuranic concentration.

			Error (%)						
Group	E_{max} (eV)	REF	2REG	UF-SD	UF-IR	EQ-SD	EQ-SD+	EQ-IR	EQ-IR+
15	9118.00	16.352	0.00	0.02	0.02	-0.11	0.03	-0.11	0.03
16	5530.00	15.063	-0.00	0.01	0.11	-0.61	-0.04	-0.61	-0.04
17	3519.10	17.145	0.01	-0.01	-0.28	-1.06	-0.06	-1.06	-0.06
18	2239.45	18.332	0.04	-0.01	-1.38	-1.93	0.03	-1.93	0.02
19	1425.10	22.447	-0.01	0.02	0.65	0.61	-0.56	0.60	-0.57
20	906.899	21.523	0.01	-0.07	-0.87	-1.72	-0.78	-1.77	-0.83
21	367.263	30.591	0.06	-0.00	-1.89	-5.62	-1.01	-5.66	-1.04
22	148.729	46.453	-0.09	-0.64	-2.91	-0.21	-2.61	-0.23	-2.63
23	75.5014	78.175	0.11	-0.83	-6.78	10.93	0.18	11.20	0.43
24	48.0520	97.880	-0.00	-1.83	-10.75	-5.50	-1.68	-5.28	-1.45
25	27.7000	32.423	1.68	1.35	-6.94	22.67	1.02	22.70	1.05
26	15.9680	7.879	0.00	-0.03	0.03	0.02	-0.11	0.02	-0.11
27	9.87700	10.818	0.00	0.19	0.60	-0.28	-0.62	-0.28	-0.62

Table 9.87: Cross sections for U-238 in a MOX pin in a UO_2-MOX lattice with radius 0.6 cm, pitch 1.26 cm, and 10% transuranic concentration.

			Error (%)						
Group	E_{max} (eV)	REF	2REG	UF-SD	UF-IR	EQ-SD	EQ-SD+	EQ-IR	EQ-IR+
15	9118.00	14.070	-0.07	-0.07	-0.09	0.07	0.15	0.05	0.14
16	5530.00	14.486	-0.03	-0.07	-0.14	0.04	0.12	-0.05	0.03
17	3519.10	15.221	-0.03	-0.04	-0.16	-0.00	0.24	-0.14	0.11
18	2239.45	14.031	-0.03	-0.03	-0.14	-0.11	0.30	-0.26	0.15
19	1425.10	14.299	-0.02	-0.06	-0.12	-0.15	0.19	-0.26	0.08
20	906.899	13.135	-0.01	-0.02	0.07	-0.11	0.21	-0.18	0.15
21	367.263	15.203	0.01	-0.41	0.75	-0.55	0.39	-0.76	0.18
22	148.729	15.310	0.09	-0.78	0.65	-0.07	0.18	-0.10	0.14
23	75.5014	13.797	0.14	-0.20	-2.21	0.72	0.70	0.55	0.54
24	48.0520	18.709	0.45	-1.59	-2.90	0.14	0.90	-1.44	-0.69
25	27.7000	15.600	0.19	-1.27	-3.07	-1.95	1.24	-4.85	-1.75
26	15.9680	9.110	-0.00	-0.22	0.16	-0.07	-0.46	-0.07	-0.46
27	9.87700	15.405	0.07	-0.84	0.86	-0.40	1.09	-0.40	1.09

Table 9.88: Cross sections for U-235 in a MOX pin in a UO_2-MOX lattice with radius 0.6 cm, pitch 1.26 cm, and 10% transuranic concentration.

			Error (%)						
Group	E_{max} (eV)	REF	2REG	UF-SD	UF-IR	EQ-SD	EQ-SD+	EQ-IR	EQ-IR+
15	9118.00	13.331	0.00	0.01	0.01	0.01	0.01	0.01	0.01
16	5530.00	13.345	0.00	-0.01	-0.01	0.00	-0.01	0.00	-0.01
17	3519.10	13.574	0.00	0.00	0.03	-0.00	-0.00	-0.00	-0.00
18	2239.45	15.016	0.00	0.01	0.00	0.18	0.01	0.18	0.01
19	1425.10	16.151	0.00	-0.01	0.11	0.14	-0.04	0.14	-0.04
20	906.899	16.798	-0.00	0.04	0.03	-0.06	0.03	-0.06	0.03
21	367.263	20.983	-0.02	0.00	1.02	1.07	-0.20	1.07	-0.20
22	148.729	24.166	-0.01	-0.08	-0.29	-0.23	-0.15	-0.23	-0.15
23	75.5014	29.846	-0.04	-0.24	0.90	-2.09	-0.36	-2.09	-0.37
24	48.0520	37.997	-0.05	0.29	0.55	-2.01	-0.36	-2.00	-0.34
25	27.7000	39.318	-0.00	-0.13	0.65	8.42	0.28	8.45	0.30
26	15.9680	47.860	0.02	-1.15	-1.61	-2.44	-0.12	-2.44	-0.13
27	9.87700	37.802	0.01	-0.36	-1.44	4.87	2.50	4.63	2.26

Table 9.89: Cross sections for Pu-239 in a MOX pin in a UO_2-MOX lattice with radius 0.6 cm, pitch 1.26 cm, and 10% transuranic concentration.

			Error (%)						
Group	E_{max} (eV)	REF	2REG	UF-SD	UF-IR	EQ-SD	EQ-SD+	EQ-IR	EQ-IR+
15	9118.00	14.673	0.00	0.02	0.03	0.04	0.03	0.04	0.03
16	5530.00	15.595	-0.00	-0.01	-0.02	0.04	0.00	0.04	0.00
17	3519.10	16.320	-0.00	-0.01	0.02	-0.21	-0.02	-0.21	-0.02
18	2239.45	16.811	0.00	0.01	-0.19	0.06	0.02	0.06	0.02
19	1425.10	17.706	0.00	-0.02	-0.18	0.47	-0.10	0.47	-0.10
20	906.899	20.139	0.02	-0.07	-0.68	-2.06	-0.43	-2.07	-0.45
21	367.263	27.963	-0.01	-0.14	-1.78	-1.99	-0.45	-2.03	-0.49
22	148.729	31.981	-0.05	-0.35	-2.10	-0.13	-1.29	-0.17	-1.33
23	75.5014	46.407	0.08	0.28	-8.10	-0.65	-0.43	-0.58	-0.36
24	48.0520	29.229	0.03	-0.38	-11.67	-6.79	-1.69	-6.77	-1.68
25	27.7000	42.626	0.01	-0.45	-1.62	-8.98	-1.68	-9.03	-1.74
26	15.9680	74.117	0.04	-0.55	-3.90	-1.17	-1.70	-1.44	-1.97
27	9.87700	28.847	0.01	-3.09	-9.43	-18.07	-1.53	-18.40	-1.92

Table 9.90: Cross sections for Pu-240 in a MOX pin in a UO_2-MOX lattice with radius 0.6 cm, pitch 1.26 cm, and 10% transuranic concentration.

			Error (%)						
Group	E_{max} (eV)	REF	2REG	UF-SD	UF-IR	EQ-SD	EQ-SD+	EQ-IR	EQ-IR+
15	9118.00	16.357	0.00	0.03	0.07	-0.18	0.01	-0.18	0.01
16	5530.00	15.067	-0.00	0.03	0.14	-0.99	-0.14	-0.99	-0.14
17	3519.10	17.142	0.00	-0.04	-0.36	-1.79	-0.36	-1.80	-0.36
18	2239.45	18.420	0.03	0.02	-2.02	-3.54	-0.80	-3.56	-0.81
19	1425.10	21.941	-0.01	0.00	0.93	0.71	-0.31	0.70	-0.33
20	906.899	20.844	0.01	0.00	-1.18	-2.06	-0.62	-2.16	-0.72
21	367.263	29.465	0.07	0.09	-4.24	-8.09	-1.52	-8.17	-1.61
22	148.729	41.221	-0.01	-1.02	-6.45	-0.51	-1.27	-0.51	-1.27
23	75.5014	63.019	0.16	0.17	-13.88	9.77	4.75	9.90	4.87
24	48.0520	81.890	0.17	-2.59	-21.21	-11.79	-0.78	-11.69	-0.67
25	27.7000	23.170	0.94	0.33	-6.07	45.02	10.84	45.04	10.86
26	15.9680	7.871	-0.00	-0.14	0.10	0.12	-0.18	0.12	-0.18
27	9.87700	10.745	-0.00	0.27	1.64	0.39	-0.51	0.39	-0.52

9.7 Chapter Summary

This chapter presented several benchmark problems—a UO_2 fuel pin, a MOX fuel pin, a UO_2 lattice with water hole, and a UO_2-MOX lattice—and used them to compare various self-shielding methods side-by-side. The methods tested included both classical methods and new methods.

Significant results included:

- a demonstration of the effect of the self-shielding of the scattering source, which effects all of the methods for groups such as the one containing the U-238 $36.6\,\text{eV}$ resonance.
- the failure of the intermediate resonance model to account for flux reduction due to resonance absorption.
- significant mutual self-shielding effects in MOX fuel.
- difficulty in the generation of subgroup with interference cross section quadratures.
- success of ultrafine with simplified scattering with the slowing down source and the difficulty with the intermediate resonance source with broad groups.
- failure of resonance interference factors when spatial mutual self-shielding effects are important.

Part V

Conclusions and References

Chapter 10

Conclusions

10.1 Summary

In Sec. 1.4, two overarching thesis objectives were defined. First, the thesis sought to measure the current status of existing self-shielding methods. Second, the thesis sought to propose new self-shielding methods to extend the range of applicability of the methods. These objectives were accomplished through the six major contributions detailed in this thesis:

1. Existing self-shielding methods were presented in great detail in Part II. Although this is not novel work, such an exhaustive description of such a wide array of methods is not readily found in literature—with [12] being the closest—and should serve as a useful reference for many future applications.

2. A framework for evaluating self-shielding methods was proposed in Ch. 6. Under this framework a simple benchmark problem was defined and applied to numerous self-shielding methods. This provided a baseline for performance of the methods.

3. The effect of using scalar-flux-weighted multigroup cross sections was quantified in Ch. 7. This approximation was shown to have a measurable and significant impact even on simple and small problems. Using angular-dependent cross sections was shown to correct the issue. Other options exist and were detailed, including Legendre expanding the angular dependence and using a corrective factor known as an SPH factor.

4. A new means of accounting for mutual self-shielding in the subgroup method was developed in Sec. 8.3. This method fits a parameter known as an interference cross section for each level of a nuclide's subgroup quadrature for each other nuclide. It allows interference effects to be modeled natively inside the subgroup method without increasing the algorithmic complexity of the method.

5. A new method known as Ultrafine with Simplified Scattering, a hybrid of ultrafine and subgroup methods, was introduced in Sec. 8.4. This method gives many of the benefits of the ultrafine method without needing to rigorously compute the scatter source. This allows self-shielding effects to be handled much more elegantly than in current methods, and allows for very straightforward parallelization and otherwise reduced computational burden of a true ultrafine method.

6. In Ch. 9, both old and new methods were compared on a series of benchmark problems. This uses the framework of Ch. 6 and applies it to realistic problems. The results not only shed light on the quality of classical self-shielding approximations but also serve to assess the quality of the newly proposed methods.

For each of these contributions, a brief summary and future work related to the area will now be discussed.

10.2 Classical Self-Shielding Approximations

Summary

Part II explained in great detail the classical approaches to self-shielding. Included were slowing down in infinite media, equivalence in dilution, the subgroup method, and ultrafine methods.

The solution of the slowing down equation is the backbone of all the subsequent self-shielding methods. It is used to generate tables of multigroup constants as a function of the dilution, i.e., the amount of moderating material other than the nuclide of interest in the the medium. These tables are used directly by the equivalence in dilution method or used to generate quadratures for the subgroup method.

The equivalence in dilution method (Ch. 3) uses a clever manipulation of the transport equation in its collision probability form on a problem with exactly two regions—fuel and moderator—to find an equivalence between a heterogeneous problem and a homogeneous problem. An equivalence cross section serves effectively as an additional background moderator and with it, the tables generated by the solution of the slowing down equation can be used in a heterogeneous problem. This equivalence cross section is obtained using a rational approximation based on the shape and size of the lumped fuel regions as well as the Dancoff factor, which accounts for the likelihood of a neutron exiting one fuel lump and entering another lump elsewhere in the geometry.

The subgroup method (Ch. 4) uses a clever change of variables to integrate the reaction rate by cross section value rather than by energy. This allows many fewer base points to be needed

in a numerical quadrature, and allows a lattice-level calculation to account for self-shielding effects through the solution of a simplified transport equation with a fixed source only a small number of times per energy group per nuclide. The quadrature needed, though, is not easily defined, and several methods for the generation of the quadrature are detailed in the main text.

Ultrafine methods (Ch. 5) discretize the energy variable sufficiently to implicitly account for self-shielding effects. If computationally feasible, one could use ultrafine methods directly on a downstream application without resorting to a multi-level cross section generation approach. However, this is not currently feasible, and ultrafine methods are typically used to generate cross sections on small geometries for use in downstream applications. In the main text, the means of treating the scatter source, which is the primary complication of these methods, is discussed.

Future Work

Although this section of the thesis was intended to be background material rather than new work, there is still future work that can and should be done. Specifically, rather than leaving this material as a textual reference, each method should be implemented in an open source framework for use by educators and researchers. In the spirit of OpenMC [38] and OpenMOC [3], this open source approach enables those in the field to make meaningful progress toward their educational and research goals, avoiding unneeded difficulties with implementation. Also, there is no better means of explaining the workings of a method than a demonstration.

Such an open source framework could come in one of two varieties (or ambitiously, both). First, the framework could be standalone, including its own transport solver and only applying these methods to small problems, such as those shown in Ch. 9. Second, the methods could be adapted to a larger scale and included in OpenMOC, effectively transforming it from a transport solver to a lattice physics code.

10.3 Framework for Evaluating Self-Shielding Methods

Summary

In Ch. 6, a framework for evaluating self-shielding methods was introduced. This framework sought to be analogous to unit testing and integral testing in a software engineering framework. Rather than evaluating a self-shielding method only by its results on a large problem with many aspects of physics working in different ways, the specific physical aspects being modeled by the method should first be isolated.

A specific benchmark problem was then given, one that was the simplest possible problem in which both energy and spatial self-shielding are important. The benchmark used two simple geometries, an isolated slab and an infinite square array of identical pins, and only a single resonance, whose height was varied, in the fuel material. Several different self-shielding methods were tested and quantitatively evaluated using this benchmark.

This test highlighted how two-term rational approximations in equivalence in dilution do a very good job of modeling the spatial self-shielding effect. Likewise, it showed the efficacy of the subgroup method when a suitable quadrature was obtained. The quadrature generation process was noted to be quite difficult in some cases. Perhaps most significantly, this test highlighted that a newer method known as the Embedded Self-Shielding Method failed to perform nearly as well on this simple benchmark. The implementation of ESSM used was based on an iterative procedure to determine the appropriate data to use from homogeneous tables. Newer implementations of ESSM—perhaps because this issue was seen in separate work—use the iterative procedure to determine the appropriate data to use from tables generated from heterogeneous calculations.

Future Work

The most desired aspect of future work for this framework is for it to be applied to any and all new self-shielding methods. While this has little to do with the framework itself, this is the means that the framework will have the most significant impact.

In terms of the benchmark problem, a plethora of future work is readily performable by considering incremental additions to the aspects of physics under consideration. Later in this thesis, realistic scattering and real cross sections were applied to the benchmark to serve as the next step in the framework. Other possibilities abound. One could study the effect of intra-pin discretization, perhaps with a temperature distribution across the pin or differing number densities in different radial zones. A second resonant nuclide was admixed in the fuel in Ch. 8, and this could be extended further by using a more realistic scattering model.

10.4 Angular Effects on Multigroup Cross Sections

Summary

In Ch. 7, the effect of using the scalar flux to collapse the total multigroup cross section was examined. Condensation errors were seen in the reaction rates and shown to be the result of improper treatment of self-shielding. Effectively, the neutron flux entering a resonant region from the moderator is not shielded; that is, there are a significant number of neutrons at the resonance energies. However, as neutrons pass through the resonant region, those neutrons

at resonance energies preferentially collide, and there is a significant reduction in the flux at those energies. Thus, the multigroup cross section is very different for neutrons entering the resonant region than those that have traversed a piece of it first. This effect is not sufficiently treated by using an average value obtained by scalar flux weighting.

It was shown that using angular dependent total multigroup cross sections alleviated this effect. Importantly, it showed that simply using angular dependent cross sections is not sufficient to alleviate the issue; they must be coupled with sufficiently fine spatial discretization.

Two possible means of accounting for this issue without resorting to angular dependent cross section data were presented. First, a transport correction can be used, where the total reaction rate is expanded in Legendre polynomials, and the anisotropic terms are moved to the right hand side as a source. This tactic can be effective, but adds anisotropy to the scatter source. More moments than desired for the scattering may be required to adequately model the total reaction rate. Second, the SPH factor can be used. The SPH factor is a correction factor that enforces conservation of reaction rates. Although a very simple concept, it was shown to be very effective on a simple test problem.

Future Work

A truly elegant means of accounting for these angular issues is desired. Correction factors, especially ones with as little physical basis as the SPH factor, are not ideal in a high-fidelity simulation. However, this desire must be balanced with the reality of computations, and a solution must not add too much computational complexity.

Some possible solutions that warrant further study include a coarse spatial discretization coupled with course angularly dependent data. Rather than use different cross sections for each angle in an MOC solution, perhaps using cross sections defined on the octant would be sufficient. Alternatively, the Legendre expansion approach could be investigated using double-Legendre expansions, i.e., separate expansions for neutrons entering the fuel region than for those exiting the region. There are difficulties applying this in 2-D, as the surface normal may not be constant in a flat source region, but further investigation is still warranted.

10.5 Subgroup with Interference Cross Sections

Summary

In Sec. 8.3, a means of accounting for mutual self-shielding in the subgroup method was proposed. This method, the subgroup method with interference cross sections, adds an extra quantity to the quadrature for a given nuclide to account for interference effects for each other nuclide. Holding the base quadrature constant, so-called interference cross sections

are obtained from a fitting process, minimizing the error between subgroup estimates and infinite medium reference solutions. This approach allows the resonance interference effect to be modeled natively inside the subgroup method without increasing algorithmic complexity.

The results in Sec. 8.3 were very promising, and the method was further tested in Ch. 9. On the UO_2 fuel pin, the method again performed adequately. However, with the MOX fuel pin, this method was not at all successful. Difficulties arose in the generation of the interference cross sections. For nuclides that had little impact on the cross section of another nuclide in a particular group, nonsensical interference cross section values were chosen by the optimizer. Furthermore, because in many cases, the base quadrature was not directly analogous to energy ranges, the obtained interference cross sections retained errors on the order of several percent.

Future Work

Despite the struggles identified in this analysis, this method still has merit, but requires much future work. There were two major issues in the generation of the interference quadratures in this work, likely each requiring its own solution.

First, the issue of the optimizer choosing large interference cross sections when an infinite medium is insensitive to the cross section must be addressed. The approach taken in this analysis, of forcing interference cross sections to zero when a lack of sensitivity was observed, is not adequate, as there is no clear cutoff between the cross section being sensitive versus not sensitive. One possibility is to generate the interference cross sections on heterogeneous geometries, similar to the approach for generating the base quadrature in [24].

Second, the base quadratures used in this study were not compatible with the interference cross sections. One means of alleviating this issue is to use a base quadrature defined by a direct approach to quadrature generation. This guarantees the quadrature will have the necessary properties for the interference cross section procedure. However, the direct approach is not typically desired in subgroup implementations, and so further work is needed to determine a procedure that is suitable with a fitting or moment-based method.

10.6 Ultrafine with Simplified Scattering

Summary

Section 8.4 presents a new method that is a hybrid of the subgroup and ultrafine methods, dubbed Ultrafine with Simplified Scattering. This method uses an ultrafine discretization of the energy variable and uses the same left hand side of the transport equation as ultrafine methods. It uses the scatter source used in the subgroup method on the right hand side, which decouples each energy point from each other point. The generation of cross sections is then

entirely analogous to the procedure used in the subgroup method, but the quadrature is much more easily defined, and mutual self-shielding effects are modeled implicitly.

Two possible right hand sides were considered. First, the intermediate resonance source, the most commonly employed scatter source in the subgroup method, was used. This approach has two primary difficulties. First, the intermediate resonance parameter must be defined for each nuclide relative to another nuclide. By treating all nuclides in the same calculation, the nuclide to use as the reference is ill-defined. Second, if wide groups are used, this method fails to account for the depression in the flux due to resonance absorption. In Ch. 9, this was seen to be significant in certain cases, including moderate errors with U-238 alone and exacerbated errors in MOX fuel for certain nuclides.

The second choice of the scatter source is that of a solution to the slowing down equation. An equivalent infinite medium is defined in the same manner as in the equivalence in dilution method, and the source is computed from the solution of the slowing down equation with this medium. The slowing down source can be tabulated by nuclide, and so these slowing down solutions can be precomputed.

In Ch. 9, both choices of scatter source were examined. As wide groups were used in this analysis, the slowing down solution performed much better than the intermediate resonance source. Overall, it was the best performing method considered in the analysis. Although this method was certainly not the most computationally efficient method considered, it was successfully identified as a possible method to use for higher fidelity calculations.

Future Work

With the positive results obtained in Ch. 9, this method warrants considerable future work. It should be applied to larger problems, such as fuel assembly calculations, and perhaps examined for full-core applications. In these applications, studies will need to be performed to quantify many outstanding issues. For instance, this work did not address the best approach for selecting the ultrafine energy mesh used in the solution. The sensitivity and trade-offs implied by the selection of the energy mesh in the context of computational efficiency should be studied. Furthermore, although this method appears to be easily performed on parallel architectures, additional studies should be performed to identify the best approach to this. Also, a study examining how this method fits into a production-level workflow is needed.

10.7 Analysis of Cross Section Generation Methods

Summary

Chapter 9 was a significant study that compared both old and new self-shielding methods on small geometries using realistic cross sections. Cases were chosen to highlight the performance of the methods with only a single resonant nuclide and with multiple resonant nuclides. In the latter case, cases were specifically chosen to stress the methods' handling of mutual self-shielding. This study was a continuation of the framework presented in Ch. 6, increasing the complexity and providing more realistic test cases.

This process was used to evaluate the two new self-shielding methods proposed in the thesis, one with a high degree of success, and one requiring considerable future work to be viable. These mixed results are precisely the reason such benchmark cases are necessary. This procedure highlights specific aspects of physics and allows any issues to be diagnosed before they are applied to larger problems and clouded by other aspects of the physics at play.

The method also included legacy methods and the correction-based approach to mutual self-shielding of resonance interference factors. These methods were compared side-by-side with the new methods, and were found to be rather effective. In some cases, the methods did break down somewhat, highlighting the limits of their application.

Future Work

The quantity of future work in this area is endless. More and more test cases can be applied, with more and more methods tested. However, this should be applied in a very systematic manner. In the spirit of software engineering's unit tests and integral tests, cases should be chosen that minimize the total burden of running the test cases while maximizing the coverage of situations tested. Although a goal of newer self-shielding methods is to be more problem agnostic, a test suite could be tailored to a specific class of reactors, and additional test suites made for other classes of reactors.

An additional area of future work is in the application of cross section generation methods to larger geometries. The small geometries considered in this study are not greatly impacted by issues such as the spatial distribution of the flux across the core. However, if one were to merge the lattice and full-core levels of the multi-level approach to reactor physics simulations, using self-shielding methods directly on full-core problems, a flat distribution of neutrons as a source would not be a sufficient approximation. In this case, an iterative approach to self-shielding may be warranted, where information from a coarse-group calculation is used to inform the self-shielding calculation.

References

[1] R. E. MACFARLANE, *PSR-480/NJOY99.0: Code System for Producing Pointwise and Multigroup Neutron and Photon Cross Sections from ENDF/B Data*, Los Alamos National Laboratory, 2000.

[2] J. R. ASKEW, "A Characteristics Formulation of the Neutron Transport Equation in Complicated Geometries," AAEW-M 1108, UK Atomic Energy Establishment (1972).

[3] W. BOYD, S. SHANER, L. LI, B. FORGET, and K. SMITH, "The OpenMOC method of characteristics neutral particle transport code," *Annals of Nuclear Energy*, **68**, 43 (2014).

[4] A. YAMAMOTO, M. TABUCHI, N. SUGIMURA, T. USHIO, and M. MORI, "Derivation of optimum polar angle quadrature set for the method of characteristics based on approximation error for the Bickley function," *Journal of Nuclear Science and Technology*, **44:2**, 129.

[5] J. J. DUDERSTADT and L. J. HAMILTON, *Nuclear Reactor Analysis*, John Wiley & Sons (1976).

[6] T. H. TRUMBULL and T. E. FIENO, "Effects of applying the Doppler broadened rejection correction method for LEU and MOX pin cell depletion calculations," *Annals of Nuclear Energy*, **64**, 184 (2013).

[7] J. LAMARSH, *Introduction to Nuclear Reactor Theory*, Addison-Wesley Publishing Company (1961).

[8] P. REUSS, *Neutron Physics*, EDP Sciences (2008).

[9] A. HÉBERT, *Applied Reactor Physics*, Presses Internationales Polytechnique (2009).

[10] R. GOLDSTEIN and E. R. COHEN, "Theory of resonance absorption of neutrons," *Nuclear Science and Engineering*, **13**, 132 (1962).

[11] B. R. SEHGAL, "Resonance Absorption for Heavy Moderators in Homogeneous Media," *Journal of Nuclear Energy Parts A/B*, **19**, 921 (1965).

[12] A. YAMAMOTO and D. NOTT, *Lattice Physics Computation*, volume 1 of *Handbook of Nuclear Engineering*, p. 913–1239, Springer, 2010.

[13] G. I. BELL and S. GLASSTONE, *Nuclear Reactor Theory*, Van Nostrand Reinhold Company (1970).

[14] R. STAMM'LER and C. ABBATE, *Methods of steady-state reactor physics in nuclear design*, Academic Press (1983), ISBN 0-12-663320-7.

[15] N. SUGIMURA and A. YAMAMOTO, "Evaluation of Dancoff factors in complicated geometry using the method of characteristics," *Journal of Nuclear Science and Technology*, **43**, 1182 (2006).

[16] M. L. WILLIAMS and K.-S. KIM, "The Embedded Self-Shielding Method," *PHYSOR 2012 – Advances in Reactor Physics Linking Research, Industry, and Education* (2012).

[17] M. A. JESSEE et al., "POLARIS: A new two-dimensional lattice physics analysis capability for the SCALE code system," *PHYSOR 2014* (2014).

[18] L. B. LEVITT, "The probability table method for treating unresolved neutron resonances in Monte Carlo calculations," *Nuclear Science and Engineering*, **49**, 450 (1972).

[19] D. E. CULLEN, "Application of the probability table method to multigroup," *Nuclear Science and Engineering*, **55**, 387 (1974).

[20] M. N. NIKOLAEV, "Comments on the probability table method," *Nuclear Science and Engineering*, **61**, 286 (1976).

[21] W. M. STACEY, *Nuclear Reactor Physics*, Wiley-VCH, second edition, (2007).

[22] A. YAMAMOTO, H. KOIKE, and Y. YAMANE, "A new framework of resonance calculation method based on the sub-group method (1); theory," *Transactions of the American Nuclear Society*, **100**, 647 (2009).

[23] A. YAMAMOTO, H. KOIKE, and Y. YAMANE, "A new framework of resonance calculation method based on the sub-group method (2); calculation," *Transactions of the American Nuclear Society*, **100**, 650 (2009).

[24] H. G. JOO, G. Y. KIM, and L. POGOSBEKYAN, "Subgroup weight generation based on shielded pin-cell cross section conservation," *Annals of Nuclear Energy*, **36**, 859 (2009).

[25] G. CHIBA and H. UNESAKI, "Improvement of moment-based probability table for resonance self-shielding calculaion," *Annals of Nuclear Energy*, **33**, 1141 (2006).

[26] P. RIBON, "Probability tables and Gauss quadrature application to neutron cross sections in the unresolved energy range," *Proceedings of the Topical Meeting on Advances in Reactor Physics and Safety*, **1**, 280 (1986).

[27] S. PENG, X. JIANG, S. Z. 1, and D. WANG, "Subgroup method with resonance interference factor table," *Annals of Nuclear Energy*, **59**, 176 (2013).

[28] A. HÉBERT, "The Ribon Extended Self-Shielding Model," *Nuclear Science and Engineering*, **151**, 1 (2005).

[29] D. J. POWNEY and T. D. NEWTON, "Overview of the WIMS 9 Resonance Treatment," ANSWERS/TASK/2004/246, Serco Assurance (2004).

[30] A. CANBAKAN, A. HÉBERT, and J.-F. VIDAL, "Accuracy of a subgroup method for pressurized water reactor fuel assembly models," *International Conference on Mathematics and Computational Methods Applied to Nuclear Science & Engineering* (2015).

[31] A. YAMAMOTO et al., "AEGIS: An Advanced Lattice Physics Code for Light Water Reactor Analyses," *Nuclear Engineering and Technology*, **42**, *5*, 500 (2010).

[32] M. L. WILLIAMS and M. ASGARI, "Computation of Continuous Energy Neutron Spectra with Discrete Ordinates Transport Theory," *Nuclear Science and Engineering*, **121**, 173 (1995).

[33] M. L. WILLIAMS, "Submoment Expansion of Neutron-Scattering Sources," *Nuclear Science and Engineering*, **134**, 218 (2000).

[34] K.-S. KIM and M. L. WILLIAMS, "The Method of Characteristics for 2-D Mutligroup and Pointwise Transport Calculations in SCALE/CENTRM," *PHYSOR 2012* (2012).

[35] N. SUGIMURA and A. YAMAMOTO, "Resonance Treatment Based on Ultra-fine-group Spectrum Calculation in the AEGIS Code," *Journal of Nuclear Science and Technology*, **44**, *7*, 958 (2007).

[36] C. H. LEE and W. S. YANG, "MC2-3: Multigroup Cross Section Generation Code for Fast Reactor Analysis," ANL-NE-11-41rev1a (2012).

[37] M. L. ZERKLE, I. K. ABU-SHUMAYS, M. W. OTT, and J. P. WINWOOD, "Theory and Application of the RAZOR Two-Dimensional Continuous Energy Lattice Physics Code," *Proceedings of the Joint International Conference on Mathematical Methods and Supercomputing for Nuclear Applications* (1997).

[38] P. K. ROMANO and B. FORGET, "The OpenMC Monte Carlo particle transport code," *Annals of Nuclear Energy*, **51**, 274 (2013).

[39] N. HORELIK, B. HERMAN, B. FORGET, and K. SMITH, "Benchmark for Evaluation and Validation of Reactor Simulations (BEAVRS)," *International Conference on Mathematics and Computational Methods Applied to Nuclear Science & Engineering* (2013).

[40] R. E. MACFARLANE, *TRANSX 2: A Code for interfacing MATXS Cross-Section Libraries to Nuclear Transport Codes*, Los Alamos National Laboratory, 1993.

[41] G. I. BELL, G. E. HANSEN, and H. A. SANDMEIER, "Multitable Treatments of Anisotropic Scattering in S_N Multigroup Transport Calculations," *Nuclear Science and Engineering*, **28**, 376 (1967).

[42] A. HÉBERT, "A Consistent Technique for the Pin-by-Pin Homogenization of a Pressurized Water Reactor Assembly," *Nuclear Science and Engineering*, **113**, 227 (1993).

[43] N. HFAIEDH and A. SANTAMARINA, "Determination of the Optimized SHEM Mesh for Neutron Transport Calculations," *Mathematics and Computation, Supercomputing, Reactor Physics and Nuclear and Biological Applications* (2005).

[44] K.-S. KIM and S. G. HONG, "A new procedure to generate resonance integral table with an explicit resonance interference for transport lattice codes," *Annals of Nuclear Energy*, **38**, 118 (2011).

[45] Y. LIU, W. MARTIN, M. WILLIAMS, and K.-S. KIM, "A Full-Core Resonance Self-Shielding Method Using a Continuous-Energy Quasi-One-Dimensional Slowing-Down Solution that Accounts for Temperature-Dependent Fuel Subregions and Resonance Interference," *Nuclear Science and Engineering*, **180**, 247 (2015).

[46] Z. GAO, Y. XU, and T. J. DOWNAR, "The treatment of resonance interference effects in the subgroup method," *Annals of Nuclear Energy*, **38**, 995 (2011).

[47] T. TAKEDA and Y. KANAYAMA, "A Multiband Method with Resonance Interference Effect," *Nuclear Science and Engineering*, **131**, 401 (1999).

[48] A. HÉBERT and A. SANTAMARINA, "Refinement of the Santamarina-Hfaiedh energy mesh between 22.5 eV and 11.4 keV," *International Conference on Reactor Physics, Nuclear Power: A Sustainable Resource* (2008).

[49] H. G. JOO, B. S. HAN, and C. H. KIM, "Implementation of Subgroup Method in Direct Whole Core Transport Calcuation Involving Nonuniform Temperature Distribution," *Mathematics and Computation, Supercomputing, Reactor Physics and Nuclear and Biological Applications* (2005).

[50] Y. S. JUNG, U. C. LEE, and H. G. JOO, "Examination of Temperature Dependent Subgroup Formations in Direct Whole Core Transport Calculation for Power Reactors," *Proceedings of ICAPP 2012* (2012).

[51] Y. S. JUNG, C. B. SHIM, C. H. LIM, and H. G. JOO, "Practical numerical reactor employing direct whole core neutron transport and subchannel thermal/hydraulic solvers," *Annals of Nuclear Energy*, **61**, 357 (2013).

[52] The MathWorks, Inc., *MATLAB and Optimization Toolbox Release 2014b*, 2014, Natick, MA.

[53] R. J. J. STAMM'LER, *HELIOS Methods*, Studsvik Scandpower, 2003.